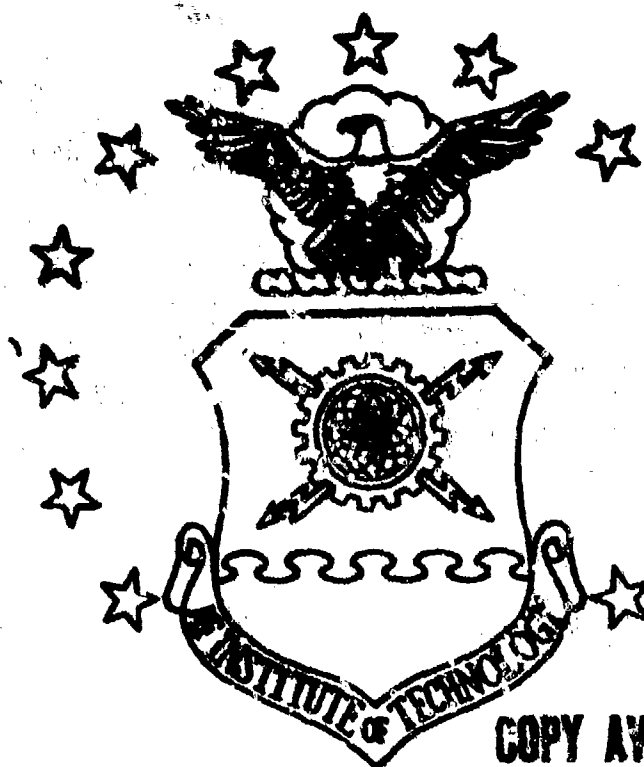
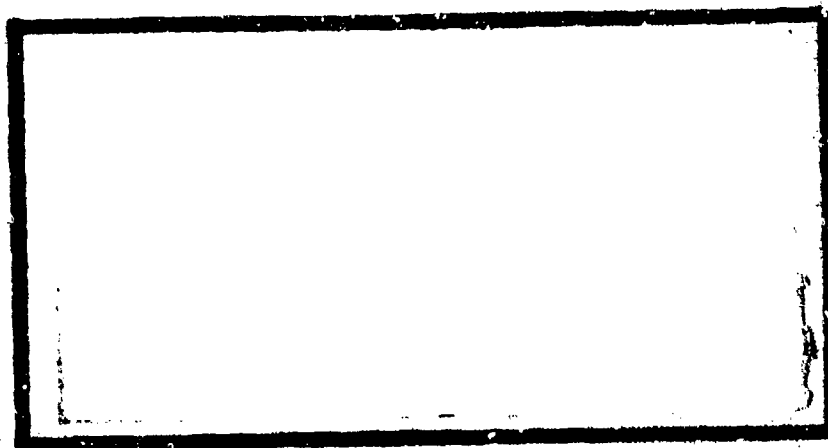


ADA032940



DDC Cy
OF

COPY AVAILABLE TO DDC DOES NOT
PERMIT FULLY LEGIBLE PRODUCTION



UNITED STATES AIR FORCE
AIR UNIVERSITY
AIR FORCE INSTITUTE OF TECHNOLOGY
Wright-Patterson Air Force Base, Ohio

DISTRIBUTION STATEMENT A

Approved for public release;
Distribution Unlimited

DDC
REF ID: A615071

UNCLASSIFIED

SECURITY CLASSIFICATION OF THIS PAGE (When Data Entered)

REPORT DOCUMENTATION PAGE		READ INSTRUCTIONS BEFORE COMPLETING FORM
1. REPORT NUMBER 14 DS/PH/76-3	2. GOVT ACCESSION NO.	3. RECIPIENT'S CATALOG NUMBER 9 Doctoral thesis
4. TITLE (and Subtitle) An Evaluation of Mass Integral Scaling as Applied to the Atmospheric Radiation Transport Problem.		5. TYPE OF REPORT & PERIOD COVERED #
6. AUTHOR(s) 10 Raymond A. Shulstad CAPT USAF		7. PERFORMING ORG. REPORT NUMBER
8. CONTRACT OR GRANT NUMBER(s)		9. PROGRAM ELEMENT, PROJECT, TASK AREA & WORK UNIT NUMBERS
9. PERFORMING ORGANIZATION NAME AND ADDRESS Air Force Institute of Technology (AFIT/EN) Wright-Patterson AFB, OH 45433		10. REPORT DATE 11 Nov 1976
11. CONTROLLING OFFICE NAME AND ADDRESS Air Force Weapons Laboratory (AFWL/SA) Kirtland AFB, NM 87117		12. NUMBER OF PAGES 197
12. MONITORING AGENCY NAME & ADDRESS (if different from Controlling Office)		13. SECURITY CLASS. (of this report) 12 Unclassified
13. DISTRIBUTION STATEMENT (of this Report) Approved for public release--distribution unlimited.		14. DECLASSIFICATION DOWNGRADING SCHEDULE 201 P.
15. DISTRIBUTION STATEMENT (of the abstract entered in Block 20, if different from Report)		
16. SUPPLEMENTARY NOTES Approved for public release IAW AFR 190-17 by JERRAL F. GUESS, Capt, USAF Director of Information Air Force Institute of Technology		
17. KEY WORDS (Continue on reverse side if necessary and identify by block number) Radiation transport Neutral-particle transport Neutron transport Secondary gamma-ray transport Atmosphere-mass scaling		
18. ABSTRACT (Continue on reverse side if necessary and identify by block number) This report presents the results of a comprehensive evaluation of mass integral scaling (MIS) as applied to the atmospheric radiation transport problem. MIS is an approximation used to predict the free-field radiation environments from atmospheric nuclear detonations. Codes like SMAUG and ATR use mass integral scaling of infinite homogeneous air transport data to generate environments which purport to reflect the near exponential vertical variation in density of air. The validity of the MIS approximation was → next page		

DD FORM 1 JAN 73 1473

EDITION OF 1 NOV 61 IS OBSOLETE

UNCLASSIFIED

SECURITY CLASSIFICATION OF THIS PAGE (When Data Entered)

012225

UNCLASSIFIED

SECURITY CLASSIFICATION OF THIS PAGE (When Data Entered)

20. ABSTRACT (Cont'd)

cont. evaluated by determining K factors defined to be the ratio of the 2-D $4\pi R^2$ variable density air dose to the 1-D $4\pi R^2$ MIS homogeneous air dose. K factors were determined for neutron and secondary gamma doses from both an unclassified fission and a thermonuclear source. Calculations were made for source altitudes between 5 and 20 km, for receiver altitudes between 1 and 25 km, and for mass ranges out to 250 g/cm^2 . The results are presented in the form of a series of ~~K factor versus~~ mass range curves for a particular source spectrum and source/receiver altitude. These curves may be used to extract multiplicative MIS correction factors. A series of MIS isoerror contours, which clearly define the error bounds over various spatial domains, is also presented.

UNCLASSIFIED

SECURITY CLASSIFICATION OF THIS PAGE (When Data Entered)

DS/PH/76-3

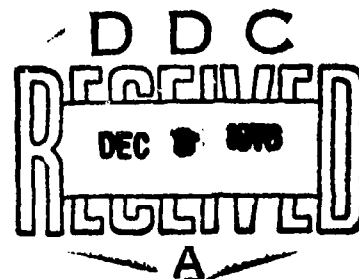
AN EVALUATION OF MASS INTEGRAL SCALING
AS APPLIED TO THE
ATMOSPHERIC RADIATION TRANSPORT PROBLEM

DISSERTATION

DS/PH/76-3

Raymond A. Shulstad
Capt USAF

Approved for public release; distribution unlimited



DS/PH/76-3

AN EVALUATION OF MASS INTEGRAL SCALING AS APPLIED
TO THE ATMOSPHERIC RADIATION TRANSPORT PROBLEM


DISSERTATION

Presented to the Faculty of the School of Engineering
of the Air Force Institute of Technology
Air University
in Partial Fulfillment of the
Requirements for the Degree of
Doctor of Philosophy

by

Raymond A. Shulstad, B.S., M.S.
Capt USAF

November 1976

ACCESSION No.	
RTIS	White Section <input checked="" type="checkbox"/>
ODS	Buff Section <input type="checkbox"/>
UNANNOUNCED	<input type="checkbox"/>
JUSTIFICATION	
BY	
DISTRIBUTION/AVAILABILITY CODES	
Dist.	AVAIL. and/or SPECIAL
	

Approved for public release; distribution unlimited

AN EVALUATION OF MASS INTEGRAL SCALING
AS APPLIED TO THE
ATMOSPHERIC RADIATION TRANSPORT PROBLEM

by

Raymond A. Shulstad, B.S., M.S.

Capt

USAF

Approved:

Charles J. Friedman
Chairman

Nov. 9 1976

Robert P. Couch

Nov 11, 1976

William J. ...

Nov 12, 1976

Peter J. Torczak

15 Nov 1976

Ronald C. Luber

15 Nov 1976

Accepted:

J. S. Premianiecki

Dean, School of Engineering

22 Nov 76

Preface

This report presents an evaluation of mass integral scaling (MIS) as applied to the atmospheric radiation transport problem. MIS is the fundamental approximation used in scaling codes like SMAUG and ATR to predict free-field radiation environments from atmospheric nuclear detonations. Such predictions are required in and are an integral part of analyses designed to assess the nuclear survivability/vulnerability of military equipment, systems, and personnel.

The results of the evaluation are summarized in a series of iso-error contour graphs which clearly define the MIS associated error over various spatial domains in the 1-25 km altitude region. These contours show that, while MIS is an acceptable approximation for source altitudes between 1 and 10 km, errors of a factor of two or more are easily incurred if applied at higher altitudes.

The purpose of the research reported here is not to condemn the use of the popular, quick-running scaling codes. Instead, my intent was to qualify the results of these codes. In fact, I believe that the codes are even more valuable now, because for the first time, users know how bad or good their results are. Furthermore, I believe that an MIS correction factor algorithm can be fairly easily constructed using the data and methodology developed in the course of this study.

I would like to acknowledge several people who provided me with significant assistance during the course of this effort. First, I want to thank my dissertation advisor, Dr. Charles J. Bridgman (Air Force Institute of Technology), for his suggestions and the encouragement

that he provided. He was one of the first to question the validity of MIS and convinced me that an evaluation of the technique was essential. Next, I want to express my appreciation to my friends and colleagues, John Burgio and Harry Murphy of the Air Force Weapons Laboratory. John processed the cross sections used in the study and, during our many discussions, provided me with a much broader insight to the problem. Harry deserves special mention. He is, without a doubt, the most competent computer programmer that I have ever met. He wrote the fitting programs used in the study and provided me with several routines which were incorporated directly into the AIRDIF code. The structured, modular nature of AIRDIF is attributable to the patient instruction he gave me. I am also indebted to Mrs. Kay Fink and Ms. Maria Garcia for typing the drafts of this report, to Mrs. Bette Shannon for typing the final manuscript, to Mr. Clarence Larson for the preparation of all figures and graphs, and to my math aide, Keith Merrifield, for the many hours he spent in helping me polish the various drafts into final form. Finally, I want to thank my family and especially my loving wife, Vicki, for the patience and understanding they showed me. Their sacrifices over the past two years were far greater than mine.

Raymond A. Shulstad

Contents

	Page
Preface	iii
List of Figures	vii
List of Tables.	xiii
Abstract.	xiv
I. Introduction.	1
Background.	1
Purpose	6
II. Mass Integral Scaling	8
The Mass Scaling Law.	8
Extension of the Mass Scaling Law to Variable Density Air	9
Deficiencies of Mass Scaling in Variable Density Air.	10
III. Method of Evaluation.	14
The K Factor.	14
Calculation Parameters.	15
IV. Atmospheric Diffusion Theory.	22
The Multigroup Diffusion Equation	23
Nonorthogonal Coordinate System	24
The Diffusion Equation in the U.S. Standard Atmosphere.	29
Numerical Solution of the Diffusion Equation.	36
The AIRDIF Code	39
V. Validity of Diffusion Calculations.	43
Comparisons of Radiation Doses in Homogeneous Air	43
Comparisons of Radiation Doses in the U.S. Standard Atmosphere.	44
K Factor Comparisons.	46
Discussion of K Factor Comparisons.	47
A Limitation.	55
VI. Evaluation of Mass Integral Scaling	58
K Factor versus Mass Range Plots.	58
Parametric Analysis	58
MIS Iso-Error Contours.	63

	Page
VII. Summary and Conclusions	81
Bibliography.	83
Appendix A: Derivation of the Mass Scaling Law	86
Appendix B: The AIRDIF Code.	90
Appendix C: Radiation Dose Comparisons	94
Appendix D: K Factor Comparisons	109
Appendix E: K Factor versus Mass Range Plots for a Fission Source	126
Appendix F: K Factor versus Mass Range Plots for a Thermonuclear Source	154
Vita.	182

List of Figures

<u>Figure</u>		<u>Page</u>
1	The U.S. Standard Atmosphere	2
2	The Mass of Air Above an Altitude Z in the U.S. Standard Atmosphere.	12
3	Orthogonal and Nonorthogonal Meshing in the Atmosphere	25
4	Coaltitude Range in the U.S. Standard Atmosphere to 100 g/cm^2 versus Altitude.	27
5	The Expanding Nonorthogonal Coordinate System.	28
6	The Density Gradient versus Altitude	31
7	Least-Squares Fit of AIRDIF Neutron Silicon Doses from a Fission Source in Homogeneous Air.	40
8	Least-Squares Fit of AIRDIF Secondary Gamma Silicon Doses from a Fission Source in Homogeneous Air	41
9	Neutron Silicon Doses from a Fission Source in Homogeneous Air: ANISN versus MORSAIR	50
10	Secondary Gamma Silicon Doses from a Fission Source in Homogeneous Air: ANISN versus MORSAIR	51
11	Neutron Silicon Doses from a Thermonuclear Source in Homogeneous Air: ANISN versus MORSAIR	52
12	Secondary Gamma Silicon Doses from a Thermonuclear Source in Homogeneous Air: ANISN versus MORSAIR	53
13	Neutron versus Secondary Gamma Coaltitude Silicon K Factors for a Fission Source at 20 km.	60
14	Sensitivity of the Coaltitude Neutron Silicon K Factor for a Fission Source to Source Altitude.	61
15	Sensitivity of the Coaltitude Secondary Gamma Silicon K Factor for a Fission Source to Source Altitude	62
16	Sensitivity of the Neutron Silicon K Factor for a Fission Source at 20 km to Receiver Altitude	64

<u>Figure</u>		<u>Page</u>
17	Sensitivity of the Coalititude Neutron Silicon K Factor for a Source at 20 km to Source Type.	65
18	Sensitivity of the Coalititude Secondary Gamma Silicon K Factor for a Source at 20 km to Source Type.	66
19	Sensitivity of the Coalititude Neutron K Factor for a Fission Source at 20 km to Dose Response	67
20	Sensitivity of the Coalititude Secondary Gamma K Factor for a Fission Source at 20 km to Dose Response	68
21	10% Maximum MIS Error Contour for a Source at 5 km	70
22	20% Maximum MIS Error Contour for a Source at 10 km.	71
23	Neutron Dose MIS Error Contours for a Fission Source at 15 km	73
24	Neutron Dose MIS Error Contours for a Thermonuclear Source at 15 km.	74
25	Secondary Gamma Dose MIS Error Contours for a Fission Source at 15 km.	75
26	Secondary Gamma Dose MIS Error Contours for a Thermonuclear Source at 15 km.	76
27	Neutron Dose MIS Error Contours for a Fission Source at 20 km	77
28	Neutron Dose MIS Error Contours for a Thermonuclear Source at 20 km.	78
29	Secondary Gamma Dose MIS Error Contours for a Fission Source at 20 km.	79
30	Secondary Gamma Dose MIS Error Contours for a Thermonuclear Source at 20 km.	80

Appendix B

B-1	Hierarchy of the AIRDIF Code	91
-----	--	----

FigurePage

Appendix C

C-1	Neutron Silicon Doses from a Fission Source in Homogeneous Air: AIRDIF versus ANISN	95
C-2	Secondary Gamma Silicon Doses from a Fission Source in Homogeneous Air: AIRDIF versus ANISN	96
C-3	Neutron Silicon Doses from a Fission Source at 15 km and Receivers at 11.3 km: AIRDIF versus MORSAIR . . .	97
C-4	Secondary Gamma Silicon Doses from a Fission Source at 15 km and Receivers at 11.3 km: AIRDIF versus MORSAIR	98
C-5	Neutron Silicon Doses from a Fission Source at 15 km and Receivers at 15.29 km: AIRDIF versus MORSAIR . .	99
C-6	Secondary Gamma Silicon Doses from a Fission Source at 15 km and Receivers at 15.29 km: AIRDIF versus MORSAIR	100
C-7	Neutron Silicon Doses from a Fission Source at 15 km and Receivers at 21.66 km: AIRDIF versus MORSAIR . .	101
C-8	Secondary Gamma Silicon Doses from a Fission Source at 15 km and Receivers at 21.66 km: AIRDIF versus MORSAIR	102
C-9	Neutron Silicon Doses from a Fission Source at 20 km and Receivers at 20.61 km: AIRDIF versus MORSAIR . .	103
C-10	Secondary Gamma Silicon Doses from a Fission Source at 20 km and Receivers at 20.61 km: AIRDIF versus MORSAIR	104
C-11	Neutron Tissue Doses from a Fission Source at 20 km and Receivers at 20.61 km: AIRDIF versus MORSAIR . .	105
C-12	Secondary Gamma Tissue Doses from a Fission Source at 20 km and Receivers at 20.61 km: AIRDIF versus MORSAIR	106
C-13	Neutron Silicon Doses from a Thermonuclear Source at 20 km and Receivers at 20.61 km: AIRDIF versus MORSAIR	107

<u>Figure</u>		<u>Page</u>
C-14	Secondary Gamma Silicon Doses from a Thermonuclear Source at 20 km and Receivers at 20.61 km: AIRDIF versus MORSAIR	108

Appendix D

D-1	Neutron Silicon K Factors for a Fission Source at 5 km and Receivers at 5.07 km	110
D-2	Secondary Gamma Silicon K Factors for a Fission Source at 5 km and Receivers at 5.07 km	110
D-3	Neutron Silicon K Factors for a Fission Source at 10 km and Receivers at 8.84 km	111
D-4	Secondary Gamma Silicon K Factors for a Fission Source at 10 km and Receivers at 8.84 km	111
D-5	Neutron Silicon K Factors for a Fission Source at 10 km and Receivers at 10 km	112
D-6	Secondary Gamma Silicon K Factors for a Fission Source at 10 km and Receivers at 10 km	112
D-7	Neutron Silicon K Factors for a Fission Source at 10 km and Receivers at 12.13 km	113
D-8	Secondary Gamma Silicon K Factors for a Fission Source at 10 km and Receivers at 12.13 km	113
D-9	Neutron Silicon K Factors for a Fission Source at 15 km and Receivers at 11.30 km	114
D-10	Secondary Gamma Silicon K Factors for a Fission Source at 15 km and Receivers at 11.30 km	114
D-11	Neutron Silicon K Factors for a Fission Source at 15 km and Receivers at 15.29 km	115
D-12	Secondary Gamma Silicon K Factors for a Fission Source at 15 km and Receivers at 15.29 km	115
D-13	Neutron Silicon K Factors for a Fission Source at 15 km and Receivers at 21.66 km	116
D-14	Secondary Gamma Silicon K Factors for a Fission Source at 15 km and Receivers at 21.66 km	116

<u>Figure</u>		<u>Page</u>
D-15	Neutron Silicon K Factors for a Fission Source at 20 km and Receivers at 14.85 km	117
D-16	Secondary Gamma Silicon K Factors for a Fission Source at 20 km and Receivers at 14.85 km	117
D-17	Neutron Silicon K Factors for a Fission Source at 20 km and Receivers at 20.61 km	118
D-18	Secondary Gamma Silicon K Factors for a Fission Source at 20 km and Receivers at 20.61 km	118
D-19	Neutron Silicon K Factors for a Fission Source at 20 km and Receivers at 22.08 km	119
D-20	Secondary Gamma Silicon K Factors for a Fission Source at 20 km and Receivers at 22.08 km	119
D-21	Neutron Tissue K Factors for a Fission Source at 20 km and Receivers at 14.85 km	120
D-22	Secondary Gamma Tissue K Factors for a Fission Source at 20 km and Receivers at 14.85 km	120
D-23	Neutron Tissue K Factors for a Fission Source at 20 km and Receivers at 20.61 km	121
D-24	Secondary Gamma Tissue K Factors for a Fission Source at 20 km and Receivers at 20.61 km	121
D-25	Neutron Tissue K Factors for a Fission Source at 20 km and Receivers at 22.08 km	122
D-26	Secondary Gamma Tissue K Factors for a Fission Source at 20 km and Receivers at 22.08 km	122
D-27	Neutron Silicon K Factors for a Thermonuclear Source at 20 km and Receivers at 14.85 km	123
D-28	Secondary Gamma Silicon K Factors for a Thermonuclear Source at 20 km and Receivers at 14.85 km	123
D-29	Neutron Silicon K Factors for a Thermonuclear Source at 20 km and Receivers at 20.61 km	124
D-30	Secondary Gamma Silicon K Factors for a Thermonuclear Source at 20 km and Receivers at 20.61 km	124
D-31	Neutron Silicon K Factors for a Thermonuclear Source at 20 km and Receivers at 22.08 km	125

<u>Figure</u>		<u>Page</u>
D-32	Secondary Gamma Silicon K Factors for a Thermonuclear Source at 20 km and Receivers at 22.08 km	125
	Appendix E contains 54 K factor versus mass range figures for a fission source. These are not listed here but are indexed on page 126.	
	Appendix F contains 54 K factor versus mass range figures for a thermonuclear source. These are not listed here but are indexed on page 154.	

List of Tables

<u>Table</u>		<u>Page</u>
I	Monte Carlo Calculations in Variable Density Air . . .	3
II	The DLC-31 Multigroup Energy Structure and Group Mean Free Paths	17
III	Neutron Dose Response Functions.	19
IV	Gamma Dose Response Functions.	20
V	Neutron Sources.	21
VI	Summary of U.S. Standard Atmosphere Comparisons: AIRDIF versus MORSAIR.	45

Abstract

This report presents the results of a comprehensive evaluation of mass integral scaling (MIS) as applied to the atmospheric radiation transport problem. MIS is an approximation used to predict the free-field radiation environments from atmospheric nuclear detonations. Codes like SMAUG and ATR use mass integral scaling of infinite homogeneous air transport data to generate environments which purport to reflect the near exponential vertical variation in density of air.

The validity of the MIS approximation was evaluated by determining K factors defined to be the ratio of the 2-D $4\pi R^2$ variable density air dose to the 1-D $4\pi R^2$ MIS homogeneous air dose. K factors were determined for neutron and secondary gamma doses from both an unclassified fission and a thermonuclear source. Calculations were made for source altitudes between 5 and 20 km, for receiver altitudes between 1 and 25 km, and for mass ranges out to 250 g/cm². The results are presented in the form of a series of K factor versus mass range curves for a particular source spectrum and source/receiver altitude. These curves may be used to extract multiplicative MIS correction factors. A series of MIS iso-error contours, which clearly define the error bounds over various spatial domains, is also presented.

The unique and distinguishing feature of this research is that the evaluation was conducted with a special form of diffusion theory which is also described in this report. By comparing the diffusion derived K factors to some recent Monte Carlo calculations, it is shown that the evaluation is not dependent on diffusion theory. This is significant

because the full-scale parametric evaluation of MIS was conducted with diffusion theory at a fraction of the cost that would have been required by a comparable Monte Carlo evaluation.

The results of this evaluation indicate that MIS is acceptable (errors less than 20%) out to mass ranges of 220 g/cm^2 for source altitudes between 1 and 10 km. At higher altitudes, however, errors of a factor of two or more are easily incurred.

AN EVALUATION OF MASS INTEGRAL SCALING
AS APPLIED TO THE
ATMOSPHERIC RADIATION TRANSPORT PROBLEM

I. Introduction

Background

The prediction of free-field radiation environments from atmospheric nuclear detonations is an integral part of analyses designed to assess the survivability/vulnerability (S/V) of military equipment, systems, and personnel. These assessments are characterized by the requirement to evaluate survivability and vulnerability under a multitude of scenarios. For example, the analyst must consider the sensitivity of his results to such parameters as weapon yield, source spectrum, and burst/receiver altitudes.

The physics of the atmospheric radiation transport problem is described by the well-known Boltzmann transport equation. Unfortunately, because of the unique problems created by the exponential-like density variation in air* (Figure 1), classical numerical solutions of the Boltzmann equation for this problem have not been attempted. Monte Carlo simulation is the only method that has been used to compute the free-field radiation environments in two-dimensional (2-D) variable density air. Table I summarizes the limited number of 2-D air Monte Carlo calculations which have been published.

*Variable density air in this study is defined to be the 1962 U.S. Standard Atmosphere (Ref. 1).

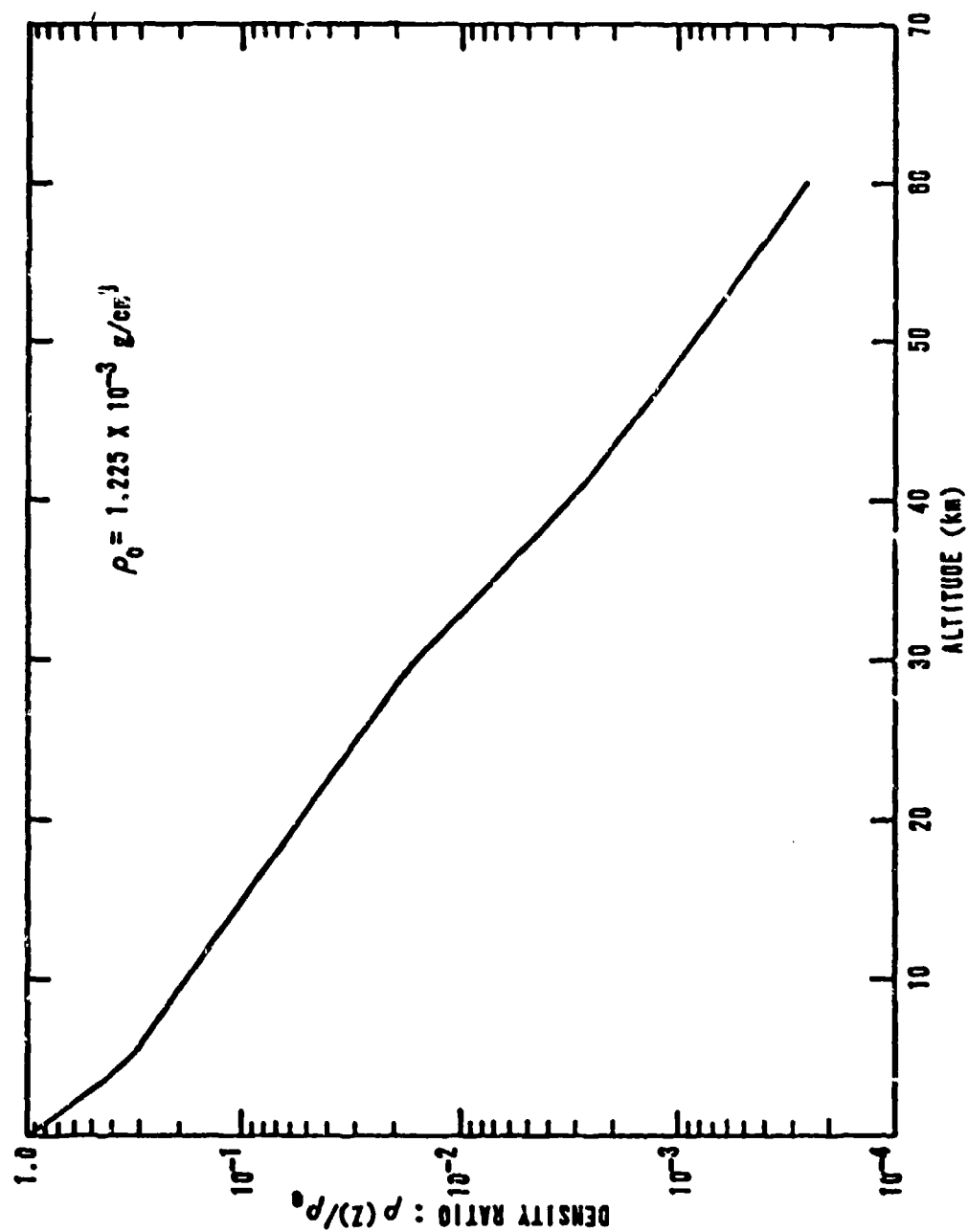


Figure 1. The U.S. Standard Atmosphere

TABLE I

Monte Carlo Calculations in Variable Density Air

<u>Author(s)</u>	<u>Year</u>	<u>Ref. No.</u>	<u>Source Height (km)</u>	<u>Source</u>
Marcum	1963	2	30.48, 60.96	14 MeV neutron
Marcum	1963	3	60.96 51.82	3 MeV gamma fission gamma
Raso and Woolf	1966	4	20.00	1.25 MeV gamma
George and Lavagnino	1966	5, 6	9.14, 15.24	12 monoenergetic neutron sources: 14.0-0.004 MeV
Shelton and Keith	1969	7	25.91, 33.53	8 monoenergetic neutron sources: 14.0-0.03 MeV
Raso	1969	8	20, 30, 40	0.5 and 1.0 MeV neutron
Celnik	1969	9	20 to 75	7 monoenergetic neutron sources: 14.1-1.5 MeV
Samon	1976	10	20, 30, 40, 60, 80	fission and thermo- nuclear neutron sources

The application of Monte Carlo methods to this problem is a science (some say art) in its own right and, unfortunately, expensive. For example, Eamon (Ref. 10) reports that CDC-7600 computer execution times of 30-40 minutes are required to obtain acceptable statistics (standard deviations less than 25%) for radiation environments from a fission source at 150 receivers located at mass ranges* varying from 10 to 200 g/cm² of air.

The high computational costs associated with Monte Carlo determinations coupled with the multiscenario nature of nuclear S/V assessments led to the development and widespread use of quick-running, user-oriented mass scaling codes like SMAUG (Ref. 11), ATR (Ref. 12), and CDR (Ref. 13). All of these codes use mass integral scaling (MIS) of infinite homogeneous air transport data to generate radiation environments which purport to reflect the exponential nature of two-dimensional (2-D) air. Their required input normally involves only a specification of the source in terms of yield and spectrum, source location, and receiver locations. They are capable of calculating environments at hundreds of receiver locations in a few seconds.

Past attempts to evaluate the accuracy of the MIS approximation have been limited in number and scope. In 1963, Marcum (Refs. 2 and 3) compared mass integral scaled doses from a 14 MeV neutron and a 3 MeV gamma source to Monte Carlo determined 2-D air doses at source altitudes of 30.48 and 60.96 km. He found that, at these altitudes, particles

*Mass range is the integral of the density along a straight line between the source and a receiver point. In constant density, homogeneous air it is simply the product of the density and the slant range between the source and receiver.

streaming out of the top of the exponential atmosphere (leakage) resulted in doses that were as much a factor of two lower than the scaled doses. In 1966, Raso and Woolf (Ref. 4) reported that MIS seemed to work pretty well for a 1.25 MeV gamma source at an altitude of 20 km. Unfortunately, their evaluation was restricted to mass ranges less than 80 g/cm².

In 1969, several evaluations of MIS were reported. Raso (Ref. 8) concluded that the MIS errors for a 0.5 MeV and a 1.0 MeV neutron source at altitudes of 20, 30, and 40 km were small. These results are somewhat misleading because his evaluation was restricted to small mass ranges of less than 20 g/cm². Celnik (Ref. 9) evaluated MIS for a number of monoenergetic neutron sources ranging in energy from 1.5 to 14.1 MeV and at altitudes ranging from 20 to 75 km. His results showed that the leakage effect cited above resulted in order of magnitude errors for source altitudes above 40 km and ranges greater than 80 g/cm².

It should be mentioned that the ATR code (Ref. 12) has a correction factor that purports to correct scaled doses for exponential air effects. The correction algorithm is based on an extension of French's (Ref. 14) "First-Last Collision Model" which was developed to predict the air/ground interface perturbation on doses from fast neutrons. An examination of the algorithm shows that the ATR correction factor is a function only of the source and receiver altitude and is independent of range. In contrast, the results of the evaluations cited above show quite clearly that the correction factor is strongly dependent on range. The ATR correction also assumes that the only perturbation is the leakage effect mentioned above. Again, the results of past evaluations (Refs. 2, 3, 7) have shown that differences in mass distribution between the source

and receiver in homogeneous and variable density air can cause an additional effect that is quite different from leakage. This effect, hereafter referred to as the mass distribution effect, can actually result in the 2-D variable density air results being higher than the scaled results rather than lower as leakage would predict.

By far, the most comprehensive evaluation to date was reported by Shelton and Keith (Ref. 7) in 1969. They compared the scaled total fluence from eight monoenergetic neutron sources ranging in energy from 0.03 to 14.1 MeV to Monte Carlo determined variable density air fluences. Source altitudes of 25.91 and 33.53 km and receiver altitudes ranging from 18 to 53 km were considered. In many cases, their evaluation extended to depths of 120 g/cm². Their results again showed that significant differences (errors >50%) existed between the scaled and actual variable density air results.

In summary, a number of attempts have been made in the past to evaluate the accuracy of the MIS approximation in variable density air. These evaluations have been limited in scope in that only a few monoenergetic sources and altitudes were considered. MIS has not been evaluated for spectra such as fission or thermonuclear sources, for source altitudes less than 20 km, or for the very important secondary gamma environments. Further, an acceptable MIS correction factor algorithm has not been developed.

Purpose

The purpose of the research reported here was to conduct a systematic evaluation of the MIS technique as applied to the atmospheric radiation transport problem. The evaluation is based on determining the ratio of

the 2-D $4\pi R^2$ variable density air dose to the 1-D $4\pi R^2$ homogeneous air MIS dose as a function of mass range, for a particular source, dose response function, and source/receiver altitude. Silicon and tissue dose ratios were determined for neutron and secondary gamma environments from both an unclassified fission and unclassified thermonuclear source for source altitudes between 5 and 20 km, for receiver altitudes between 1 and 25 km, and out to mass ranges of 250 g/cm².

The unique and distinguishing feature of this research is that the evaluation was conducted with a special form of diffusion theory which is defined later. The complete parametric evaluation via diffusion theory was conducted at a fraction of the cost ($\sim 1/30$) that would have been required by a comparable Monte Carlo evaluation. Further, by comparing diffusion derived results to available Monte Carlo results, it is shown that the diffusion evaluation is an adequate model for predicting the MIS evaluation ratios.

This report contains seven sections and six appendixes. In Section II, the mass scaling law is described, and the application of MIS in the scaling codes is discussed. The method used to evaluate MIS is described in detail in Section III. The diffusion equation in variable density air is developed in Section IV. Section V contains an examination of the validity of the diffusion calculations. Comparisons of diffusion derived radiation environments and MIS evaluation ratios are discussed here. The actual evaluation of mass integral scaling is presented in Section VI. Finally, a summary and concluding remarks are presented in Section VII.

II. Mass Integral Scaling

The Mass Scaling Law

The mass scaling law is widely used and is rigorously applicable to the transport of radiation in homogeneous media. For application to the atmospheric radiation transport problem, it can be stated as follows:

In an infinite homogeneous medium with an isotropic point source, the $4\pi R^2$ fluence (time integrated flux) or dose is a function only of ρR ,* the mass per unit area between the source and a receiver. In 1956, Zerby (Ref. 15) presented a very simple derivation of the mass scaling law using the Boltzmann transport equation. As shown in Appendix A, the scaling law can be derived from the diffusion equation in a similar manner and under the exact same set of assumptions.

To further clarify how mass scaling is applied in homogeneous air, let's consider the following example. If identical isotropic point sources are placed in two infinite homogeneous air media (medium A and medium B), and if two slant ranges, R_A and R_B , in the two media are related by

$$\rho_B R_B = \rho_A R_A \quad (2.1)$$

where ρ is the density in the respective media, then, as shown in Appendix A, the energy dependent fluences, $F(R,E)$, at ranges R_A and R_B

*In homogeneous air, " ρR " is the mass range or areal density and is given by the product of the density and slant range between the source and receiver.

must be related as

$$4\pi R_B^2 F(R_B, E) = 4\pi R_A^2 F(R_A, E) \quad (2.2)$$

It is convenient to refer to the quantity on the left- (or right-) hand side of equation (2.2) as the " $4\pi R^2$ fluence."

If the atmosphere were homogeneous, the mass scaling law could be rigorously applied, without error, to quickly compute radiation environments under a wide variety of scenarios. Unfortunately, this is not the case; the density in the U.S. Standard Atmosphere, as shown in Figure 1, is not constant but decreases in an exponential-like fashion with altitude. In the next subsection, it is shown how the mass scaling law is extended to variable density air and becomes an approximation whose accuracy varies and depends on a number of parameters.

Extension of the Mass Scaling Law to Variable Density Air

Since the density is not constant in variable density air, defined here to be the U.S. Standard Atmosphere (Ref. 1), the application of mass scaling here requires a careful definition of mass range. The mass range in this atmosphere is defined to be the mass integral, $\langle \rho R \rangle$, which can be written as

$$\langle \rho_B R_B \rangle \triangleq \int_0^{R_B} \rho(z) dR_B \quad (2.3)$$

and is also sometimes referred to as the areal density.

To show how the mass scaling law is applied in variable density air, assume that medium A is homogeneous air and that medium B is the U.S. Standard Atmosphere. The mass integral scaling (MIS) approximation

assumes that if the mass range between a source and receiver in variable density air is equal to the mass range in homogeneous air, then the $4\pi R^2$ fluences will be the same, i.e., if

$$\langle \rho_B R_B \rangle = \rho_A R_A \quad (2.4)$$

then

$$4\pi R_B^2 F(R_B, E) = 4\pi R_A^2 F(R_A, E) \quad (2.5)$$

So, the fundamental assumption made in MIS codes is that homogeneous air transport results can be mass integral scaled to generate radiation environments which purport to reflect the near-exponential nature of the U.S. Standard Atmosphere. All of these codes have an infinite homogeneous air transport data base like the one presented by Burgio in reference 16. The data base is stored as $4\pi R^2$ fluence as a function of mass range (areal density). To calculate the approximate 2-D atmospheric dose, a user specifies the source spectrum, dose response function, source height, receiver height, and slant range. The code then evaluates the mass integral and uses its data base to compute the 1-D MIS $4\pi R^2$ dose at this mass range. Finally, the dose is found by simply dividing by $4\pi R^2$.

Deficiencies of Mass Scaling in Variable Density Air

Since the mass scaling law was derived under the assumption of an infinite homogeneous media, it should be clear that it becomes an approximation when extended to variable density air. The most obvious deficiency of MIS when applied in this medium is its inability to account for the streaming of particles out the top of the exponential-like atmosphere (leakage). In homogeneous air, the medium is infinite in that every point

is theoretically surrounded by an infinite amount of mass. Therefore, it is not possible for particles to "leak." In the U.S. Standard Atmosphere, the density decreases in an exponential-like fashion with altitude. Figure 2, which depicts the integral with respect to altitude of the density function given in Figure 1, shows that the mass of air above an altitude z also decreases exponentially with altitude. At altitudes above 40 km, there are only a few grams/cm² of air above, and particles directed upward at these altitudes can and do stream out the top of the atmosphere. Since mass integral scaling cannot account for leakage, the scaled doses must be higher than the actual 2-D variable density air doses. The severity of the leakage effect obviously increases with altitude.

Another more subtle deficiency of MIS is due to the differences in mass distribution in homogeneous air and in the U.S. Standard Atmosphere. In homogeneous air, which is used to construct the scaling data base, the mass is uniformly distributed between the source and all receiver points. In contrast, the mass is nearly exponentially distributed in the vertical direction in the U.S. Standard Atmosphere. In this medium, a substantial number of particles can reach receivers after traveling great distances in the less dense air above the source. Although their paths are much greater than the simple slant range between the source and these receivers, the particles encounter much less air in traversing these distances than predicted by the simple mass integral. Therefore, they suffer less attenuation. The net effect of the mass distribution difference is to enhance the 2-D variable density air dose at large mass ranges and depress it at smaller ranges. The mass distribution effect is clearly present in

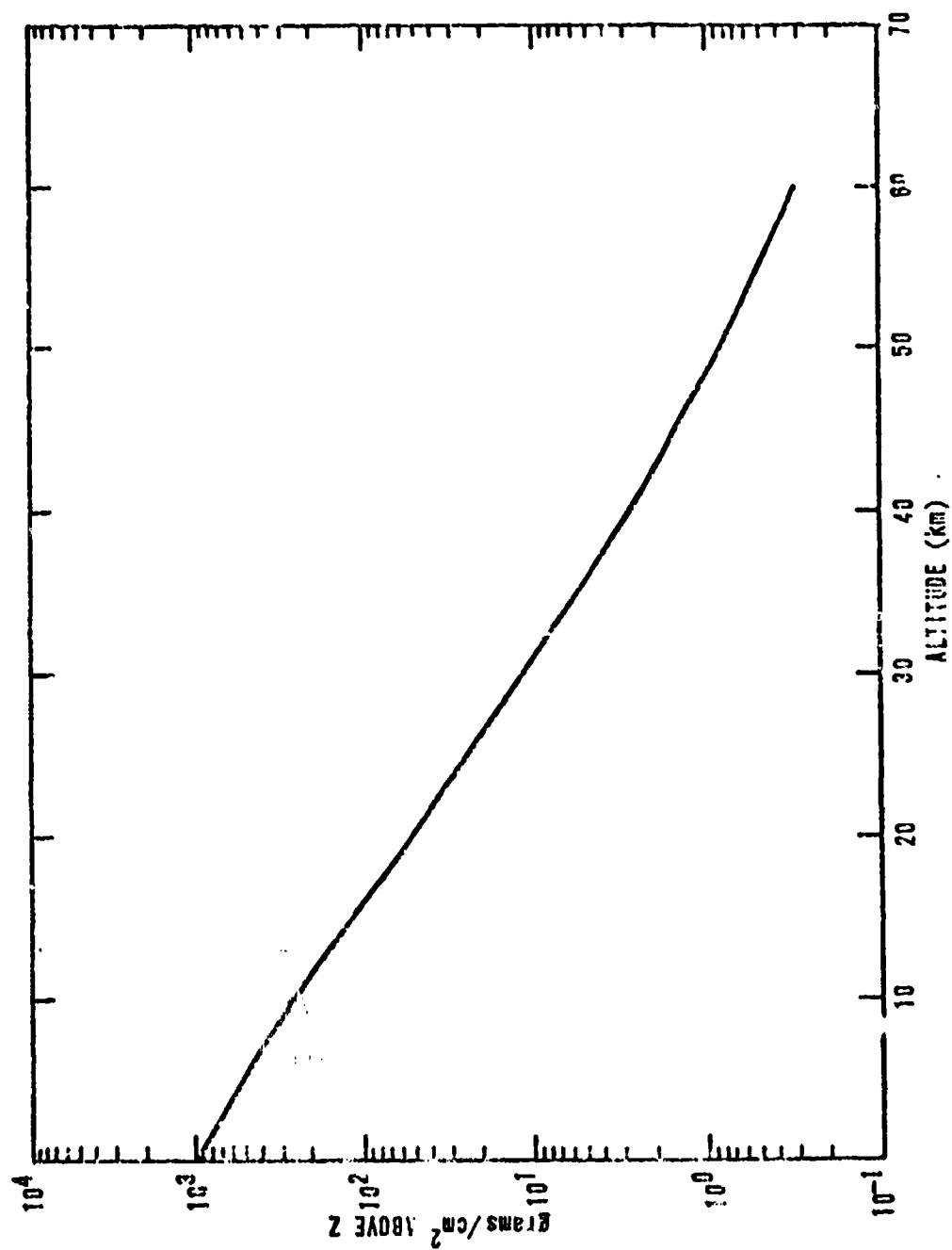


Figure 2. The Mass of Air Above an Altitude z in the U.S. Standard Atmosphere

Marcum's data (Refs. 2, 3) and has been discussed previously by Shelton and Keith (Ref. 7).

Finally, MIS is clearly inadequate for accurately predicting doses from low altitude bursts and for receivers near the air/ground interface. This, of course, is due to the change of medium and drastic discontinuity of density that occurs at the air/ground interface. Straker's (Ref. 17) analysis showed that the ground acts as a reflector at ranges close to the source and as an absorber at ranges far from the source. Therefore, the scaled doses are low in-close and high at greater ranges. Recently, Huszar (Ref. 18:38) compared some actual 2-D air/ground transport calculations (Ref. 19) to scaled results. He reports that if the source/receiver altitude is greater than 1000 meters and the corresponding receiver/source altitude is greater than 200 meters, then the air/ground perturbation of the scaled dose is negligible.

In summary, the effects of leakage, mass distribution, and the air/ground interface can all produce perturbations in the mass integral scaled dose in variable density air. As stated at the outset, the purpose of the research reported here was to conduct a systematic evaluation of the MIS technique as applied to the atmospheric radiation transport problem. Air/ground perturbations, which have recently been examined in detail (Refs. 18, 19), were not evaluated in the effort reported here. Results will be presented later which clearly define the error due to leakage and mass distribution over various spatial domains in the 1-25 km altitude region. In the next section, the method of evaluation used in this study is defined.

III. Method of Evaluation

The K Factor

Many nuclear S/V assessments do not require such details as the angular or energy dependent fluence and are conducted using scalar quantities like dose which is defined by

$$\text{Dose}(\vec{r}) = \sum_{g=1}^G F^g(\vec{r}) D_R^g \quad (3.1)$$

where

$F^g(\vec{r})$ = the angle integrated scalar fluence at a distance of $|\vec{r}|$ from the source for energy group g of a multigroup energy set which contains G groups (particles/cm²).

D_R^g = the experimentally determined dose response function for group g in units of dose (e.g., rads silicon or tissue)/unit scalar fluence.

Therefore, in this study mass integral scaling was evaluated by determining K factors which were defined as

$$K \text{ factor} = \frac{2\text{-D } 4\pi R^2 \text{ VARIABLE DENSITY AIR DOSE}}{1\text{-D } 4\pi R^2 \text{ MIS DOSE}} \quad (3.2)$$

Since the $4\pi R^2$ variable density air dose is a function of the source height, receiver altitude, mass range, source type, and response function, the K factor must also be dependent on these parameters. This evaluation method is convenient because the K factor can be used not only as a measure of the error due to MIS but also as a simple multiplicative correction factor for the scaled doses. The error due to MIS, which is

defined to be the absolute value of the difference between the 2-D and 1-D $4\pi R^2$ doses divided by the 2-D $4\pi R^2$ dose, is related to the K factor by

$$\epsilon = \left| \frac{\text{K factor} - 1}{\text{K factor}} \right| \quad (3.3)$$

Calculation Parameters

In this study, K factors were determined for neutrons and secondary gammas, for a fission and a thermonuclear source, for source altitudes between 5 and 20 km, for receiver altitudes between 1 and 25 km, for mass ranges out to 250 g/cm², and for silicon and tissue doses. The calculations reported here were made using the DLC-31, 37/21 coupled neutron and gamma, multigroup energy structure (Ref. 20) shown in Table II, the silicon and tissue response functions shown in Tables III and IV, and the unclassified fission and thermonuclear sources shown in Table V. The DLC-31 fission weighted multigroup cross section set described in reference 16 was used. Macroscopic cross sections were obtained under the assumption that air at a density of 1.11 mg/cm³ is composed of 79% nitrogen and 21% oxygen by volume (3.6609×10^{19} N atoms/cm³ and 9.7316×10^{18} O atoms/cm³).

As pointed out earlier, the unique and distinguishing feature of this research is that the computation of K factors and MIS evaluation were conducted with a special form of diffusion theory. This approach was chosen because an insufficient number of Monte Carlo calculations existed (Table I). Further, the cost to make the number of Monte Carlo calculations that might be required to adequately account for the sensitivity of the K factor to source/response type, source/receiver altitude, and range was thought to

be prohibitive. The special form of diffusion theory is developed in the next section, and the adequacy of its use in the MIS evaluation is examined in Section V.

TABLE II^a

The DLC-31 Multigroup Energy Structure and Group Mean Free Paths

Group	Upper Energy (MeV)	Mean Free Path ^c (g/cm ²)	Group	Upper Energy (MeV)	Mean Free Path (g/cm ²)
<u>Neutron Groups</u>					
1	1.9640+1 ^b	15.2	20	1.8268	10.9
2	1.6905+1	15.1	21	1.1080	10.7
3	1.4918+1	15.0	22	5.5023-1	6.8
4	1.4191+1	15.2	23	1.5764-1	6.1
5	1.3840+1	15.2	24	1.1109-1	5.2
6	1.2840+1	15.3	25	5.2475-2	4.3
7	1.2214+1	16.1	26	2.4788-2	4.0
8	1.052+1	17.1	27	2.1875-1	3.7
9	1.0000+1	18.6	28	1.0333-2	3.5
10	9.0484	19.0	29	3.3546-3	3.2
11	8.1873	17.0	30	1.2341-3	3.1
12	7.4082	18.8	31	5.8295-4	2.9
13	6.3763	17.3	32	1.0130-4	2.8
14	4.9659	21.6	33	2.9023-5	2.8
15	4.7237	13.3	34	1.0677-5	2.7
16	4.0657	12.5	35	3.0590-6	2.7
17	3.0119	17.5	36	1.1254-6	2.7
18	2.3852	19.9	37	4.1400-7	2.4
19	2.3069	14.8			

^aFrom reference 16.^bRead 1.9640+1 as 1.9640×10^1 .^cThe mean free path in mass units is independent of altitude and computed by multiplying the mean free path ($1/\Sigma_t$) at altitude z by the density at altitude z .

TABLE II (continued)

The DLC-31 Multigroup Energy Structure and Group Mean Free Paths

<u>Group</u>	<u>Upper Energy (MeV)</u>	<u>Mean Free Path (g/cm²)</u>
<u>Gamma Groups</u>		
38/1	1.4000+1	52.3
39/2	1.0000+1	47.4
40/3	8.0000	44.2
41/4	7.0000	41.4
42/5	6.0000	38.2
43/6	5.0000	34.5
44/7	4.0000	30.3
45/8	3.0000	26.7
46/9	2.5000	24.0
47/10	2.0000	20.9
48/11	1.5000	17.5
49/12	1.0000	14.5
50/13	7.0000-1	12.1
51/14	4.50000-1	10.2
52/15	3.0000-1	8.4
53/16	1.5000-1	7.1
54/17	1.0000-1	6.4
55/18	7.0000-2	5.6
56/19	4.5000-2	4.4
57/20	3.0000-2	2.6
58/21	2.0000-2	0.7

TABLE III

Neutron Dose Response Functions

Group	Silicon Response ^a Rads/(n/cm ²)	Tissue Response ^b Rads/(n/cm ²)
1	1.9106E-09	8.67241E-09
2	1.7792E-09	7.41901E-09
3	1.6818E-09	6.81154E-09
4	1.6231E-09	6.54471E-09
5	1.5144E-09	6.14729E-09
6	1.3851E-09	5.95478E-09
7	1.2370E-09	5.89361E-09
8	1.0530E-09	5.55077E-09
9	8.7897E-10	5.28824E-09
10	7.9629E-10	5.04731E-09
11	7.8141E-10	5.00452E-09
12	4.7092E-10	4.75953E-09
13	2.1394E-10	4.48311E-09
14	1.8267E-10	4.25311E-09
15	1.4195E-10	4.17110E-09
16	1.0582E-10	3.97837E-09
17	1.0006E-10	3.39051E-09
18	8.2995E-11	3.13766E-09
19	9.4778E-11	3.03449E-09
20	6.5328E-11	2.63932E-09
21	4.9785E-11	2.05699E-09
22	3.1515E-11	1.33305E-09
23	1.7897E-12	7.62280E-10
24	2.8022E-12	5.48897E-10
25	1.2327E-12	3.11644E-10
26	7.9084E-13	2.07393E-10
27	5.8930E-13	1.46624E-10
28	2.9804E-13	6.61426E-11
29	1.0498E-13	2.27582E-11
30	4.3305E-14	9.13150E-12
31	1.4421E-14	3.66325E-12
32	4.5895E-15	1.17590E-12
33	3.9377E-15	1.10948E-12
34	5.6286E-15	1.61171E-12
35	9.4023E-15	2.74157E-12
36	1.5380E-14	4.45699E-12
37	7.4244E-13	1.12382E-11

^aProvided by Dave Bartine of ORNL.^bBased on rebanding of data in reference 21 by H. M. Murphy.

TABLE IV

Gamma Dose Response Functions

Group	Silicon Response ^a Rad/(G/cm ²)	Tissue Response ^b Rad/(G/cm ²)
1	3.41838E-09	2.74311E-09
2	2.57121E-09	2.25643E-09
3	2.16121E-09	1.98395E-09
4	1.89915E-09	1.79216E-09
5	1.63669E-09	1.59277E-09
6	1.38348E-09	1.38972E-09
7	1.13348E-09	1.18027E-09
8	9.43338E-10	1.00980E-09
9	8.20339E-10	8.83204E-10
10	6.83433E-10	7.42810E-10
11	5.28457E-10	5.80300E-10
12	3.85046E-10	4.23930E-10
13	2.71224E-10	2.96950E-10
14	1.77718E-10	1.92834E-10
15	1.04590E-10	1.07596E-10
16	6.85104E-11	4.93830E-11
17	7.98544E-11	3.43145E-11
18	1.45429E-10	2.94789E-11
19	3.44112E-10	4.37499E-11
20	8.26793E-10	9.66468E-11
21	2.64927E-09	3.25042E-10

^aBased on rebanding of data given in reference 22 by H. M. Murphy.

^bBased on rebanding of data given in reference 23 by H. M. Murphy.

TABLE V

Neutron Sources^a

<u>Group</u>	<u>Thermonuclear</u>	<u>Fission</u>
1	0.0	0.0
2	0.0	0.0
3	1.38714-02*	0.0
4	9.34254-03	0.0
5	2.66169-02	0.0
6	1.66622-02	0.0
7	1.68678-02	0.0
8	1.23974-02	0.0
9	7.48258-03	3.83946-03
10	6.82320-03	3.50150-03
11	6.77521-03	5.38923-03
12	1.03201-02	7.34895-03
13	1.80706-02	1.83674-02
14	3.61700-03	3.24954-03
15	1.24302-02	8.46880-03
16	2.60380-02	5.50022-02
17	2.37305-02	3.24354-02
18	3.74662-03	1.05785-02
19	2.56418-02	9.72362-02
20	6.44472-02	1.46769-01
21	8.84954-02	2.15670-01
22	9.13765-02	1.50179-01
23	1.16335-02	1.92973-02
24	1.10777-01	1.20983-01
25	5.40049-02	5.72919-02
26	5.68196-03	5.99914-03
27	9.26377-02	2.39968-02
28	1.16267-01	1.43980-02
29	7.38166-02	0.0
30	2.32454-02	0.0
31	2.02810-02	0.0
32	1.90145-03	0.0
33	0.0	0.0
34	0.0	0.0
35	0.0	0.0
36	0.0	0.0
37	0.0	0.0
Total	1.00000	1.00000

^aFrom reference 24*Read 1.88714-02 as 1.88714×10^{-2}

IV. Atmospheric Diffusion Theory

This section contains a development of the atmospheric diffusion theory used in this research. There are two features of the theory which are unique and deserve special mention. First, the 1962 U.S. Standard Atmosphere (Ref. 1) was incorporated directly into the diffusion equation. Secondly, a nonorthogonal coordinate system, which expands exponentially with altitude, was developed and used. As will be shown below, this coordinate system is essential to the numerical solution of the diffusion or transport equation in variable density air.

Two additional features, which were included to minimize the inherent limitations of diffusion theory, are also worthy of mention. First, although the group-to-group scatter was assumed to be isotropic as required by diffusion theory, the in-group scatter was treated as anisotropic (limited to linear angular variations) by applying a transport correction to the diffusion coefficient. Secondly, diffusion theory restricts the angular dependence of the fluence to linear variation with the cosine of the angle, θ_0 , which is defined by arc cosine $(\hat{r} \cdot \hat{v})$, where \hat{r} is the unit position vector and \hat{v} is the unit particle velocity vector (Ref. 25:234). Since the uncollided particles (direct fluence) emanating from an isotropic point source are all directed radially outward, their angular variation must be represented by a dirac delta function in $\cos \theta_0$ which, of course, is poorly treated by the diffusion theory assumption of linearity with $\cos \theta_0$. This limitation was circumvented by using an analytical first collided source. With this source, diffusion theory is

applied only to particles which have scattered at least one time, and the direct or uncollided portion of the fluence is computed analytically.

The Multigroup Diffusion Equation

The multigroup diffusion equation in general coordinates, x_1, x_2, x_3 , can be written as

$$\begin{aligned} \nabla \cdot \left(D^g(x_1, x_2, x_3) \nabla F^g(x_1, x_2, x_3) \right) - \Sigma_R^g(x_1, x_2, x_3) F^g(x_1, x_2, x_3) \\ = -S^g(x_1, x_2, x_3) \\ - \sum_{g'=1}^{g-1} \Sigma_S^{g' \rightarrow g}(x_1, x_2, x_3) F^{g'}(x_1, x_2, x_3) \end{aligned} \quad (4.1)$$

where

g = the energy group number which varies from 1 for the highest energy to G for the lowest energy

D^g = the group g diffusion coefficient in units of cm

F^g = the angle integrated group g scalar fluence in units of particles/cm²

Σ_R^g = the macroscopic removal cross section for group g in units of cm⁻¹

$\Sigma_R^g = \Sigma_T^g - \Sigma_S^{g \rightarrow g}$

Σ_T^g = the macroscopic total interaction cross section for group g in units of cm⁻¹

$\Sigma_S^{g' \rightarrow g}$ = the macroscopic cross section for scatter from group g' to group g in units of cm⁻¹

S^g = the source of particles for group g in units of particles/
cm³

It should be noted that the assumption of no up-scatter in energy has been made in writing equation (4.1).

A Nonorthogonal Coordinate System

McLaren (Ref. 26) was the first to recognize that a nonorthogonal coordinate system was essential to the solution of the diffusion or transport equation in variable density air. This requirement arises from the exponential-like density variation of the U.S. Standard Atmosphere (Figure 1). Since the density decreases exponentially with altitude, the particle mean free paths* increase exponentially with altitude. As shown below, this phenomenon imposes a unique problem on the numerical solution of equation (4.1).

Consider Figure 3a which shows a generalized set of mesh lines in a right circular cylindrical coordinate system which might be used in the numerical solution of equation (4.1) in 2-D variable density air. The vertical mesh spacing is set at some arbitrary fraction of a mean free path (e.g., three lines per mean free path) and increases with altitude, because the mean free path increases with altitude. Although the horizontal meshing is shown to be constant in Figure 3a, classical finite differencing methods do permit the radial mesh to vary in the radial

*The mean free path can be conveniently expressed in altitude independent mass units by multiplying the mean free path at altitude z by the density at altitude z . As shown earlier in Table II, the DLC-31 neutron groups have mean free paths which vary from 2 to 20 g/cm² while a 1-50 g/cm² variation exists for the gamma groups.

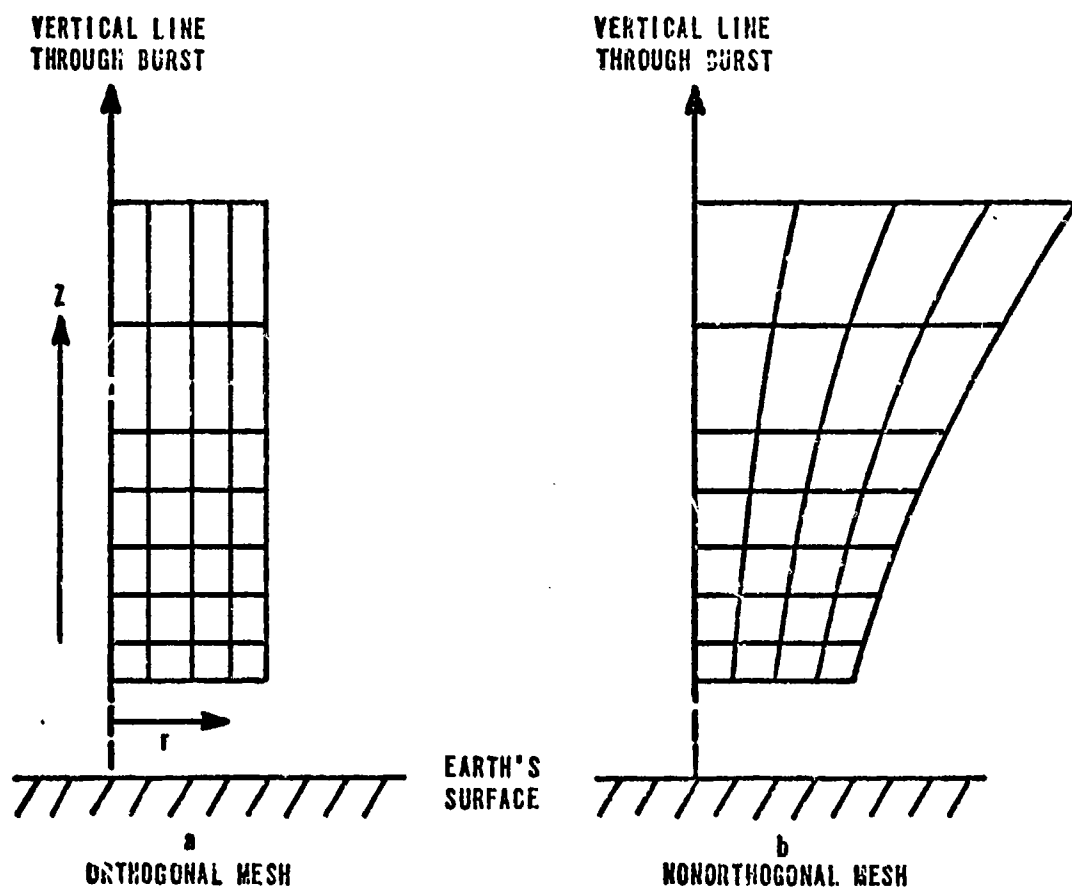


Figure 3. Orthogonal and Nonorthogonal Meshing in the Atmosphere

direction. However, variation of the radial mesh with altitude, which is clearly required if a constant mean free path separation between mesh points is to be maintained, is not permitted. In practice, the radial mesh spacing would be fixed by the bottom row where the air is most dense. This would result in a radial mesh which would become finer in a mean free path sense with increasing altitude. This continuously decreasing mesh (in mean free paths) introduces numerical instabilities into the solution.

This problem can be overcome by using a mesh which expands with altitude as shown in Figure 3b. The penalty of this approach is non-orthogonal coordinates. (Note that the mesh lines in Figure 3b no longer intersect at right angles.) With such a coordinate system, it is possible to maintain a constant mean free path radial mesh spacing by simply allowing the coordinate system to expand at a rate which approximates the exponential-like density variation of the U.S. Standard Atmosphere. Figure 4, which shows the coaltitude range to 100 g/cm^2 as a function of altitude in the U.S. Standard Atmosphere, indicates the rate of expansion required.

Finally, it is important to note that an additional advantage is realized by the introduction of the nonorthogonal coordinates. Specifically, solutions can be obtained over a much larger area without increasing the number of mesh points. This is significant because this increase in solution domain does not require any additional computer memory or computation time.

The coordinate system developed for this study is similar to the one proposed by McLaren. It is shown in Figure 5 and defined by the following transformation equations:

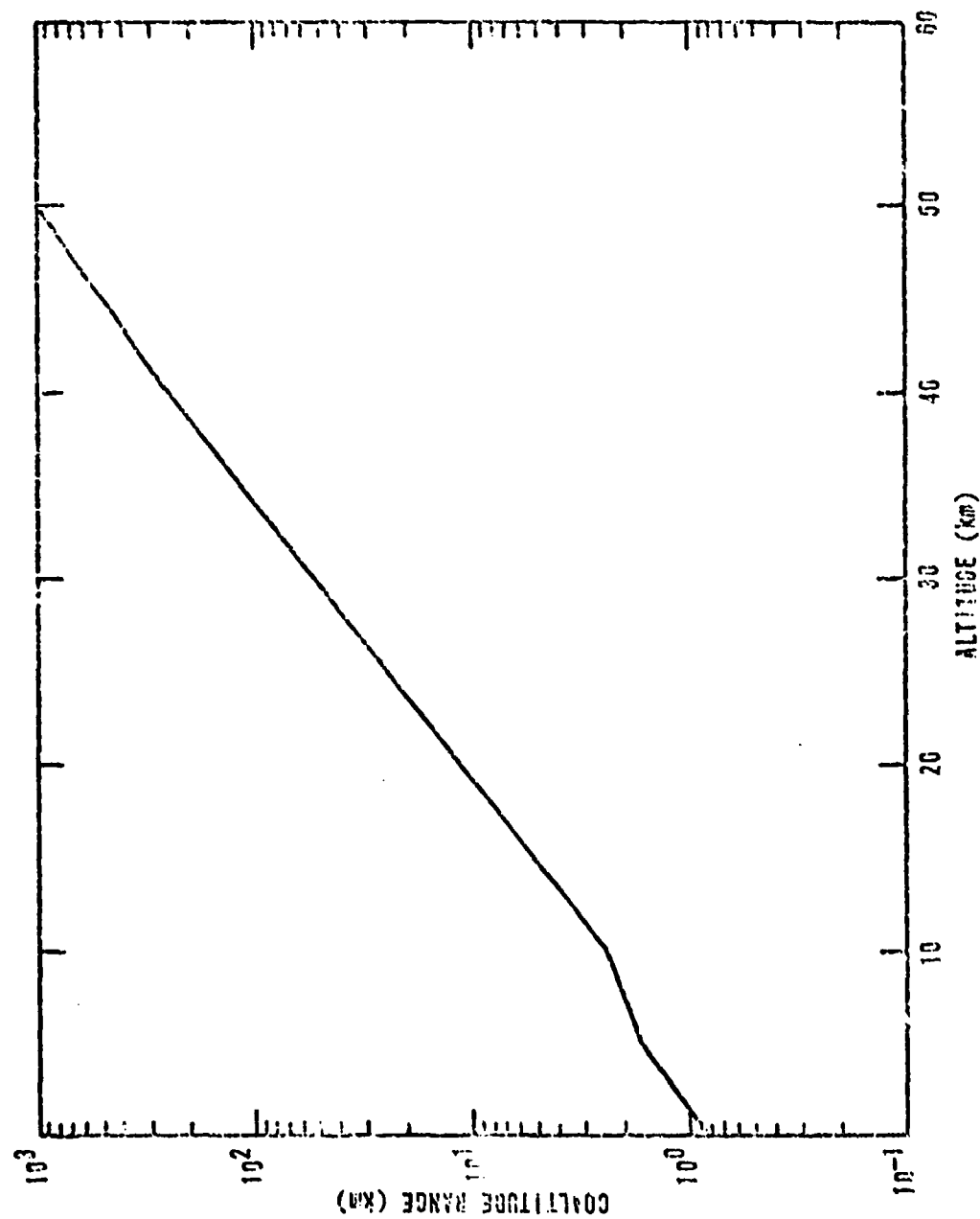
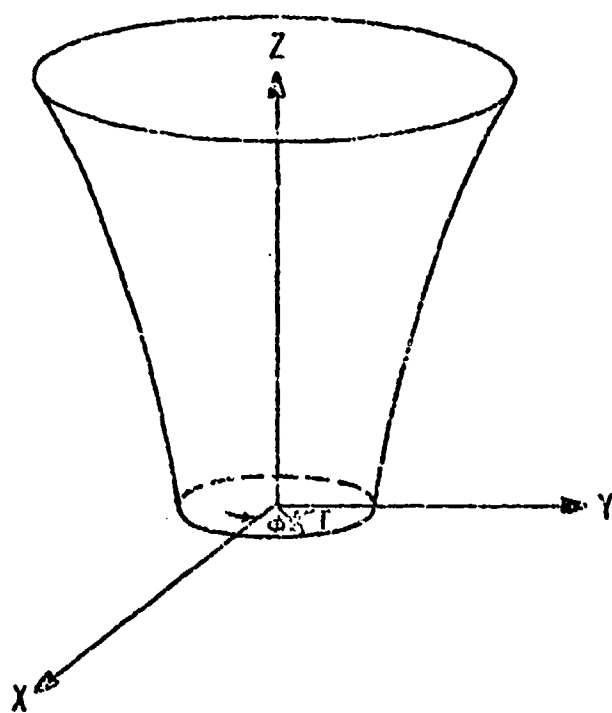


Figure 4. Coaltitude Range in the U.S. Standard Atmosphere to 100 g/cm^2 Versus Altitude



$$x = re^{Z/H} \cos \phi$$

$$y = re^{Z/H} \sin \phi$$

$$z = z$$

Figure 5. The Expanding Nonorthogonal Coordinate System

$$x_1 = r \quad (4.2)$$

$$x_2 = \phi \quad (4.3)$$

$$x_3 = z \quad (4.4)$$

and

$$x = r e^{z/H} \cos \phi \quad (4.5)$$

$$y = r e^{z/H} \sin \phi \quad (4.6)$$

$$z = z \quad (4.7)$$

where x, y, z are standard rectangular coordinates and H is the mesh expansion parameter.

The Diffusion Equation in the U.S. Standard Atmosphere

A simple and direct approach for incorporating the U.S. Standard Atmosphere into the diffusion equation is to express all cross sections, which are functions of altitude only in this medium, in terms of sea level values. If $f(z)$ is the ratio of the density at altitude z to the density at sea level (i.e., $f(z) = \rho(z)/\rho_0$), then

$$\Sigma_R^g(z) = \Sigma_R^g f(z) \quad (4.8)$$

$$\Sigma_S^{g' \rightarrow g}(z) = \Sigma_S^{g' \rightarrow g} f(z) \quad (4.9)$$

$$D^g(z) = D^g/f(z) \quad (4.10)$$

where Σ_R^g , $\Sigma_S^{g' \rightarrow g}$, and D^g are all defined at sea level ($\rho_0 = 1.225 \times 10^{-3}$ g/cm³). As pointed out at the beginning of this section, the 1962 U.S. Standard Atmosphere (Ref. 1) was adopted as the atmospheric model in this study. An algorithm, which uses reference 1's equations (ideal gas

law and hydrostatic equation) and defining atmospheric parameter base values, was incorporated into the AIRDIF code to generate the density ratio, $f(z)$, at any altitude z .

An examination of equation (4.10) and the spatial leakage term in equation (4.1) shows that an additional parameter is required in defining the atmosphere. Specifically, the gradient of $\rho_0/\rho(z)$ ($g(z) = \frac{d}{dz}(1/f(z))$) as a function of altitude is also required. In this study, a model based on the assumption of local exponential density variation in some small altitude increment Δz about z was developed to generate the value of $g(z)$ at any altitude z . Under this assumption, it can be easily shown that

$$g(z) = \frac{d}{dz} (\rho_0/\rho(z)) = \frac{-\ln(f(z_1)/f(z_2))}{2\Delta z f(z)} \quad (4.11)$$

where

$$z_1 = z + \Delta z \quad (4.12)$$

$$z_2 = z - \Delta z \quad (4.13)$$

Figure 6 shows how $g(z)$ varies with altitude.

Since the density and hence all cross sections are functions of altitude only, symmetry with respect to the angle, ϕ , exists and the multi-group diffusion equation given in equation (4.1) can be written in the U.S. Standard Atmosphere and in the nonorthogonal coordinate system as

$$\begin{aligned} \nabla \cdot \left(\frac{D^g}{f(z)} \nabla F^g(r, z) \right) - \Sigma_R^g f(z) F^g(r, z) \\ = -S^g(r, z) - \sum_{g'=1}^{g-1} \Sigma^{g' \rightarrow g} f(z) F^{g'}(r, z) \end{aligned} \quad (4.14)$$

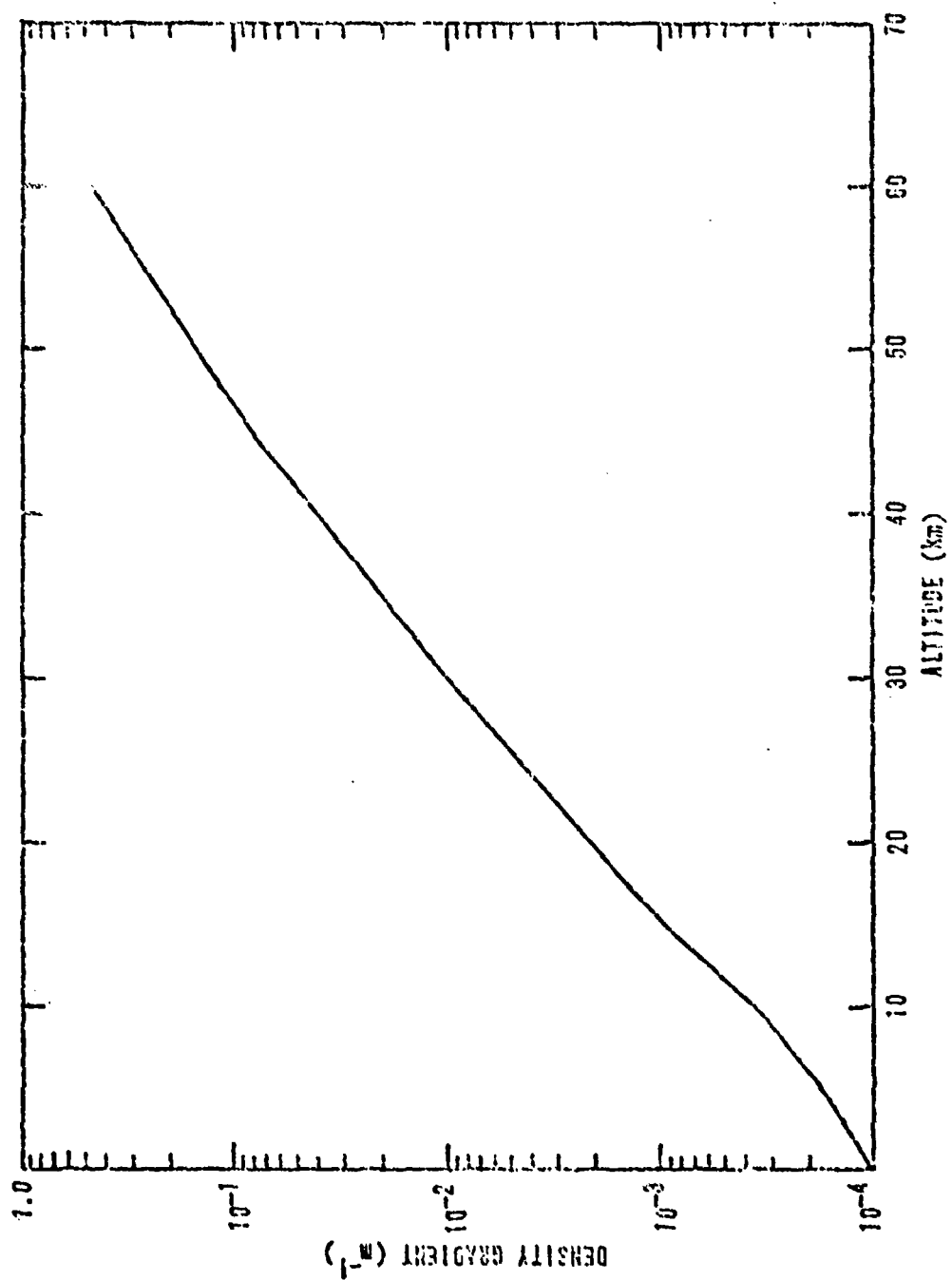


Figure 6. The Density Gradient Versus Altitude

The generalized form of the spatial leakage term, $\nabla \cdot (D(z) \nabla F(r,z))$, is given by

$$\nabla \cdot (D(z) \nabla F(r,z)) = \frac{1}{\sqrt{g}} \frac{\partial}{\partial x^K} \left(D(x_3) \sqrt{g} g^{KP} \frac{\partial F}{\partial x^P} \right) \quad (4.15)$$

where g^{KP} are the elements of the contravariant metric tensor associated with the coordinate transformation defined by equations (4.2) through (4.7), and g is the determinant of the metric tensor, g_{KP} , associated with that transformation.

Under the coordinate transformation defined by equations (4.2) through (4.7), the elements of the metric tensor are

$$g_{11} = e^{2z/H} \quad (4.16)$$

$$g_{12} = g_{21} = 0 \quad (4.17)$$

$$g_{13} = g_{31} = \frac{r}{H} e^{2z/H} \quad (4.18)$$

$$g_{22} = r^2 e^{2z/H} \quad (4.19)$$

$$g_{23} = g_{32} = 0 \quad (4.20)$$

$$g_{33} = \frac{r^2 e^{2z/H}}{H^2} + 1 \quad (4.21)$$

and

$$g = r^2 e^{4z/H} \quad (4.22)$$

The elements of the contravariant metric tensor, g^{KP} , are

$$g^{11} = \left(\frac{r^2}{H^2} + e^{-2z/H} \right) \quad (4.23)$$

$$g^{12} = g^{21} = 0 \quad (4.24)$$

$$g^{13} = g^{31} = -r/H \quad (4.25)$$

$$g^{22} = \frac{e^{-2z/H}}{r^2} \quad (4.26)$$

$$g^{23} = g^{32} = 0 \quad (4.27)$$

$$g^{33} = 1 \quad (4.28)$$

When equation (4.15) is expanded using the expressions just given, it can be shown that the multigroup spatial leakage term, $\nabla \cdot (D^g(z) \nabla F^g)$, can be reduced to

$$\begin{aligned} \frac{D^g}{f(z)} & \left(\left(\frac{r^2}{H^2} + e^{-2z/H} \right) \frac{\partial^2 F^g}{\partial r^2} + \left(\frac{3r}{H^2} + \frac{e^{-2z/H}}{r} - \frac{r}{H} f(z)g(z) \right) \frac{\partial F^g}{\partial r} \right. \\ & \left. - \frac{2r}{H} \frac{\partial^2 F^g}{\partial r \partial z} + \left(-\frac{1}{H} + f(z)g(z) \right) \frac{\partial F^g}{\partial z} + \frac{\partial^2 F^g}{\partial z^2} \right) \end{aligned} \quad (4.29)$$

where superscript g now again is the energy group designation and $g(z)$ is the gradient defined by equation (4.11).

To permit linear isotropy in the i -group scatter, a transport correction was used in defining the diffusion coefficient. Specifically,

$$D^g = 1/3 \Sigma_{TR}^g \quad (4.30)$$

where

Σ_{TR}^g = the transport cross section at sea level for group g in units of cm^{-1}

$$\Sigma_{TR}^g = \Sigma_T^g - \Sigma_{S1}^{g-g}$$

$\Sigma_{s_1}^{g-g} = P_1$ coefficient in the Legendre expansion of the angular dependence of the scattering cross section for group g in-group scatter

For the reasons given at the beginning of this section and also to avoid the numerical problems associated with using a point source, an analytical first collided source was used for $S^g(r, z)$ in equation (4.14). Specifically,

$$S^g(r, z) = \sum_{g'=1}^g \Sigma_s^{g'+g} f(z) F_V^{g'}(r, z) \quad (4.31)$$

where

$F_V^{g'}(r, z)$ = the uncollided fluence in group g'

$$F_V^{g'}(r, z) = \frac{S_0^{g'}}{4\pi R^2} \exp \left(- \frac{\Sigma_T^{g'}}{\rho_0} \langle \rho R \rangle \right) \quad (4.32)$$

and where

$S_0^{g'}$ = the number of group g' particles emanating from an isotropic point source at $r = 0$ and $z = z_s$

R = the slant range between the source at altitude z_s and receiver at altitude z in units of cm = $\left((z_s - z)^2 + r^2 e^{2z/H} \right)^{1/2}$

$\Sigma_T^{g'}$ = the total macroscopic cross section at sea level ($z = 0$)

$\langle \rho R \rangle$ = mass range or areal density defined by equation (2.3)

It is important to note that the use of the first collided source in equation (4.14) means that only the collided fluence is actually found by diffusion theory. The total fluence is computed by simply

adding the uncollided and collided fluences, i.e.,

$$F_T^g(r,z) = F^g(r,z) + F_V^g(r,z) \quad (4.33)$$

where

$F_T^g(r,z)$ = total group g scalar fluence

$F^g(r,z)$ = collided fluence found by numerically solving equation
(4.14)

$F_V^g(r,z)$ = uncollided fluence found by analytically evaluating
equation (4.32)

The specification of boundary conditions completes the definition of atmospheric diffusion theory. On the sides of the expanding cylinder ($r = r_{max}$) zero fluence boundary conditions were applied. This condition, of course, is artificial but does not introduce significant error as long as the boundary is placed several mean free paths (20-30 g/cm²) from the domain of interest. At the top and bottom of the expanding cylinder, zero return (partial) current conditions were applied; for example, at $z = z_{max}$, the condition

$$J_{-z}^g(r,z) \Big|_{z=z_{max}} = 0 \quad (4.34)$$

was applied. In the expanding coordinate system and U.S. Standard Atmosphere, this condition becomes

$$\frac{F^g(r,z)}{4} + \frac{D^g}{2f(z)} \left(\frac{r^2}{H^2} e^{2z/H} + 1 \right)^{1/2} \left(-\frac{r}{H} \frac{\partial F^g}{\partial r} + \frac{\partial F^g}{\partial z} \right) \Big|_{z=z_{max}} = 0 \quad (4.35)$$

The bottom condition is again artificial and is equivalent to assuming that the air below z_{\min} acts as a perfect absorber. The top condition, however, is a good approximation of the true vacuum condition (which can't be applied in diffusion theory) as long as z_{\max} is set at an altitude where there is not much air above (30 km in this study).

An important characteristic of the equations just derived should be mentioned. Under the conditions,

$$H \rightarrow \infty \quad (4.36)$$

$$g(z) = 0 \quad (4.37)$$

$$f(z) = \rho(zs)/\rho_0 \quad (4.38)$$

all of the equations developed here reduce directly to a description of the diffusion equation in normal cylindrical coordinates and homogeneous, constant density air. It is this property that enables the AIRDIF code described in Appendix B to compute diffusion environments in both variable density and homogeneous air.

Numerical Solution of the Diffusion Equation

Standard operator differencing techniques (Ref. 27:184) were used to derive the multigroup finite differenced form of equation (4.14). The resulting nine point (five point in homogeneous air) difference equation for interior points is

$$\begin{aligned} & b_{i-1,j-1} F_{i-1,j-1}^g + b_{i,j-1} F_{i,j-1}^g + b_{i+1,j-1} F_{i+1,j-1}^g \\ & + b_{i-1,j} F_{i-1,j}^g + b_{i,j} F_{i,j}^g + b_{i+1,j} F_{i+1,j}^g \\ & + b_{i-1,j+1} F_{i-1,j+1}^g + b_{i,j+1} F_{i,j+1}^g + b_{i+1,j+1} F_{i+1,j+1}^g \end{aligned}$$

$$\begin{aligned}
&= \frac{-S_{i,j} f_j}{D^g} \\
&\quad - \frac{f_j}{D^g} \sum_{g=1}^{g-1} \Sigma_s^{g' \rightarrow g} f_j f_{i,j}^{g'}
\end{aligned} \tag{4.39}$$

where

$$b_{i-1,j-1} = - \frac{r_i \Delta z_j}{H \Delta r \Delta z_{j-1} (\Delta z_j + \Delta z_{j-1})} \tag{4.40}$$

$$b_{i,j-1} = \frac{1}{\Delta z_{j-1} (\Delta z_j + \Delta z_{j-1})} \left(2 - f_j g_j \Delta z_j + \frac{\Delta z_j}{H} \right) \tag{4.41}$$

$$b_{i+1,j-1} = -b_{i-1,j-1} \tag{4.42}$$

$$\begin{aligned}
b_{i-1,j} &= \frac{1}{\Delta r^2} \left(\frac{r_i^2}{H^2} + e^{-2z_j/H} \right) - \frac{1}{2\Delta r} \left(\frac{r_i}{H^2} + \frac{e^{-2z_j/H}}{r_i} - \frac{r_i f_j g_j}{H} \right) \\
&\quad + \frac{r_i}{H \Delta r \Delta z_j \Delta z_{j-1}} (\Delta z_j - \Delta z_{j-1}) - \frac{r_i}{\Delta r H^2}
\end{aligned} \tag{4.43}$$

$$\begin{aligned}
b_{i,j} &= - \frac{2}{\Delta r^2} \left(\frac{r_i^2}{H^2} + e^{-2z_j/H} \right) + \frac{f_j g_j}{\Delta z_j \Delta z_{j-1}} (\Delta z_j - \Delta z_{j-1}) \\
&\quad - \frac{2}{\Delta z_j \Delta z_{j-1}} - \frac{\Sigma_R^g}{D^g} f_j^2 - \frac{(\Delta z_j - \Delta z_{j-1})}{H \Delta z_j \Delta z_{j-1}}
\end{aligned} \tag{4.44}$$

$$\begin{aligned}
b_{i+1,j} &= \frac{1}{\Delta r^2} \left(\frac{r_i^2}{H^2} + e^{-2z_j/H} \right) + \frac{1}{2\Delta r} \left(\frac{e^{-2z_j/H}}{r_i} + \frac{r_i}{H^2} - \frac{f_j g_j r_i}{H} \right) \\
&\quad - \frac{r_i (\Delta z_j - \Delta z_{j-1})}{H \Delta r \Delta z_j \Delta z_{j-1}} + \frac{r_i}{\Delta r H^2}
\end{aligned} \tag{4.45}$$

$$b_{i-1,j+1} = \frac{r_i \Delta z_{j-1}}{H \Delta r \Delta z_j (\Delta z_j + \Delta z_{j-1})} \quad (4.46)$$

$$b_{i,j+1} = \frac{1}{\Delta z_j (\Delta z_j + \Delta z_{j-1})} (2 + f_j g_j \Delta z_{j-1}) - \frac{\Delta z_{j-1}}{H \Delta z_j (\Delta z_j + \Delta z_{j-1})} \quad (4.47)$$

$$b_{i+1,j+1} = -b_{i-1,j+1} \quad (4.48)$$

and where

$$S_{i,j} = \sum_{g=1}^g f_j \frac{\Sigma_s^{g'} - g S_0^{g'}}{4\pi R_{i,j}^2} \exp\left(-\frac{\Sigma_T^{g'}}{\rho_0} \langle \rho R \rangle_{i,j}\right) \quad (4.49)$$

and $S_0^{g'}$ = the number of particles in energy group g' emanating from the point source

The difference equations for boundary points can be written in a similar fashion.

The difference equations were written into the matrix form

$$A \vec{\Phi}^g = \vec{\Sigma}^g \quad (4.50)$$

where

A is a block, tridiagonal matrix and a function of the mesh, atmospheric model, and energy group

$\vec{\Sigma}^g$ is the source vector for group g and is composed of the scatter of both the collided and uncollided particles into g from energy groups above g

Φ_g is the unknown scalar fluence for group g

The matrix equations were incorporated into the AIRDIF code and solved group-by-group via a block-iterative method known as successive line overrelaxation (SLOR) (Ref. 28:199). As pointed out earlier, only the collided fluence was found by numerically solving equation (4.50). The total fluence in each group was found by adding the uncollided fluence (equation (4.32)) and the numerically determined collided fluence.

The AIRDIF Code

The AIRDIF code is based on the atmospheric diffusion theory just presented. It is capable of computing the radiation dose environments in both homogeneous air and in the U.S. Standard Atmosphere from atmospheric nuclear detonations. In addition to environment definition, it is also capable of directly computing the MIS K factors. Appendix B contains a summary of the detailed description of the AIRDIF code presented in reference 29.

To compute K factors, an AIRDIF homogeneous air run for the source and dose response of interest is made first. The homogeneous air doses are then least squares fit to a radiation transmission equation developed by Murphy (Ref. 16:36),

$$T(x) = \exp(A + Bx + Cx^2 + Dx^{3/2} + Ex^{1/2} + Fx^{1/3} + G\ln(x)) \quad (4.51)$$

where $T(x) = 4\pi R^2$ 1-D MIS dose at a mass range of x g/cm².

Figures 7 and 8 show the fit and actual AIRDIF data for neutron and secondary gamma silicon doses from a fission source in homogeneous air.

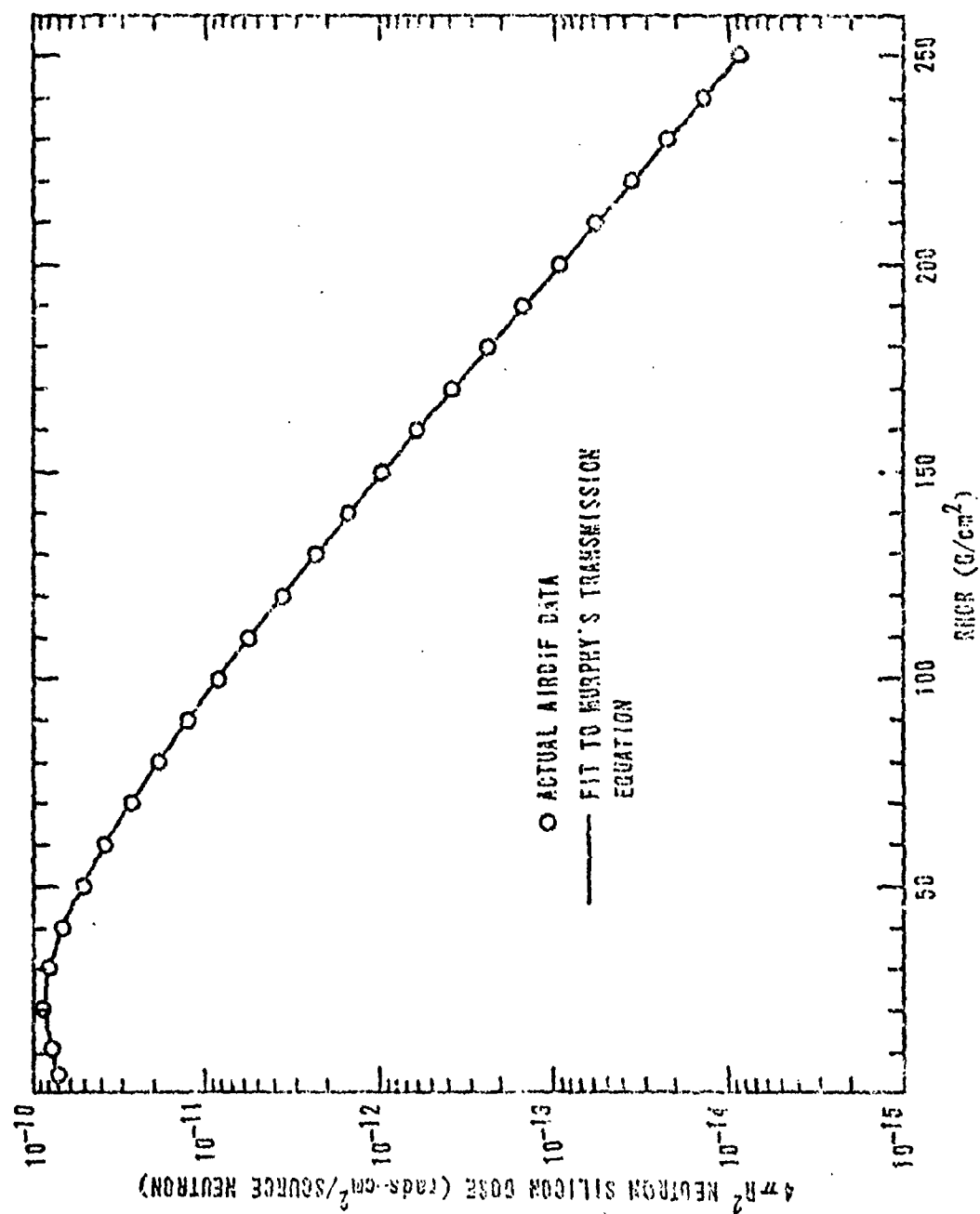


Figure 7. Least-Squares Fit of AIRDIF Neutron Silicon Doses from a Fission Source in Homogeneous Air

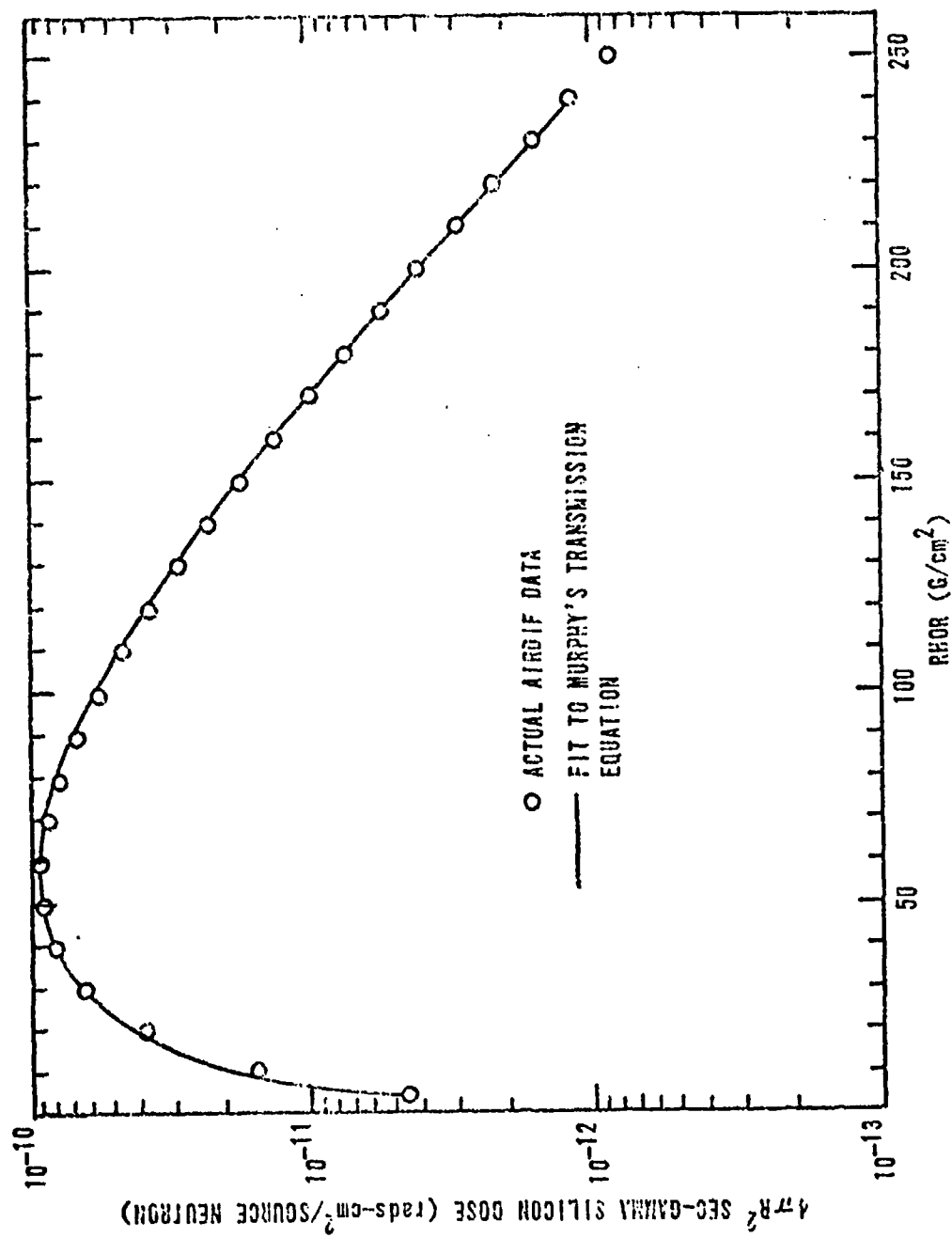


Figure 8. Least-Squares Fit of AIRDIF Secondary Gamma Silicon Doses from a Fission Source in Homogeneous Air

These results are typical and demonstrate that good fits to equation (4.51) can be obtained. Note that in these and all other figures to follow, the symbol used for mass range (equation (2.3)) is "RHOR."

The fit coefficients for both neutrons and gammas are included as part of the input for the 2-D variable density air run. Using these coefficients and equation (4.51), AIRDIF computes the $4\pi R^2$ 1-D MIS doses which are required in computing the K factors.

It should be emphasized that this parameterization of the homogeneous data is essential to the direct computation of K factors within AIRDIF. It should also be noted that scaling codes like SMAUG have small central memory requirements because they also utilize these kinds of fits to store their data bases.

V. Validity of Diffusion Calculations

The validity of the AIRDIF diffusion calculations was first tested by comparing the diffusion environments to discrete ordinates transport results in homogeneous air and to Monte Carlo results in variable density air. Comparisons were made for neutron and secondary gamma environments, for silicon and tissue dose response, for a fission and thermonuclear source, and out to mass ranges of 200 g/cm². Next, to test the adequacy of the diffusion model for predicting the MIS evaluation ratios, comparisons of K factors derived from diffusion theory and Monte Carlo techniques were made. Typical results of these comparisons are presented and discussed in this section.

Comparisons of Radiation Doses in Homogeneous Air

In homogeneous air, the AIRDIF neutron and secondary gamma doses were compared to Burgio's (Ref. 16) discrete ordinates results which were produced with the ANISN code (Ref. 30). Results were compared for the fission and thermonuclear source shown in Table V and using the silicon and tissue response functions presented in Tables III and IV. It is worth mentioning that the ANISN data are actually Murphy's (Ref. 16:36) fits of Burgio's data to equation (4.51). These fits are in good agreement with the ANISN calculations with maximum differences of about 5%. The AIRDIF results were compared to the ANISN fits rather than the actual data because, in the future, these fits will become the new data base for SMAUG. This approach is consistent with the real objective of

this research, i.e., evaluate the results from mass scaling codes.

Figures C-1 and C-2 in Appendix C are typical of the results achieved. For both sources and response functions, the AIRDIF diffusion results for neutrons are approximately 10-20% low for mass ranges less than 20 g/cm². Over the mass range of 20 to about 140 g/cm², the AIRDIF results are 1-15% higher. For ranges between 140 and 200 g/cm², the AIRDIF results become increasingly lower than ANISN with maximum differences of about 30% occurring at 200 g/cm². The agreement in secondary gamma doses was similar. However, the differences were somewhat larger with maximum errors of about 40% occurring at 200 g/cm². In general, the agreement was better for tissue response which emphasizes the low energy particle contribution (where the scatter is more isotropic) more than the silicon response. Also, the agreement was a little better, as one would expect, for the fission source than for the thermonuclear source.

Comparisons of Radiation Doses in the U.S. Standard Atmosphere

Similar comparisons were made in the U.S. Standard Atmosphere. In this medium, the comparisons were made to Eamon's recent Monte Carlo calculations (Ref. 10) performed with the MORSAIR (Ref. 31) code. Table VI lists the comparisons which were made. Note that AIRDIF is about 30 times faster than MORSAIR while making determinations at 10 times the number of mesh or receiver points. This result was not unexpected and, in fact, was the primary reason why the diffusion approach was pursued. Representative samples of Table VI's comparisons are presented in Appendix C (Figures C-3 to C-14).

In general, the MORSAIR data considered in these comparisons had standard deviations less than 10% for ranges less than 100 g/cm², 10-20%

TABLE VI

Summary of U.S. Standard Atmosphere Comparisons:
AIRDIF versus MORSAIR

<u>No.</u>	<u>Source</u>	<u>Source Altitude</u>	<u>Run Time^a MORSAIR/AIRDIF</u>	<u>Receiver Altitude</u>	<u>Response</u>
1	Fission	5.0	35.	5.07	Silicon
2	Fission	10.0	30.	8.84	Silicon
3	Fission	10.0		10.00	Silicon
4	Fission	10.0		12.13	Silicon
5	Fission	15.0	32.	11.30	Silicon
6	Fission	15.0		15.29	Silicon
7	Fission	15.0		21.66	Silicon
8	Fission	20.0	37.	14.85	Silicon
9	Fission	20.0		14.85	Tissue
10	Fission	20.0		20.61	Silicon
11	Fission	20.0		20.61	Tissue
12	Fission	20.0		22.08	Silicon
13	Fission	20.0		22.08	Tissue
14	Thermonuclear	20.0	29.	14.85	Silicon
15	Thermonuclear	20.0		20.61	Silicon
16	Thermonuclear	20.0		22.08	Silicon

^aRatio of MORSAIR to AIRDIF 7600 execution times. MORSAIR times were for 50,000 histories and 150 receivers (30-40 min). AIRDIF times are for on the average around 1500 mesh points.

for ranges between 100 and 150 g/cm², and 20-30% for ranges from 150 to 200 g/cm². In many cases, the AIRDIF/MORSAIR differences were within the statistical scatter of the Monte Carlo data.

It is significant that the agreement between diffusion theory and transport theory (Monte Carlo in variable density air) is about the same in the U.S. Standard Atmosphere as it is in homogeneous air. This result supports the validity of the use of diffusion theory to compute K factors and is clearly shown in the K factor comparisons presented next.

K Factor Comparisons

Figures D-1 through D-32 in Appendix D present comparisons of the diffusion and transport (Monte Carlo) derived K factors for all of the determinations listed in Table VI. For reasons which are discussed below, the agreement is better in some cases than others. However, in all cases the K factor trends, which are indicative of the previously discussed leakage and mass distribution effects, are clearly the same.

The Monte Carlo data used in the comparisons were produced with the MORSAIR code by Eamon of Kaman Sciences Corporation under contract with the Air Force Weapons Laboratory (Ref. 10). In the odd-numbered figures, D-1 through D-20, the MORSAIR and AIRDIF neutron silicon K factors for a fission source at source altitudes of 5, 10, 15, and 20 km are compared. Comparisons of the secondary gamma silicon K factors are made in the even-numbered figures in this sequence. Comparisons are also made for tissue K factors for this source at 20 km in Figures D-21 through D-26. Finally, the silicon K factors for a thermonuclear

source at 20 km are compared in Figures D-27 through D-32. The sources and response functions listed in Tables III-V were used in these calculations.

The AIRDIF and MORSAIR neutron K factors are in excellent agreement with each other for almost all of the cases shown in Figures D-1 through D-32. In fact, most of the time the AIRDIF results are within the statistics of the MORSAIR data. It is important to remember that the AIRDIF results were produced at a fraction of the cost ($\sim 1/30$) required by the Monte Carlo calculations.

The agreement in the secondary gamma K factors is good but not quite as good as the agreement in neutron K factors. In general, the AIRDIF secondary gamma K factors are lower than the MORSAIR K factors for ranges less than 40 g/cm² (e.g., Figure D-12) and higher for ranges greater than 140 g/cm² (e.g., Figure D-18). These differences are due to a combination of the factors discussed below.

Discussion of K Factor Comparisons

Ideally, the K factor comparisons should indicate only whether

$$K \text{ factor})_{\text{AIRDIF}} \approx K \text{ factor})_{\text{MORSAIR}} \quad (5.1)$$

where

$$K \text{ factor})_{\text{AIRDIF}} = \frac{2-D)_{\text{AIRDIF}}}{1-D)_{\text{AIRDIF}}} \quad (5.2)$$

$$K \text{ factor})_{\text{MORSAIR}} = \frac{2-D)_{\text{MORSAIR}}}{1-D)_{\text{MORSAIR}}} \quad (5.3)$$

and where "2-D" and "1-D" are the $4\pi R^2$ 2-D variable density air and 1-D

MIS doses, respectively. Unfortunately, the automation of the K factor calculations in both the AIRDIF and MORSAIR codes introduced several additional factors which must be considered in analyzing the results of the comparisons. Specifically, the quantities that are actually compared in Figures D-1 through D-32 are

$$K \text{ factor})_{\text{AIRDIF}} = \frac{2-D)_{\text{AIRDIF}}}{1-D)_{\text{AIRDIF FIT}}} \quad (5.4)$$

and

$$K \text{ factor})_{\text{MORSAIR}} = \frac{2-D)_{\text{MORSAIR}}}{1-D)_{\text{ANISN FIT}}} \quad (5.5)$$

where the fits indicated are least squares fits of the AIRDIF and ANISN homogeneous air data to Murphy's radiation transmission equation (equation (4.51)).

Fits were used to represent the homogeneous air data for several reasons. First, these fits are essential to the direct computation of K factors within the AIRDIF and MORSAIR codes. Next, the fits of the 1-D ANISN data, as mentioned before, will form the new data base of the next version of the SMAUG code. The ATR code also uses these kinds of fits. Finally, because of the statistical nature of Monte Carlo data, some fit had to be used to represent the homogeneous air MORSAIR data. As will be shown below, the fits of the 1-D ANISN data are also a good representation of the homogeneous air MORSAIR data.

The following things must be considered in evaluating the comparison of results from equations (5.4) and (5.5):

1. How well do the fits of the 1-D AIRDIF and ANISN data represent the actual data?

2. What type of statistics are associated with the MORSAIR data?

3. How well does MORSAIR agree with ANISN in homogeneous air?

In general, the fits to Murphy's transmission equation are excellent representations of the actual homogeneous air transport results. The comparisons presented earlier in Figures 7 and 8 are typical of the accuracy achievable with these fits. Except in the steep build-up region ($0 \sim 40 \text{ g/cm}^2$) which characterizes the secondary gamma $4\pi R^2$ dose/range curves, the fit values are within 5% of the actual data. In the secondary gamma build-up region, the fit values are generally 10-15% higher than the actual data.

All of the 2-D MORSAIR data reflect statistical oscillations inherent in Monte Carlo results. For ranges less than 100 g/cm^2 , the standard deviations ran between 10 and 20% for ranges between 100 and 150 g/cm^2 and between 20 and 30% for ranges between 150 and 200 g/cm^2 . The scatter in the MORSAIR K factors is due mostly to these statistics. However, some of the oscillations clearly lie outside of these statistics. In particular, at mass ranges greater than about 140 g/cm^2 , the MORSAIR secondary gamma doses seemed to be biased low.

Figures 9-12 show that the ANISN fits and MORSAIR homogeneous air results are in good agreement. In fact, the primary reason the ANISN fits were used in defining the MORSAIR K factors is that these fits also appear to be good fits of the MORSAIR homogeneous air results. The biggest differences occur in the secondary gamma dose. In the build-up region, the 1-D MORSAIR results seemed to be about 10% higher than the 1-D ANISN fits. Also, as mentioned above, the MORSAIR secondary gamma results are somewhat lower (10-20%) at ranges greater than 140 g/cm^2 .

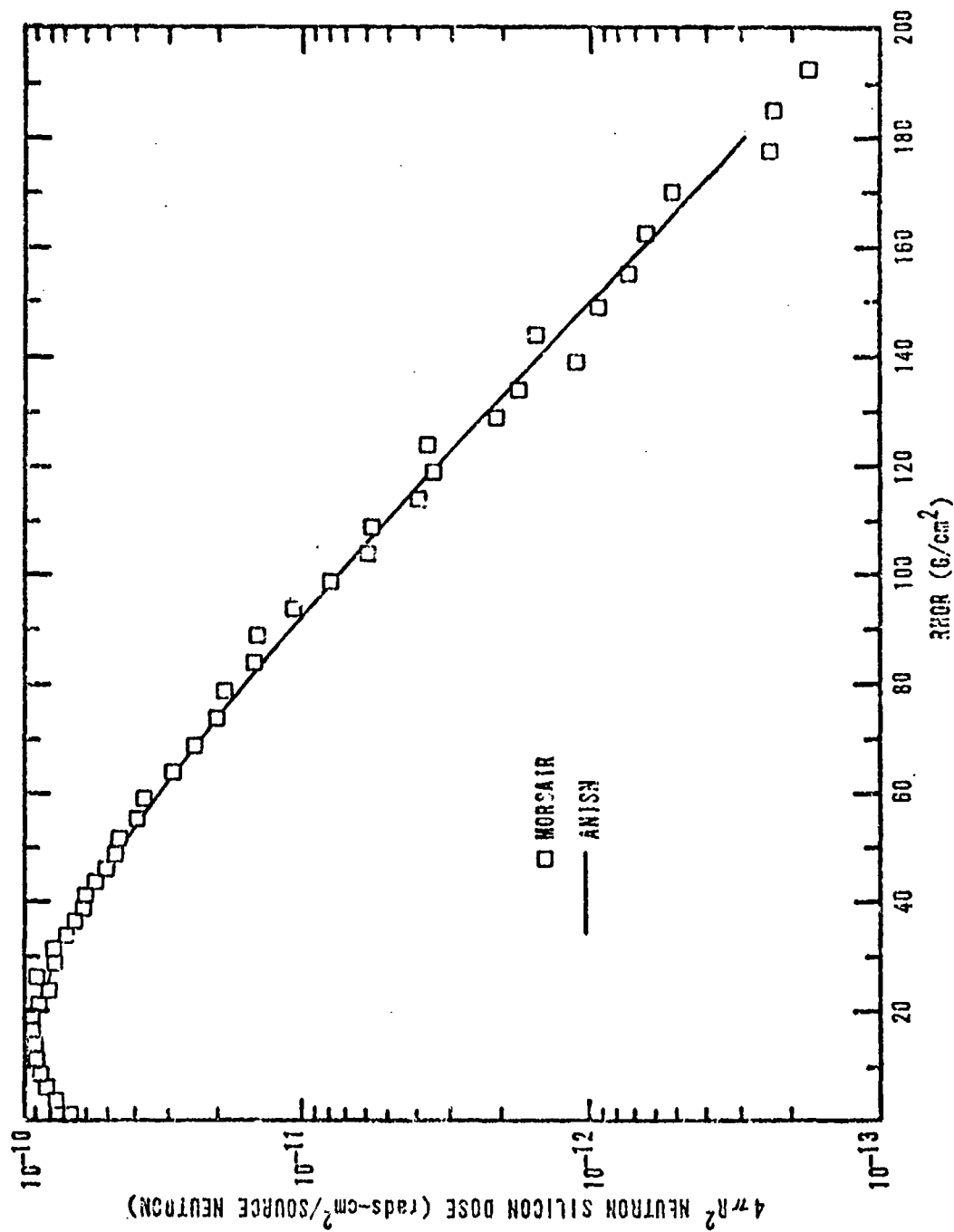


Figure 9. Neutron Silicon Doses from a Fission Source in Homogeneous Air

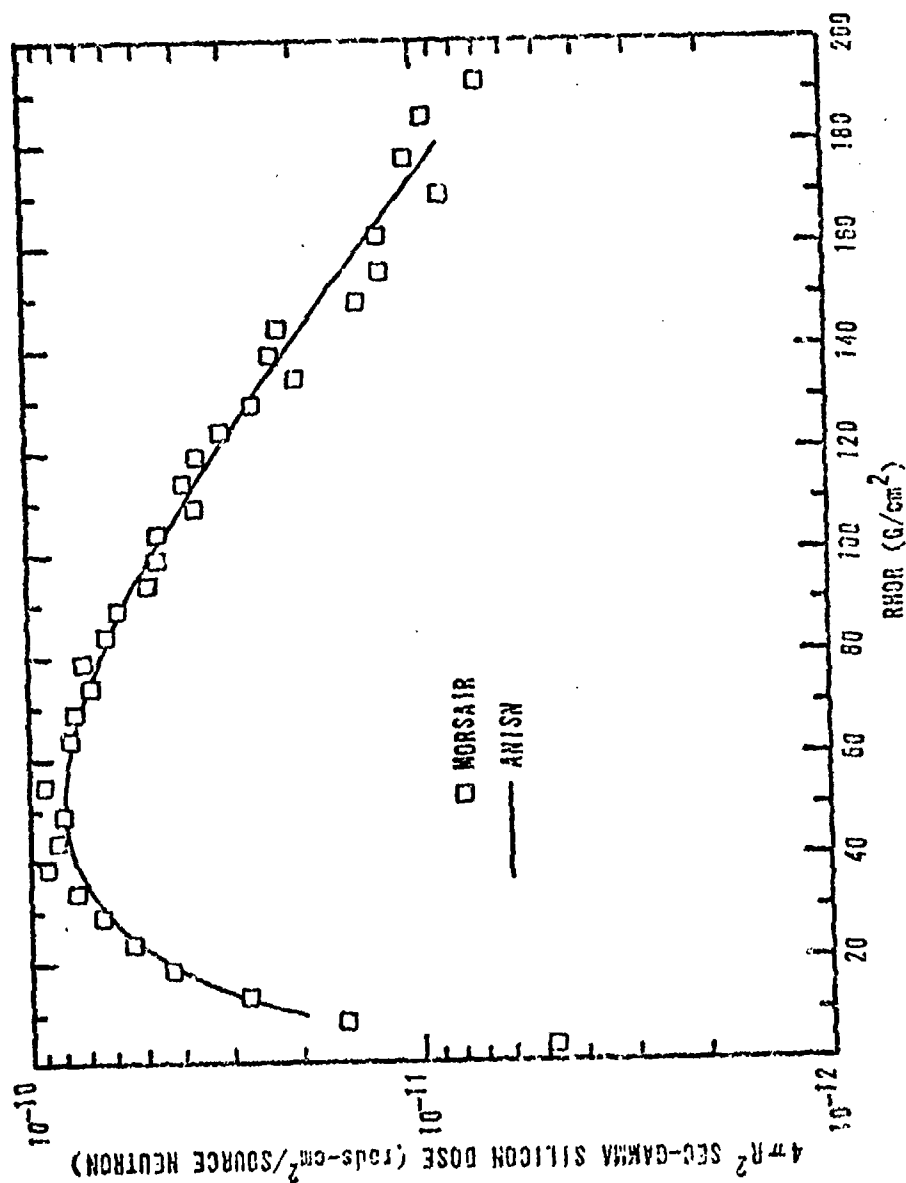


Figure 10. Secondary Gamma Silicon Doses from a Fission Source in Homogeneous Air

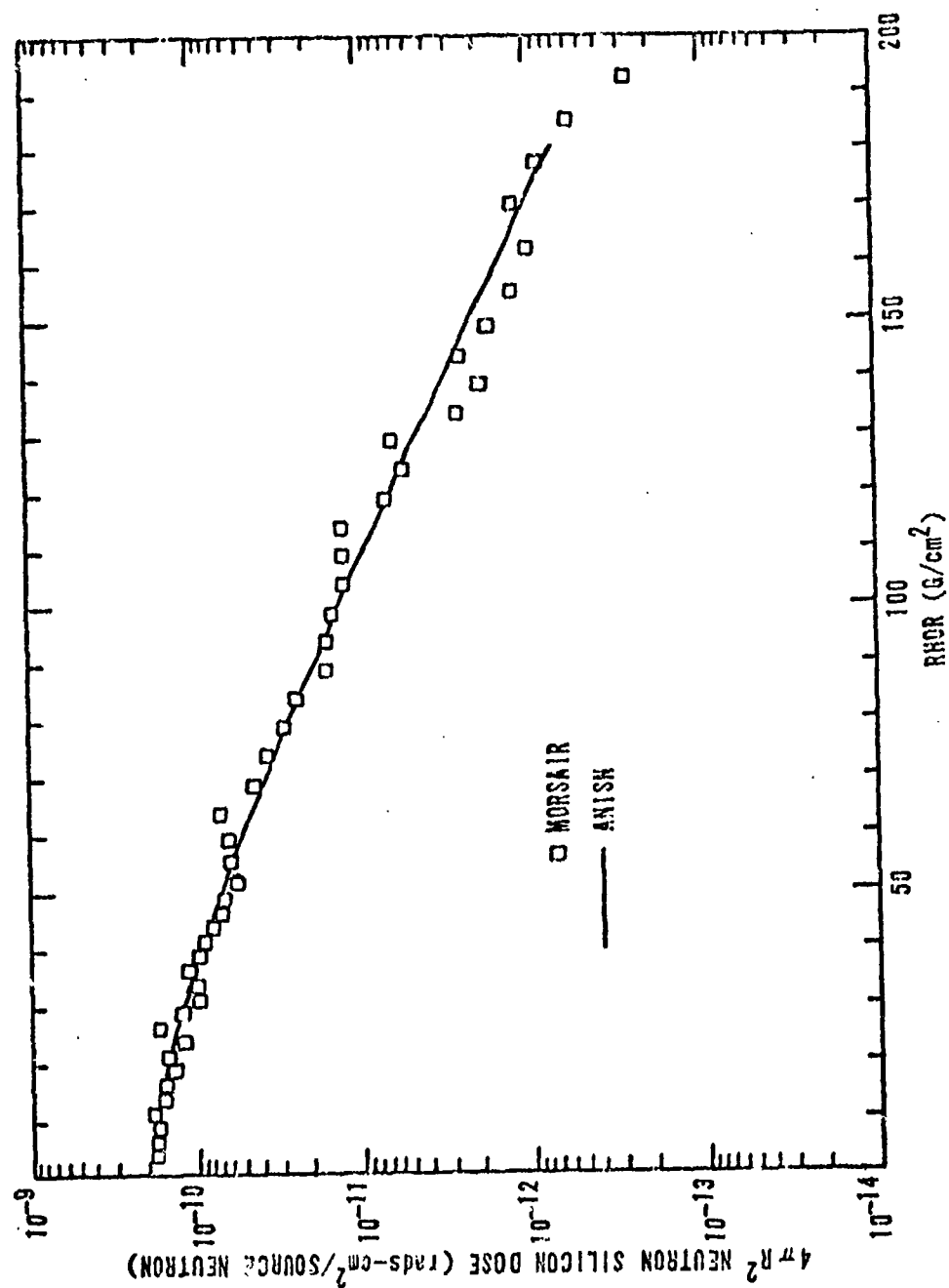


Figure 11. Neutron Silicon Doses from a Thermonuclear Source in Homogeneous Air

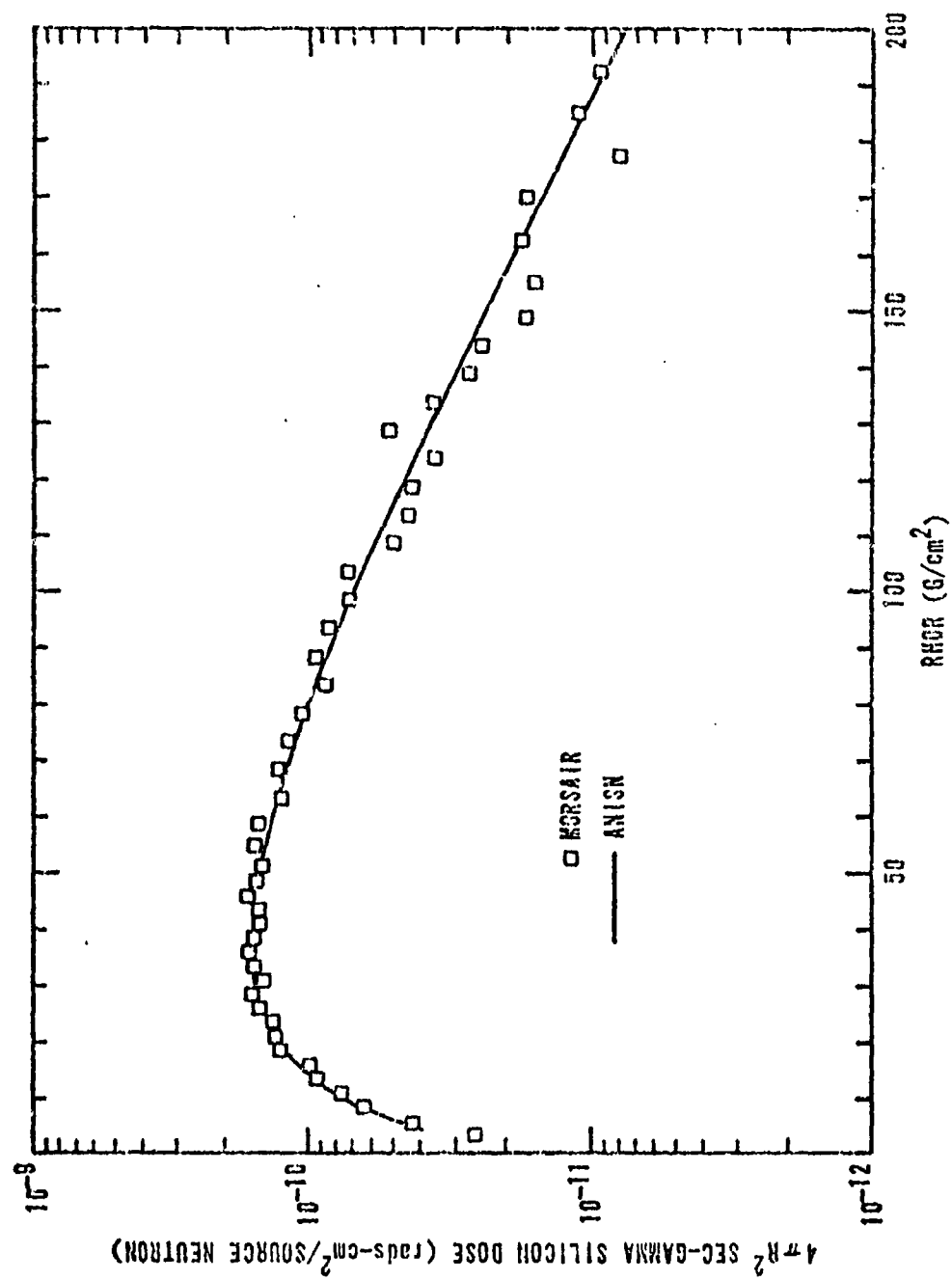


Figure 12. Secondary Gamma Silicon Doses from a
Thermonuclear Source in Homogeneous Air

In summary, all three of the factors just discussed have a bearing on the results of the K factor comparisons and must be considered in analyzing the results. Without exception, it can be shown that any significant differences that exist between the AIRDIF and MORSAIR K factors are due to these factors rather than differences in the way MIS perturbs the diffusion results and the Monte Carlo simulation of the transport doses. For example, earlier it was pointed out that for ranges less than 40 g/cm^2 , the AIRDIF secondary gamma K factors were lower ($\sim 20\%$) than the MORSAIR results. This difference is due to the fact that over this range the fit of the 1-D AIRDIF data is higher than the actual AIRDIF data, while the fit of the 1-D ANISN data is somewhat lower than the actual MORSAIR homogeneous air results over this same range. Also, recall that the AIRDIF secondary gamma K factors were higher than the corresponding MORSAIR results for ranges greater than 140 g/cm^2 . This difference is due to the combination of the 2-D air MORSAIR results being biased low and the 1-D homogeneous air MORSAIR results being lower than the fits of the 1-D ANISN data over this range.

In conclusion, comparisons of the AIRDIF and MORSAIR K factors have been made using a fission and thermonuclear source, for silicon and tissue dose, for source altitudes between 5 and 20 km, and for ranges out to 200 g/cm^2 . In almost all cases, the AIRDIF and MORSAIR K factors for neutrons and secondary gammas are in good agreement. These results support the validity of the use of diffusion theory to evaluate the mass integral scaling approximation as applied to the atmospheric radiation transport problem. This result was not unexpected for several reasons. First, it must be remembered that diffusion theory is a low order approx-

imation of transport theory. Comparisons have been presented in this section that show diffusion theory is more than an adequate model for predicting integral quantities like dose. Finally, as pointed out in Section II, the mass scaling law can be derived from both the diffusion and Boltzmann transport equations under the exact same set of assumptions.

A Limitation

During the course of this research, several problems were encountered which ultimately limited the validity of the diffusion model to source altitudes under 20 km and to receiver altitudes less than 25 km. First, at altitudes above 25 km, the air is so thin (see Figures 1 and 2) that the radiation streams for great distances between interactions. The angular dependence of the fluence at these altitudes again approaches that of a delta function which diffusion theory, with its inherent assumption of linear angular variation, is simply incapable of properly treating. Use of the first collided source minimizes but does not eliminate this problem.

Secondly, numerical problems (slow convergence rates, negative fluences, etc.) were encountered when AIRDIF was run at altitudes greater than 25 km. An extensive investigation into this problem revealed that the source of the numerical instabilities was the expanding coordinate system. Specifically, at altitudes above 25 km, the expansion rates necessary to match the atmospheric density gradient produce two undesirable effects. First, the horizontal mesh becomes too coarse in a physical distance sense at the higher altitudes. This is particularly disturbing because although the mesh interval becomes large physically,

it is still about equal from a mean free path standpoint to the intervals at the lower altitudes, where instability problems were not encountered. Secondly, the most severe problems were encountered in that domain where "line of sight" between the mesh points and source point was interfered with by the outer, exponentially curved boundary of the mesh envelope. This is also disturbing, because it is simply not possible to preserve "line of sight" and at the same time maintain the appropriate mesh expansion rate at these altitudes with an exponentially expanding coordinate system.

Finally, it should be mentioned that even if solutions to the problems just discussed could be found, at least one additional problem associated with the characteristics of the U.S. Standard Atmosphere would remain. Specifically, as shown in Figure 2, at an altitude of 25 km, there are only about 25 g/cm² above. This means that no matter how high physically the top boundary is placed, receivers located at altitudes above 25 km will still be within a couple of mean free paths (20-30 g/cm²) of the top boundary where a zero return current condition is applied. The angular dependence of the fluence here is drastically different from linear. Therefore, the diffusion approach would have questionable validity within a couple of mean free paths of the top boundary (i.e., above 25 km). It should be noted that this problem cannot be alleviated by using better boundary conditions. The zero partial return current condition, which is applied in AIRDIF, is the best approximation of the true vacuum condition that is possible to apply with diffusion theory.

Since the nonorthogonal expanding coordinate system (or one similar to it) and an exponential-like atmospheric model would be required for any order of numerical solution of the transport equation in variable density air, it was felt that the problems just discussed probably would not be unique to diffusion theory. Therefore, higher order transport solutions for altitudes above 25 km were not pursued. It turns out that the computational efficiency of Monte Carlo techniques improves* at the higher altitudes, because only a few collisions need be followed before particles escape out the top of the atmosphere. Further, the Monte Carlo method is ideally suited for handling the streaming radiation problem. For these reasons, about six months prior to the completion of the research reported here, the Air Force Weapons Laboratory awarded a contract to Kaman Sciences Corporation to conduct a high altitude evaluation of MIS with the MORSAIR Monte Carlo code (Ref. 31).

Eamon has recently completed this evaluation (Ref. 10). His assessment is based on the same sources and response functions used in this study and concentrates on source altitudes between 20 and 80 km. Eamon's results show, as expected, that at these altitudes leakage is the dominant effect. Neutron and secondary gamma K factors as low as 0.1 are reported for many cases.

*Monte Carlo, even at high altitudes, is still too expensive to run on a repeated basis as required in S/V analyses.

VI. Evaluation of Mass Integral Scaling

K Factor versus Mass Range* Plots

The AIRDIF code was used to generate silicon and tissue MIS K factors for the fission and thermonuclear sources shown in Table V. The neutron and secondary gamma silicon K factors are presented as a function of mass range in Appendix E for the fission source and in Appendix F for the thermonuclear source. In each case, plots are included at source altitudes of 5, 10, 15, and 20 km and at seven receiver altitudes for each source altitude. These data were used to assess the validity of the MIS approximation and are the basis of the discussion below.

Parametric Analysis

The K factor is a function of mass range, particle type, source altitude, receiver altitude, source type, and dose response type. In this subsection, the sensitivity of the K factor to each of these parameters is examined.

Sensitivity to Mass Range. An examination of the data in the Appendixes shows that over the 5-25 km altitude domain, the K factor is a parabolic-shaped function of mass range. For points close to the Z-axis, the K factor is less than one and, in general, is decreasing. Then it levels off and starts to increase at ranges around 100 g/cm². The increase continues over the 100-200 g/cm² range with the K factor achieving

*In this section's figures, the symbol "RHOR" is used for mass range which was defined in equation (2.3).

values that can be much greater than one at large mass ranges.

These trends are due to the combination of the leakage and mass distribution effects described in Section II. Leakage which results in the scaled doses being higher is the primary reason why the K factors are less than one over such wide ranges. The curvature and rise portion of the K factor curves are due to the mass distribution effect.

As explained in Section II, in variable density air many particles reach receivers at large mass ranges after traveling great distances in the less dense air above the source. These particles traverse, on the average, much less air than predicted by the simple mass integral and, therefore, suffer less attenuation. This phenomenon results in the 2-D variable density air doses being higher than the scaled doses at these depths and gives K factors which are increasing to values that can be much greater than one. Particle conservation dictates that if there is an enhancement at these depths, there must also be a corresponding depression in the 2-D air doses at smaller mass ranges (i.e., K factor < 1). This effect is responsible for the close-in K factors being less than one at low altitudes where leakage is insignificant.

Sensitivity to Particle Type. Since leakage of both neutrons and gammas can decrease the secondary gamma doses, the secondary gamma K factors are, in general, depressed more than the corresponding neutron K factors. This is illustrated in Figure 13 for silicon response at coaltitude for a fission source at 20 km.

Sensitivity to Source Altitude. As expected, the depression due to leakage increases as the source altitude increases. This is illustrated for a fission source in Figure 14 for neutrons and in Figure 15 for secondary gammas.

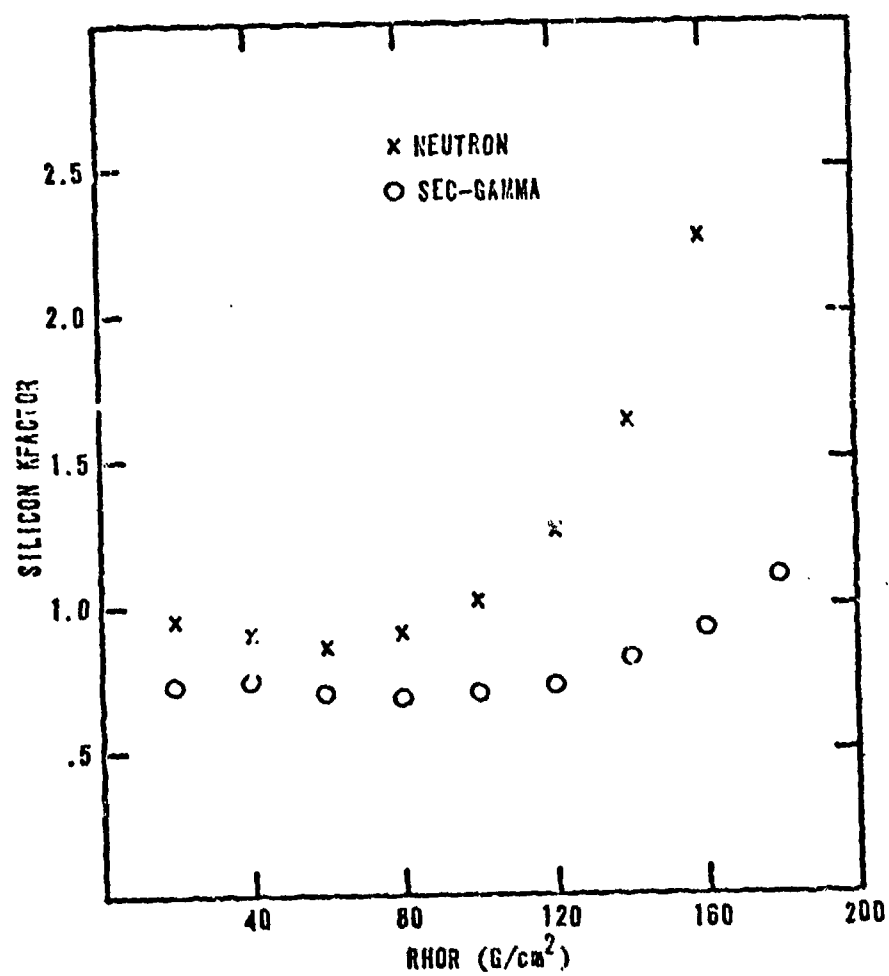


Figure 13. Neutron Versus Secondary Gamma Coaltitude Silicon K Factors for a Fission Source at 20 km

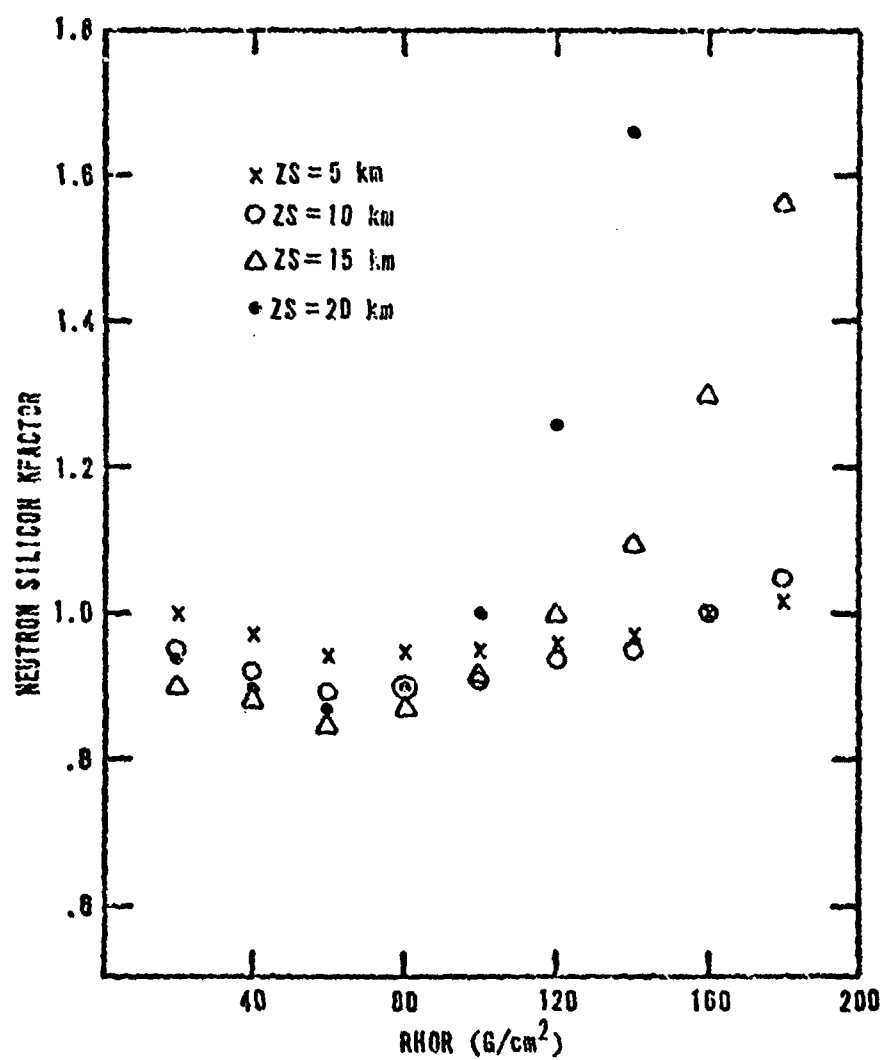


Figure 14. Sensitivity of the Coaltilute Neutron Silicon K Factor for a Fission Source to Source Altitude

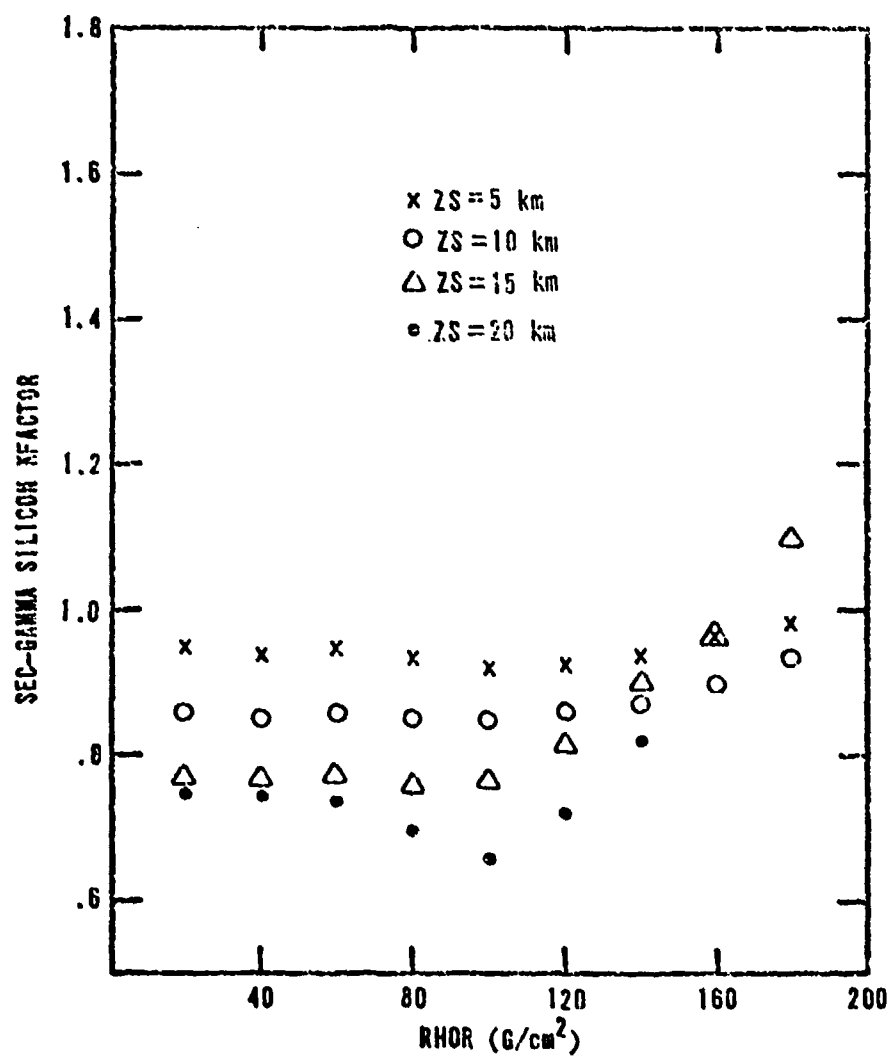


Figure 15. Sensitivity of the Coaltilute Secondary Gamma Silicon K Factor for a Fission Source to Source Altitude

Sensitivity to Receiver Altitude. In general, the depression due to leakage is greater for receiver altitudes below the source than for those above. Also, the K factor seems to rise more sharply for receivers above the source. These effects are illustrated in Figure 16 for neutron silicon K factors for a fission source at 20 km.

Sensitivity to Source Spectrum. As illustrated in Figure 17, at 20 km the neutron silicon K factor is not very sensitive to source type for mass ranges out to 160 g/cm². At larger ranges the fission K factor increases faster than the thermonuclear K factor. The corresponding comparison of secondary gamma K factors is made in Figure 18. This figure shows that the secondary gamma K factor is somewhat more sensitive to source type than the neutron K factor. In particular, leakage seems to depress the secondary gamma dose from a fission source more than that from a thermonuclear source.

Sensitivity to Dose Response. For source altitudes less than 20 km where mass distribution actively competes with leakage, the K factor is not very sensitive to the type of dose response used in defining the K factor. This is illustrated for the fission source at 20 km in Figure 19 for neutrons and in Figure 20 for secondary gammas. It should be mentioned that at higher altitudes where leakage is clearly the dominant effect, Eamon (Ref. 10) reports that the K factor is quite sensitive to the type of response used.

MIS Iso-Error Contours

A major task in studies of this type is to find a concise and yet definitive method of summarizing the results. The method developed here was to use the K factor versus mass range plots to construct MIS

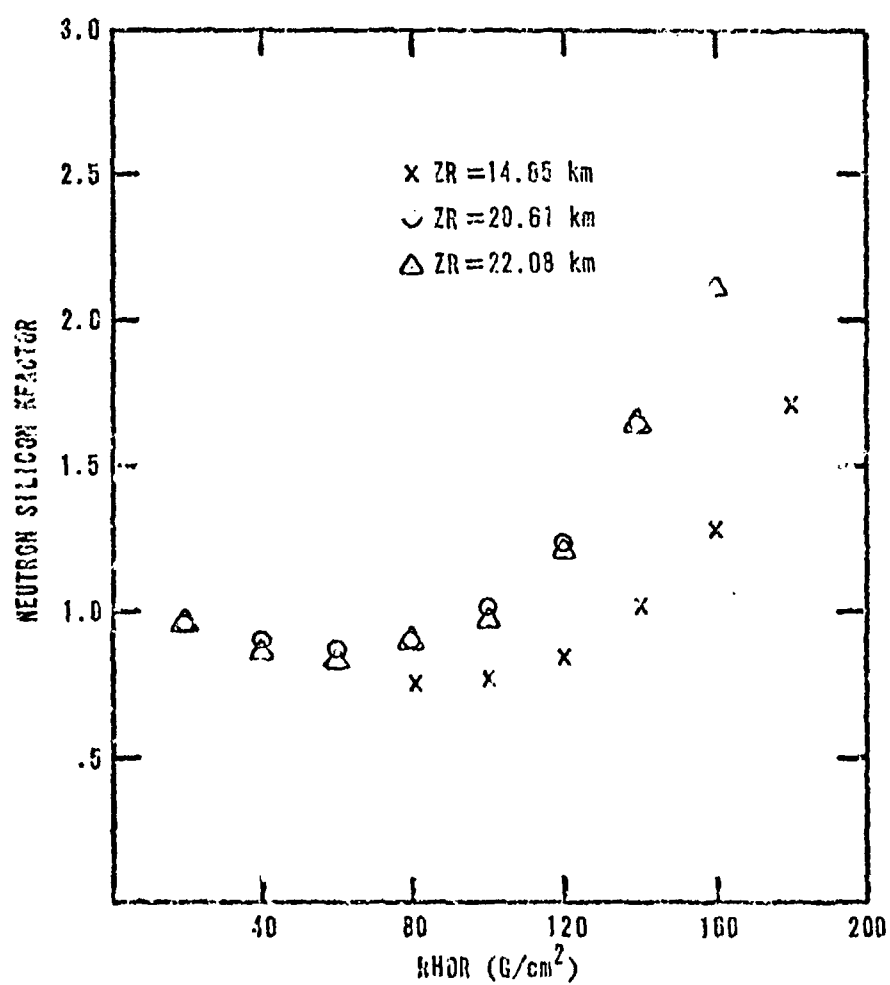


Figure 17. Sensitivity of the Neutron Silicon K Factor for a Fission Source at 20 km to Receiver Altitude

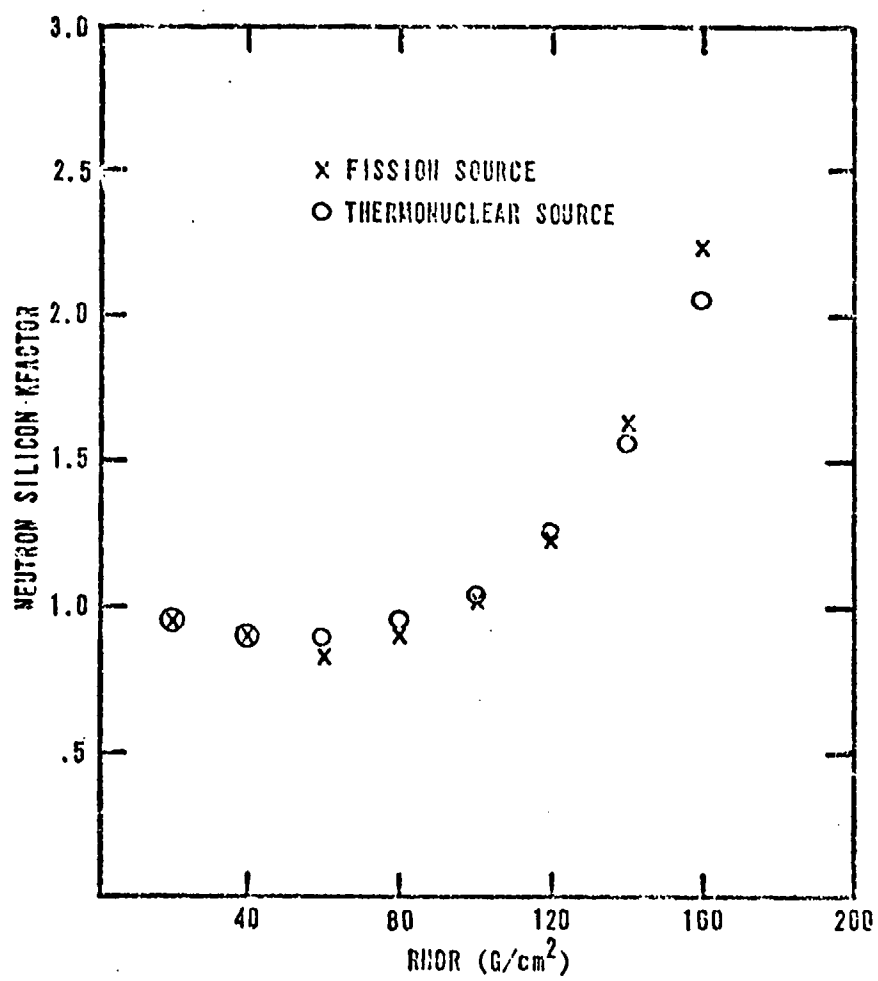


Figure 17. Sensitivity of the Coalitide Neutron Silicon K Factor for a Source at 20 km to Source Type

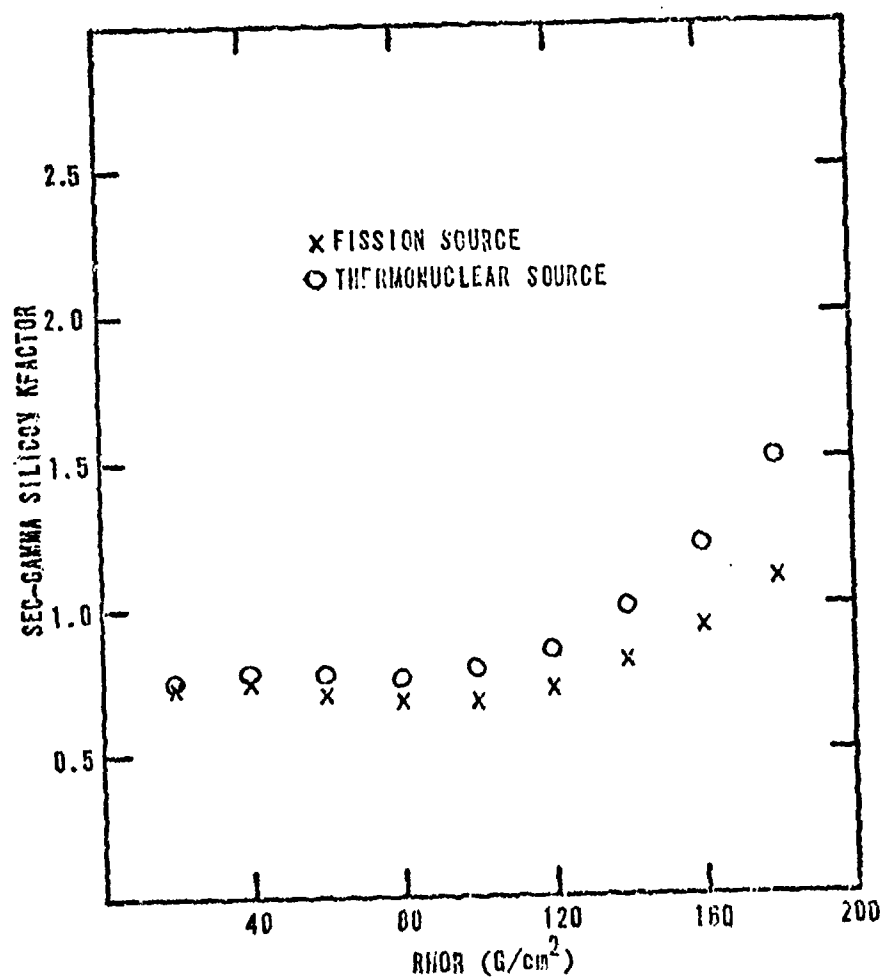


Figure 18. Sensitivity of the Coalitute Secondary Gamma Silicon K Factor for a Source at 20 km to Source Type

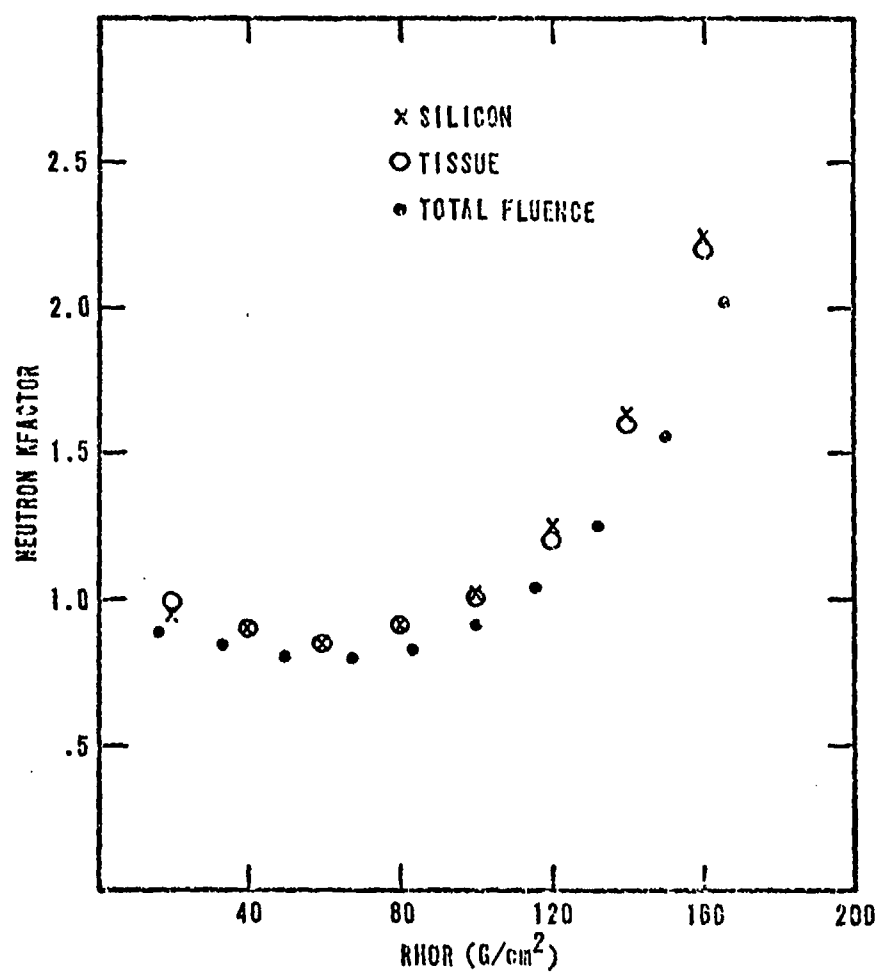


Figure 19. Sensitivity of the Coalititude Neutron K Factor for a Fission Source at 20 km to Dose Response

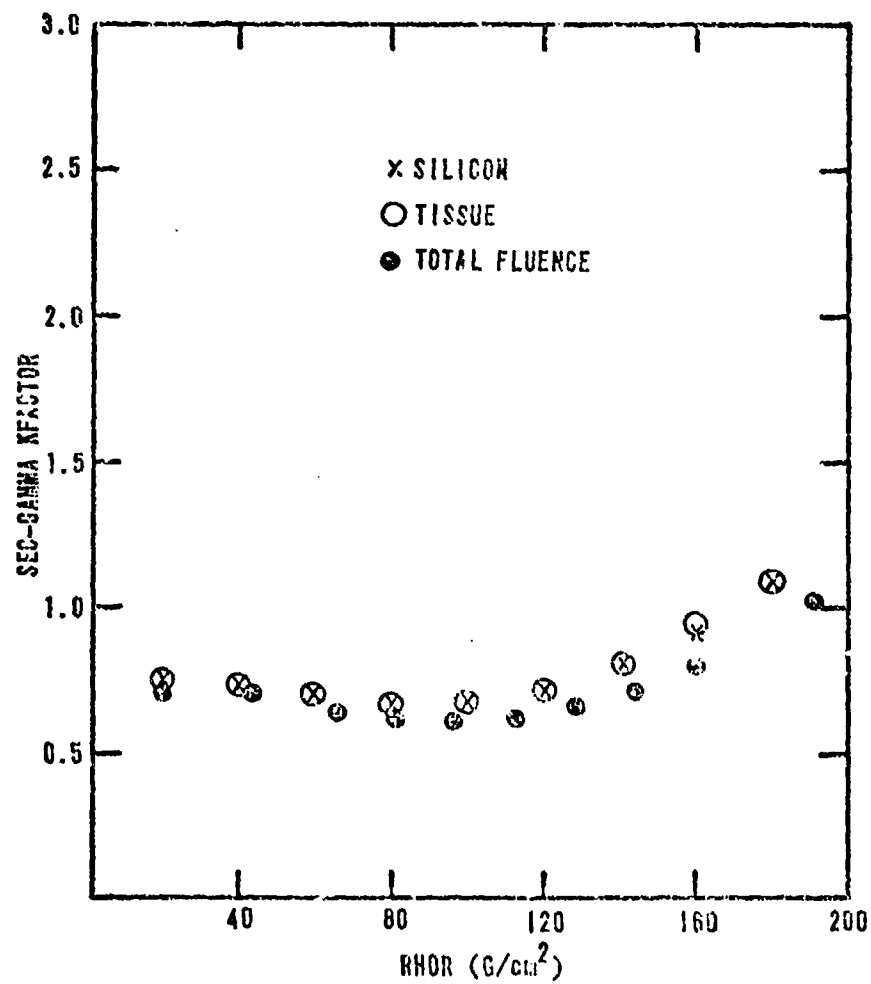


Figure 20. Sensitivity of the Coalititude Secondary Gamma K Factor for a Fission Source at 20 km to Dose Response

iso-error contours. These graphs bound the MIS associated error over various spatial domains in the 1-25 km region. They were constructed using silicon K factors and the K factor/error relationship defined by equation (3.3). Since the K factor in this domain was found to be insensitive to dose response, they also apply to tissue response. The contours are defined in terms of altitude and horizontal range from the z-axis.

Contour for a Source at 5 km. The 250 g/cm^2 contour about a source at 5 km is shown in Figure 21. This line also happens to represent the 10% maximum MIS error contour, i.e., scaled doses for receivers inside Region 1 have at most a 10% MIS error associated with them. Actually, most of the errors in Region 1 are less than 7%. The errors associated with Region 2 were not determined in this study because this region extends much beyond the depths to which the diffusion model was verified. This contour is valid for both neutrons and secondary gammas and for both the fission and thermonuclear source. Since the MIS errors are smaller at lower altitudes where the inhomogenieties in the air are smaller, the indicated results are also valid for source altitudes between 1 and 5 km. At altitudes below 1 km, the air/ground interface, which was not considered in this study, can significantly perturb the scaled dose.

Contour for a Source at 10 km. Figure 22 shows the 220 g/cm^2 and the 20% maximum MIS error contour about a source at 10 km. The contour is again valid for both sources, both responses, and for neutrons and secondary gammas. Typical errors in Region 1 are around 10% for neutron dose and 15% for secondary gamma dose. The errors associated with Region

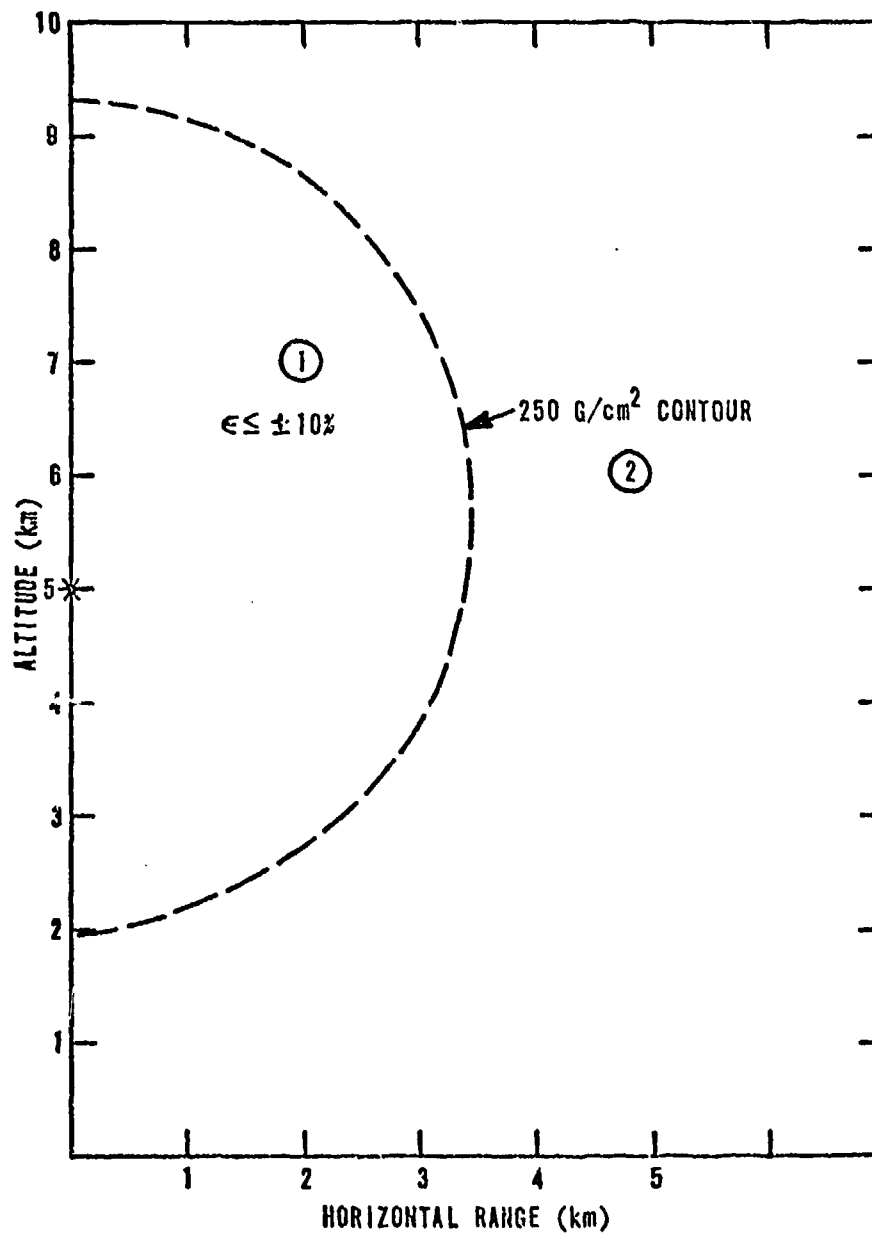


Figure 21. 10% Maximum MIS Error Contour for a Source at 5 km

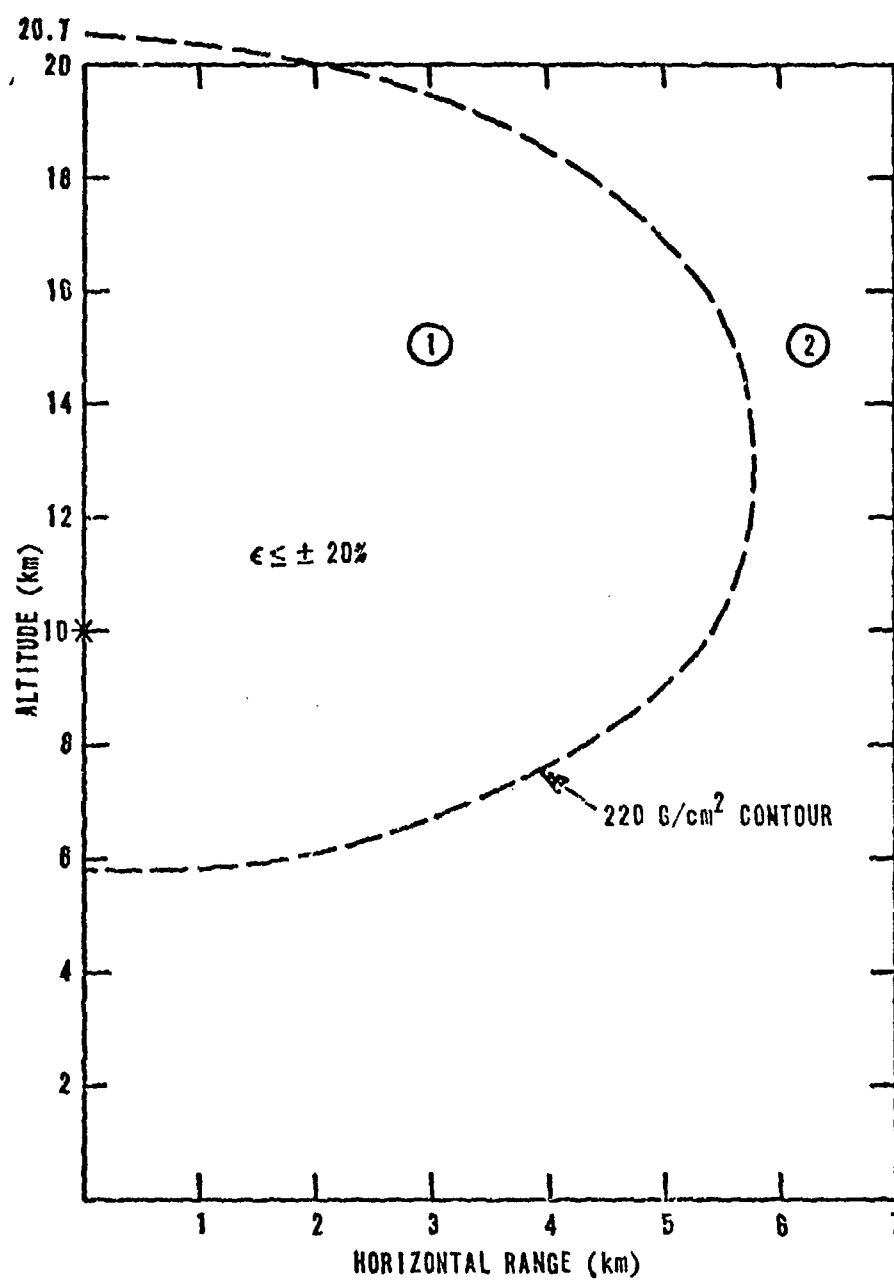


Figure 22. 20% Maximum MIS Error Contour for a Source at 10 km

2 were not determined in this study for the reason cited above.

Contour for Sources at 15 km. At this altitude the deficiencies of MIS are more pronounced and, therefore, more details must be included in defining the error contours. Figure 23 shows MIS error contours for neutron dose from a fission source at 15 km. In Region 1, the MIS errors vary from 0 to 25% with the scaled doses being higher than the actual 2-D variable density air dose. The errors in Region 2 are also in the 0-25% range, but now the scaled doses are lower than the 2-D results. In Region 3, the MIS errors are in the 25-50% range with the scaled doses again low. Errors greater than 50% are incurred in Region 4. Determinations were not made in Region 5. The corresponding MIS error contours for neutron dose from a thermonuclear source are shown in Figure 24. Note that the fission and thermonuclear source contours are almost identical.

The secondary gamma error contours for these sources at 15 km are shown in Figures 25 and 26. In these figures, the errors in Region 1 vary from 0-33%. In Region 2 the scaled doses are low with the errors ranging from 0-25%. In Region 3 errors greater than 25% are incurred. Determinations were not made in Region 4. Again, the contours for the fission and thermonuclear source are very similar.

Contours for Sources at 20 km. The MIS error contour for sources at 20 km are shown in Figures 27-30. The fission and thermonuclear contours indicate that very significant MIS errors are easily incurred at this altitude because of leakage and mass distribution effects.

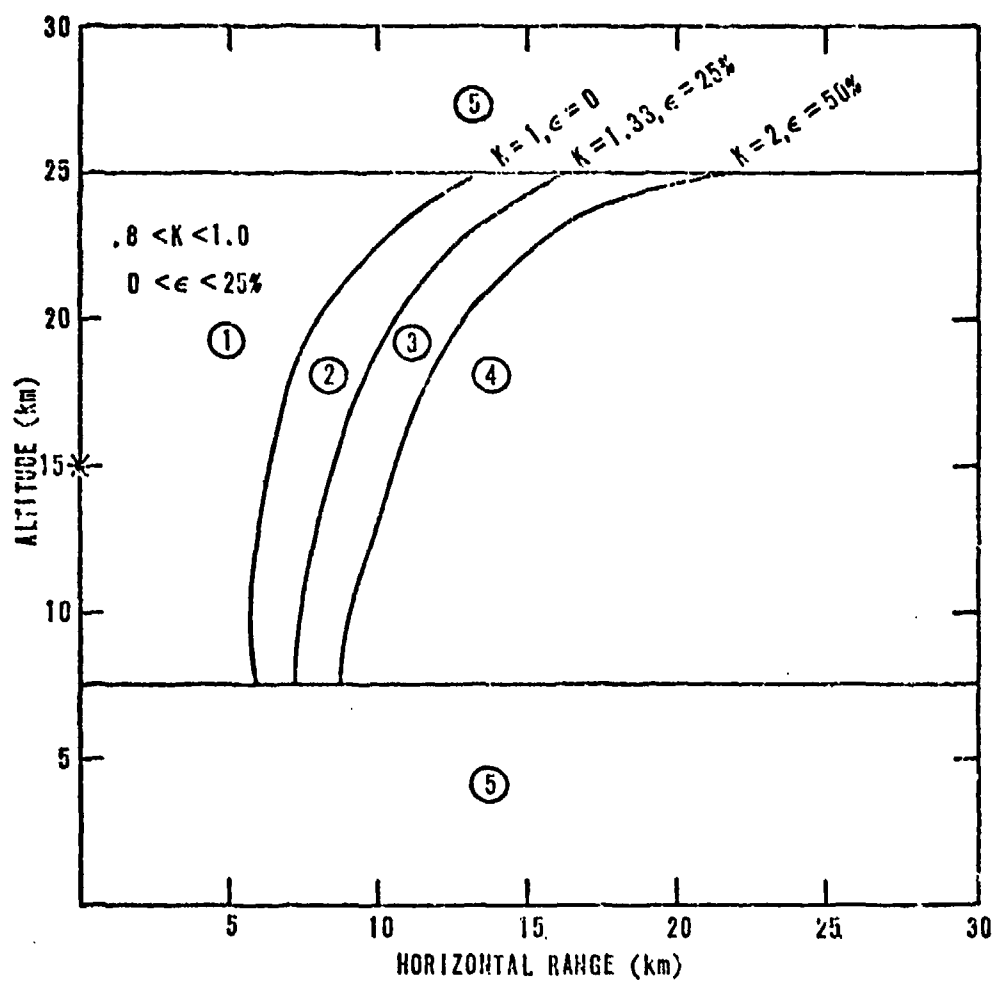


Figure 23. Neutron Dose MIS Error Contours for a Fission Source at 15 km

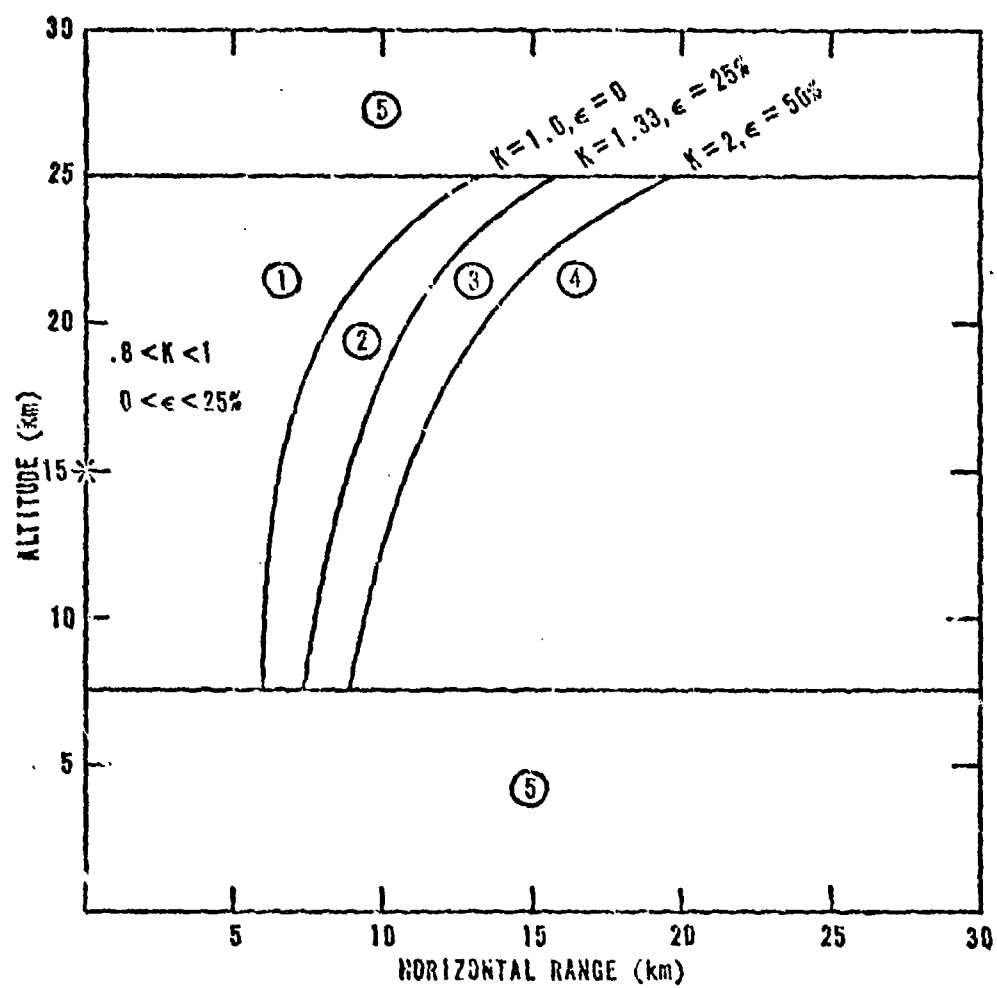


Figure 24. Neutron Dose MIS Error Contours for a Thermonuclear Source at 15 km

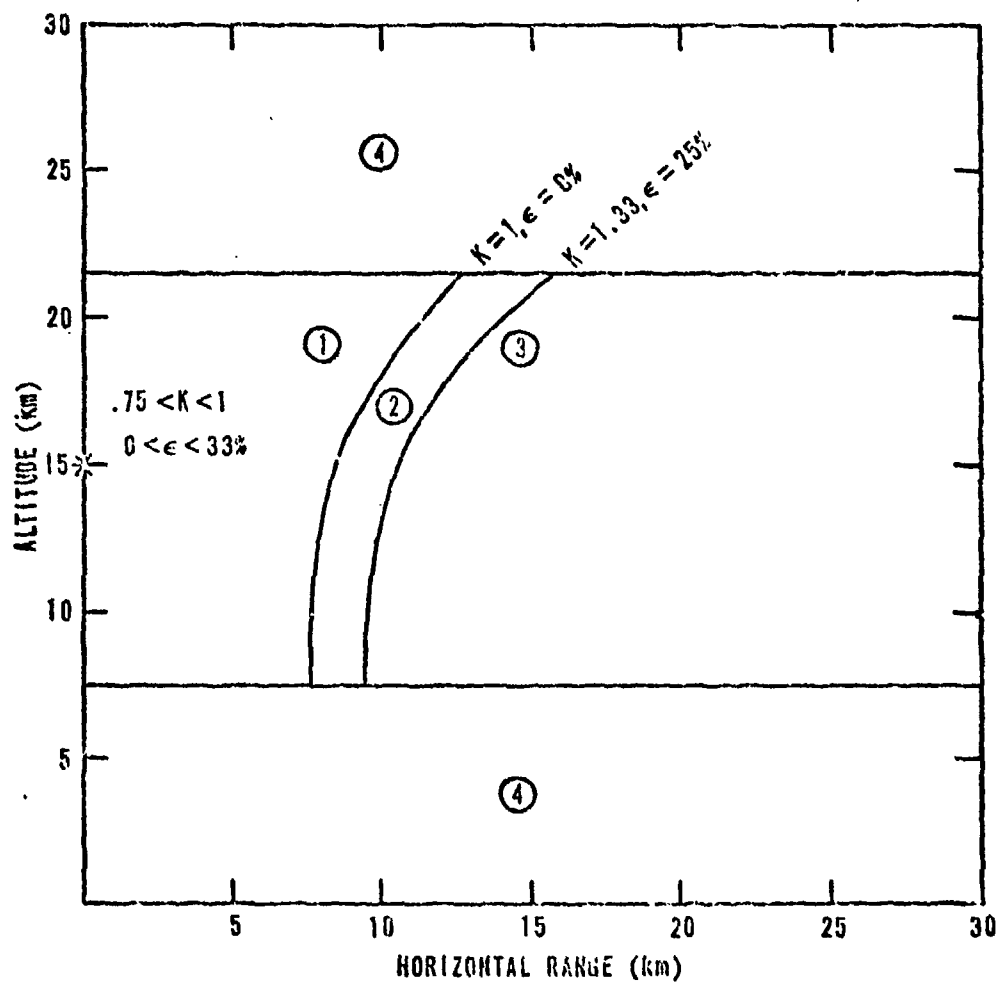


Figure 25. Secondary Gamma Dose MIS Error Contours for a Fission Source at 15 km

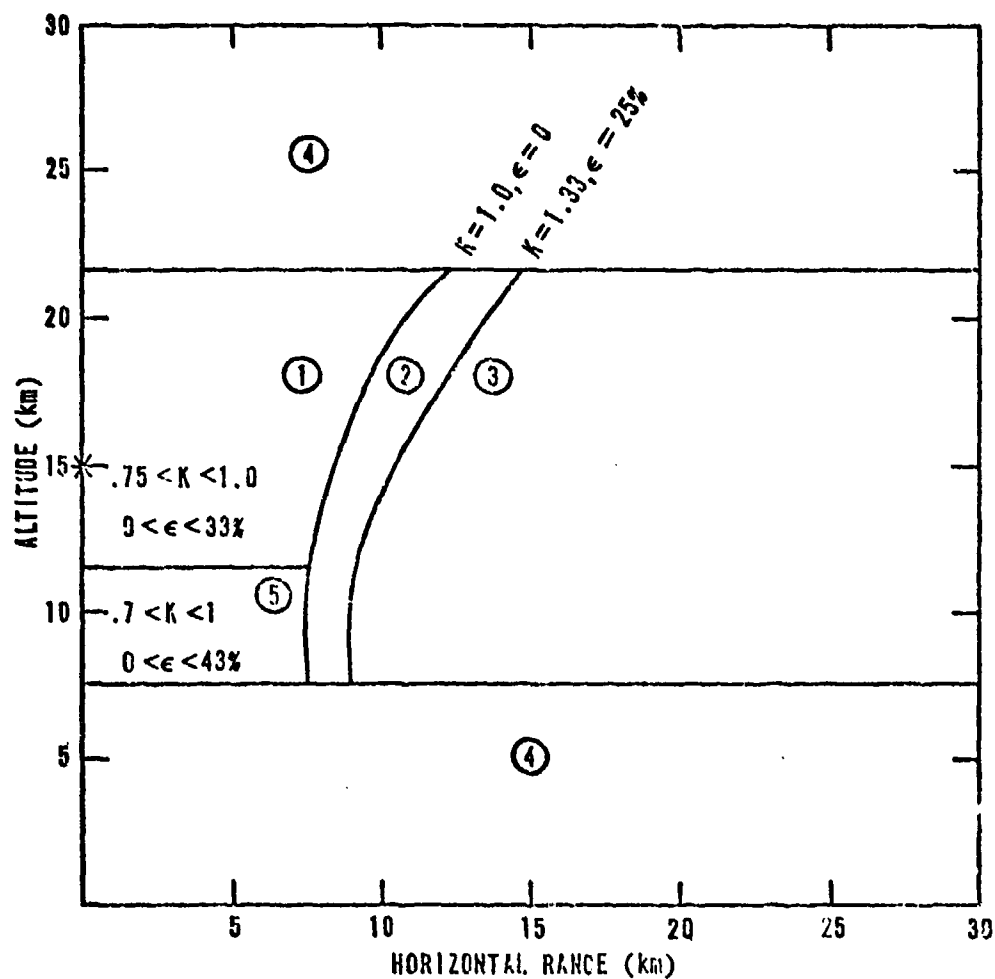


Figure 26. Secondary Gamma Dose MIS Error Contours for a Thermonuclear Source at 15 km

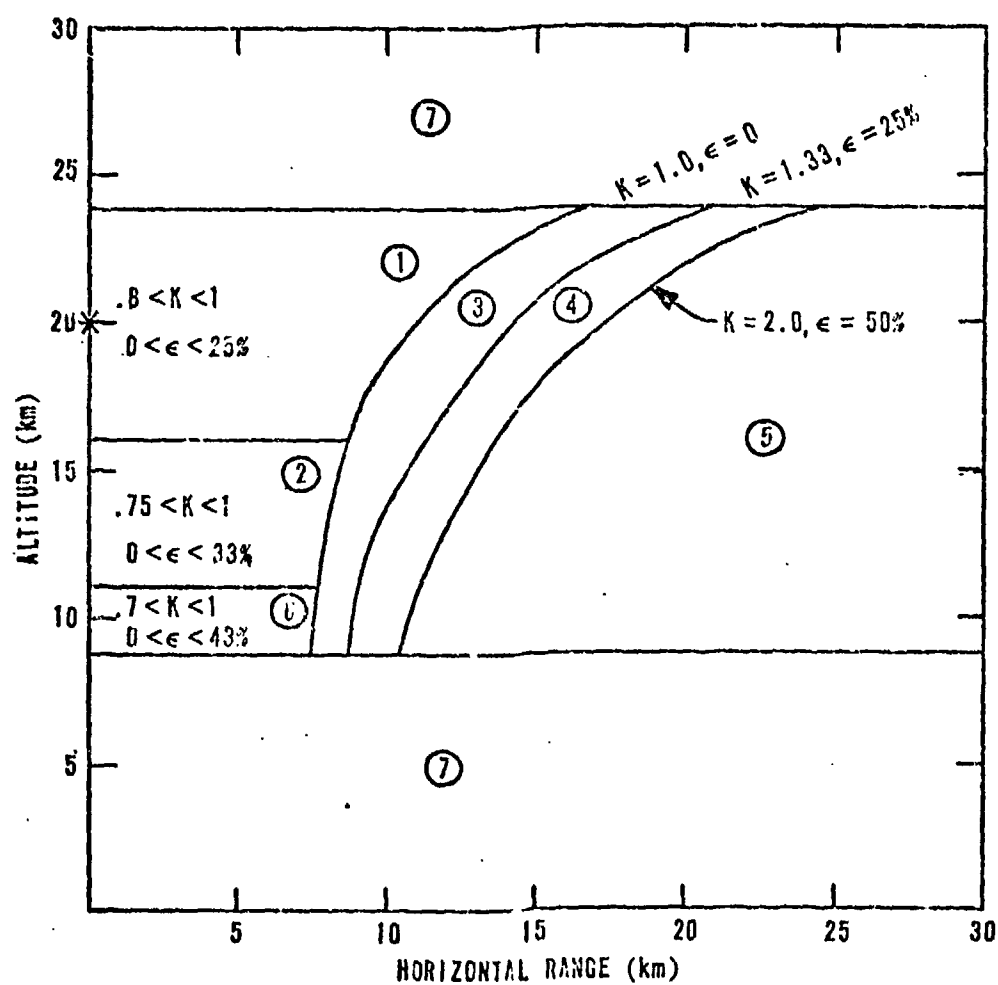


Figure 27. Neutron Dose MIS Error Contours for a Fission Source at 20 km

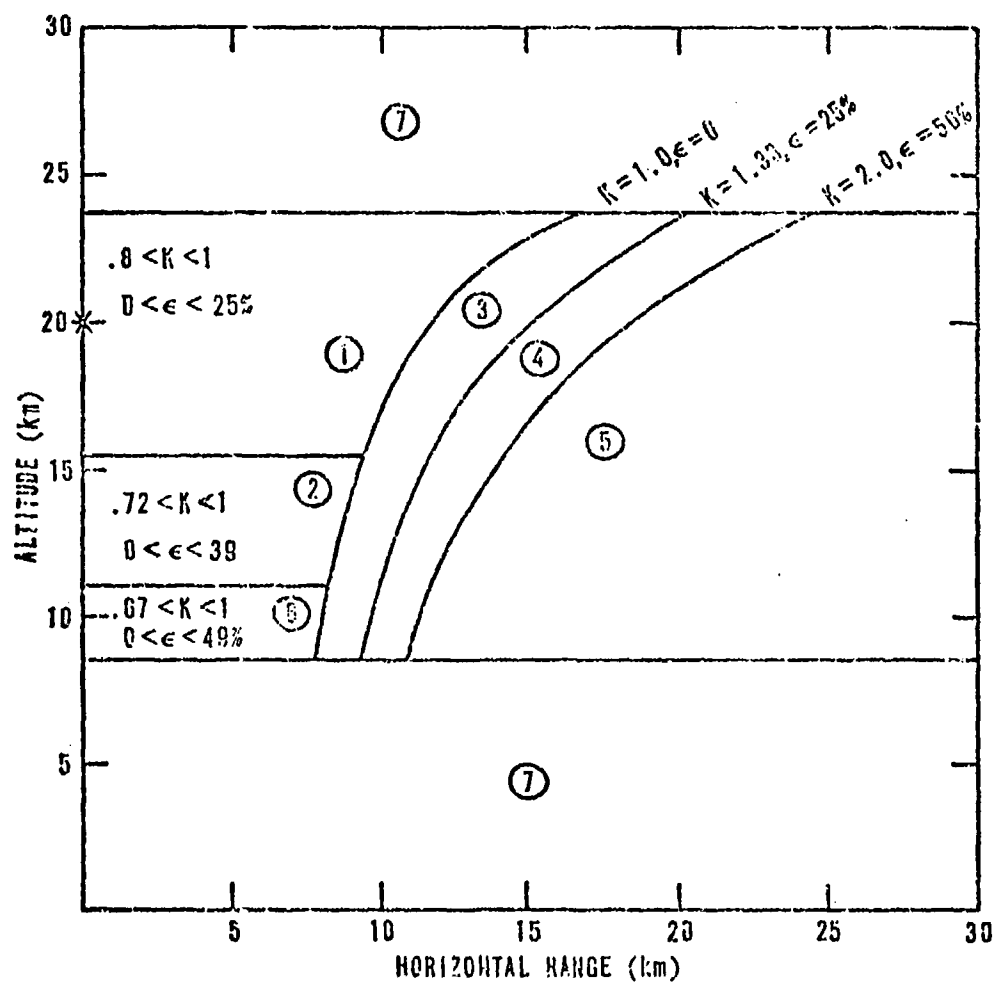


Figure 28. Neutron Dose MIS Error Contours for a Thermonuclear Source at 20 km

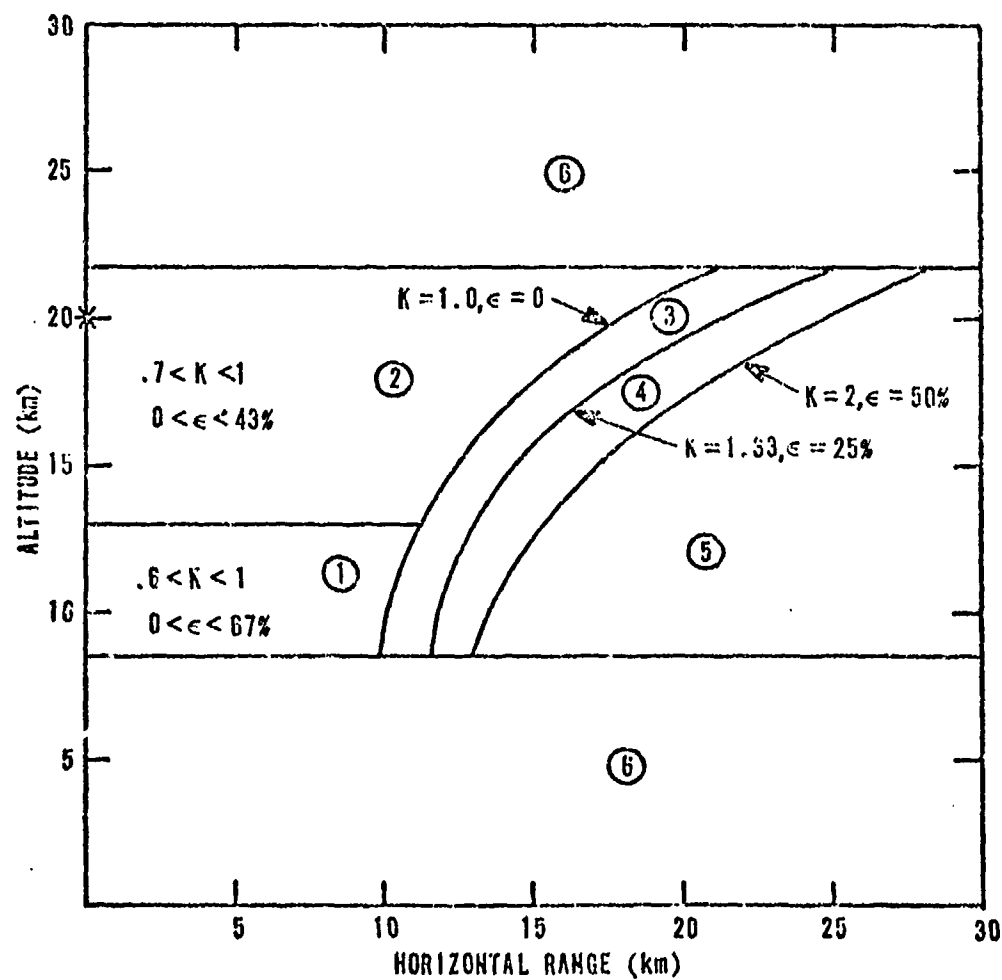


Figure 29. Secondary Gamma Dose MIS Error Contours for a Fission Source at 20 km

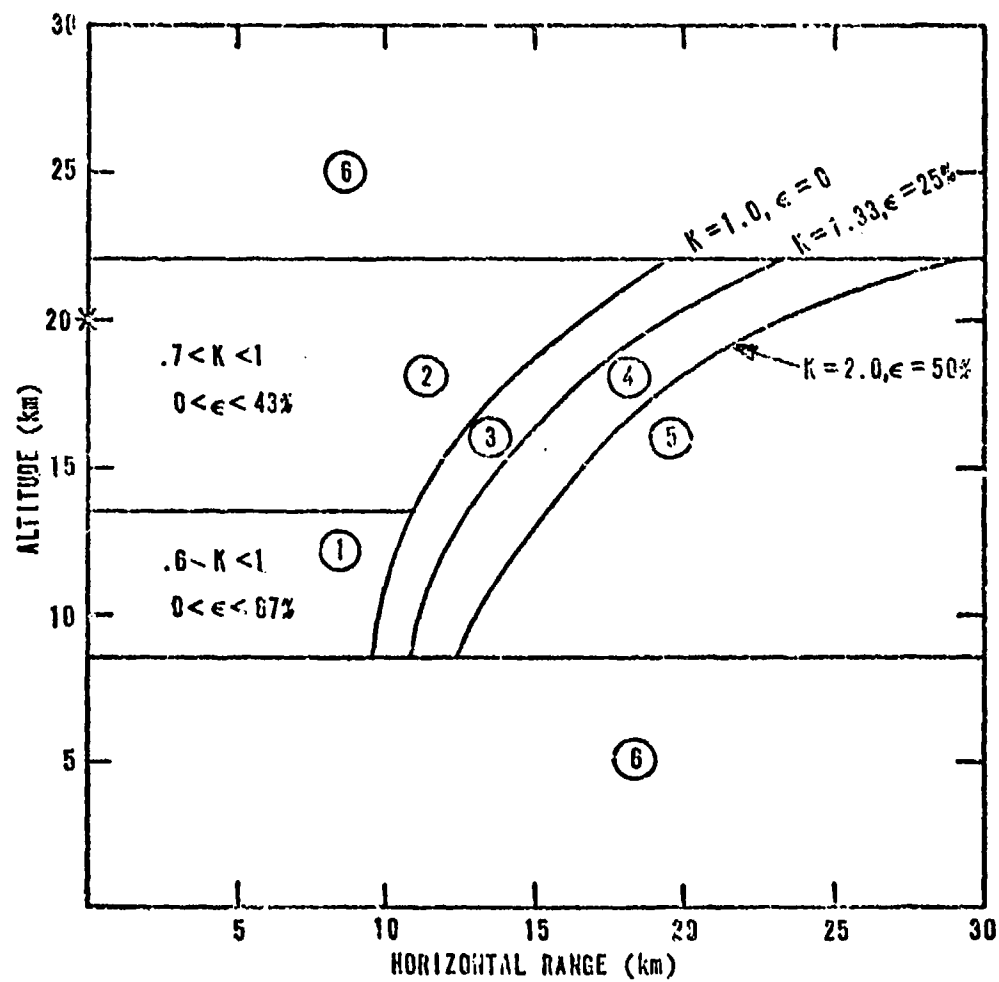


Figure 30. Secondary Gamma Dose MIS Error Contours for a Thermonuclear Source at 20 km

VII. Summary and Conclusions

The purpose of the research reported here was to conduct a systematic evaluation of the MIS approximation as applied to the atmospheric radiation transport problem. The unique feature of this research is that the evaluation was conducted with a special form of diffusion theory. By comparing the diffusion results to Monte Carlo calculations, it was shown that the diffusion approach is an adequate method for evaluating MIS. This is significant because the evaluation was conducted with diffusion theory at a fraction of the cost that would have been required by a comparable Monte Carlo evaluation.

The evaluation was conducted by determining the K factor, defined to be the ratio of the $4\pi R^2$ dose in 2-D variable density air to the $4\pi R^2$ MIS dose, as a function of mass range, source altitude, and receiver altitude. K factors were determined for neutron and secondary gamma doses, for silicon and tissue response, and for a fission and a thermonuclear source. Plots of the K factor versus mass range for source altitudes of 5, 10, 15, and 20 km were prepared and are included in the appendixes. As pointed out in Section III, these data can be used as a multiplicative correction for scaled doses. They were also used to construct a series of MIS iso-error contours which clearly define the MIS error bounds over various spatial domains.

The results of the evaluation show that MIS is acceptable (errors less than 20%) out to mass ranges of 220 g/cm^2 for source altitudes

between 1-10 km. At higher altitudes, the error contour graphs show that significant errors due to scaling are easily incurred. These contours indicate where an MIS correction is necessary, and the K factor versus mass range plots can be used to extract multiplicative correction factors for the scaled doses in these regions. A significant conclusion derived from the evaluation is that at altitudes between 10 and 20 km the mass distribution effect completely overwhelms leakage at large mass ranges. This results in scaled doses that can be much lower than the actual 2-D variable density air results. Extreme caution should be exercised in using scaled results at depths greater than 200 g/cm².

Finally, a couple of recommendations are in order. First, an accurate, efficient, and validated MIS correction factor algorithm should be developed and incorporated into the scaling codes. The results of a preliminary investigation at the Air Force Weapons Laboratory (AFWL) indicate that this is an achievable goal. The AFWL study utilized the AIRDIF K factor data reported here, and indications are that these data can be efficiently and accurately parameterized. Secondly, because of the importance of their environments at high altitudes, it is recommended that the mass integral scaling approximation be evaluated for prompt gammas* and X-rays.

*As stated earlier, this study considered only the secondary gammas produced by neutron inelastic scatter with air.

Bibliography

1. U.S. Standard Atmosphere, 1962. Wash DC: U.S. Government Printing Office, December 1962.
2. Marcum, J. I. Monte Carlo Calculations of the Transport of 14 MeV Neutrons in the Atmosphere. RM-3531-PR. Santa Monica, CA: Rand Corp., April 1963.
3. Marcum, J. I. Energy Deposition in the Atmosphere from High Altitude Gamma-Ray Sources. RM-3594-PR. Santa Monica, CA: Rand Corp., November 1963.
4. Raso, D. J., and S. Woolf. "Comparison of the Gamma-Ray Dose in an Exponential Atmosphere Calculated by the Monte Carlo and the Moment Method." Nucl. Sci. Eng., 25: 198-199 (1966).
5. George, P. and A. Lavagnino. Time Dependent Neutron Transport from a Point Isotropic Source at an Altitude of 30 kft. DASA-1820-II. October 1966.
6. George, P. and A. Lavagnino. Time Dependent Neutron Transport from a Point Isotropic Source at an Altitude of 50 kft. DASA-1820-III. November 1966.
7. Shelton, F. H. and J. R. Keith. Neutron Transport in Non-Uniform Air by Monte Carlo Calculation. KN-774-69-1. Colorado Springs, CO: Kaman Sciences Corp., January 1969.
8. Raso, D. J. "Neutron Energy Flux in an Exponential Atmosphere." Trans. Amer. Nucl. Soc., 12-2: 957-958 (1969).
9. Celnik, J. "Infinite-Medium Neutron Air Transport Buildup and Corrections for an Exponential Atmosphere." Trans. Amer. Nucl. Soc., 12-2: 955-957 (1969).
10. Eamon, James C. High Altitude Atmospheric Radiation Transport Calculations. AFWL-TR-76-142. Kirtland AFB, NM: Air Force Weapons Laboratory, August 1976. (Work done under contract to AFWL by Kaman Sciences Corp., Colorado Springs, CO.)
11. Murphy, Harry M. A User's Guide to the SMAUG Computer Code. AFWL-TR-72-3. Kirtland AFB, NM: Air Force Weapons Laboratory, May 1972.
12. Harris, R. J., Lonergan, J. H., and L. Huszar. Models of Radiation Transport in Air - The ATR Code. SAI-71-557-LJ. La Jolla, CA: Science Applications, Inc., May 1972.

13. Campbell, J. E., Dupree, S. A., and M. L. Forsman. CDR: A Program to Calculate Constant Dose Ranges from a Point Source of Radiation in the Atmosphere. NWEF 1081. Kirtland AFB, NM: Naval Weapons Effects Facility, 1971.
14. French, R. L. "A First-Last Collision Model of the Air/Ground Interface Effects on Fast-Neutron Distributions." Nucl. Sci. Eng., 19: 151-157 (1964).
15. Zerby, C. D. Radiation Flux Transformation as a Function of Density in an Infinite Medium with Anisotropic Point Sources. ORNL 2100. Oak Ridge, TN: Oak Ridge National Laboratory, October 1956.
16. Burgio, J. J. Gamma, Neutron, and Secondary Gamma Transport in Infinite Homogeneous Air. AFWL-TR-75-303, Vols I and II. Kirtland AFB, NM: Air Force Weapons Laboratory, December 1975.
17. Straker, E. A. "The Effect of the Ground on the Steady-State and Time-Dependent Transport of Neutrons and Secondary Gamma Rays in the Atmosphere." Nucl. Sci. Eng., 46: 334-355 (1971).
18. Huszar, L. and W. A. Woolson. Version 3 of Air Transport of Radiation (ATR). SAI-75-585-LJ. La Jolla, CA: Science Applications, Inc., July 1975.
19. Pace, J. V., III, Bartine, D. E., and F. R. Mynatt. Neutron and Secondary-Gamma-Ray Transport Calculations for 14-MeV and Fission Neutron Sources in Air-Over-Ground and Air-Over-Seawater Geometries. ORNL-TM-4841. Oak Ridge, TN: Oak Ridge National Laboratory, August 1975.
20. Radiation Shielding Information Center Data Library Collection, DLC-31/(DPL-1/FEWG1), contributed by Oak Ridge National Laboratory, Oak Ridge, TN.
21. Ritts, J. J., Solomito, E., and P. N. Stevens. Calculations of Neutron Fluence-to-Kerma Factors for the Human Body. ORNL-TM-2079. Oak Ridge, TN: Oak Ridge National Laboratory, February 1969.
22. Storm, L. and H. I. Israel. Photon Cross Sections from .001 to 100 MeV for Elements 1 through 100. LA-3753. Los Alamos, NM: Los Alamos Scientific Laboratory, November 1967.
23. National Bureau of Standards. Measurement of Absorbed Doses of Neutrons and of Gamma Rays. NBS Handbook 75. Wash, DC: NBS, February 1961.
24. Bartine, D. G., et al. Production and Testing of the DNA Few Group Cross Section Library. ORNL-TM-4840. Oak Ridge, TN: Oak Ridge National Laboratory (to be published).

25. Weinberg, A. M. and E. P. Wigner. The Physical Theory of Neutron Chain Reactors. Chicago: The University of Chicago Press, 1958.
26. McLaren, R. D. A Code for Aircraft Survivability Analysis - Gamma and Neutron Effects. Unpublished thesis: GNE-PH/72-8. Wright-Patterson AFB, OH: Air Force Institute of Technology, June 1972.
27. Forsythe, G. E. and W. R. Wasow. Finite Difference Methods for Partial Differential Equations. New York: John Wiley & Sons, Inc., 1960.
28. Varga, R. S. Matrix Iterative Analysis. Englewood Cliffs, NJ: Prentice-Hall, Inc., 1962.
29. Shulstad, R. A. and E. Wolf. AIRDIF: A Real Air Diffusion Theory Computer Code for the Computation of Prompt Radiation Environments and Mass Integral Scaled Dose Correction Factors for Atmospheric Nuclear Detonations. AFWL-TR-(to be published). Kirtland AFB, NM: Air Force Weapons Laboratory.
30. Engle, W. W., Jr. A User's Manual for ANISN - A One-Dimensional Discrete Ordinates Transport Code with Anisotropic Scattering. K-1693. Oak Ridge, TN: Union Carbide Corp., 1967.
31. Straker, E. A., Stevens, P. N., Irving, D. C., and V. R. Cain. The MORSE Code - A Multigroup Neutron and Gamma-Ray Monte Carlo Transport Code. ORNL-4585. Oak Ridge, TN: Oak Ridge National Laboratory, September 1970. (MORSAIR is a version of MORSE tailored for air by J. Eamon of Kaman Sciences Corp., Colorado Springs, CO.)
32. Roberds, R. M. Application of Space-Angle Synthesis to Two-Dimensional Neutral-Particle Transport Problems of Weapon Physics. AFWL-TR-75-299. Kirtland AFB, NM: Air Force Weapons Laboratory, January 1976.

Appendix A

Derivation of the Mass Scaling Law

In this Appendix, the mass scaling law is derived from the energy dependent diffusion equation. The derivation parallels Zerby's derivation of the law from the Boltzmann transport equation (Ref. 15).

First, consider the time independent diffusion equation with an isotropic point source in an infinite homogeneous medium of density ρ_A which is given by

$$D_A(E) \left(\frac{d^2}{dR_A^2} F(R_A, E) + \frac{2}{R_A} \frac{d}{dR_A} F(R_A, E) \right) - \Sigma_T^A(E) F(R_A, E) + \int dE' \Sigma_S^A(E' \rightarrow E) F(R_A, E') + \frac{\delta(R_A)}{4\pi R_A^2} S^A(E) = 0 \quad (A.1)$$

where

$D_A(E)$ = the energy dependent diffusion coefficient in units of cm

$F(R_A, E)$ = the energy dependent particle fluence at a distance of R_A from the source in units of particles/cm²-eV

$\Sigma_T^A(E)$ = the energy dependent macroscopic total interaction cross section at density ρ_A in units of cm⁻¹

$\Sigma_S^A(E' \rightarrow E)$ = the macroscopic cross section for scatter from energy E' to energy E in units of cm⁻¹ per eV

$\delta(R_A)$ = the dirac delta function (cm⁻¹)

$S^A(E)$ = the energy dependent particle source in units of
particles/eV

Now consider a second medium, medium B, composed of the same material as medium A but having density ρ_B which may be different. In this medium the diffusion equation can be written as

$$D_B(E) \left(\frac{d^2}{dR_B^2} F(R_B, E) + \frac{2}{R_B} \frac{d}{dR_B} F(R_B, E) \right) - \Sigma_T^B(E) F(R_B, E) + \int dE' \Sigma_S^B(E' \rightarrow E) F(R_B, E') + \frac{\delta(R_B)}{4\pi R_B^2} S^B(E) = 0 \quad (A.2)$$

The macroscopic cross sections in medium A can be expressed as the product of medium B cross sections and the density ratio between the media, i.e.,

$$\Sigma_T^A = \Sigma_T^B \frac{\rho_A}{\rho_B} \quad (A.3)$$

$$\Sigma_S^A = \Sigma_S^B \frac{\rho_A}{\rho_B} \quad (A.4)$$

$$D_A = D_B \frac{\rho_B}{\rho_A} \quad (A.5)$$

Using these relationships and under the assumptions that

$$\rho_A R_A = \rho_B R_B \quad (A.6)$$

and

$$S^A(E) = S^B(E) \quad (A.7)$$

equation (A.2) can be rewritten as

$$\begin{aligned}
D_A(E) & \left(\frac{d^2}{dR_A^2} F\left(R_A \frac{\rho_A}{\rho_B}, E\right) + \frac{2}{R_A} \frac{d}{dR_A} F\left(R_A \frac{\rho_A}{\rho_B}, E\right) \right) - \Sigma_T^A(E) F\left(R_A \frac{\rho_A}{\rho_B}, E\right) \\
& + \int dE' \Sigma_S^A(E' \rightarrow E) F\left(R_A \frac{\rho_A}{\rho_B}, E'\right) \\
& + \frac{\delta\left(R_A \rho_A / \rho_B\right) S^A(E)}{4\pi R_A^2} \frac{\rho_B}{\rho_A} = 0
\end{aligned} \tag{A.8}$$

A comparison of equation (A.1) to (A.8) shows that they are identical except for the source term. The volume integrated source in medium A is

$$\int_0^\infty \frac{\delta(R_A)}{4\pi R_A^2} S^A(E) 4\pi R_A^2 dR_A = S^A(E) \tag{A.9}$$

In medium B, however, the volume integrated source is given by

$$\int_0^\infty \frac{\delta\left(R_A \rho_A / \rho_B\right)}{4\pi R_A^2} S^A(E) \frac{\rho_B}{\rho_A} 4\pi R_A^2 dR_A = \left(\frac{\rho_B}{\rho_A}\right)^2 S^A(E) \tag{A.10}$$

Since the volume integrated in medium B differs by a factor of $\left(\frac{\rho_B}{\rho_A}\right)^2$ from the source in medium A, it must follow that

$$F(R_B, E) = \left(\frac{\rho_B}{\rho_A}\right)^2 F(R_A, E) \tag{A.11}$$

or

$$4\pi R_B^2 F(R_B, E) = 4\pi R_A^2 F(R_A, E) \tag{A.12}$$

where we have used equation (A.6) and included a factor of 4π , as is commonly done, to write the scaling law in terms of quantities in which geometric attenuation has been removed.

In summary, the mass scaling law states that if two infinite homogeneous media composed of identical material and containing identical isotropic point sources are related by

$$\rho_B R_B = \rho_A R_A \quad (A.6)$$

then,

$$4\pi R_B^2 F(R_B, E) = 4\pi R_A^2 F(R_A, E) \quad (A.12)$$

Appendix B

The AIRDIF Code

General Description

The AIRDIF code is based on the atmospheric diffusion theory presented in Section IV and is capable of computing both the radiation environments and MIS K factors for atmospheric nuclear detonations. It is a structured computer code composed of 42 independent subroutine modules and written in ANSI standard FORTRAN.

Figure B-1 shows the major hierarchy of the AIRDIF code. The logic in a structured code, like AIRDIF, always flows from the top downward. For example, the executive routine, EXEC, calls three routines: DATAIN, CALC, and RESOUT. EXEC first calls DATAIN to read in the input data. Control then shifts back to EXEC where subroutine CALC which performs all of the required calculations is called. Control again shifts back to EXEC, and RESOUT which outputs and stores the results is called.

There are many advantages inherent to the characteristic modularity of such structured programs. While it is beyond the scope of this appendix to enumerate on all of them, one in particular is worthy of mention. Specifically, such codes are inherently very versatile. For example, the only routine which is unique to diffusion theory is MATRIX which defines the finite differenced diffusion equations. A higher order method such as Roberd's synthesis method (Ref. 32) could be incorporated into AIRDIF by simply replacing this routine with one based on the finite differencing of the synthesis equation.

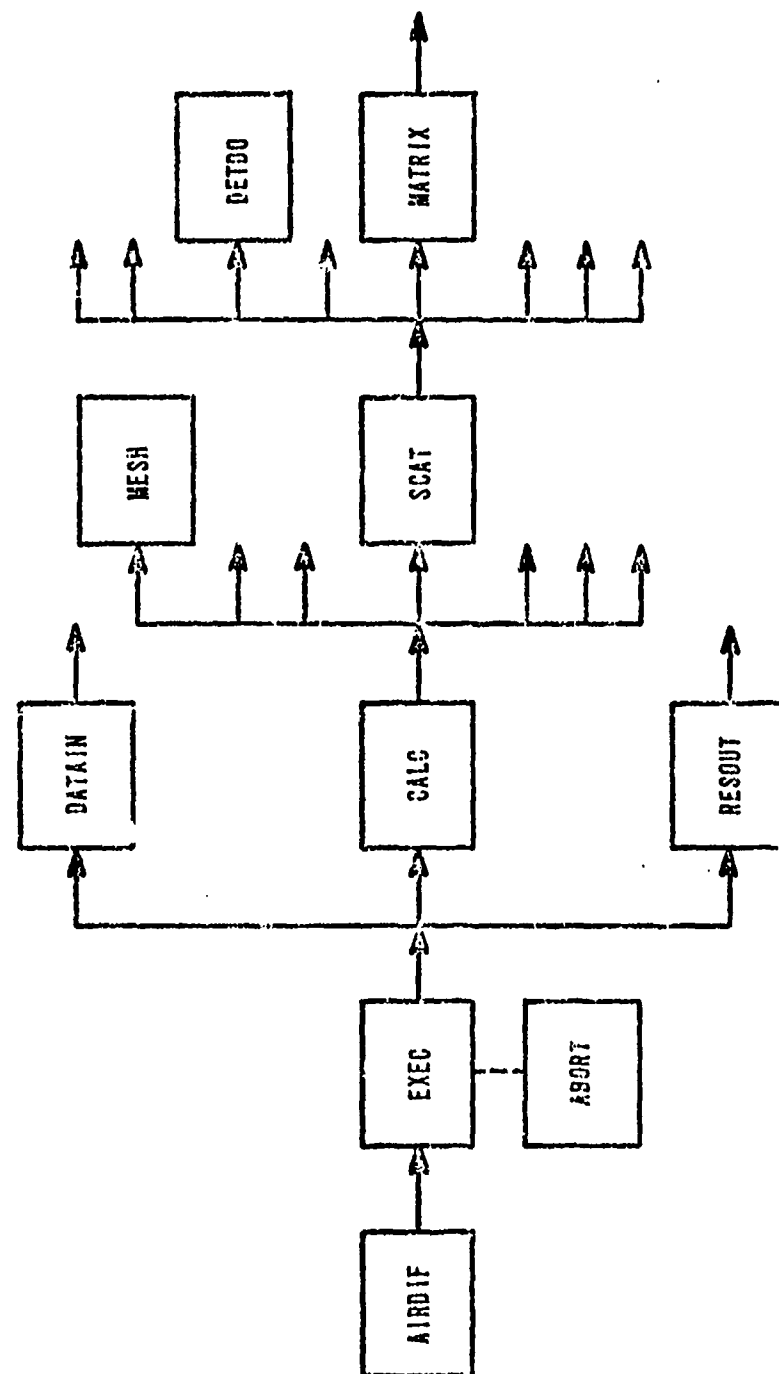


Figure B-1. Hierarchy of the AIRDIF Code

AIRDIF has been successfully run on both the CDC-6600 and 7600 computers. Execution times of about 0.05 sec per mesh point (for 37 neutron and 21 gamma groups) are required on the 7600. Since most problems require somewhere between 1500 and 3000 mesh points, a couple of minutes of 7600 CP time is normally required for each run. In its current form, AIRDIF has storage set aside for up to 5000 mesh points and requires approximately 33 octal K of small core memory (SCM) and 220 octal K of large core memory (LCM) on the 7600.

Computation of Radiation Environments

AIRDIF utilizes the analytical first collided source defined by equation (4.31) and numerically solves equation (4.50) group by group to obtain the collided fluence at all mesh points. Total fluences in each group are then obtained by combining the uncollided and collided fluences. User-supplied dose response functions and equation (3.1) are then used to compute the dose at all mesh points.

As pointed out in Section IV, AIRDIF is capable of determining the radiation environments in both homogeneous air and in the U.S. Standard Atmosphere (2-D air). The user simply specifies the option desired. For homogeneous air, the conditions specified by equations (4.36) through (4.38) are applied internally and the resulting five-point difference equations are solved iteratively. In 2-D air, a nine-point difference equation is solved.

There is also an option in AIRDIF for storing all results including the differential energy fluence at each mesh point on a permanent file. This data file can then be accessed later, and environments in any dose units can be quickly computed with a simple editing code.

Computation of K Factors

AIRDIF is also capable of directly computing K factors defined by equation (3.2). An AIRDIF homogeneous air run is made first, and the results for a particular source are stored on a permanent file. An edit code called MISFIT (Ref. 29) is then used to access this file and to perform a least squares fit of the dose for a user-supplied dose response function to Murphy's radiation transmission equation (Ref. 16:36),

$$T(x) = \exp(A + Bx + Cx^2 + Dx^{3/2} + Ex^{1/2} + Fx^{1/3} + G\ln(x)) \quad (4.51)$$

where

$$T(x) = 4\pi R^2 \text{1-D MIS dose at a mass range of } x \text{ g/cm}^2.$$

The fit coefficients for both neutrons and gammas are included as part of the input for the 2-D variable density air run. Using these coefficients and equation (4.51), AIRDIF computes the $4\pi R^2$ 1-D MIS doses. These results, the calculated 2-D air doses, and the K factor equation (3.2) are then used by AIRDIF to compute the K factors for the specified source and dose response at all mesh points.

Appendix C

Radiation Dose Comparisons

This appendix presents graphs which compare the diffusion radiation environments to transport theory and Monte Carlo environments.* In homogeneous air, the AIRDIF diffusion results are compared to ANISN discrete ordinates results. In 2-D air (U.S. Standard Atmosphere), the comparisons are made against MORSAIR Monte Carlo results. The comparisons include results for neutron and secondary gamma environments, for silicon and tissue dose response (Tables III and IV), for a fission and thermonuclear source (Table V), and out to mass ranges of 200 g/cm².

*Note that $4\pi R^2$ dose is plotted as a function of mass range in all graphs. Mass range, $\langle \rho R \rangle$, is defined by equation (2.3). In this appendix, the symbol "RHOR" is used for $\langle \rho R \rangle$.

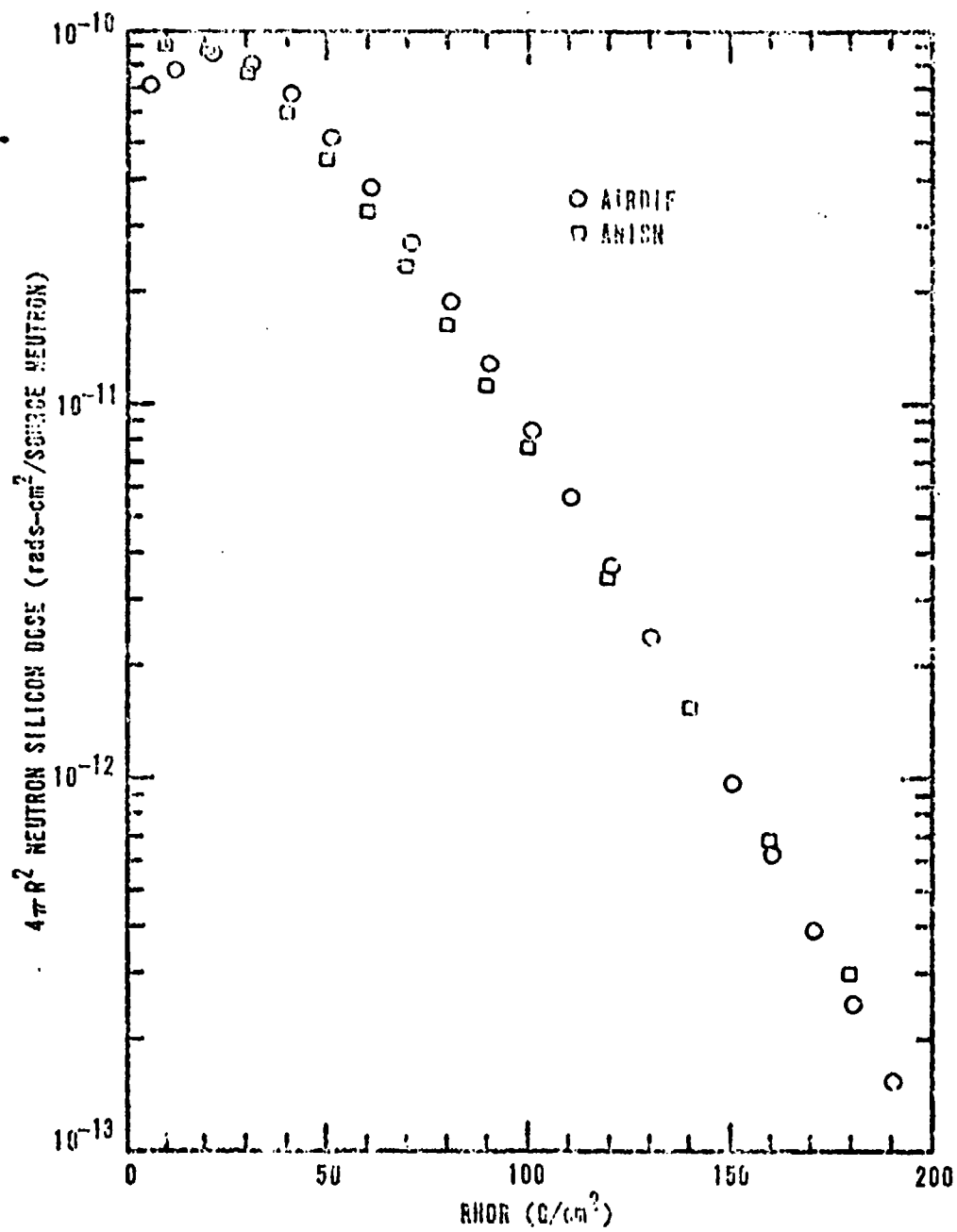


Figure C-1. Neutron Silicon Doses from a Fission Source in Homogeneous Air

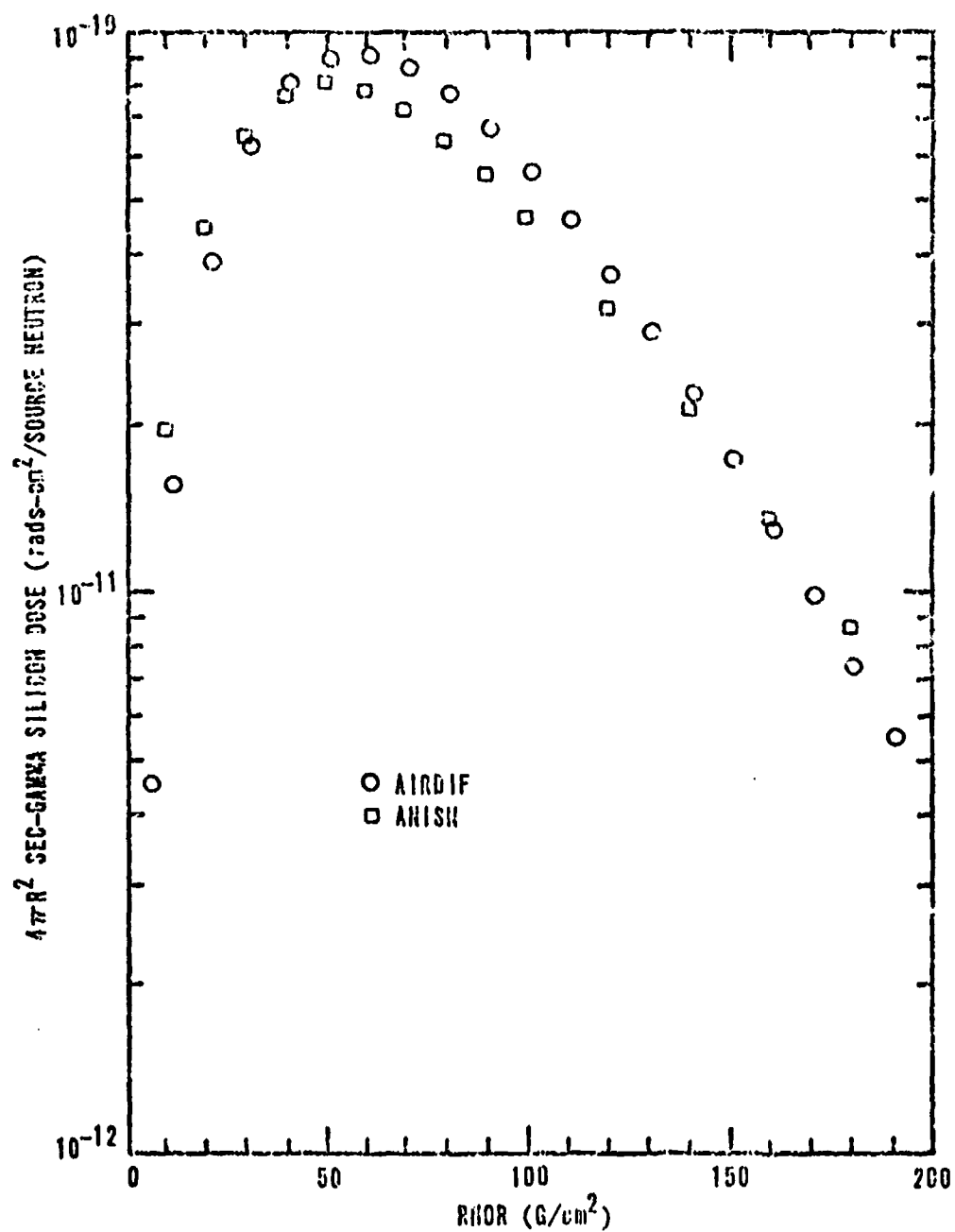


Figure C-2. Secondary Gamma Silicon Doses from a Fission Source in Homogeneous Air

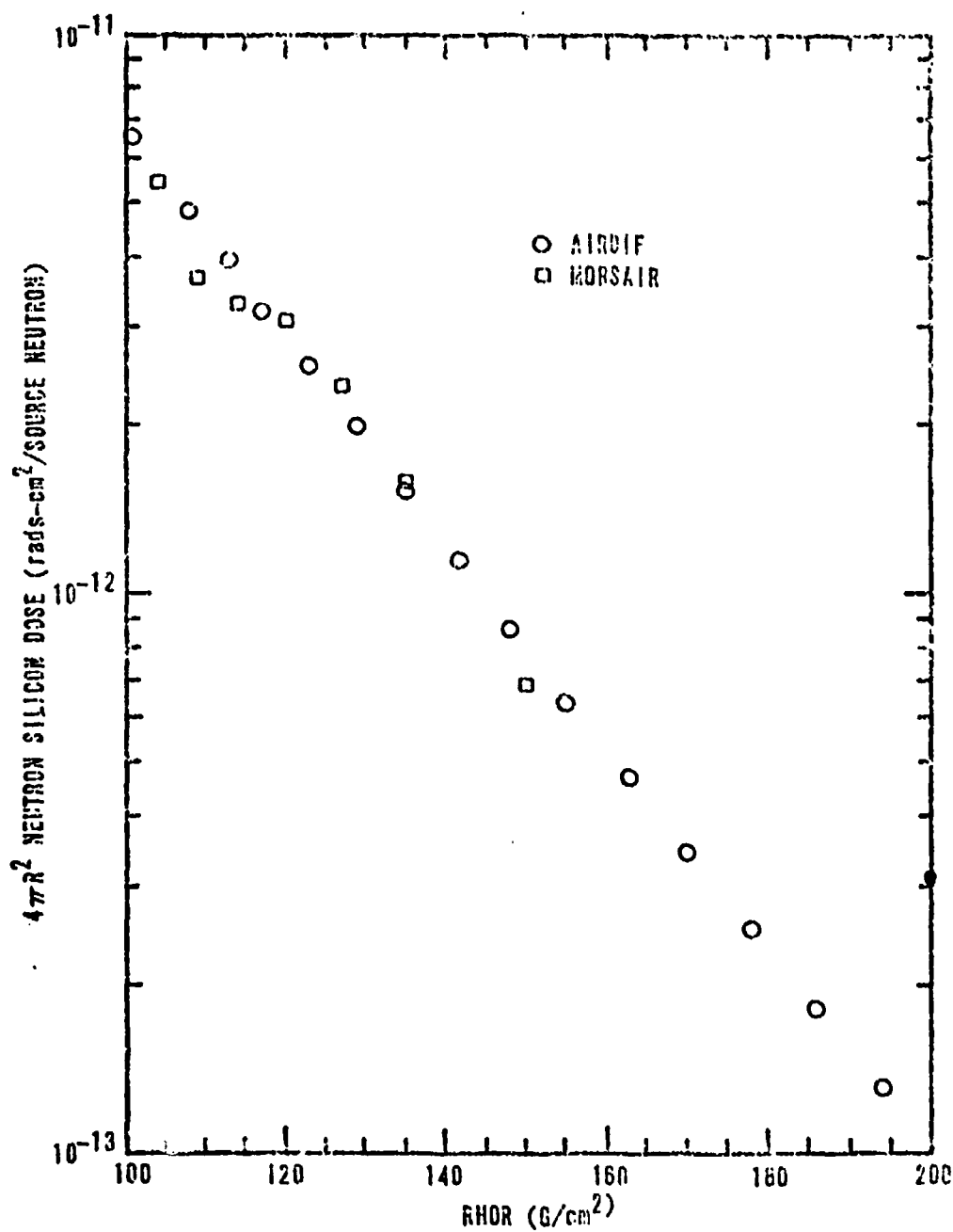


Figure C-3. Neutron Silicon Doses from a Fission Source at 15 km and Receivers at 11.3 km

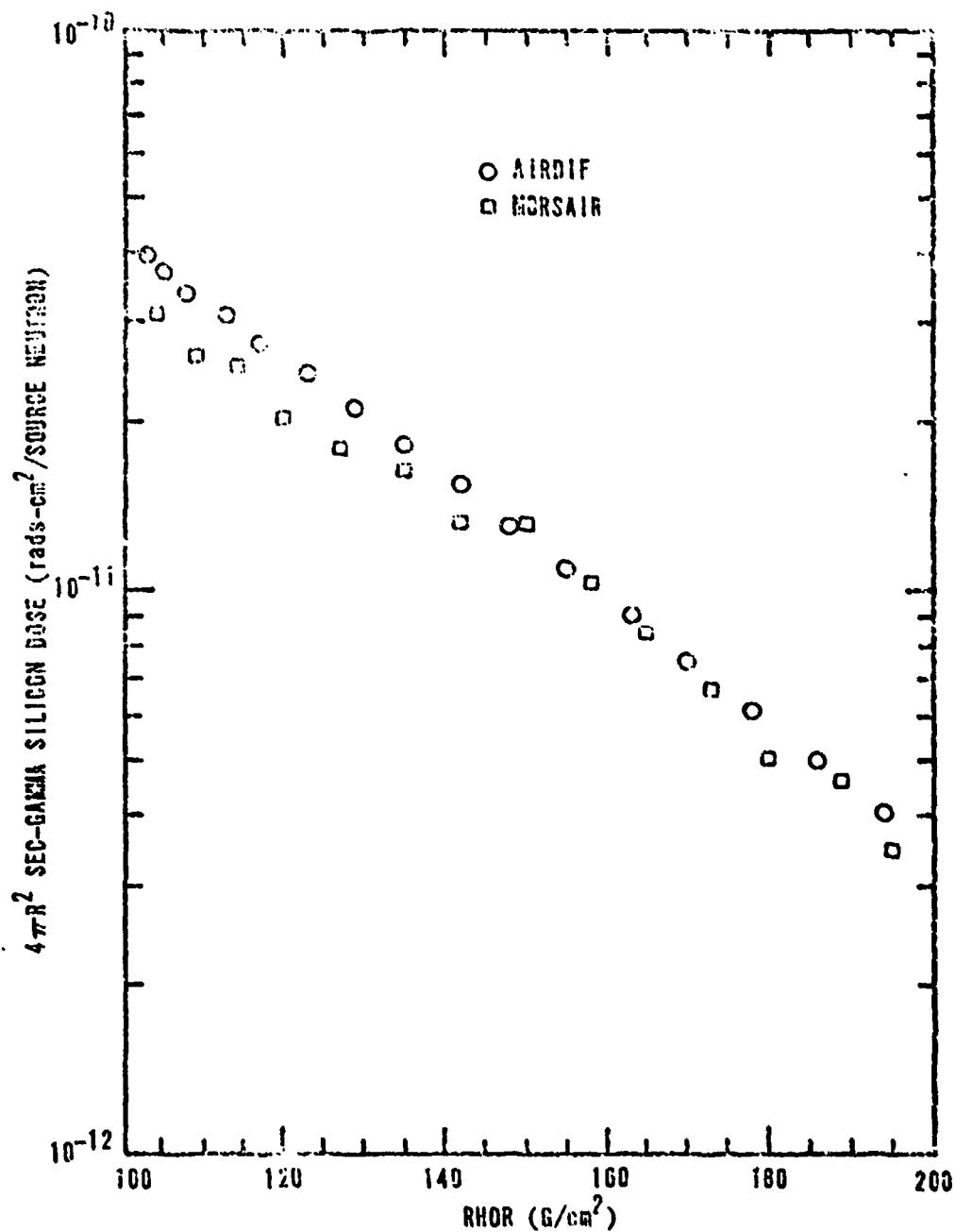


Figure C-4. Secondary Gamma Silicon Doses from a Fission Source at 15 km and Receivers at 11.3 km

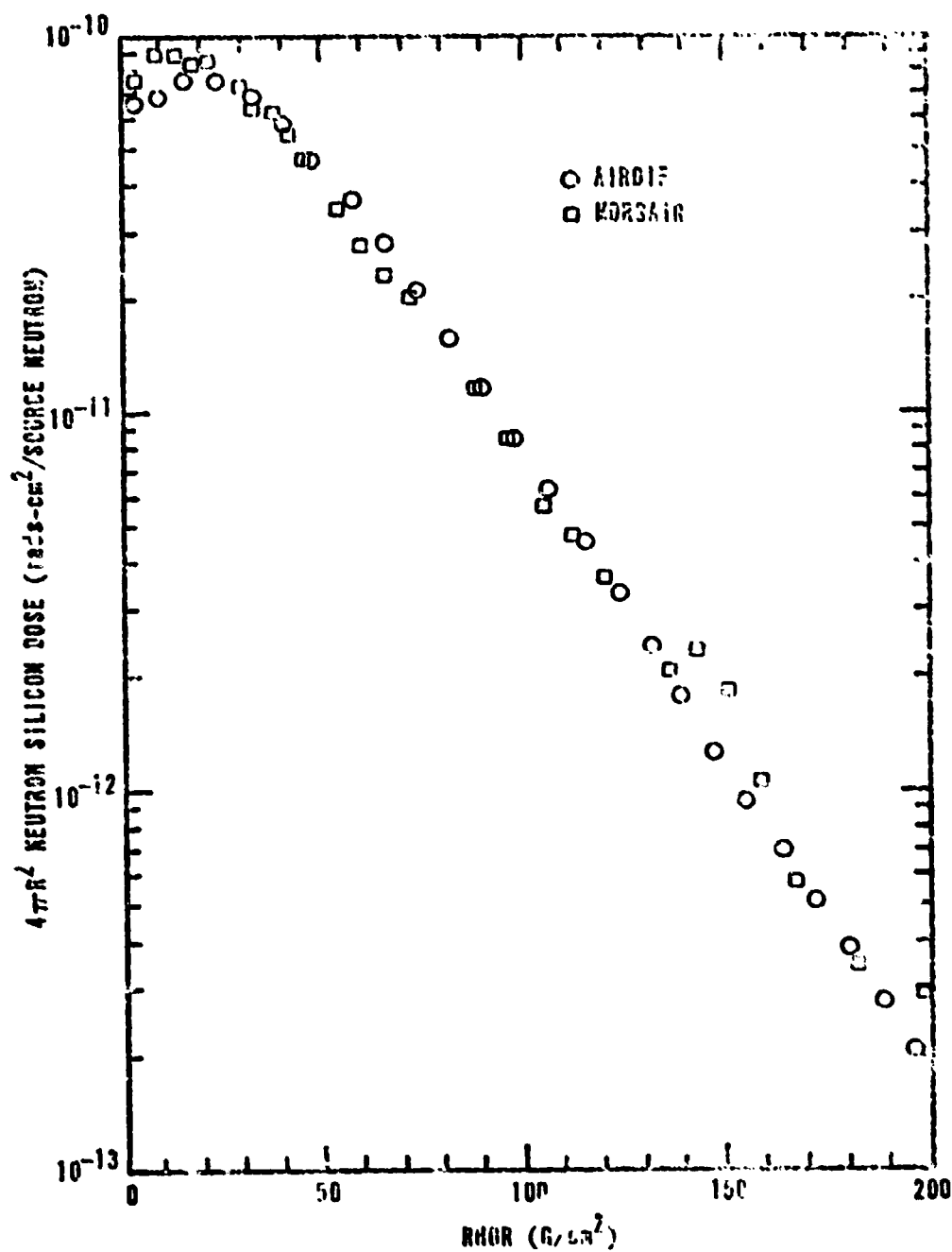


Figure C-5. Neutron Silicon Doses from a Fission Source at 15 km and Receivers at 15.29 km

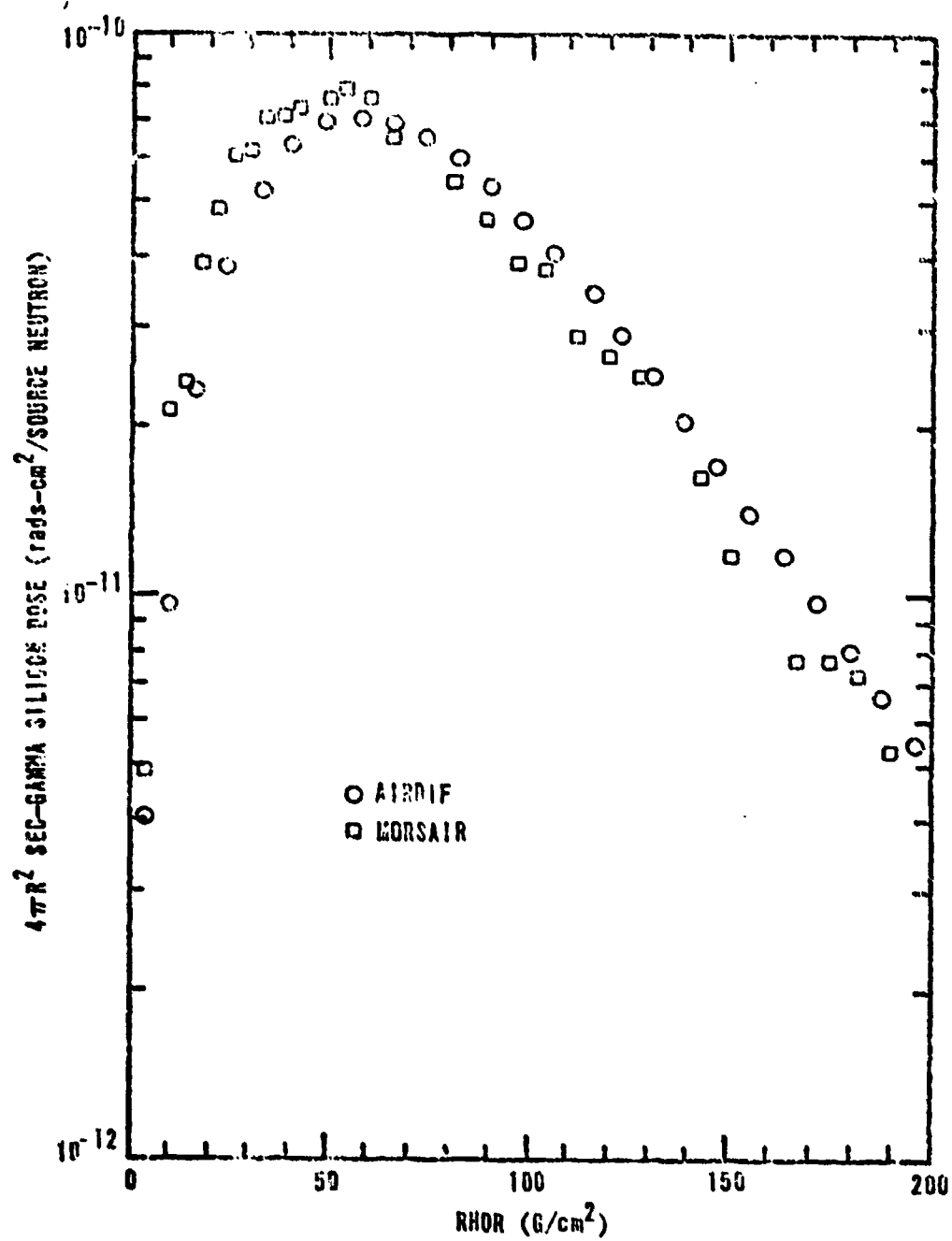


Figure C-6. Secondary Gamma Silicon Doses from a Fission Source at 15 km and Receivers at 15.29 km

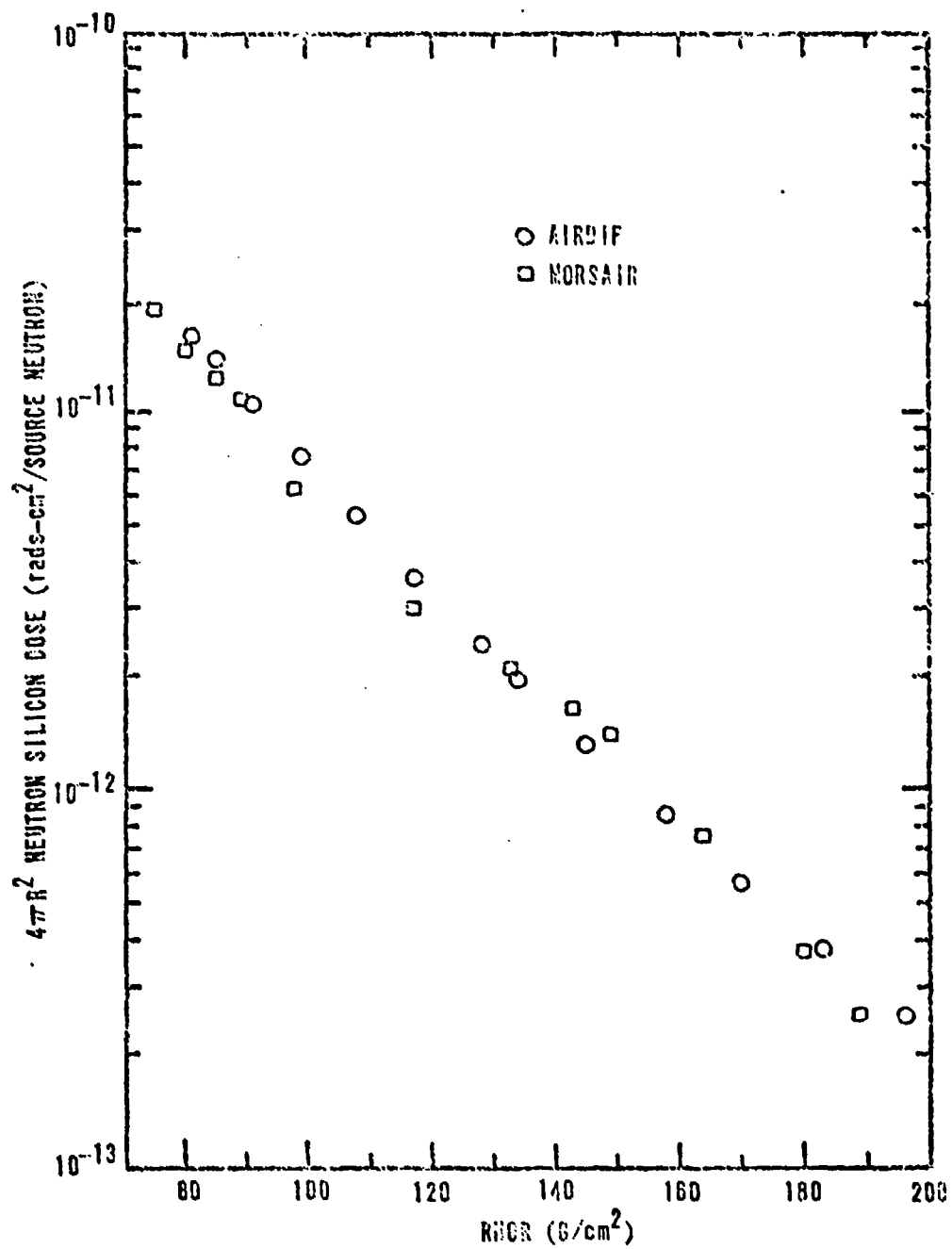


Figure C-7. Neutron Silicon Doses from a Fission Source at 15 km and Receivers at 21.66 km

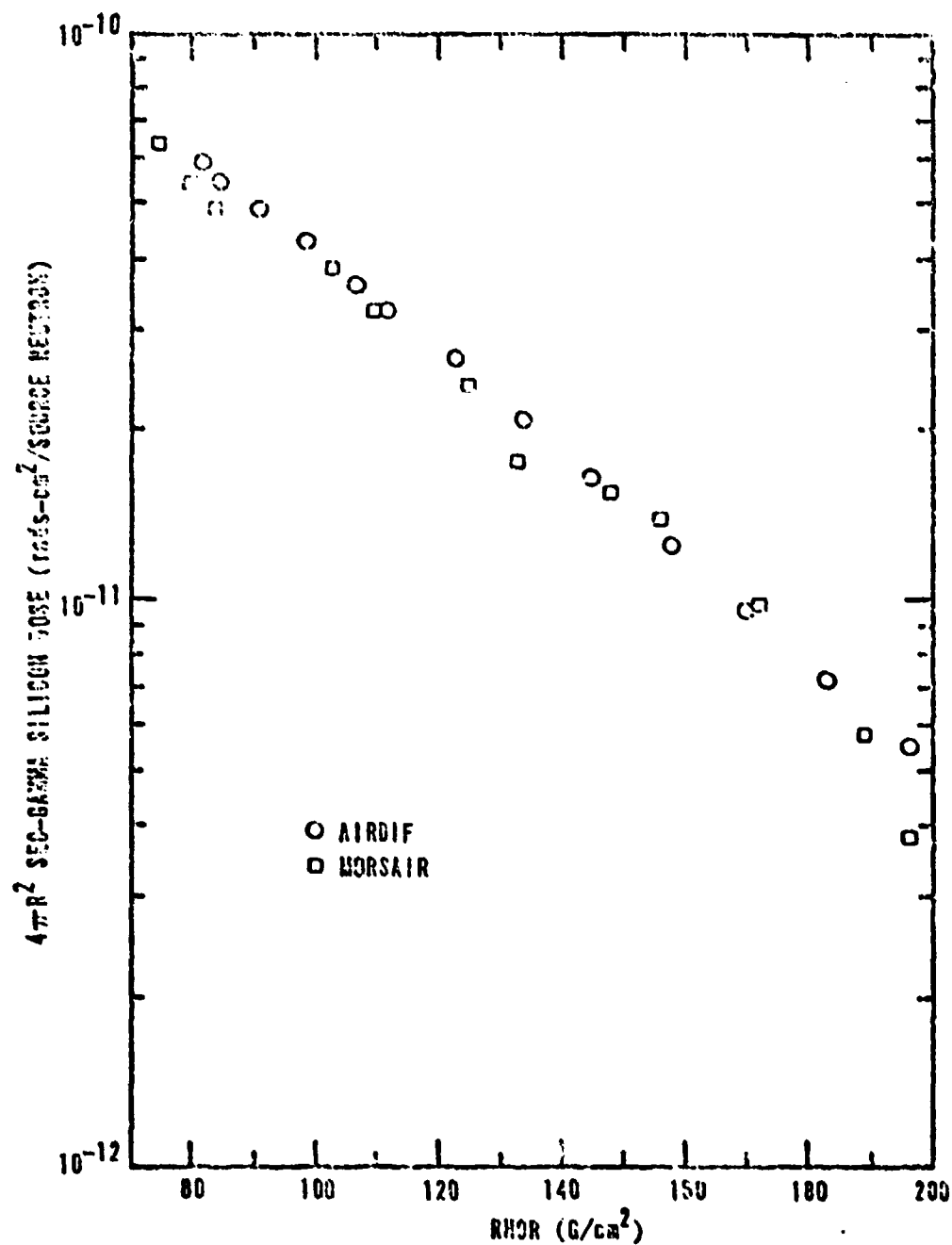


Figure C-8. Secondary Gamma Silicon Doses from a Fission Source at 15 km and Receivers at 21.66 km

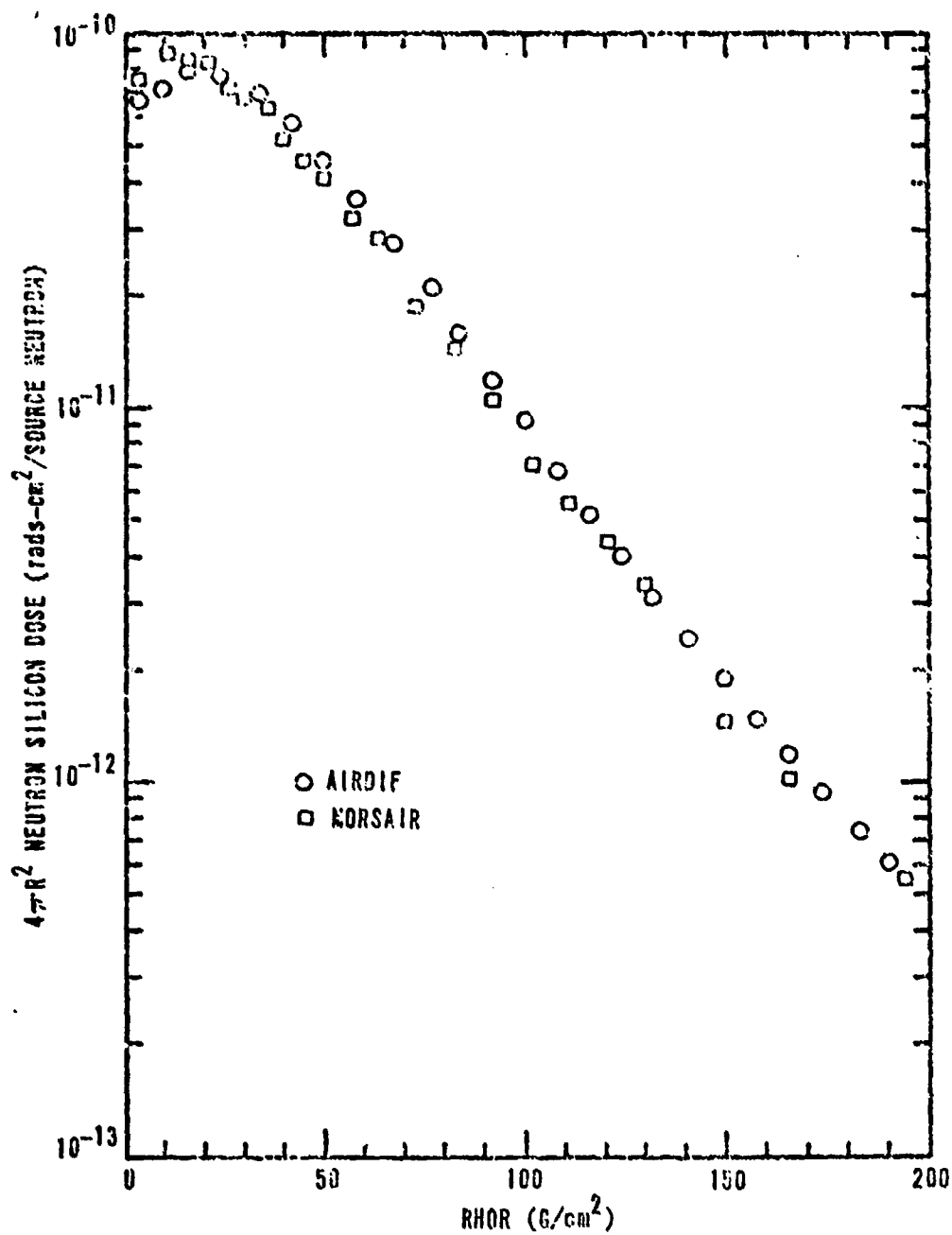


Figure C-9. Neutron Silicon Doses from a Fission Source at 20 km and Receivers at 20.61 km

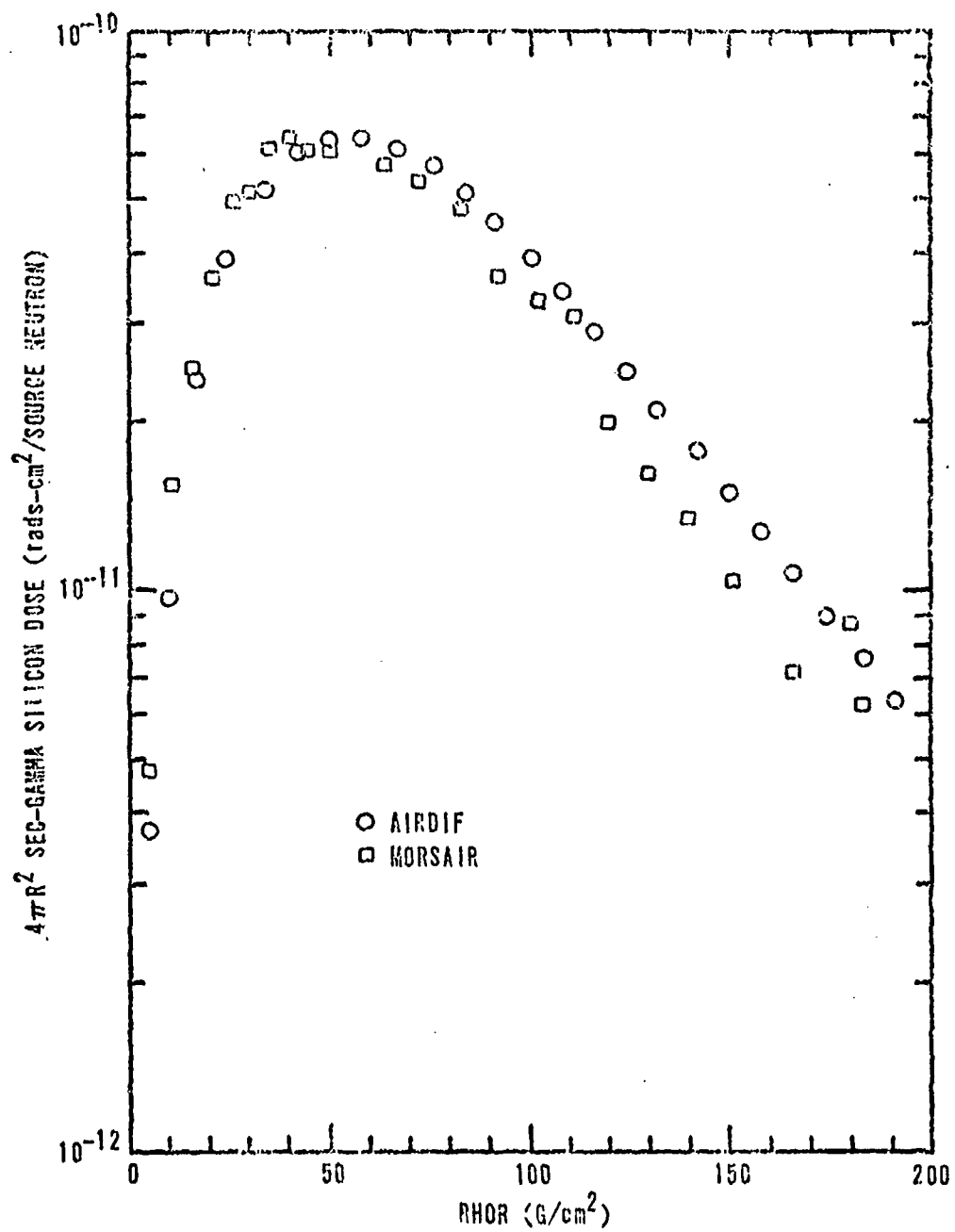


Figure C-10. Secondary Gamma Silicon Doses from a Fission Source at 20 km and Receivers at 20.61 km

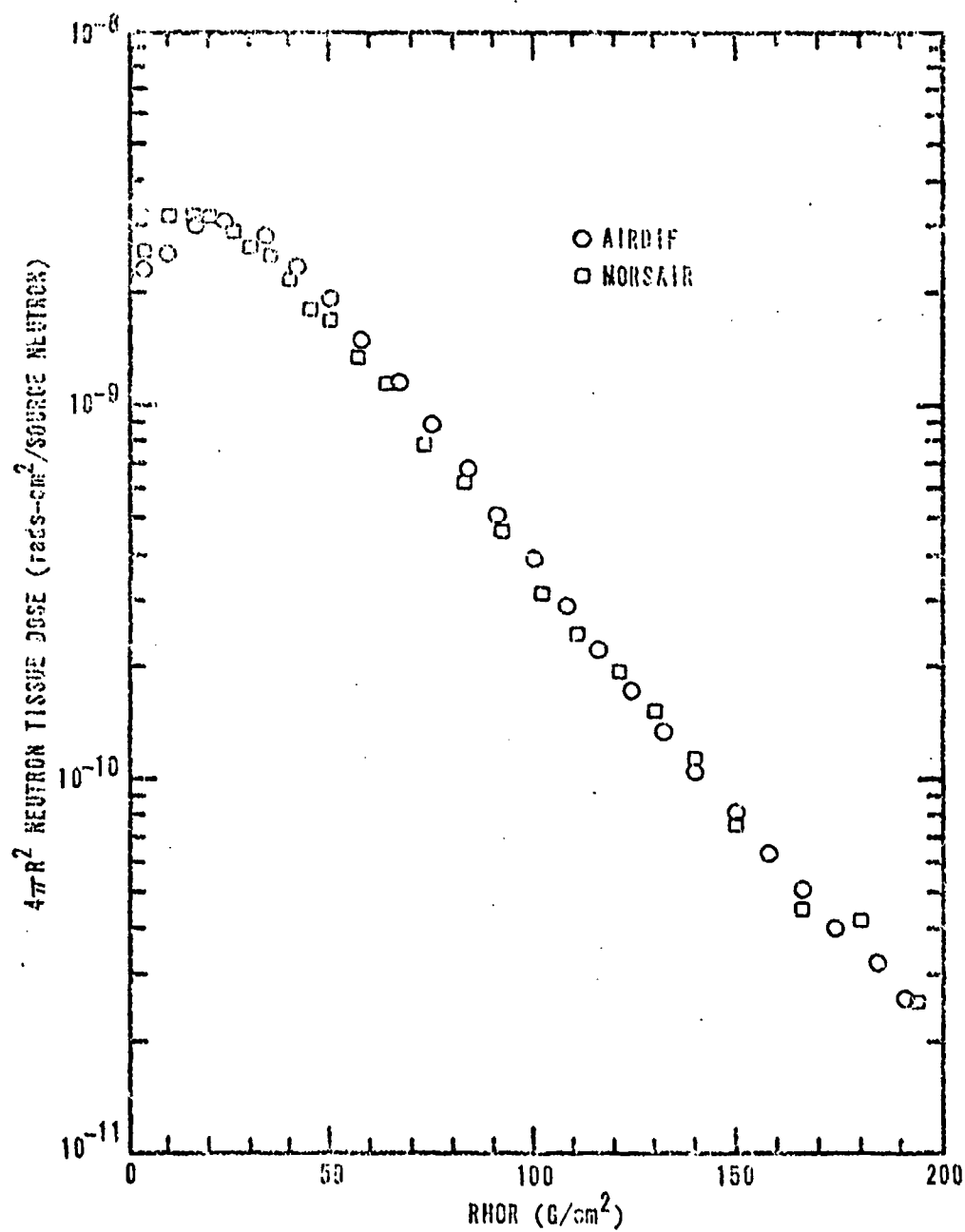


Figure C-11. Neutron Tissue Doses from a Fission Source at 20 km and Receivers at 20.61 km

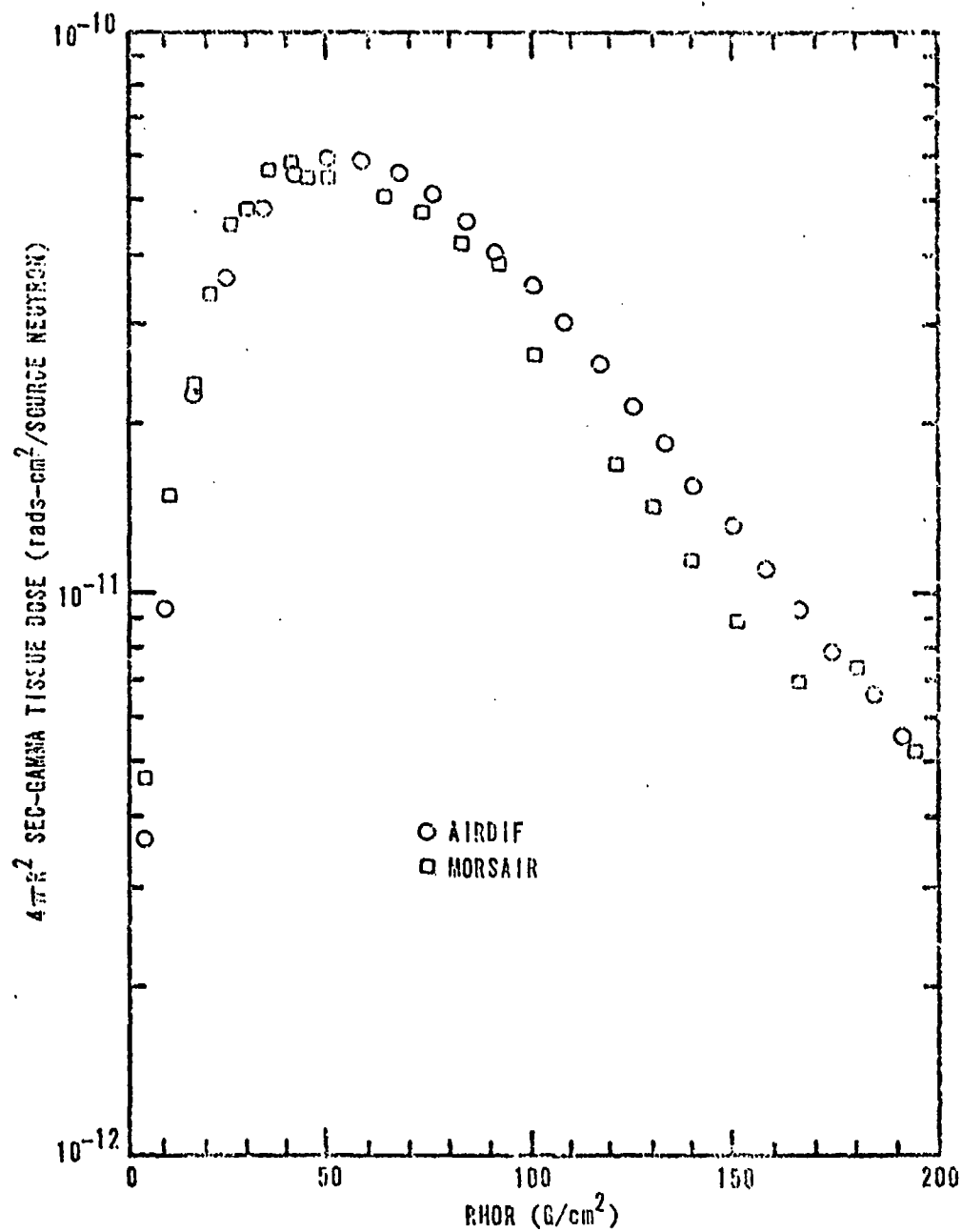


Figure C-12. Secondary Gamma Tissue Doses from a Fission Source at 20 km and Receivers at 20.61 km

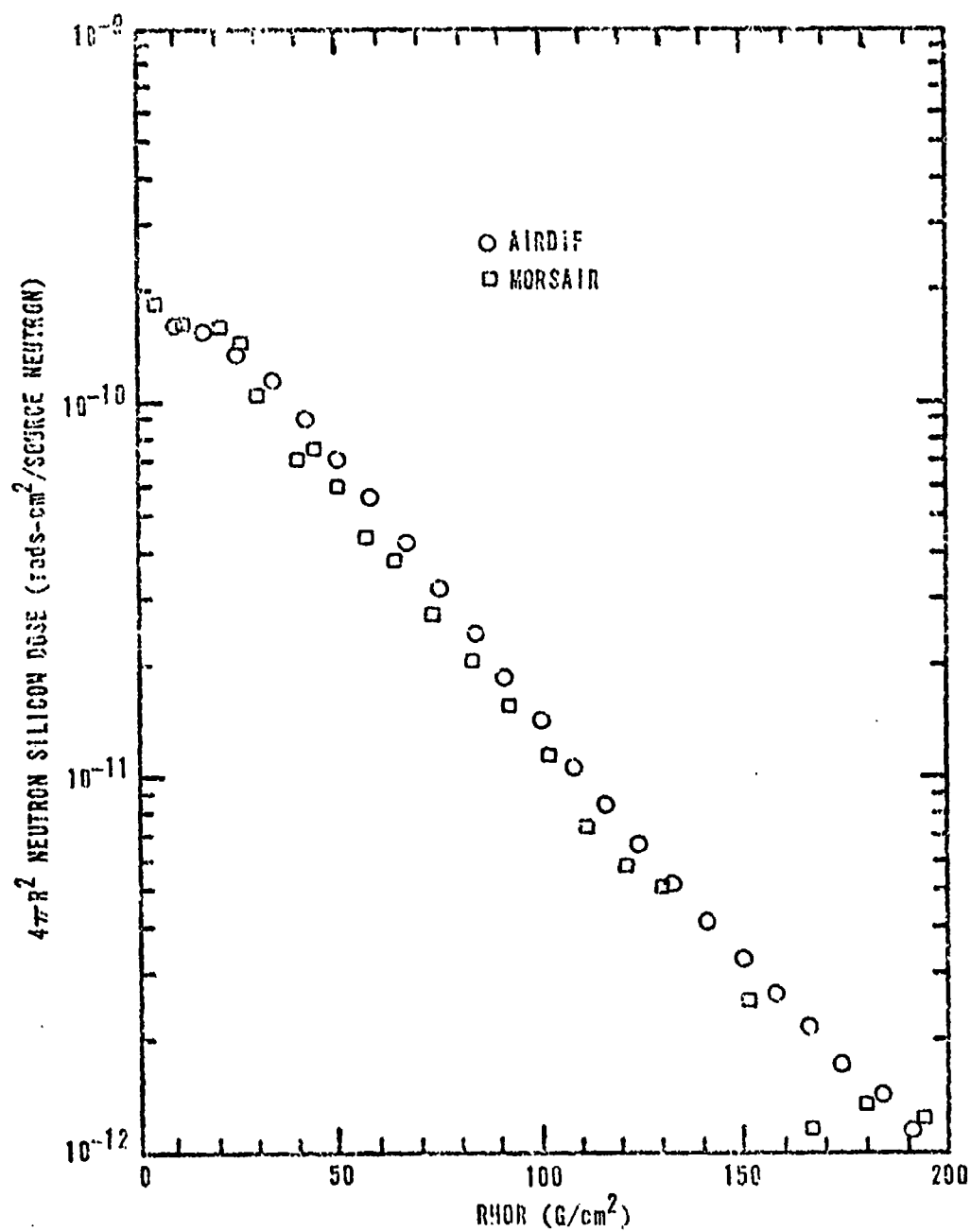


Figure C-13. Neutron Silicon Doses from a Thermonuclear Source at 20 km and Receivers at 20.61 km

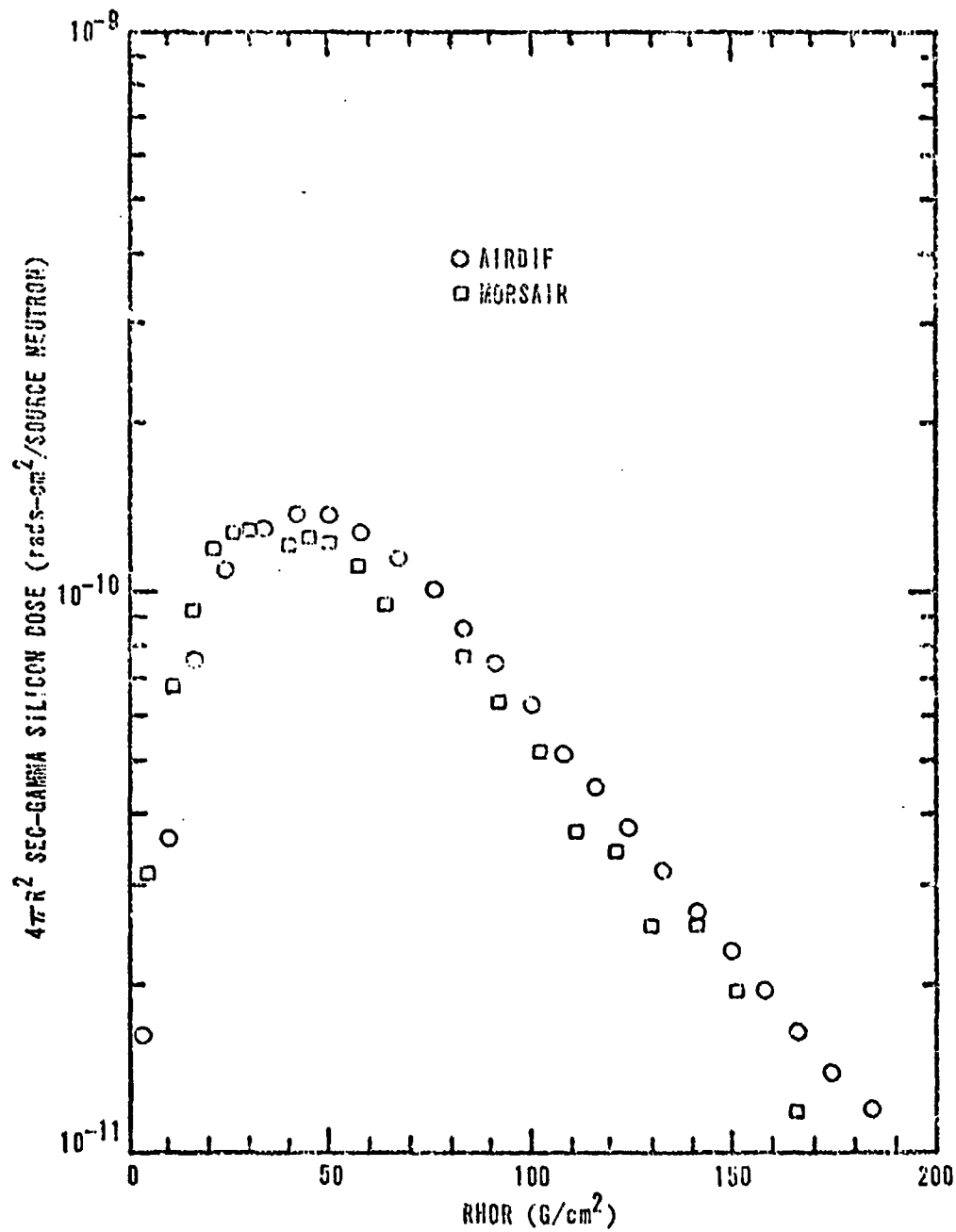


Figure C-14. Secondary Gamma Silicon Doses from a Thermonuclear Source at 20 km and Receivers at 20.61 km

Appendix D

K Factor Comparisons

This appendix contains comparisons of the AIRDIF and MORSAIR K factors. These comparisons are listed in Table VI and discussed in Section V. K factor comparisons are made for neutrons and secondary gammas, in terms of silicon and tissue dose response, for a fission and thermonuclear source, and out to mass ranges* of 200 g/cm².

*Mass range, $\langle \rho R \rangle$, is defined by equation (2.3). In this appendix, the symbol "RHOR" is used for $\langle \rho R \rangle$.

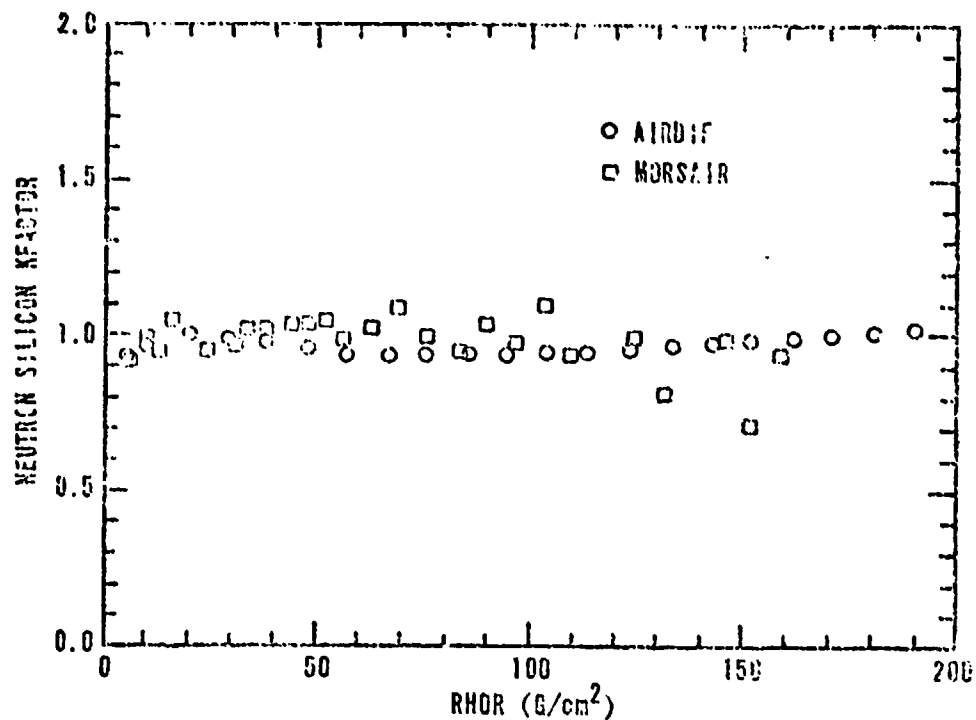


Figure D-1. Neutron Silicon K Factors for a Fission Source at 5 km and Receivers at 5.07 km

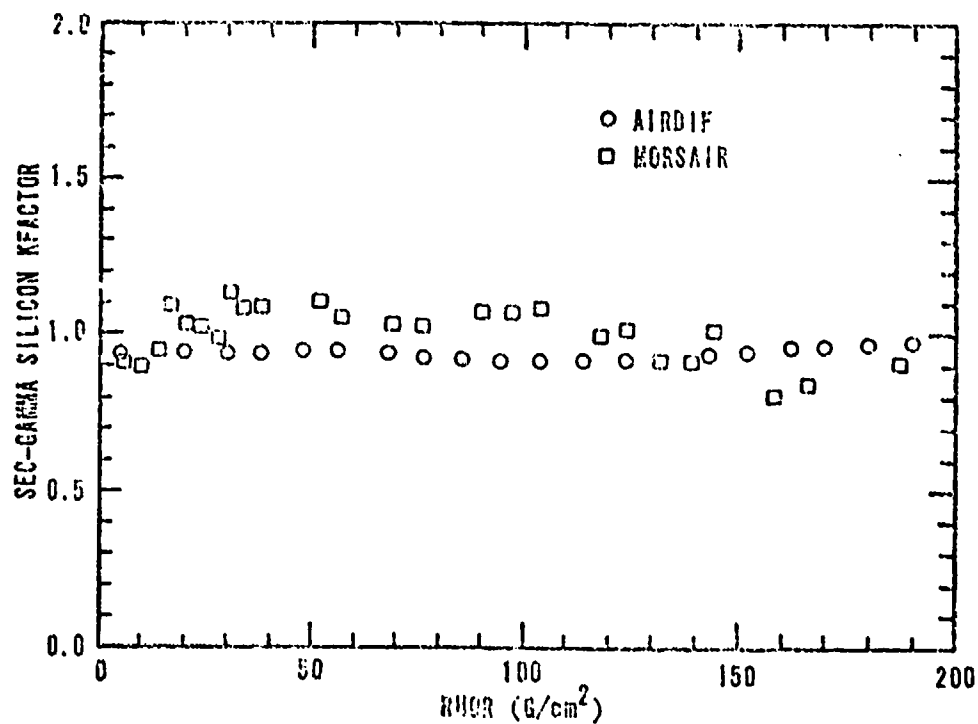


Figure D-2. Secondary Gamma Silicon K Factors for a Fission Source at 5 km and Receivers at 5.07 km

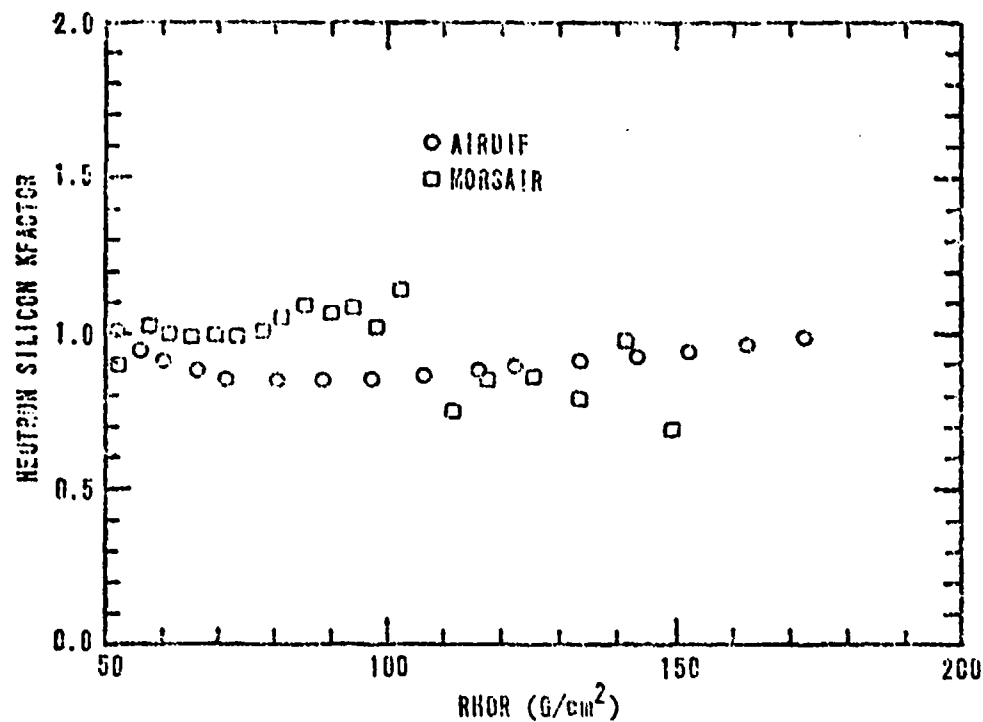


Figure D-3. Neutron Silicon K Factors for a Fission Source at 10 km and Receivers at 8.84 km

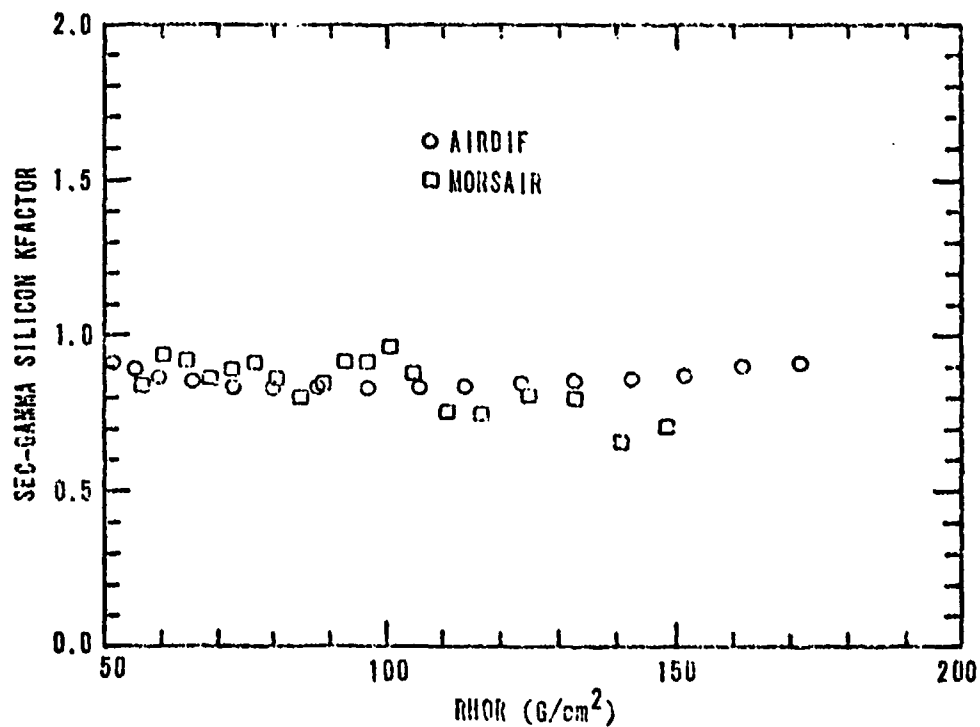


Figure D-4. Secondary Gamma Silicon K Factors for a Fission Source at 10 km and Receivers at 8.84 km

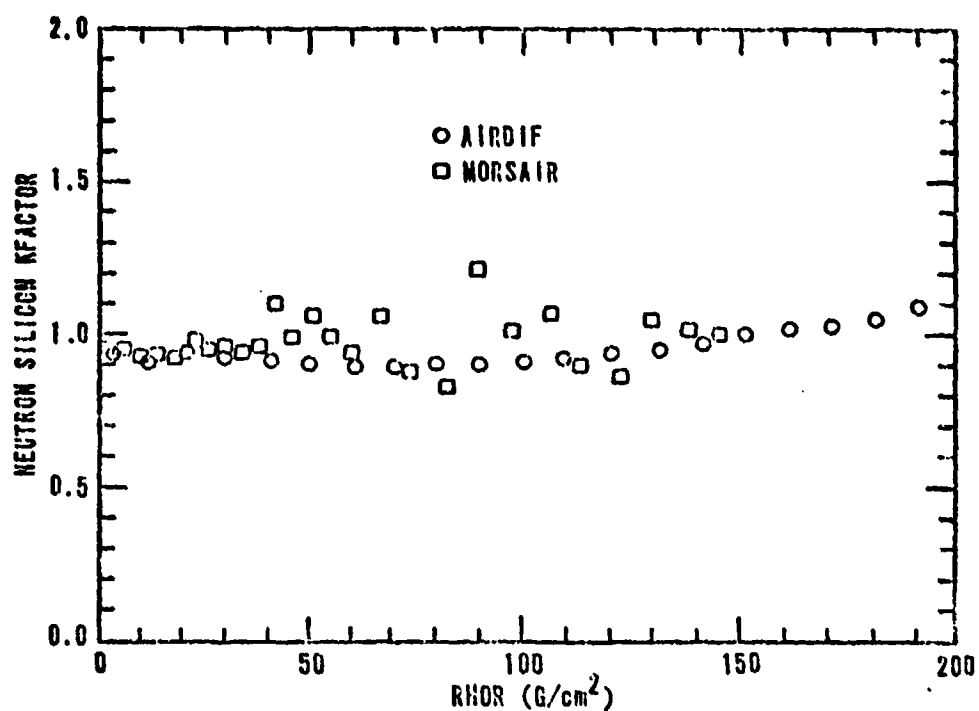


Figure D-5. Neutron Silicon K Factors for a Fission Source at 10 km and Receivers at 10 km

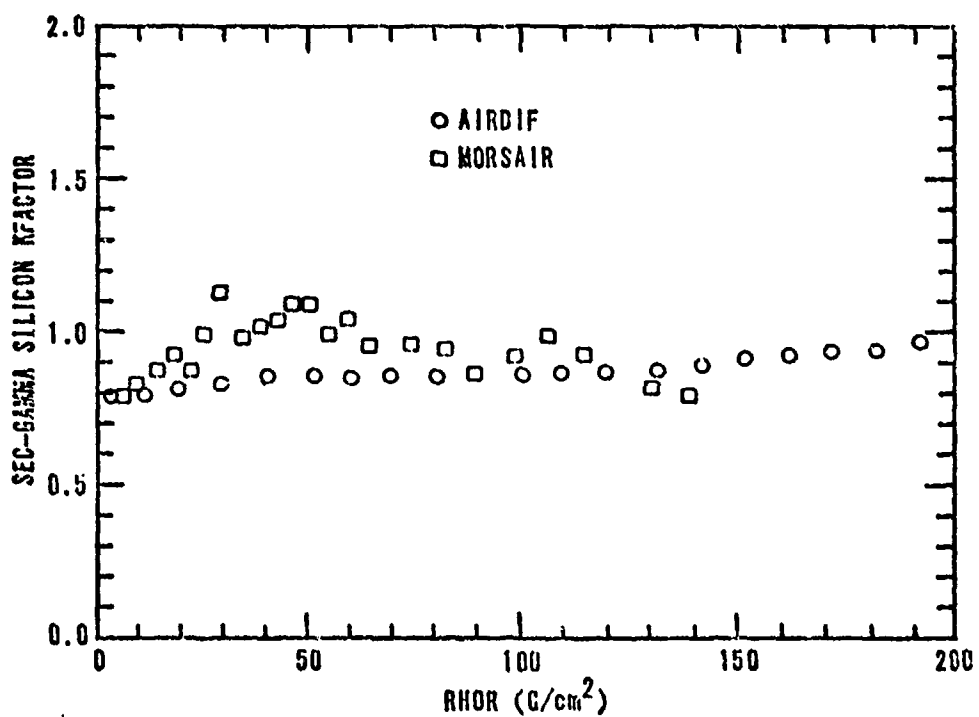


Figure D-6. Secondary Gamma Silicon k Factors for a Fission Source at 10 km and Receivers at 10 km

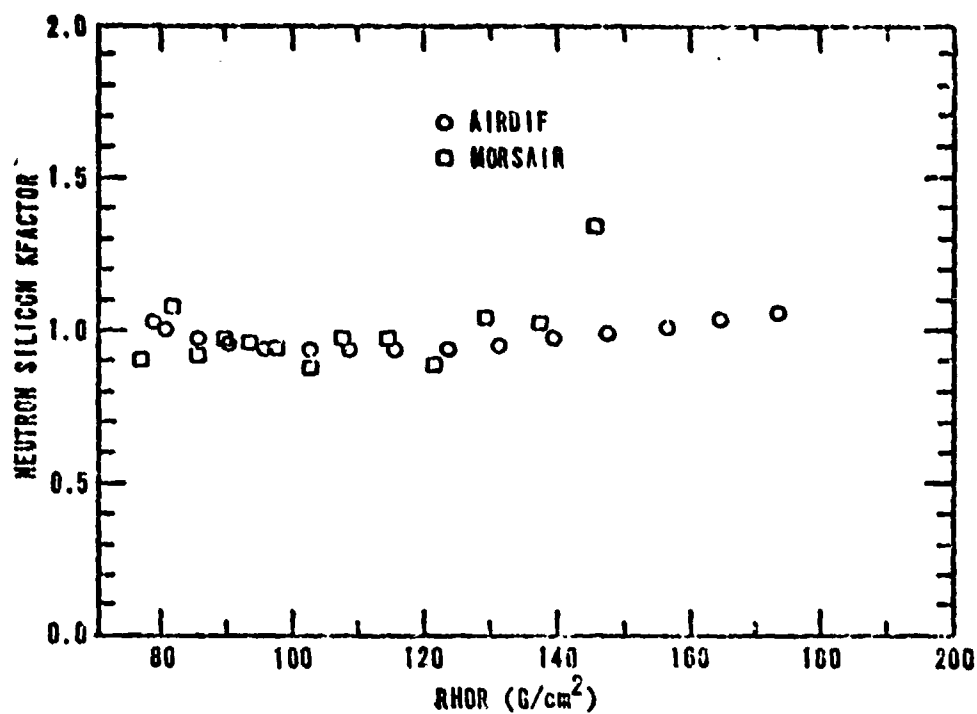


Figure D-7. Neutron Silicon K Factors for a Fission Source at 10 km and Receivers at 12.13 km

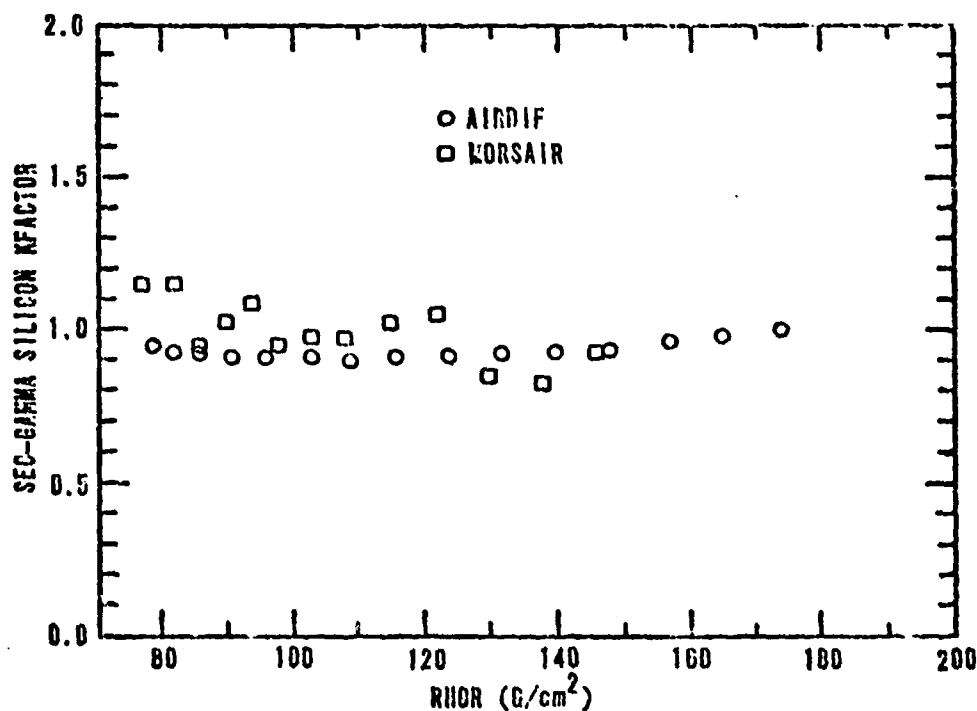


Figure D-8. Secondary Gamma Silicon K Factors for a Fission Source at 10 km and Receivers at 12.13 km

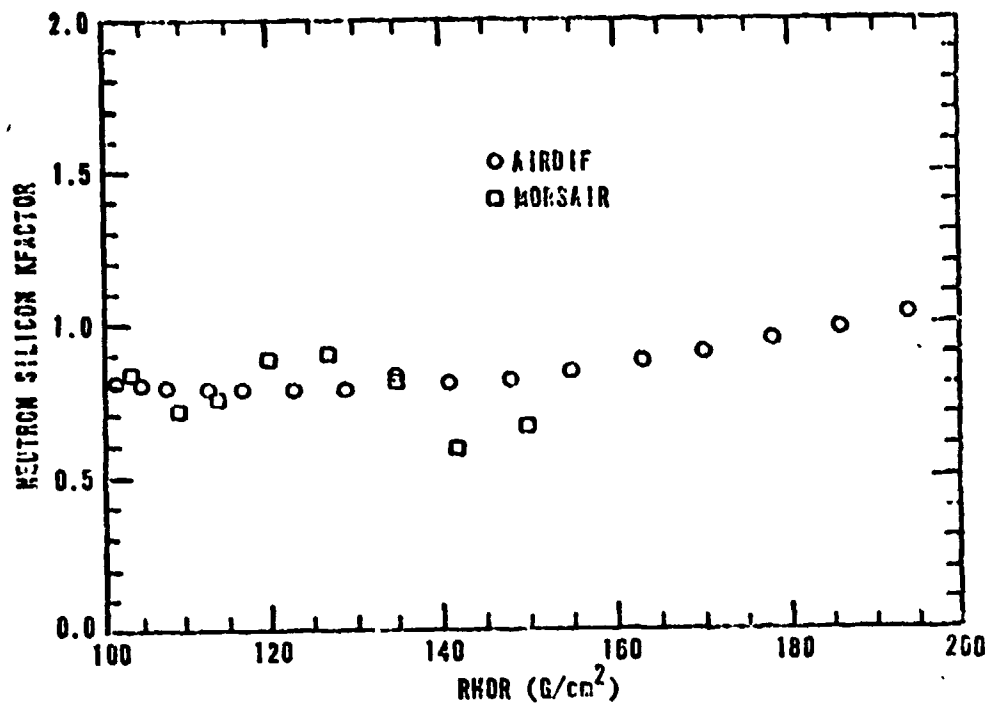


Figure D-9. Neutron Silicon K Factors for a Fission Source at 15 km and Receivers at 11.30 km

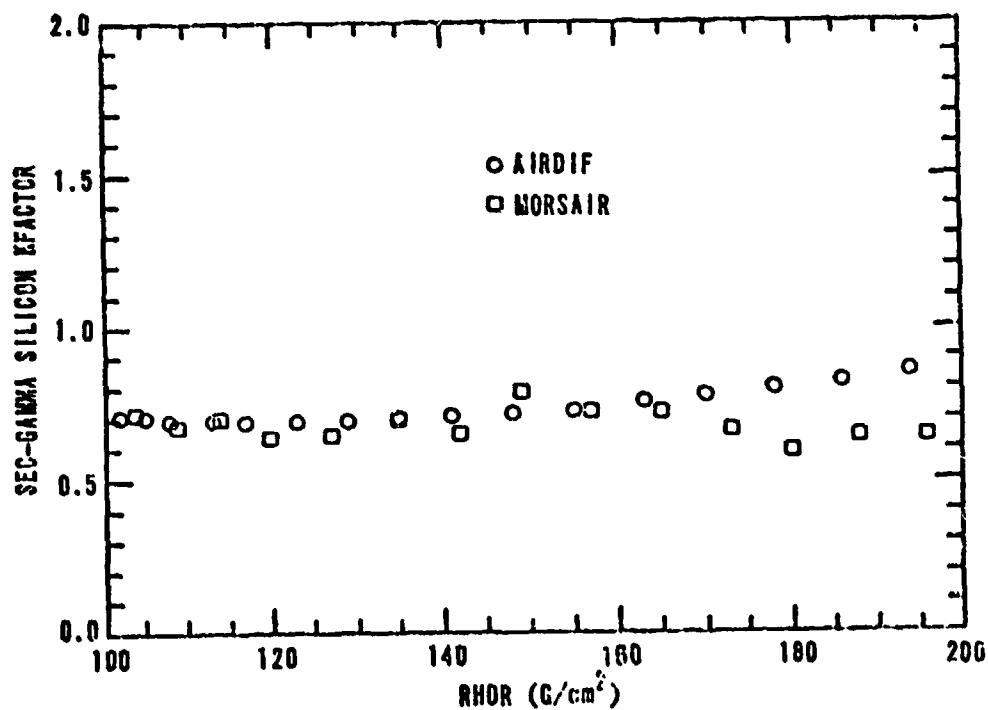


Figure D-10. Secondary Gamma Silicon K Factors for a Fission Source at 15 km and Receivers at 11.30 km

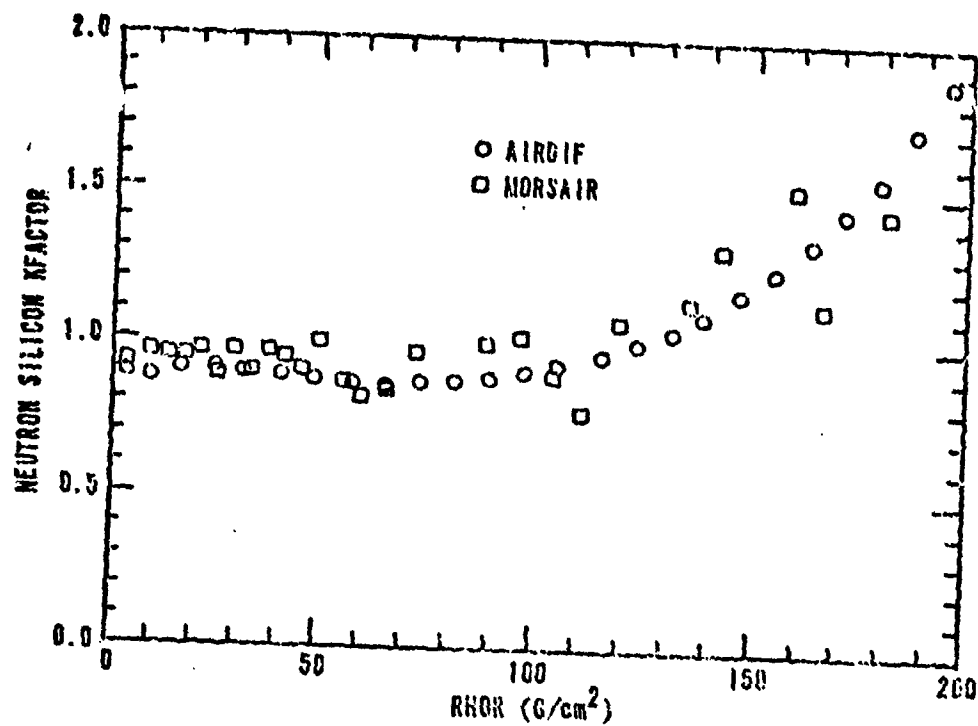


Figure D-11. Neutron Silicon K Factors for a Fission Source at 15 km and Receivers at 15.29 km

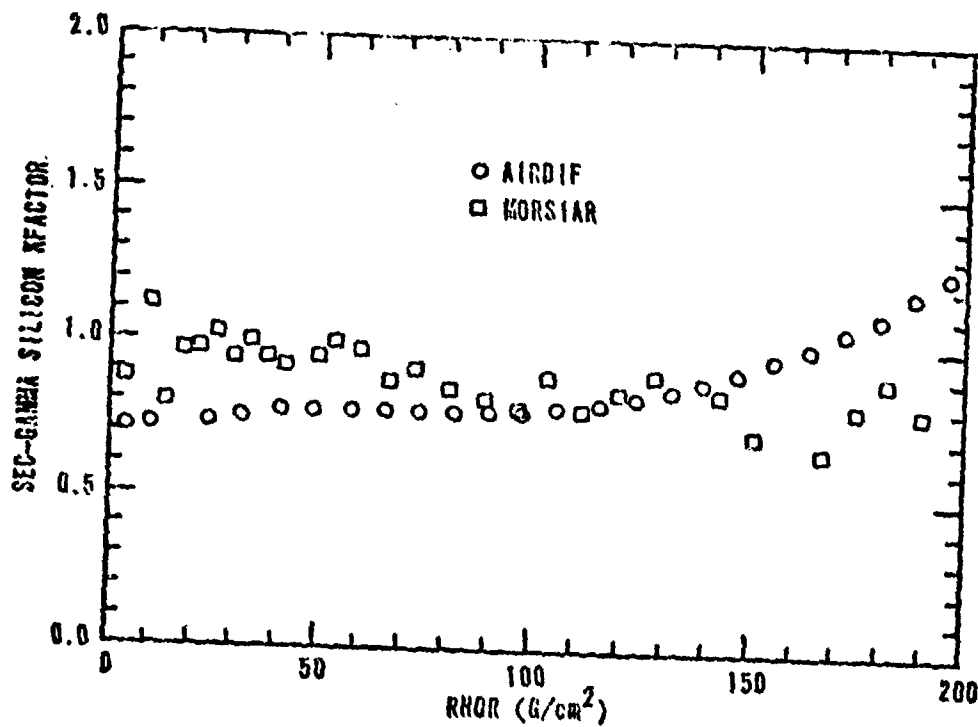


Figure D-12. Secondary Gamma Silicon K Factors for a Fission Source at 15 km and Receivers at 15.29 km

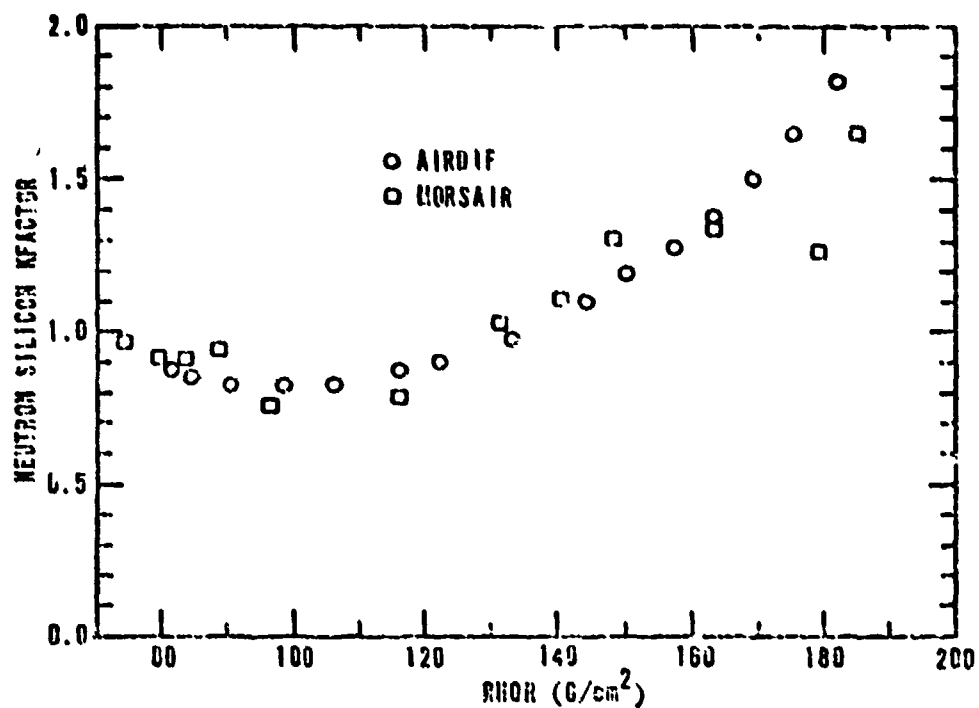


Figure D-13. Neutron Silicon K Factors for a Fission Source at 15 km and Receivers at 21.66 km

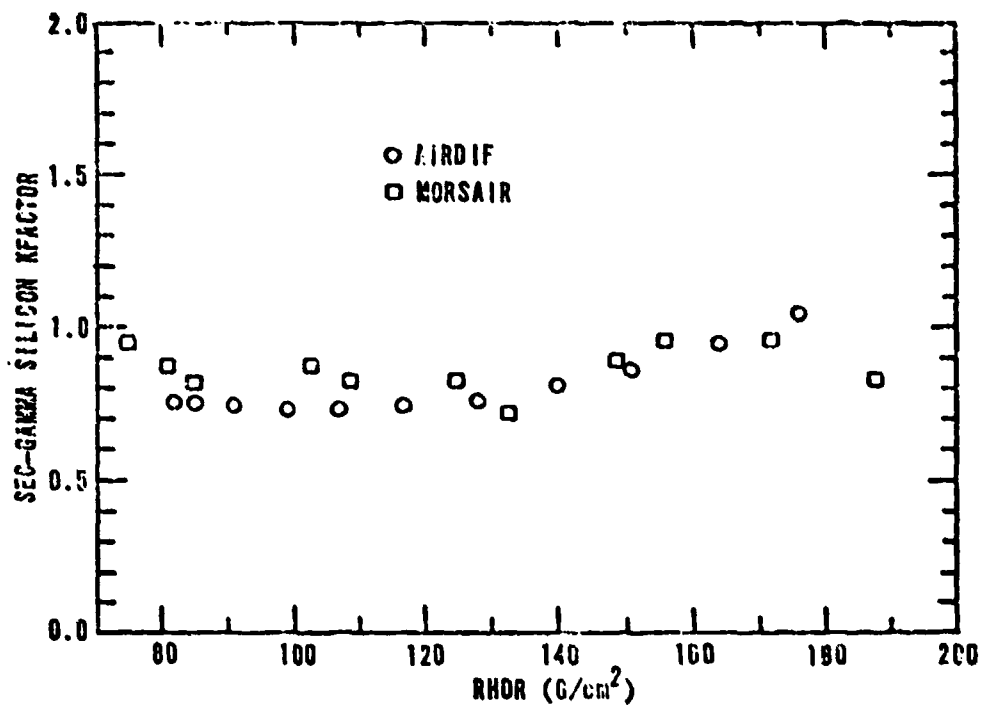


Figure D-14. Secondary Gamma Silicon K Factors for a Fission Source at 15 km and Receivers at 21.66 km

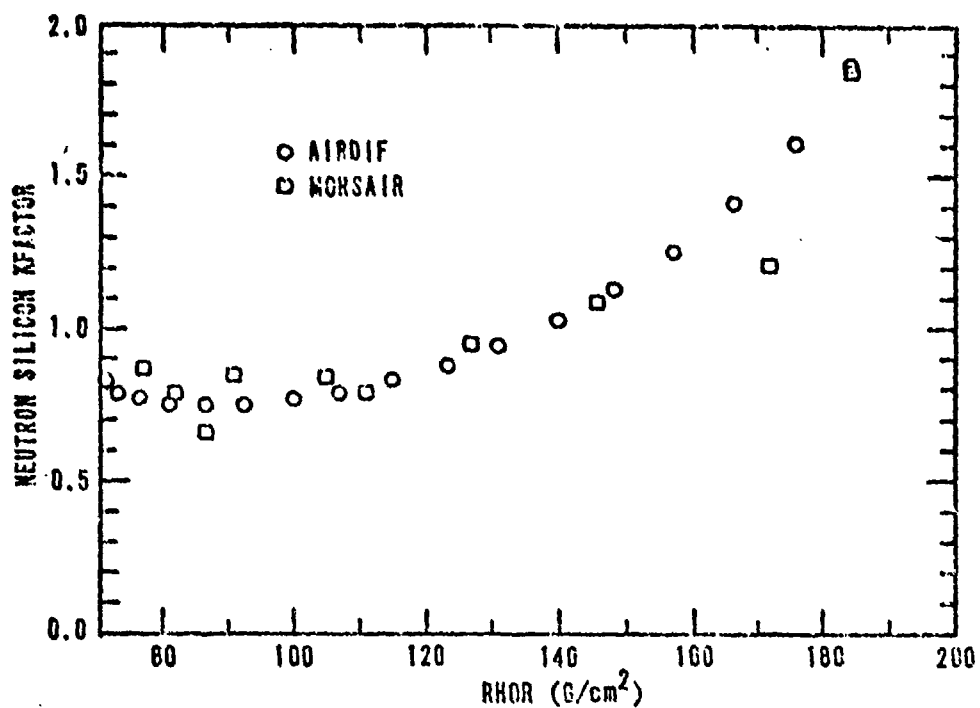


Figure D-15. Neutron Silicon K Factors for a Fission Source at 20 km and Receivers at 14.85 km

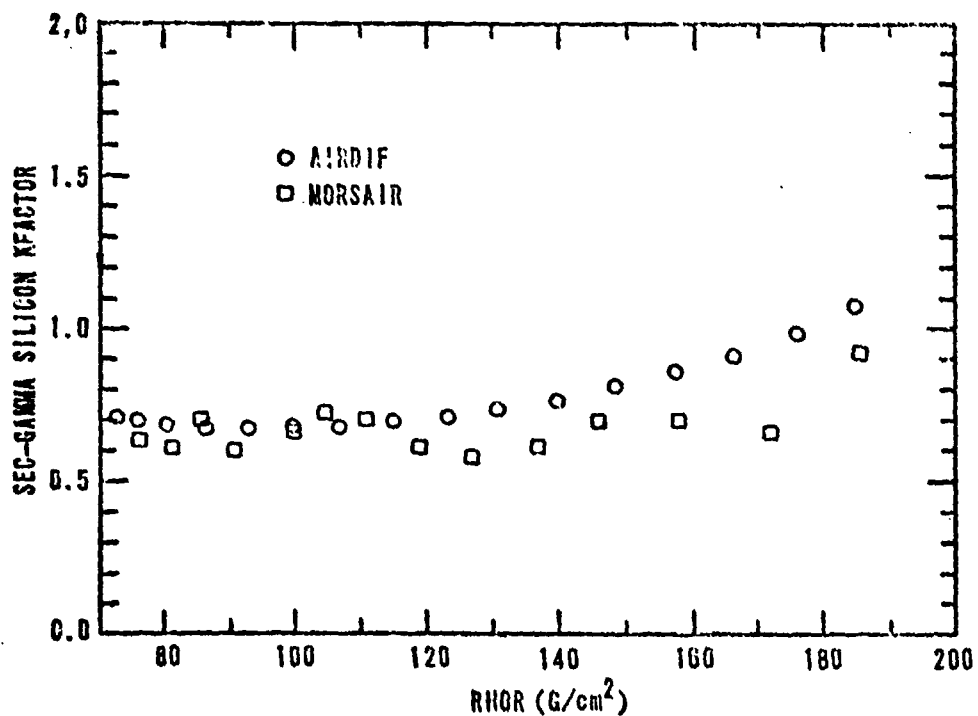


Figure D-16. Secondary Gamma Silicon K Factors for a Fission Source at 20 km and Receivers at 14.85 km

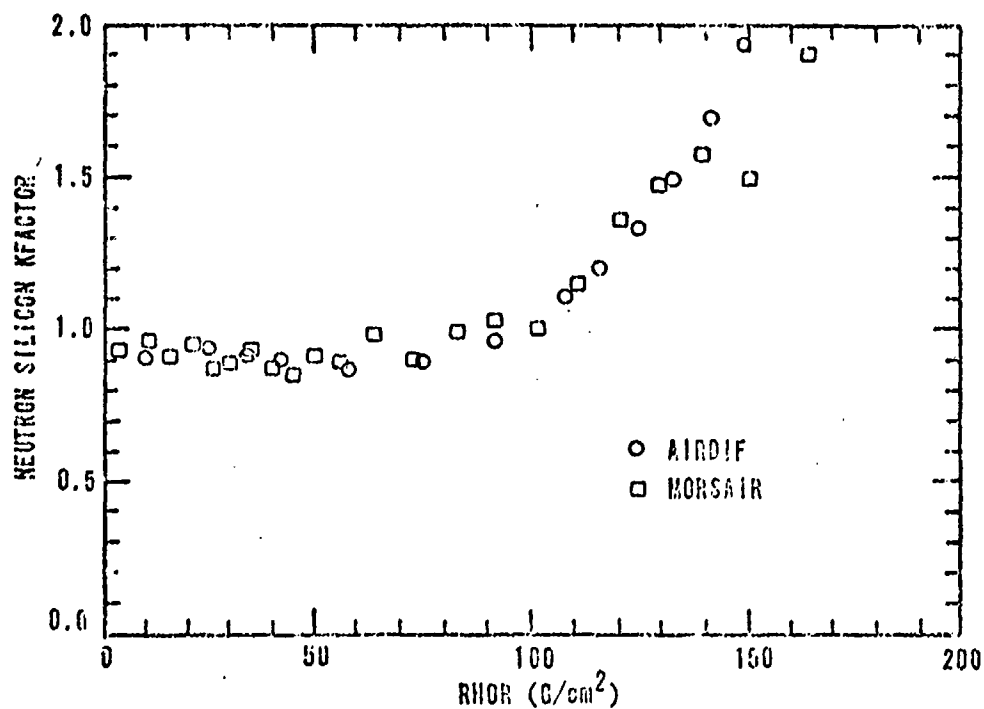


Figure D-17. Neutron Silicon K Factors for a Fission Source at 20 km and Receivers at 20.61 km

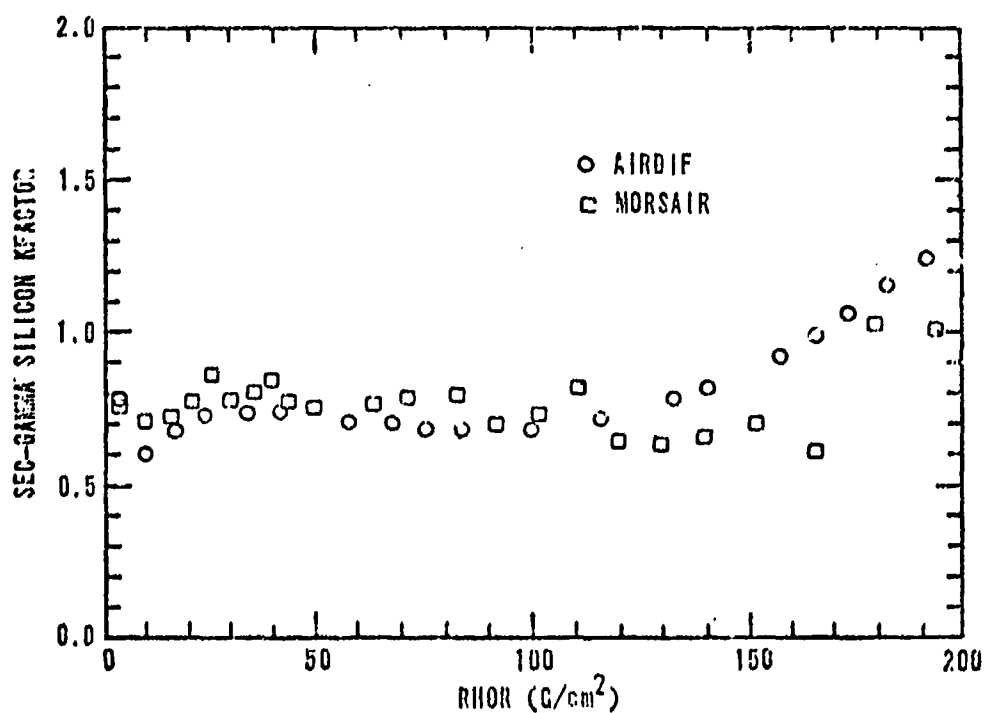


Figure D-18. Secondary Gamma Silicon K Factors for a Fission Source at 20 km and Receivers at 20.61 km

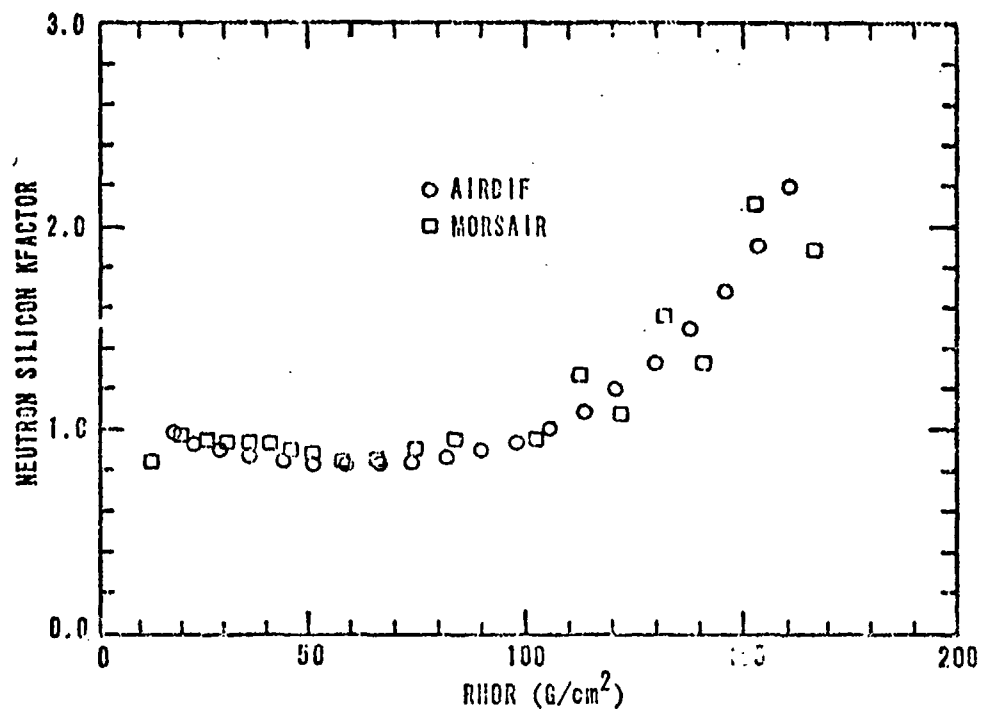


Figure D-19. Neutron Silicon K Factors for a Fission Source at 20 km and Receivers at 22.08 km

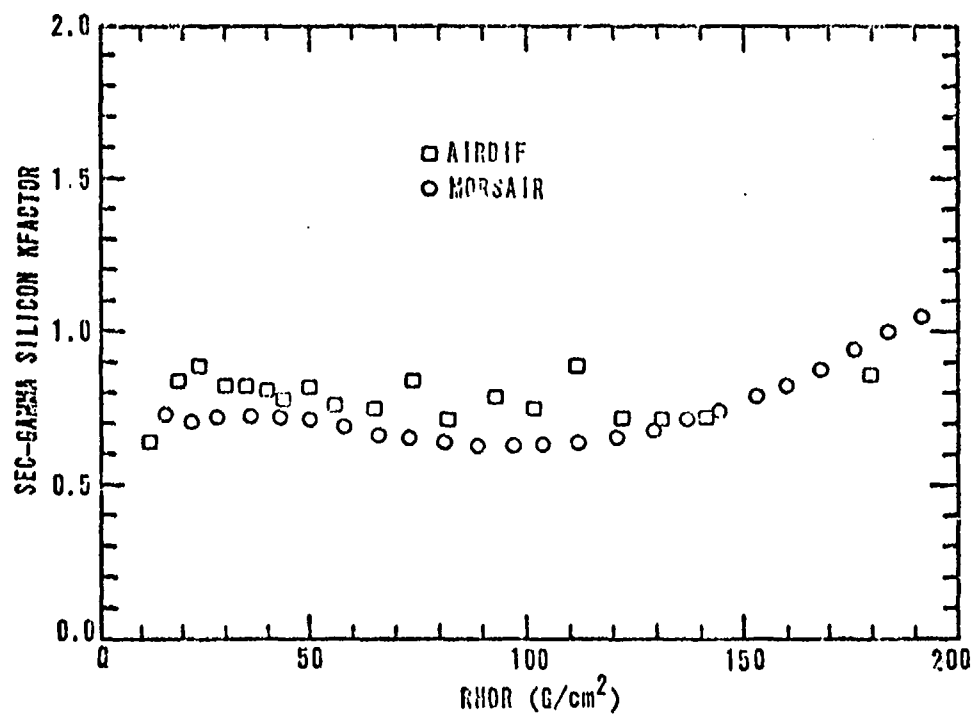


Figure D-20. Secondary Gamma Silicon K Factors for a Fission Source at 20 km and Receivers at 22.08 km

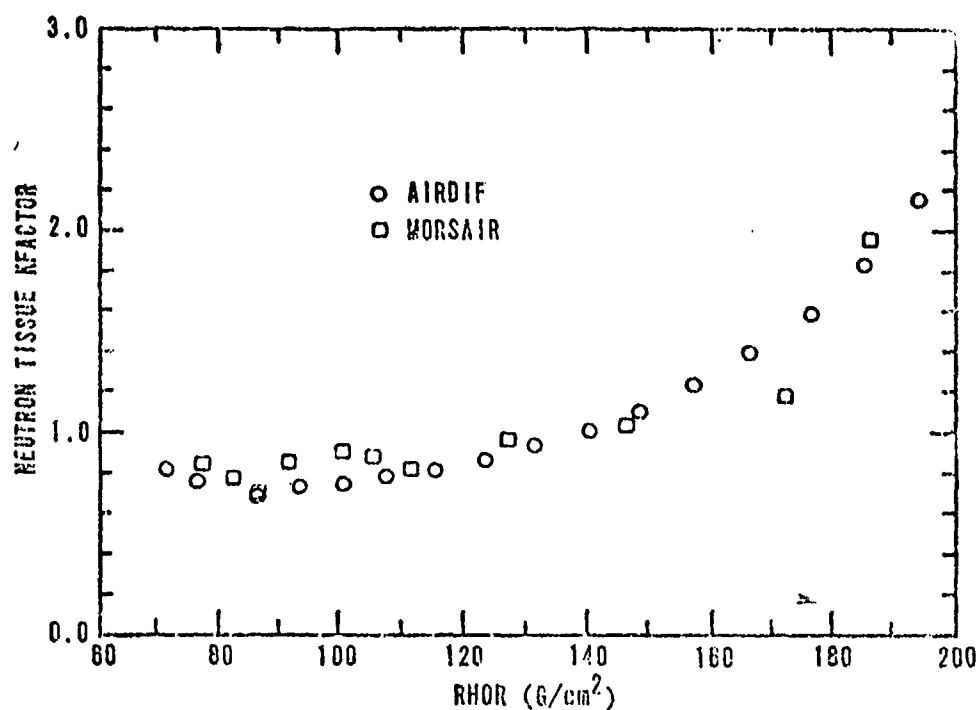


Figure D-21. Neutron Tissue K Factors for a Fission Source at 20 km and Receivers at 14.85 km

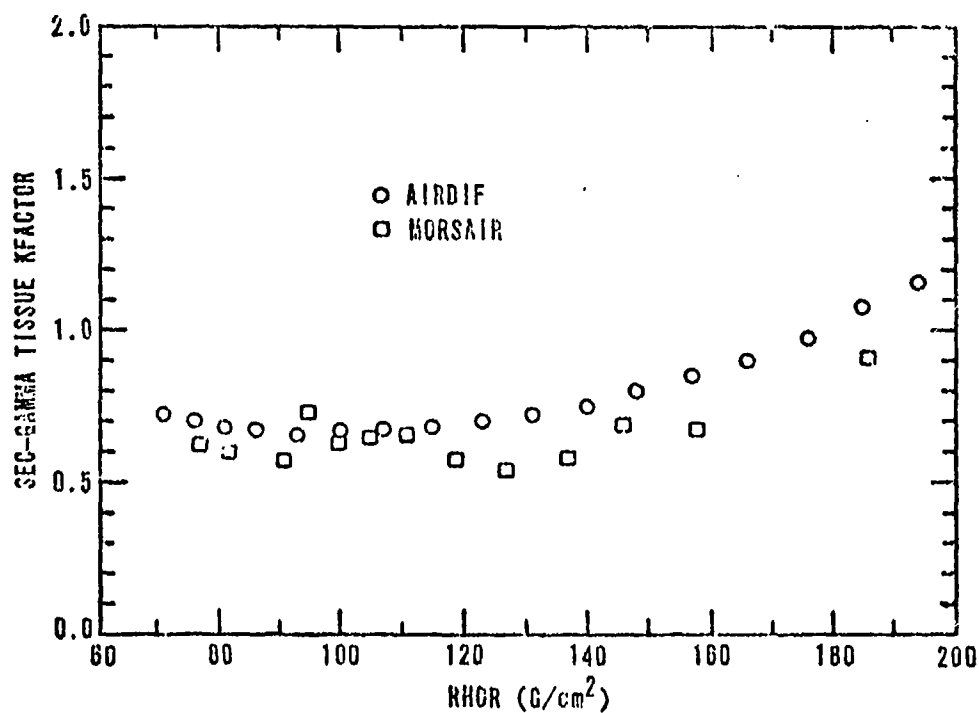


Figure D-22. Secondary Gamma Tissue K Factors for a Fission Source at 20 km and Receivers at 14.85 km

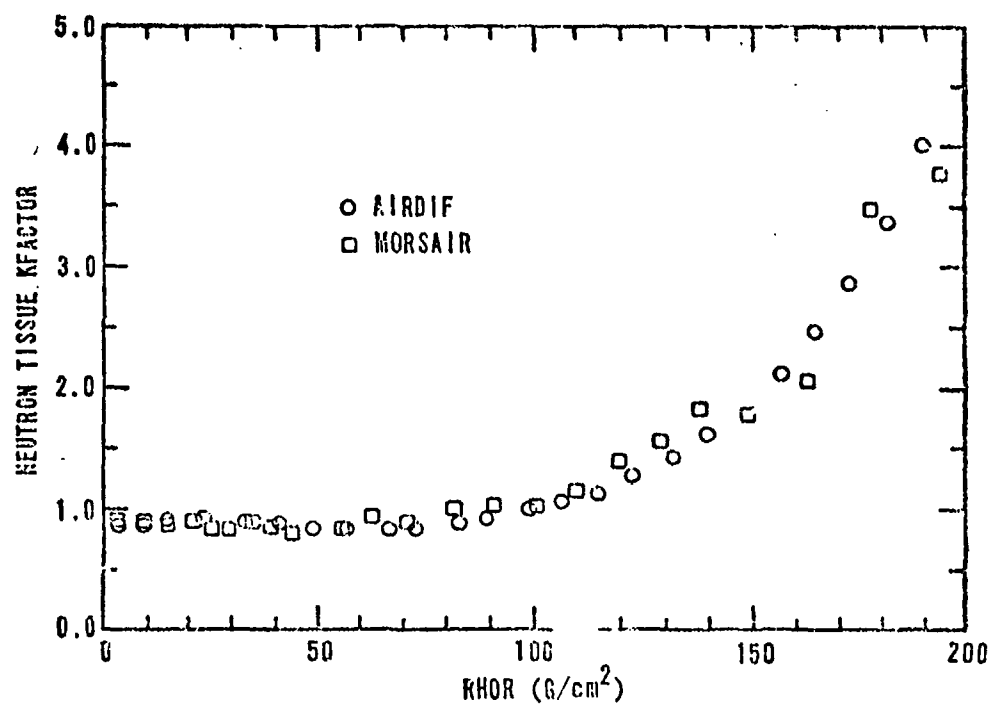


Figure D-23. Neutron Tissue K Factors for a Fission Source at 20 km and Receivers at 20.61 km

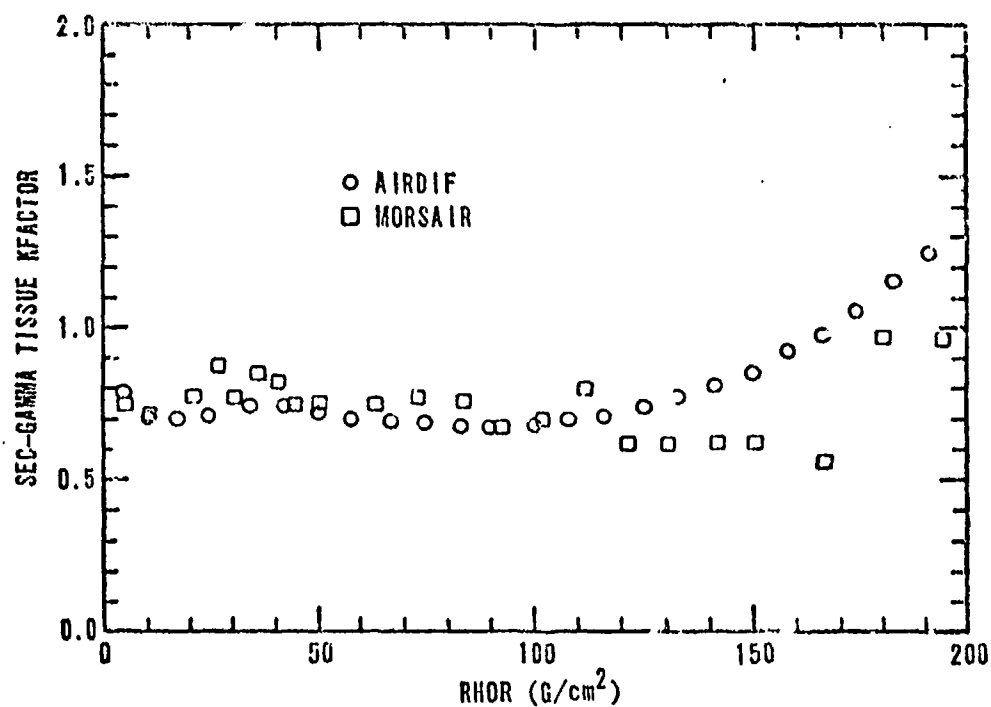


Figure D-24. Secondary Gamma Tissue K Factors for a Fission Source at 20 km and Receivers at 20.61 km

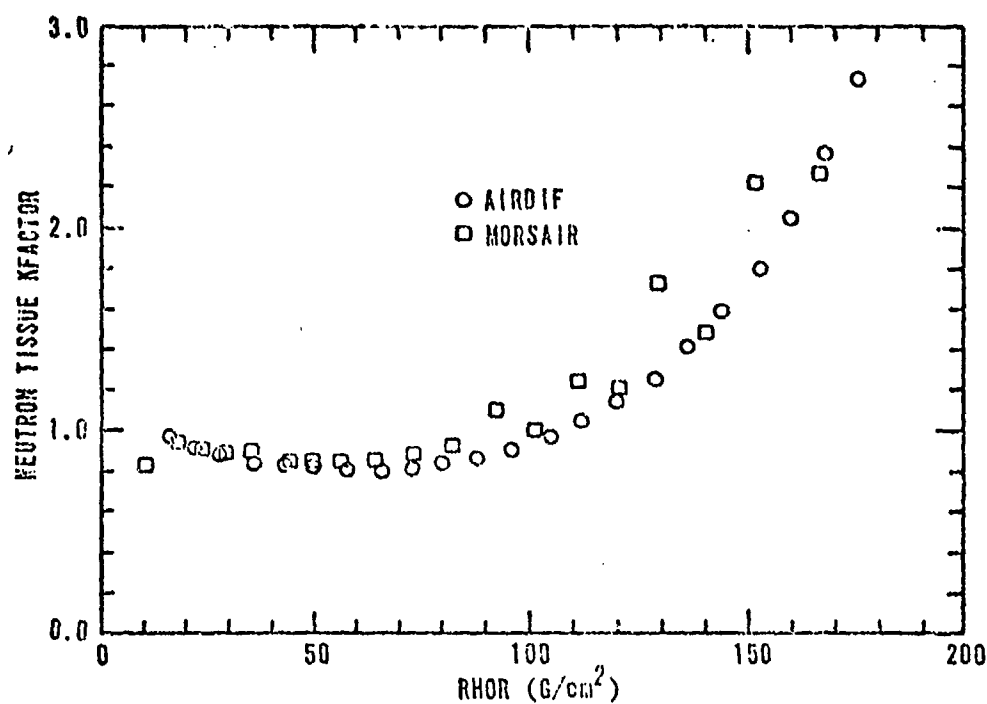


Figure D-25. Neutron Tissue K Factors for a Fission Source at 20 km and Receivers at 22.08 km

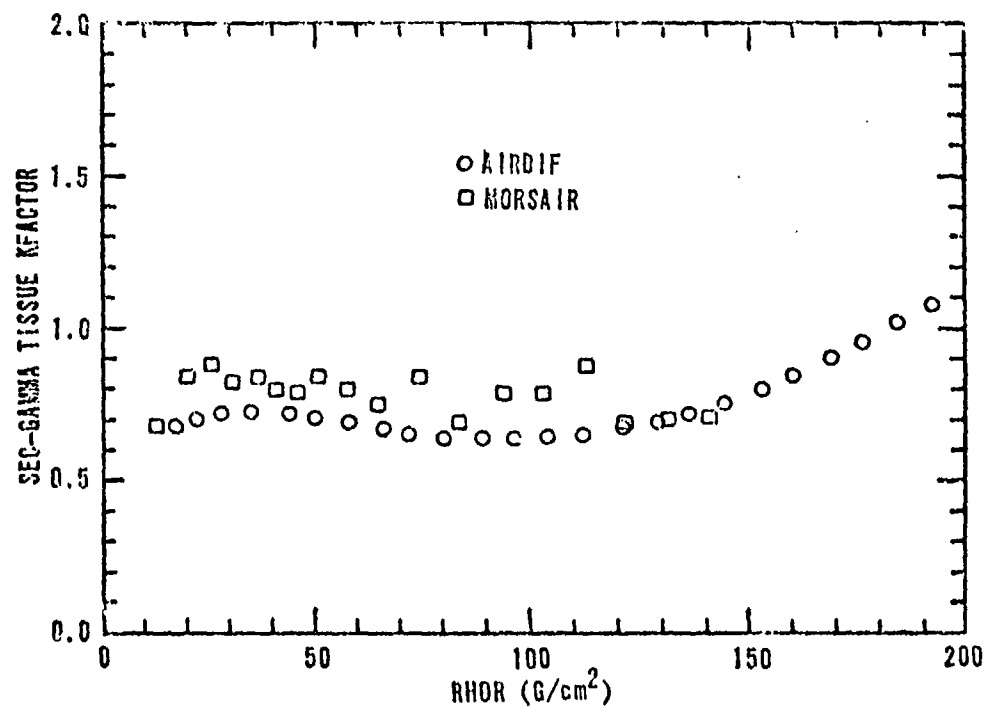


Figure D-26. Secondary Gamma Tissue K Factors for a Fission Source at 20 km and Receivers at 22.08 km

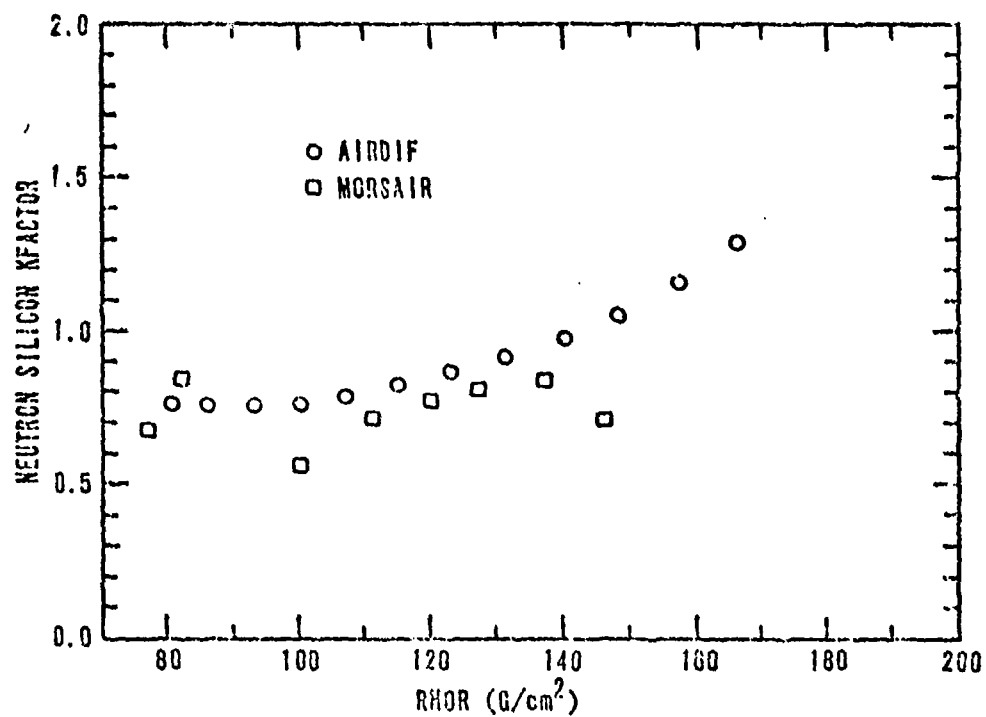


Figure D-27. Neutron Silicon K Factors for a Thermonuclear Source at 20 km and Receivers at 14.85 km

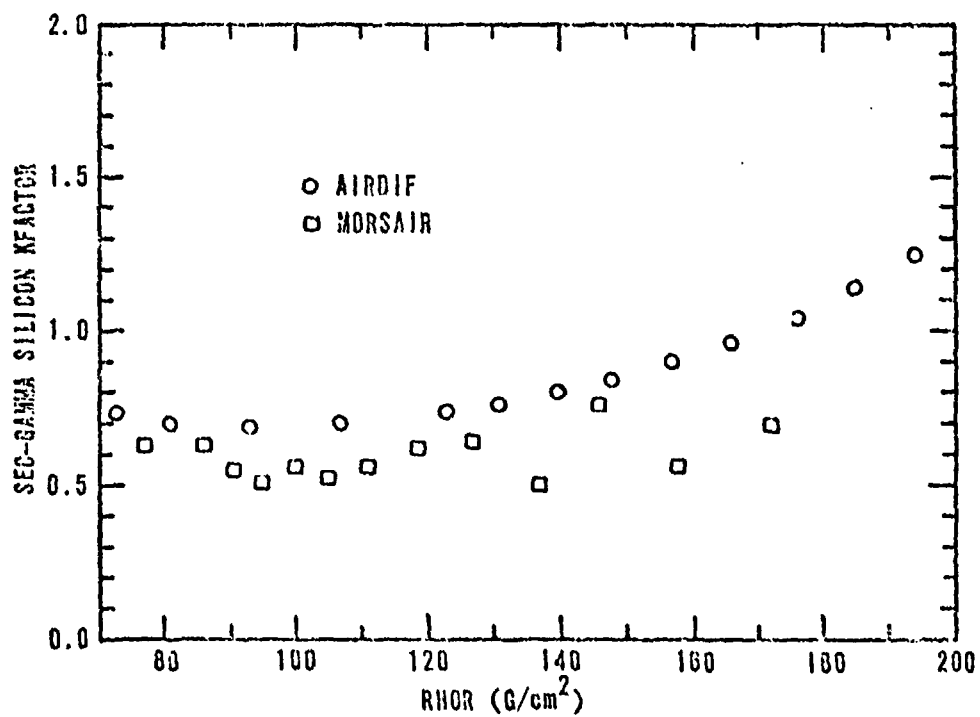


Figure D-28. Secondary Gamma Silicon K Factors for a Thermonuclear Source at 20 km and Receivers at 14.85 km

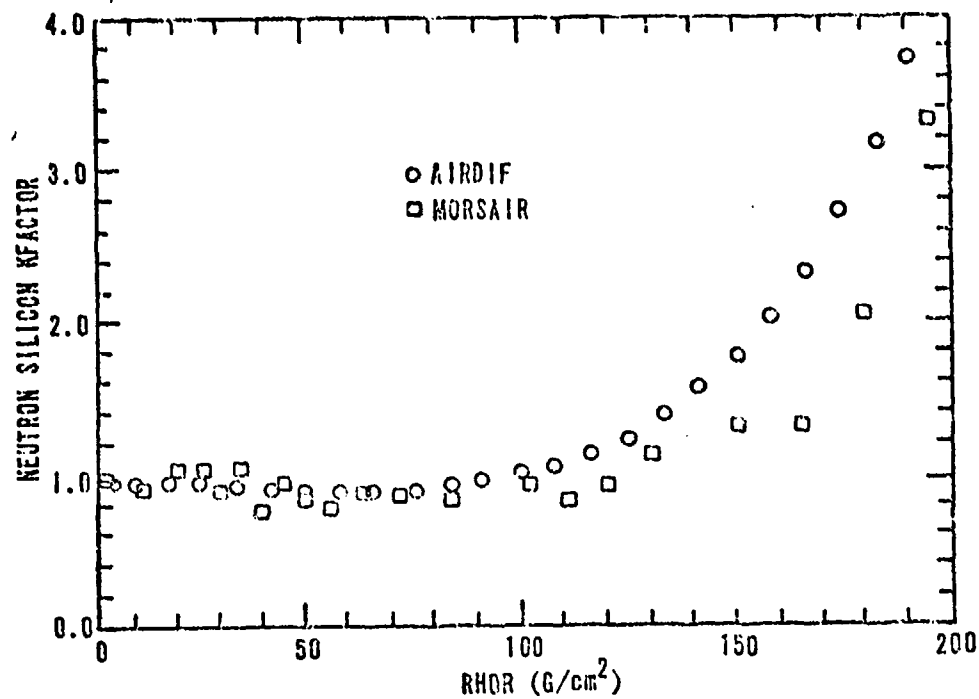


Figure D-29. Neutron Silicon K Factors for a Thermonuclear Source at 20 km and Receivers at 20.61 km

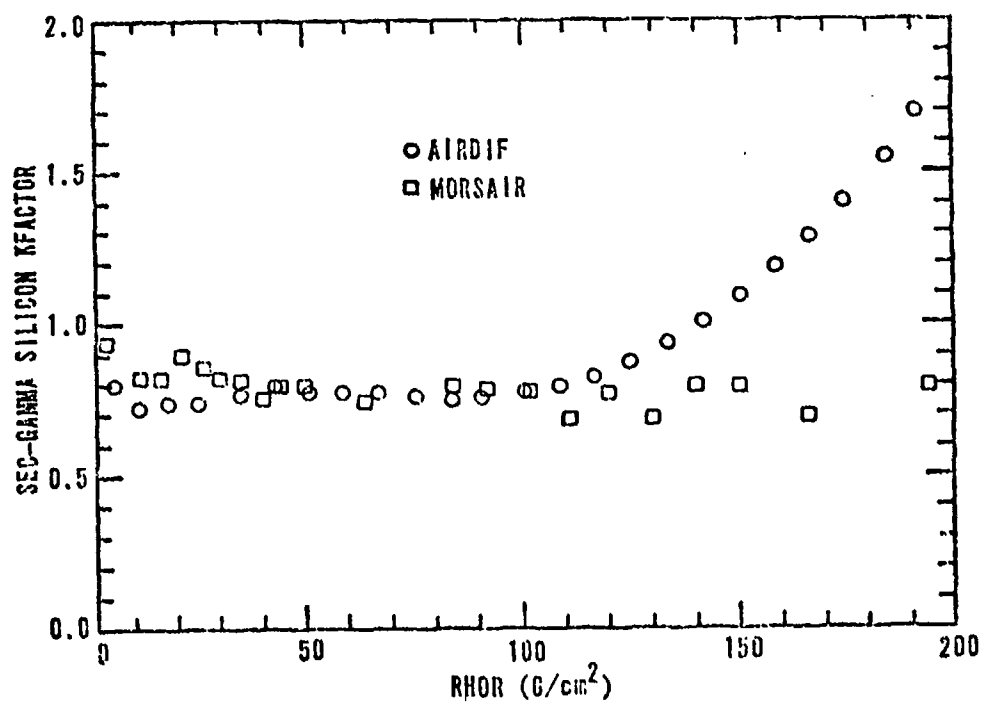


Figure D-30. Secondary Gamma Silicon K Factors for a Thermonuclear Source at 20 km and Receivers at 20.61 km

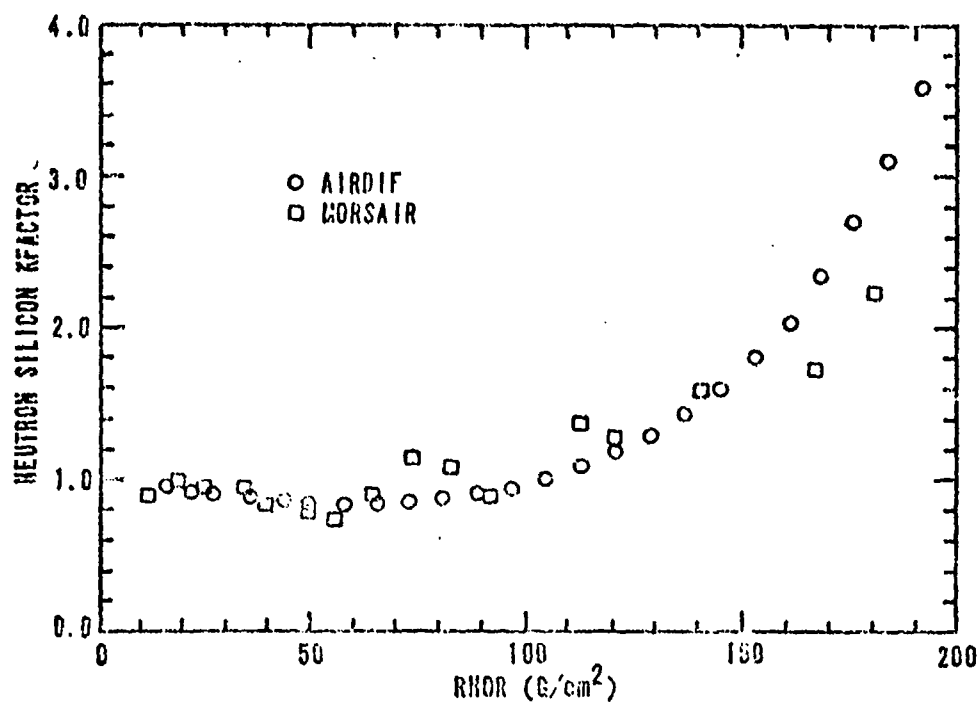


Figure D-31. Neutron Silicon K Factors for a Thermonuclear Source at 20 km and Receivers at 22.08 km

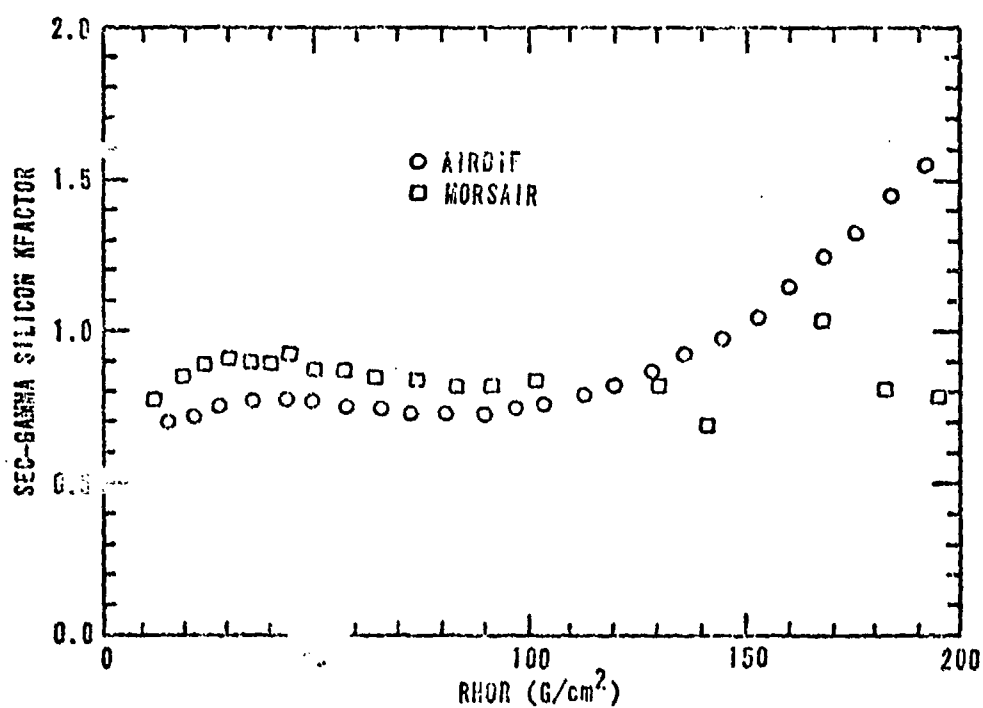


Figure D-32. Secondary Gamma Silicon K Factors for a Thermonuclear Source at 20 km and Receivers at 22.08 km

Appendix E

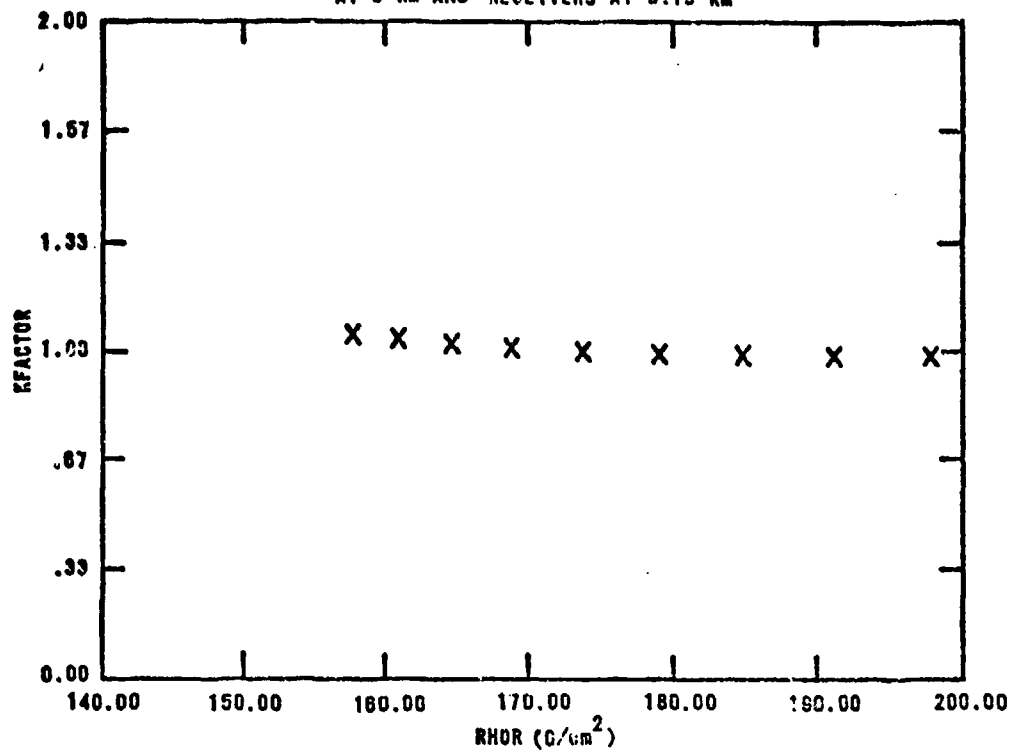
K Factor versus Mass Range Plots for a Fission Source

This appendix presents a series of K factor versus mass range* plots for the fission source in Table V. The K factors are based on the silicon dose response functions shown in Tables III and IV. Plots are included for neutrons and secondary gammas, at source altitudes of 5, 10, 15, and 20 km, and at seven receiver altitudes for each source altitude.

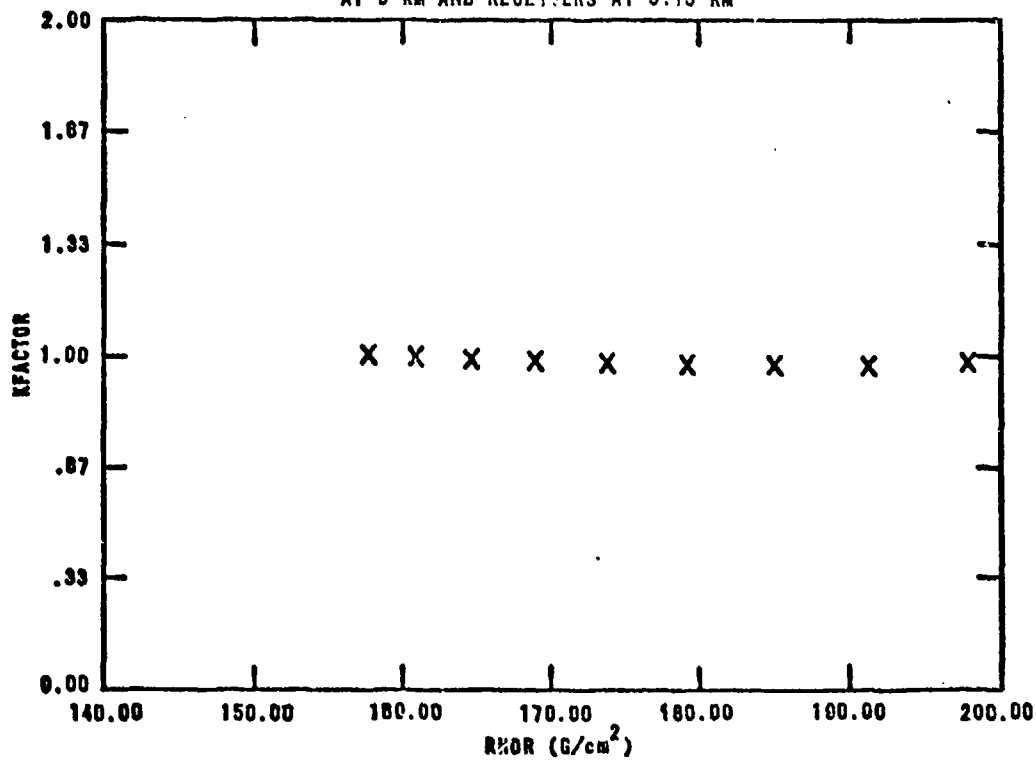
<u>Run No.</u>	<u>Index</u>	<u>Page</u>
	<u>Source Altitude (km)</u>	
1	5	127
2	10	134
3	15	141
4	20	148

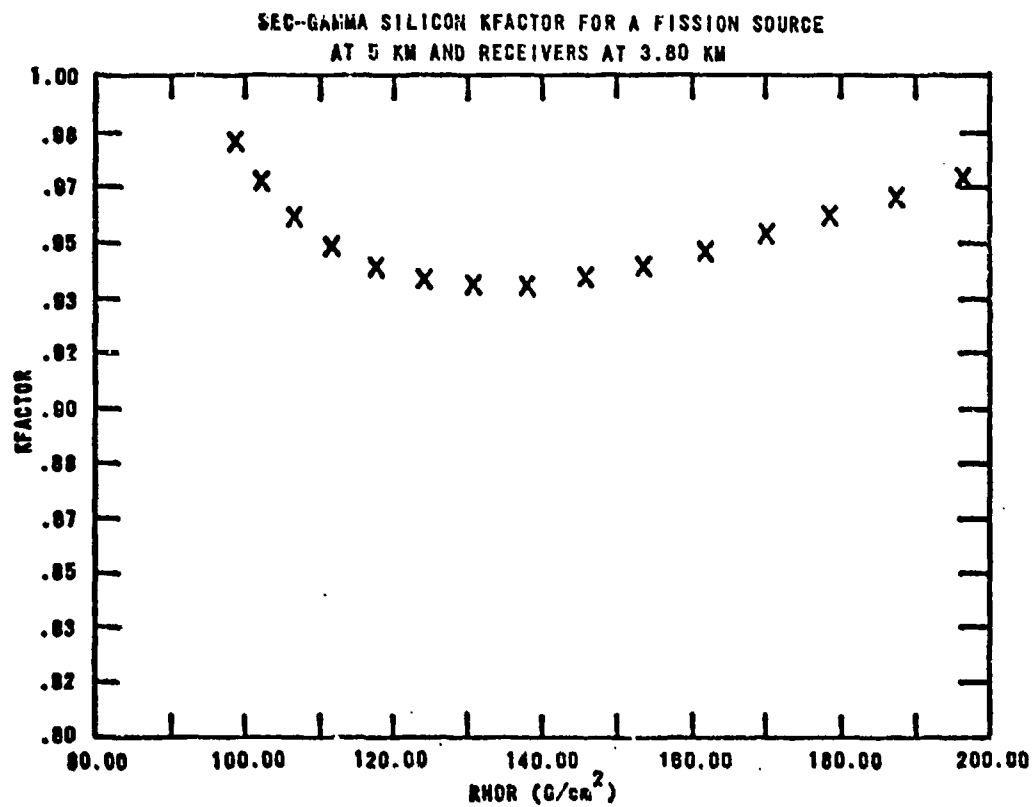
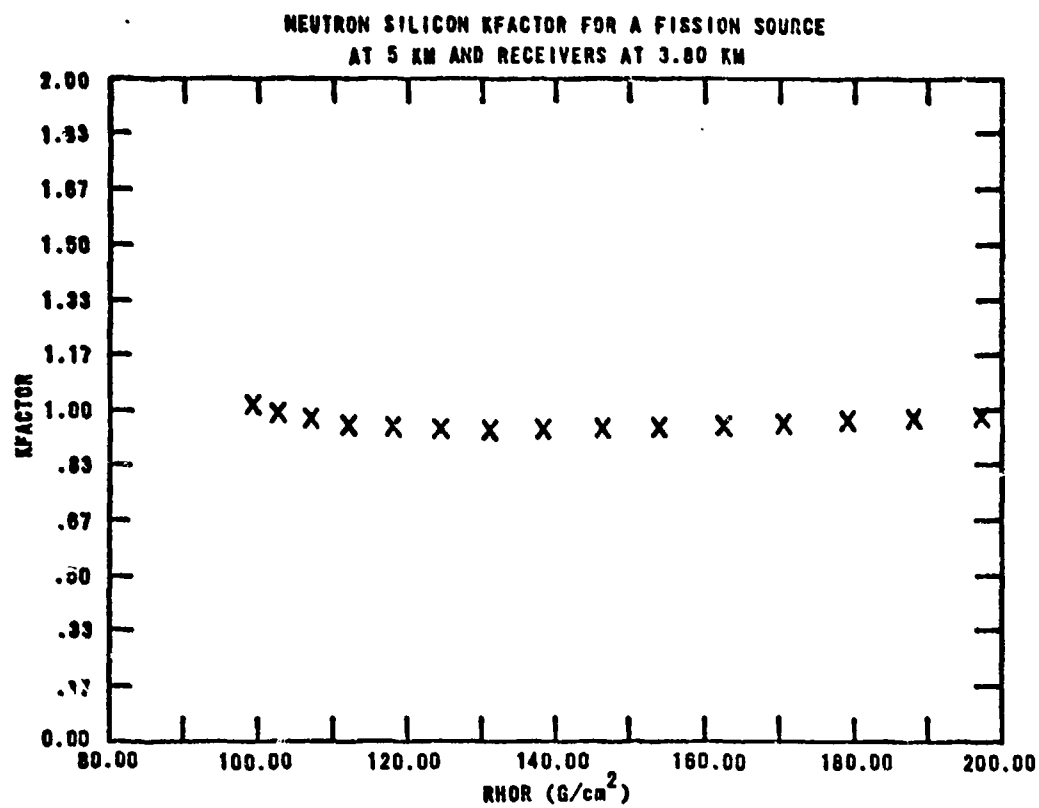
*Mass range, $\langle pR \rangle$, is defined by equation (2.3) in Section II. In this appendix, the symbol "RHOR" is used for $\langle pR \rangle$.

NEUTRON SILICON KFACTOR FOR A FISSION SOURCE
AT 5 KM AND RECEIVERS AT 3.13 KM

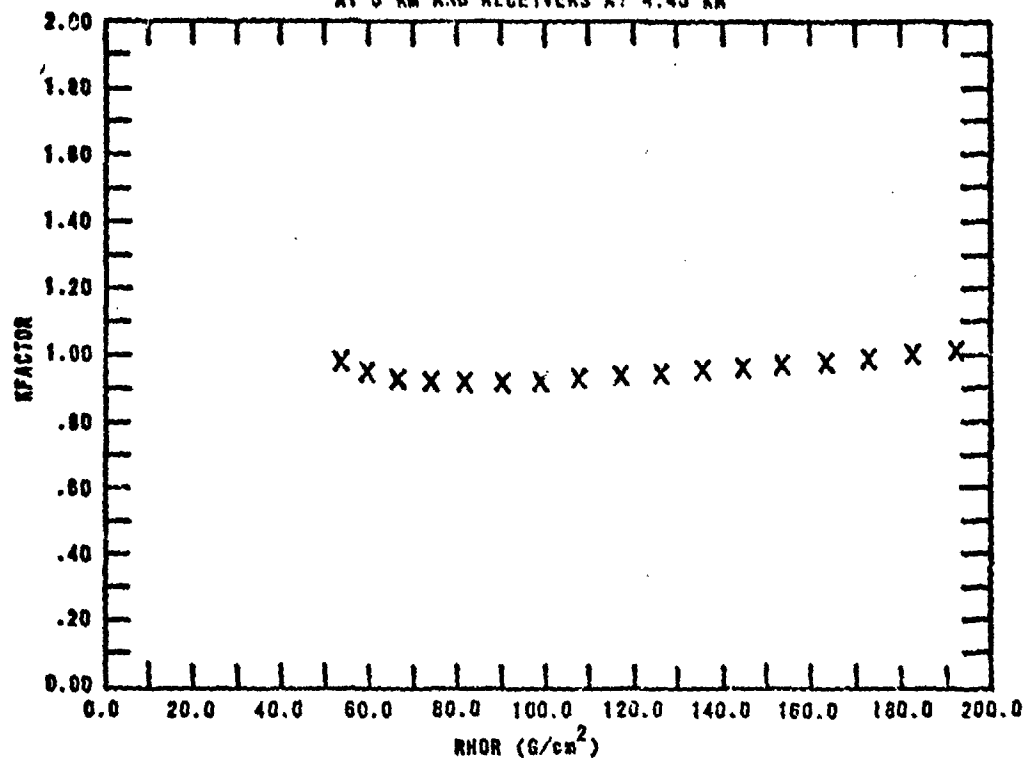


SEC-GAMMA SILICON KFACTOR FOR A FISSION SOURCE
AT 5 KM AND RECEIVERS AT 3.13 KM

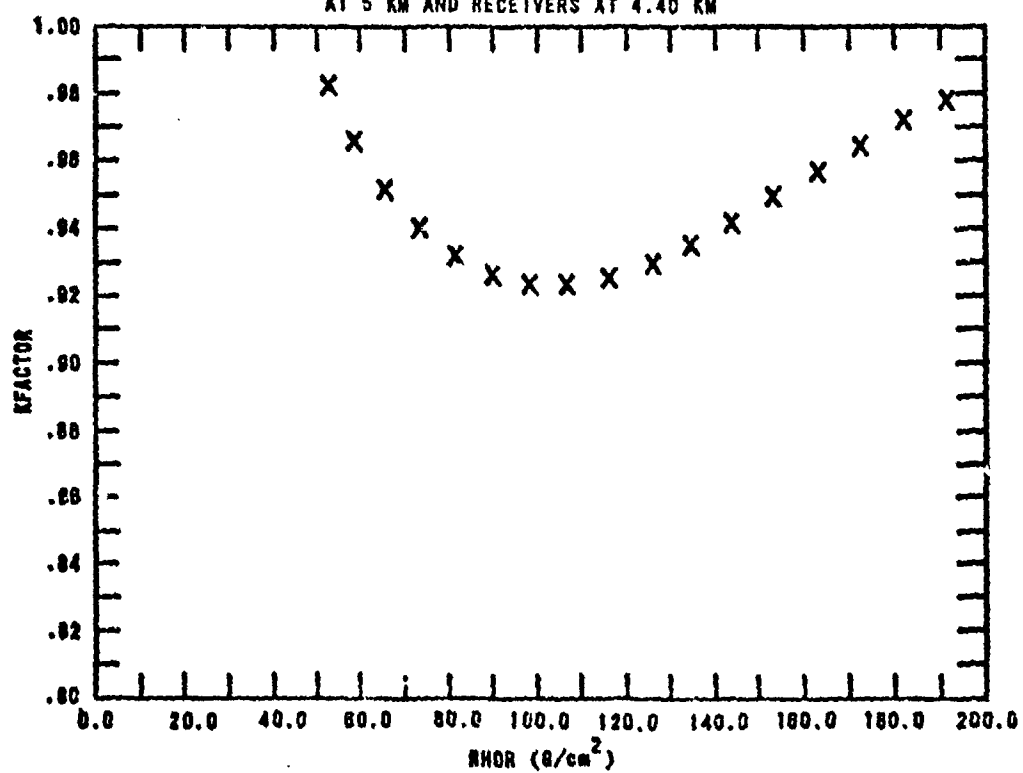




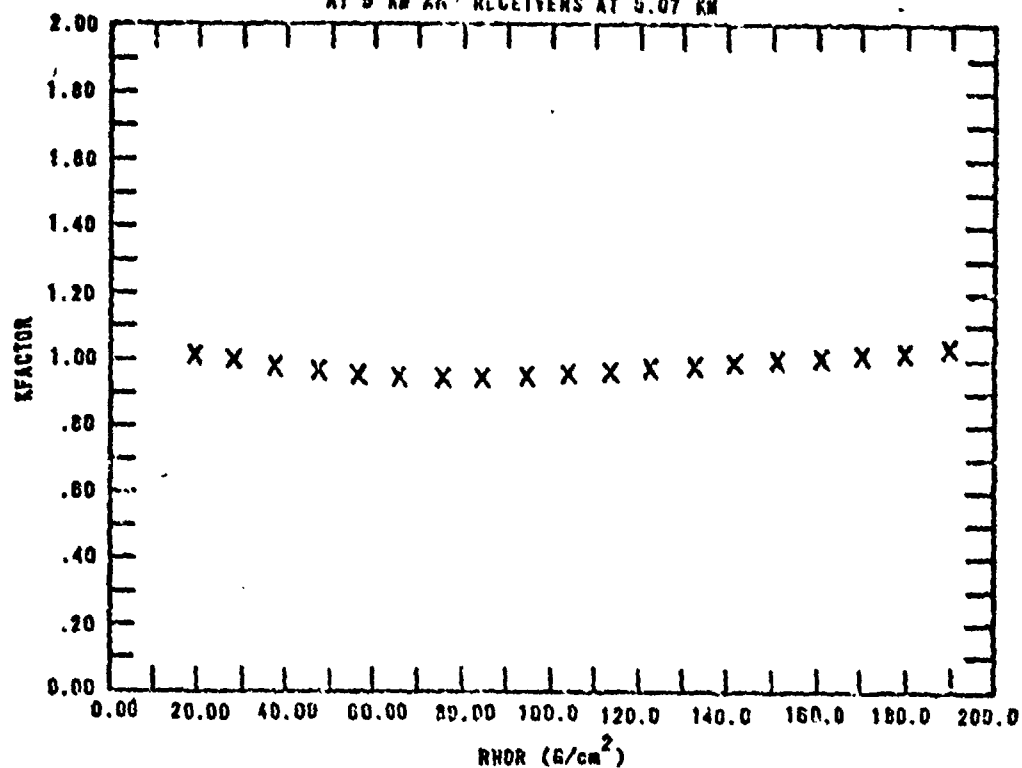
NEUTRON SILICON KFACTOR FOR A FISSION SOURCE
AT 5 KM AND RECEIVERS AT 4.40 KM



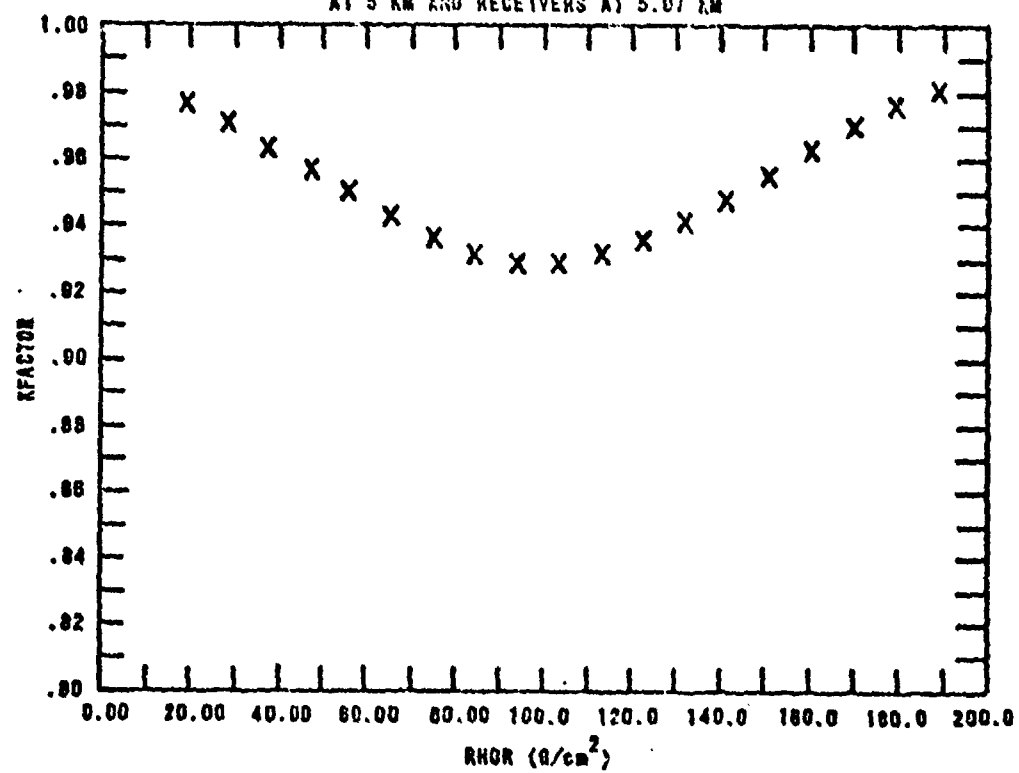
SEC-GAMMA SILICON KFACTOR FOR A FISSION SOURCE
AT 5 KM AND RECEIVERS AT 4.40 KM



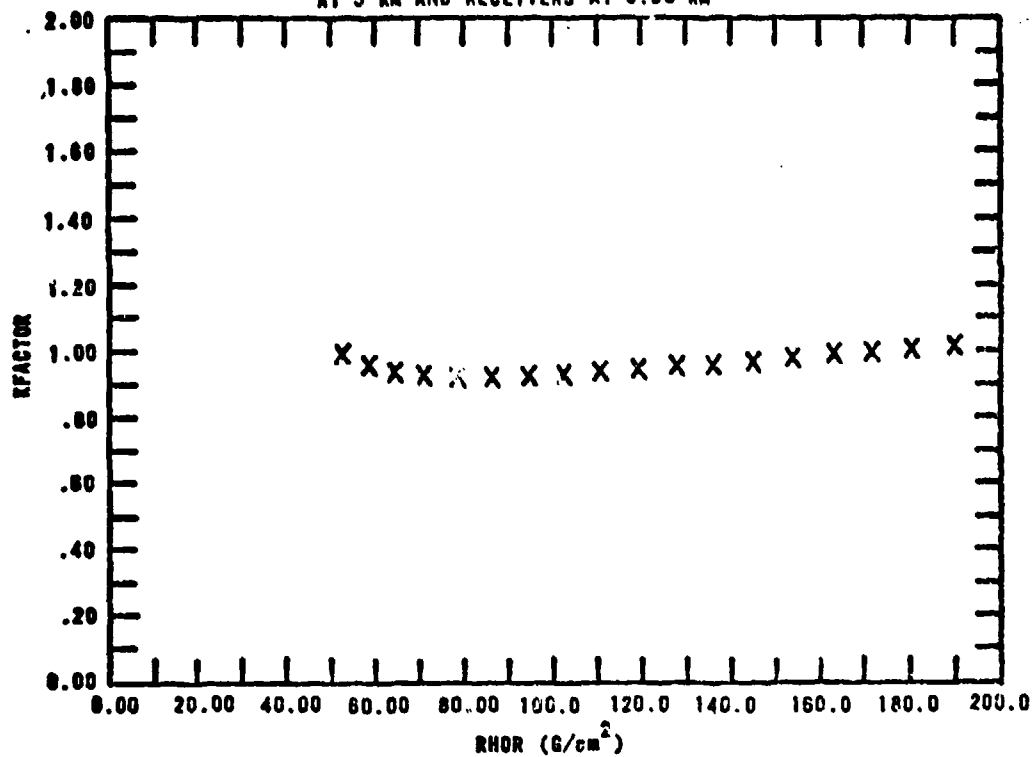
NEUTRON SILICON KFACTOR FOR A FISSION SOURCE
AT 5 KM AND RECEIVERS AT 5.07 KM



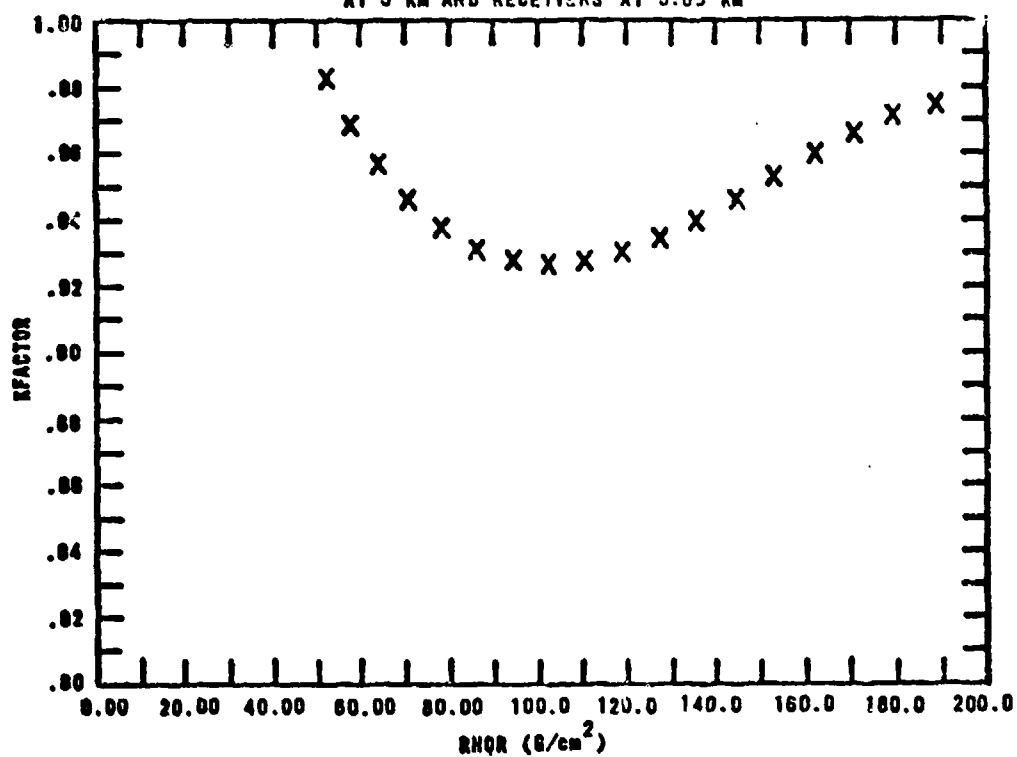
SEC-GAMMA SILICON KFACTOR FOR A FISSION SOURCE
AT 5 KM AND RECEIVERS AT 5.07 KM

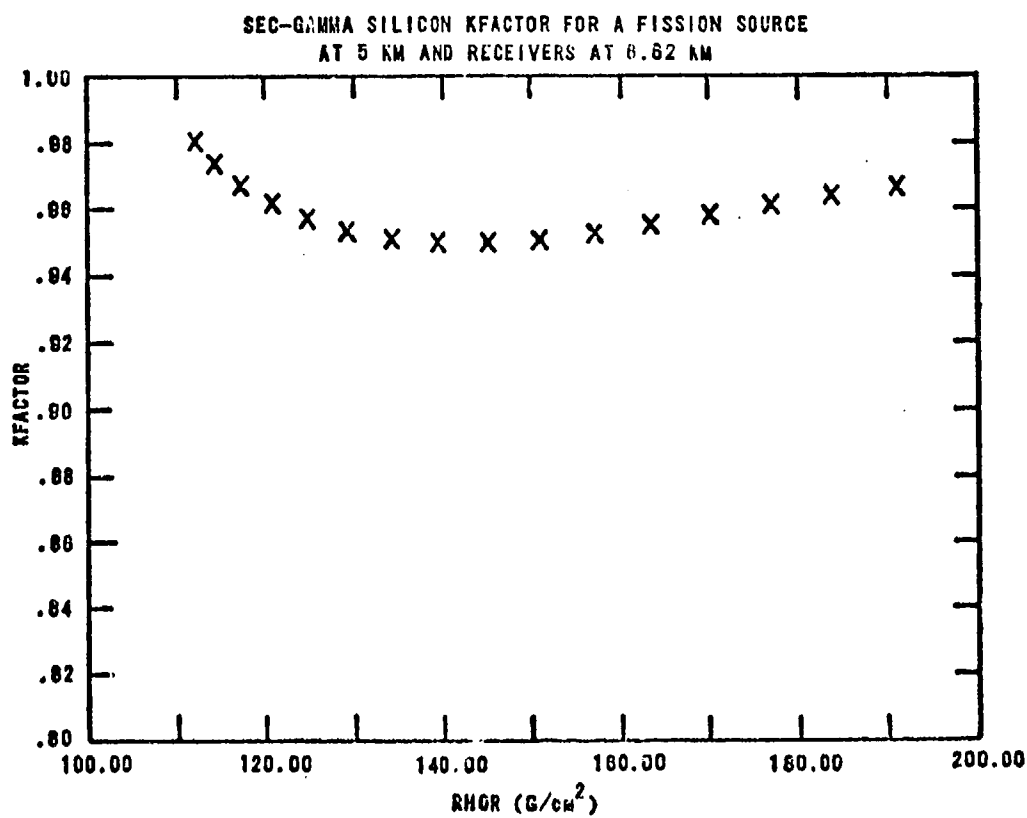
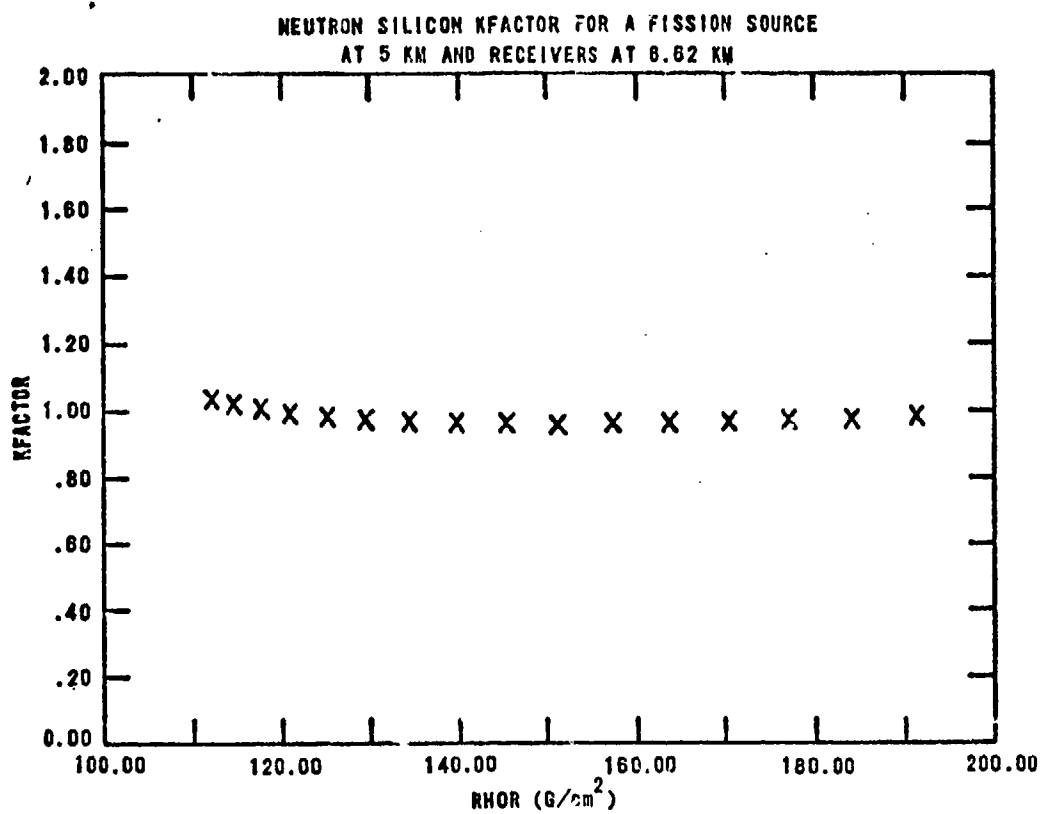


NEUTRON SILICON KFACTOR FOR A FISSION SOURCE
AT 5 KM AND RECEIVERS AT 5.65 KM

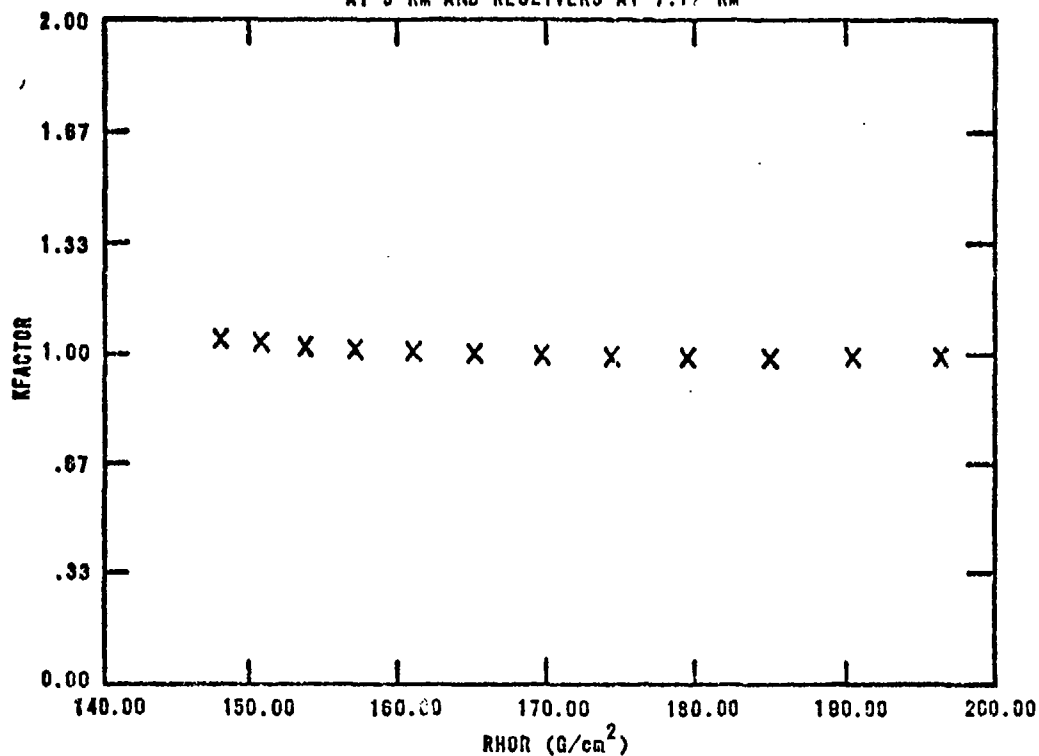


SEC-GAMMA SILICON KFACTOR FOR A FISSION SOURCE
AT 5 KM AND RECEIVERS AT 5.65 KM

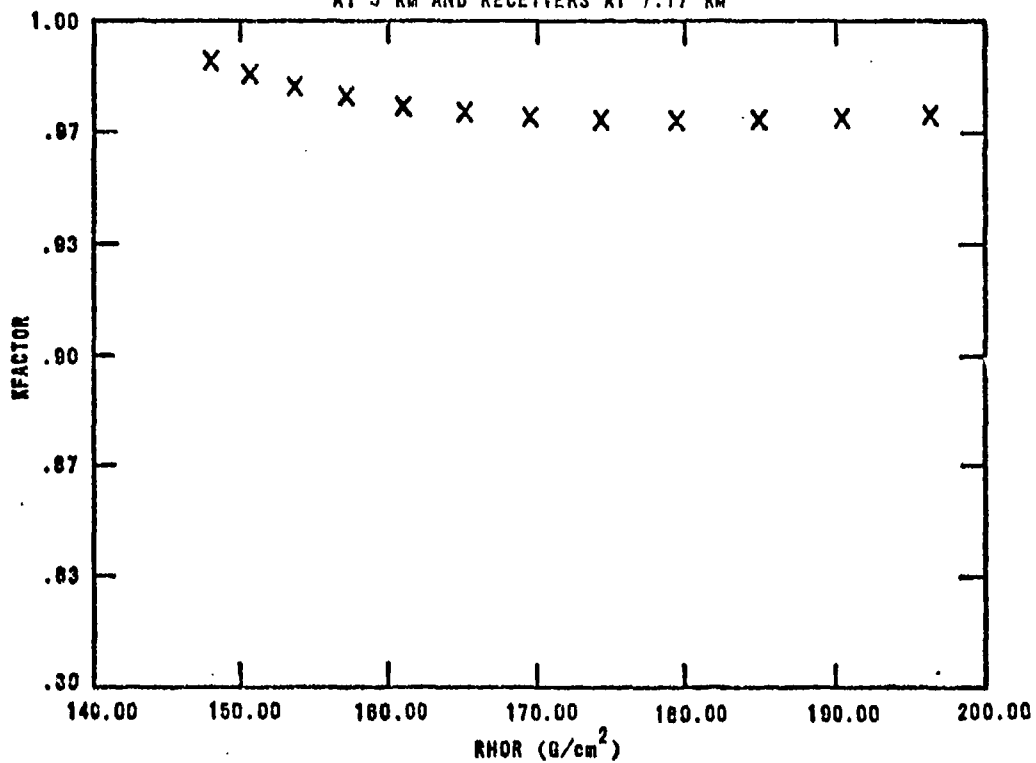




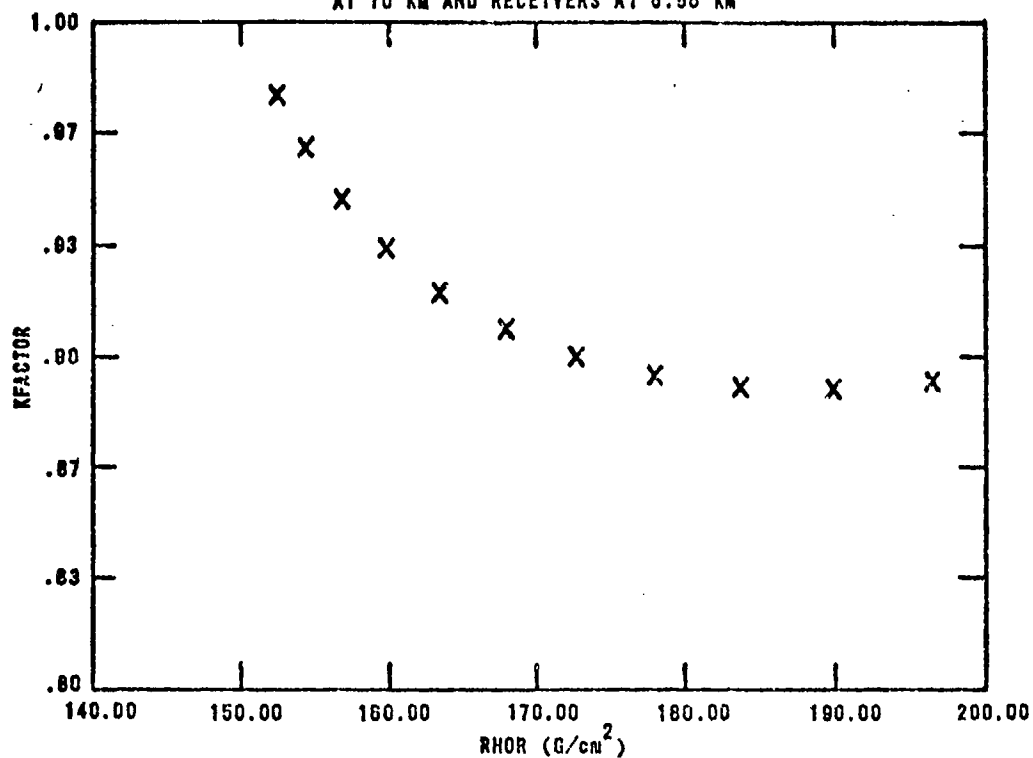
NEUTRON SILICON KFACTOR FOR A FISSION SOURCE
AT 5 KM AND RECEIVERS AT 7.17 KM



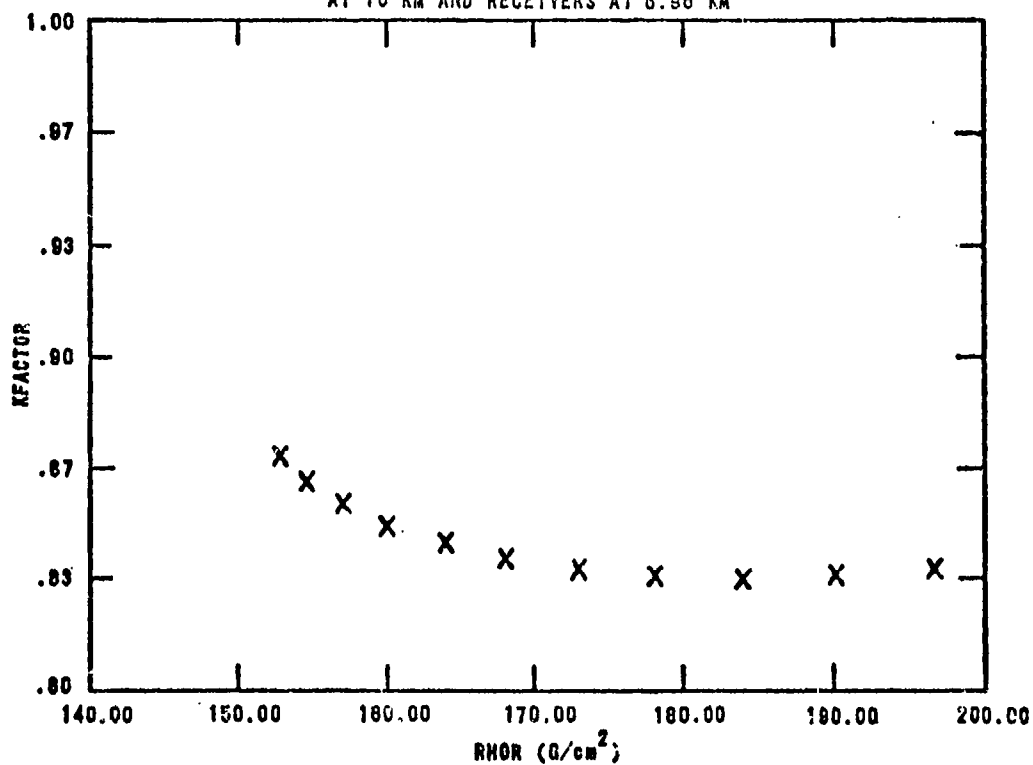
SEC-GAMMA SILICON KFACTOR FOR A FISSION SOURCE
AT 5 KM AND RECEIVERS AT 7.17 KM



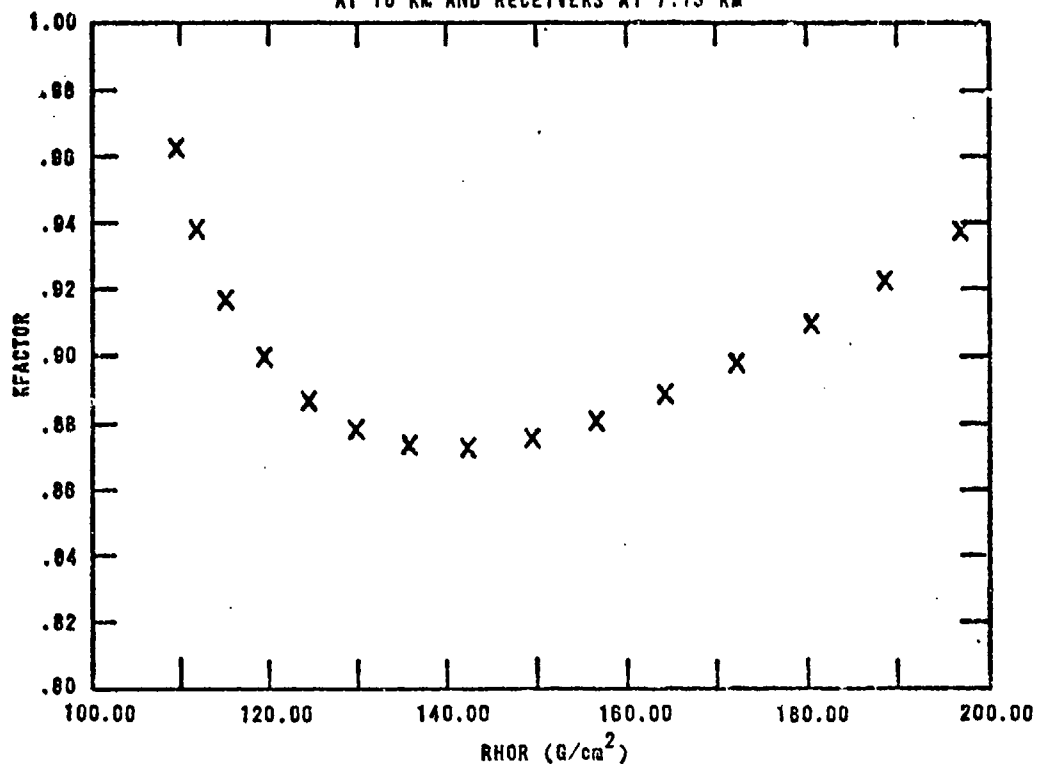
NEUTRON SILICON KFACTOR FOR A FISSION SOURCE
AT 10 KM AND RECEIVERS AT 6.98 KM



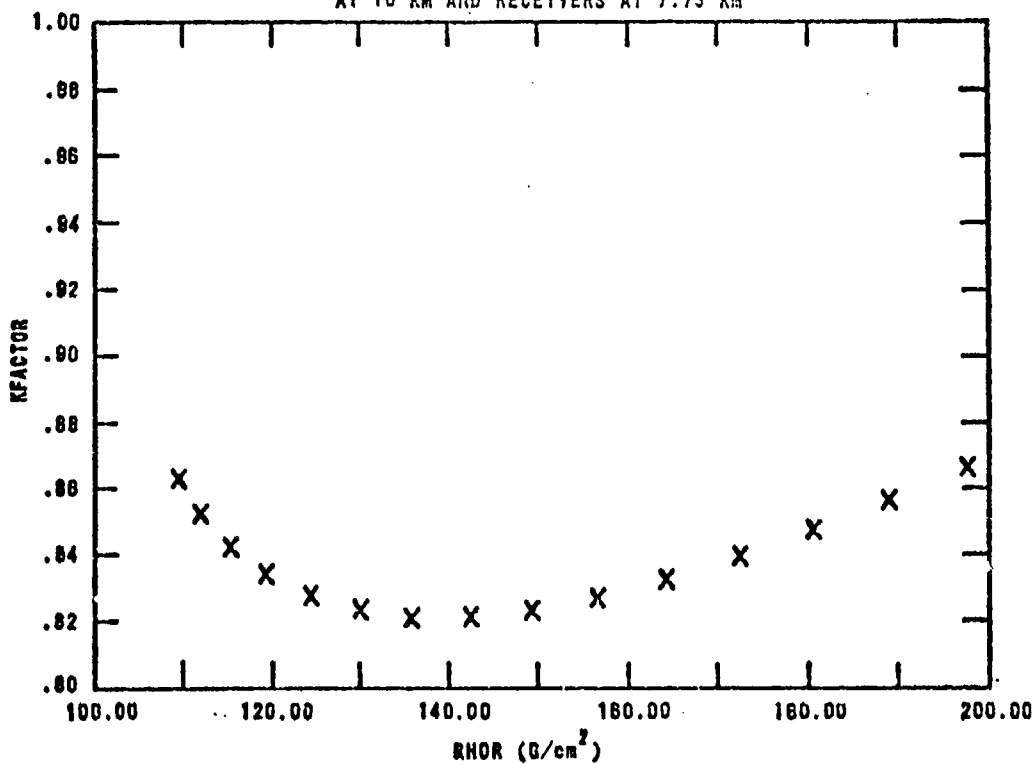
SEC-GAMMA SILICON KFACTOR FOR A FISSION SOURCE
AT 10 KM AND RECEIVERS AT 6.96 KM

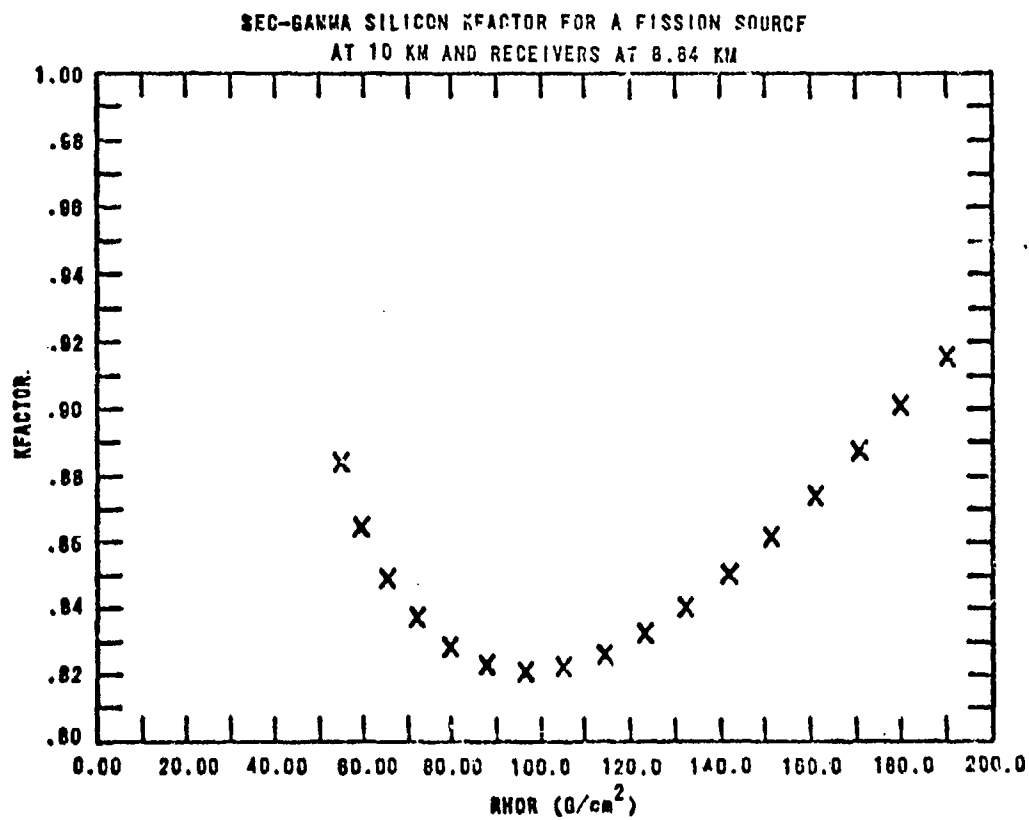
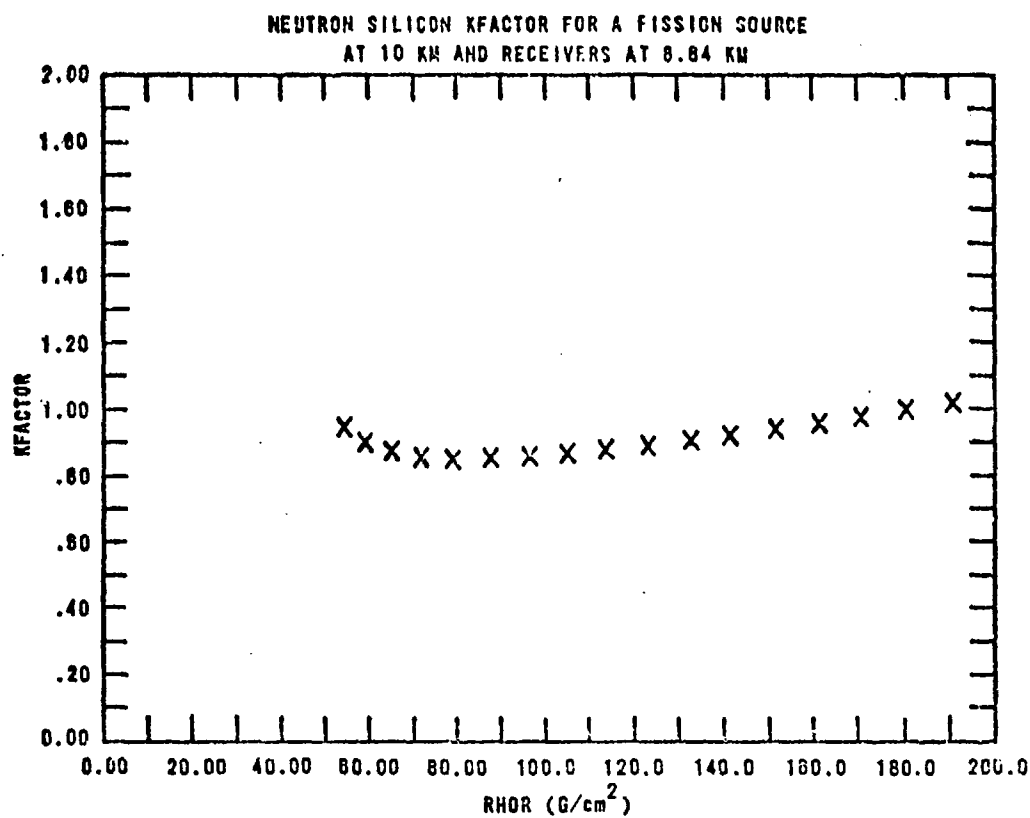


NEUTRON SILICON KFACTOR FOR A FISSION SOURCE
AT 10 KM AND RECEIVERS AT 7.73 KM

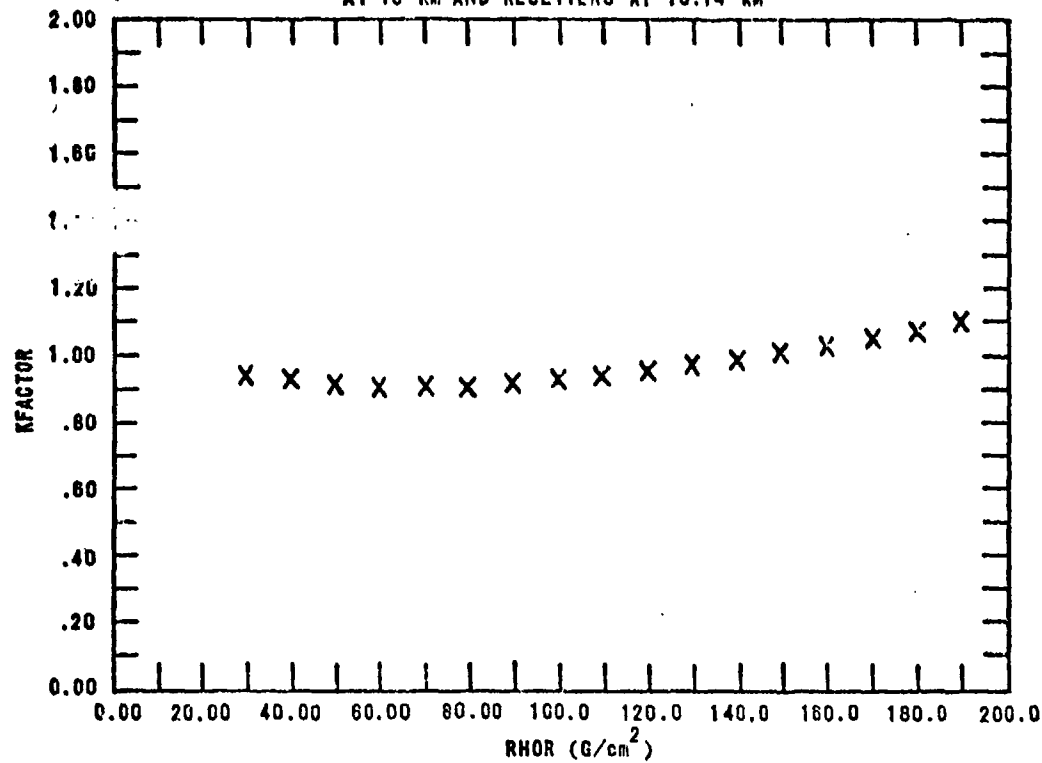


SEC-GAMMA SILICON KFACTOR FOR A FISSION SOURCE
AT 10 KM AND RECEIVERS AT 7.73 KM

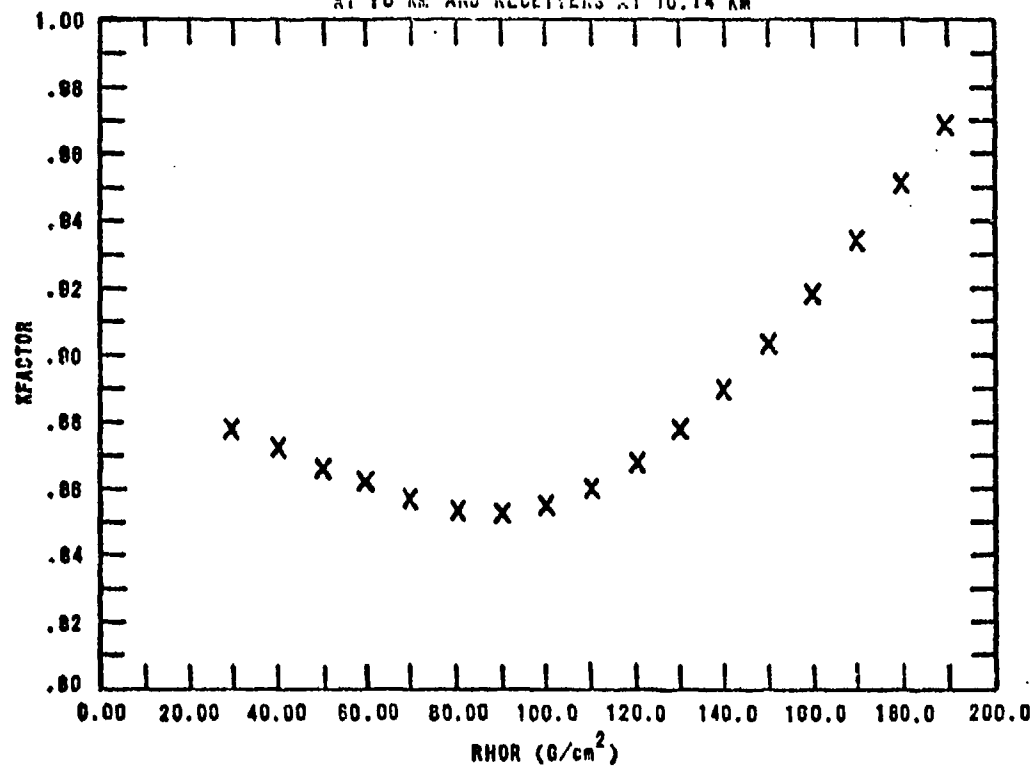


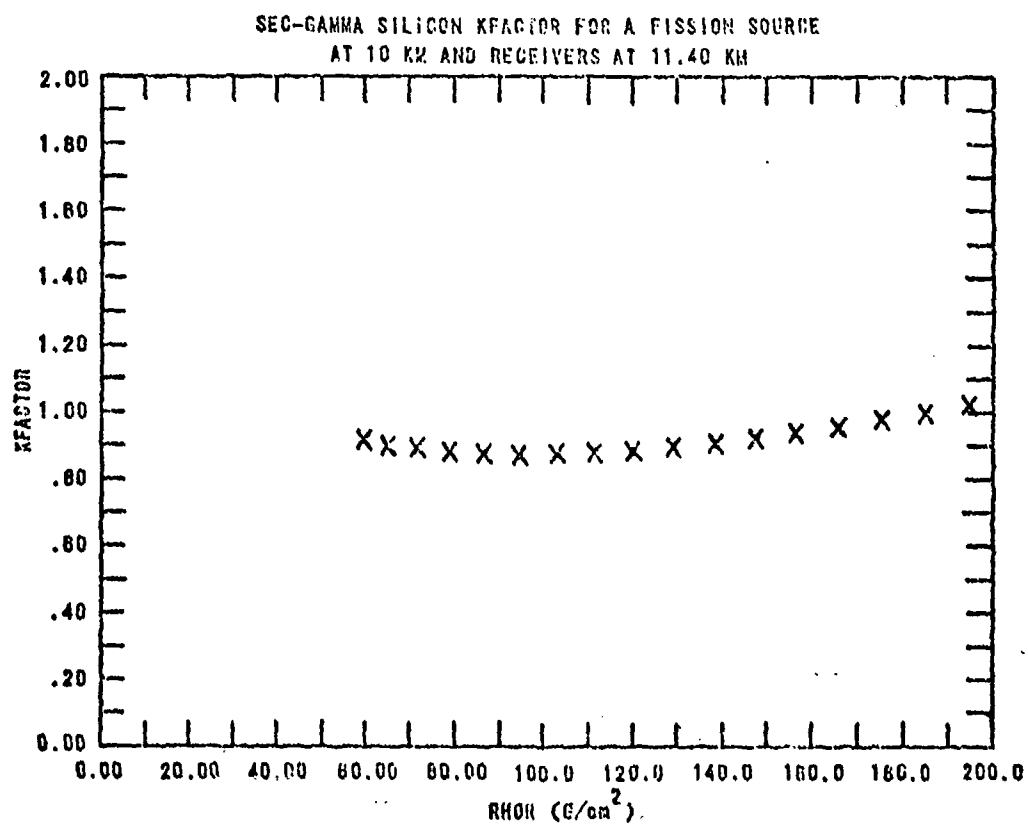
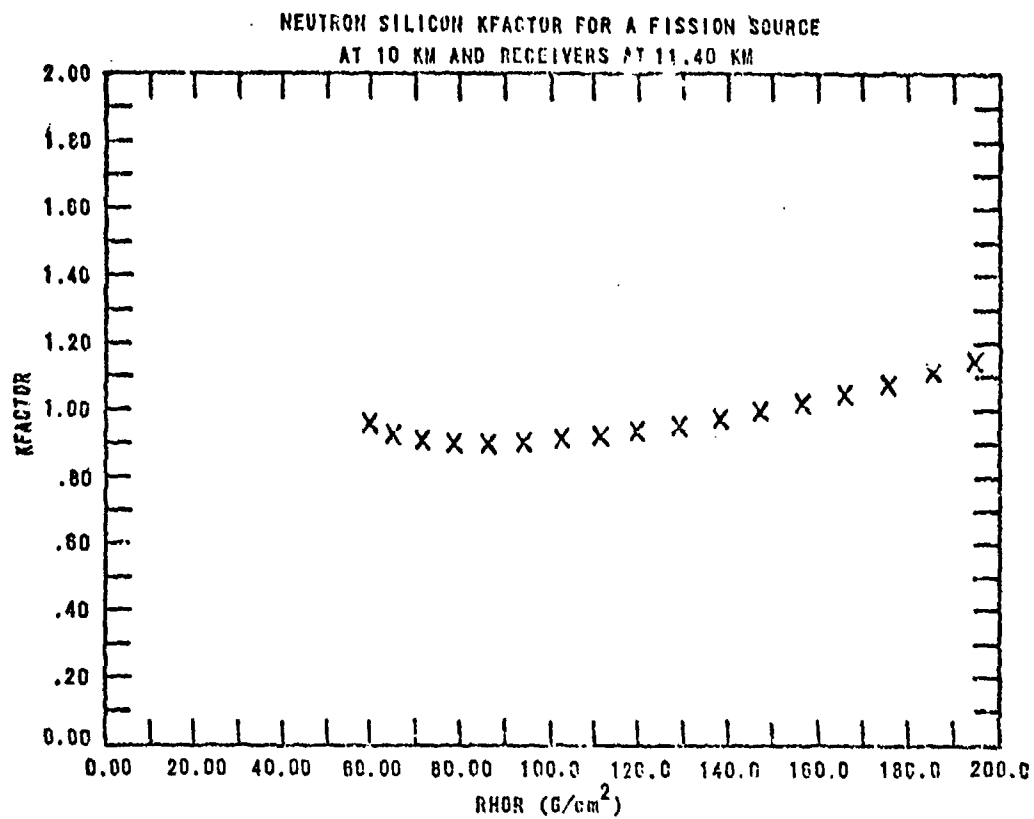


NEUTRON SILICON KFACTOR FOR A FISSION SOURCE
AT 10 KM AND RECEIVERS AT 10.14 KM

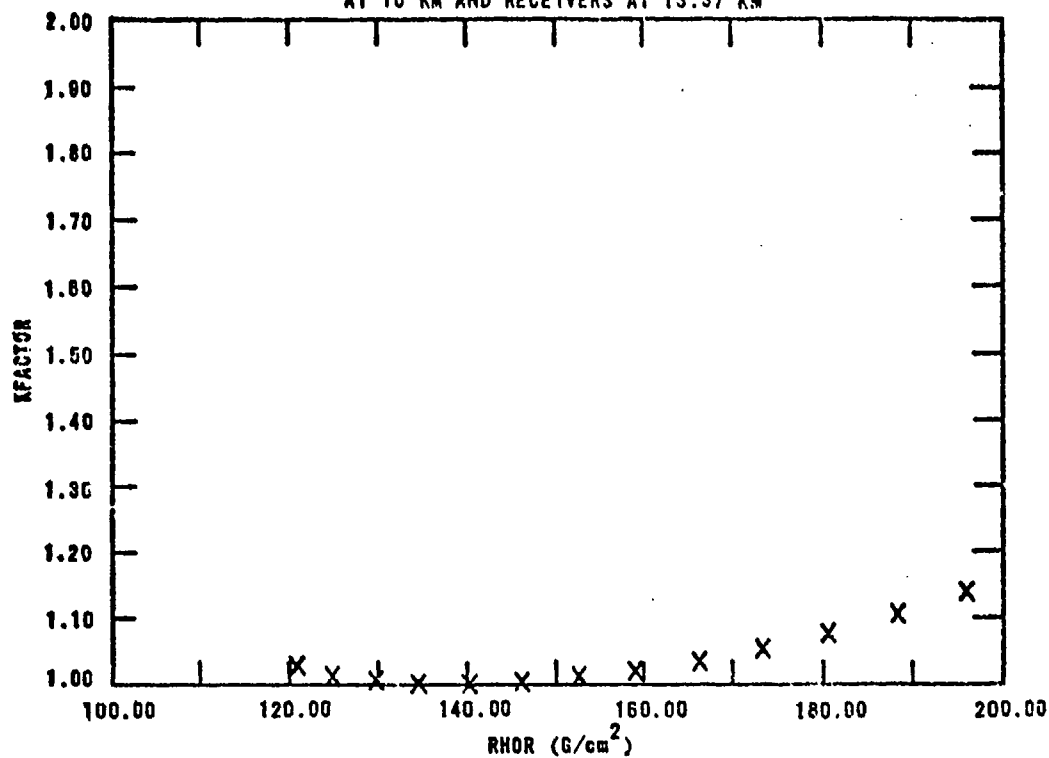


SEC-GAMMA SILICON KFACTOR FOR A FISSION SOURCE
AT 10 KM AND RECEIVERS AT 10.14 KM

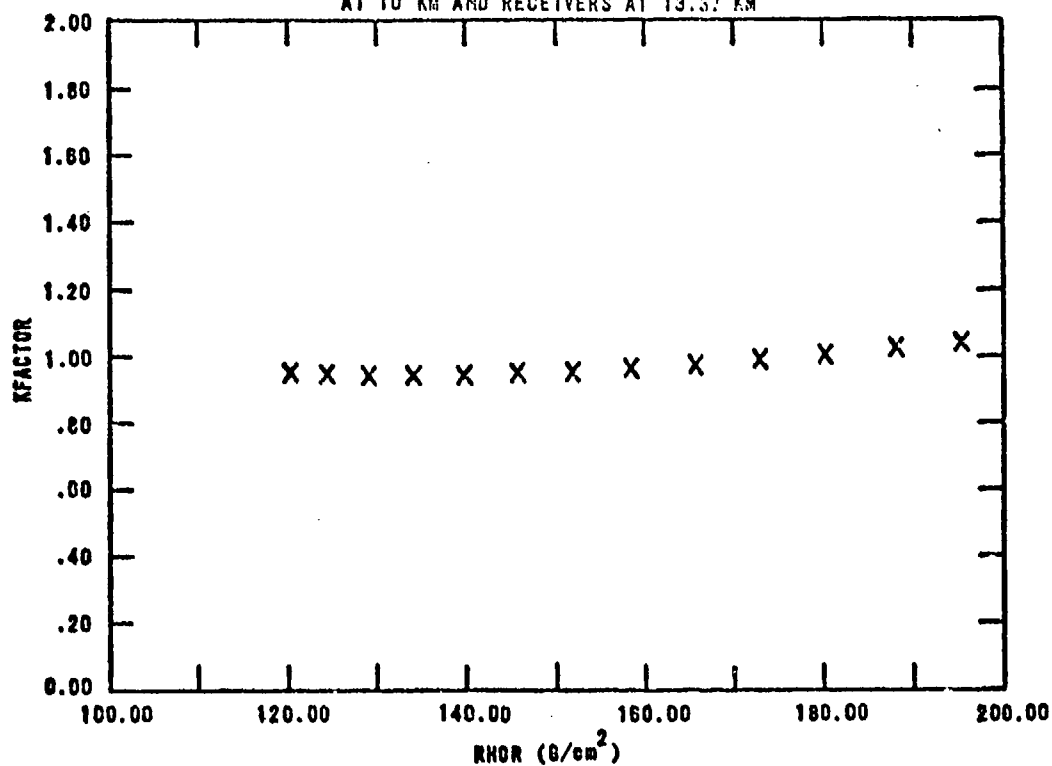


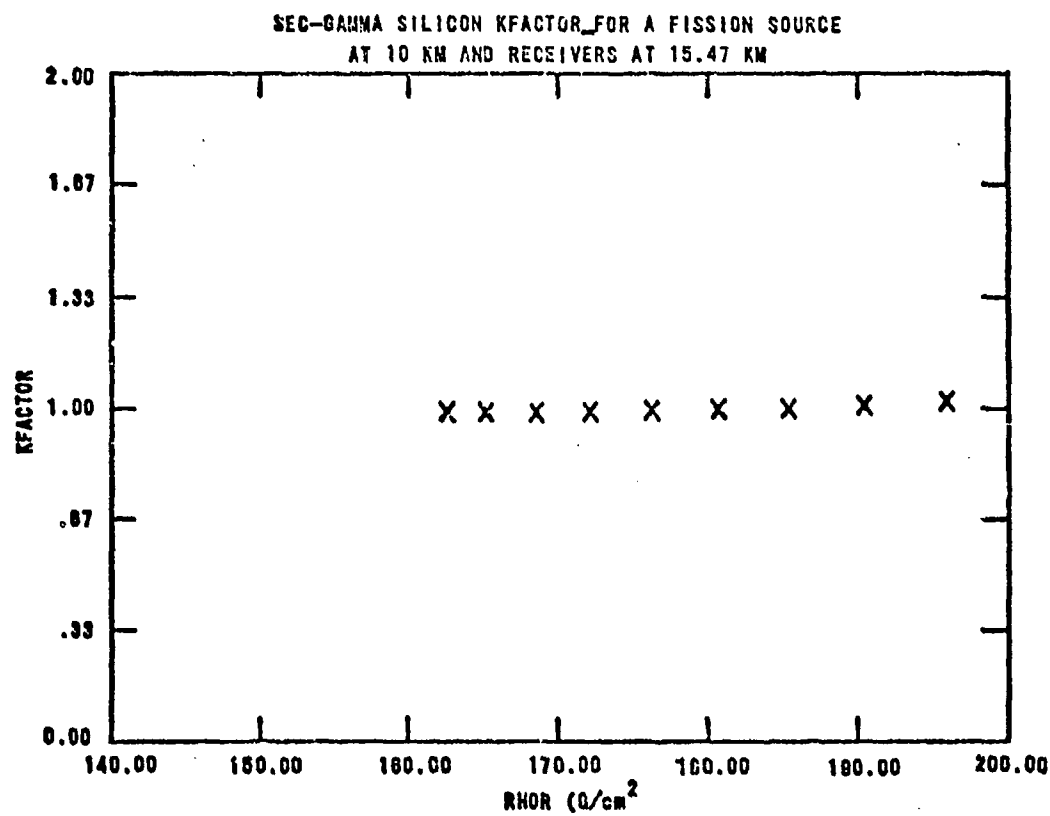
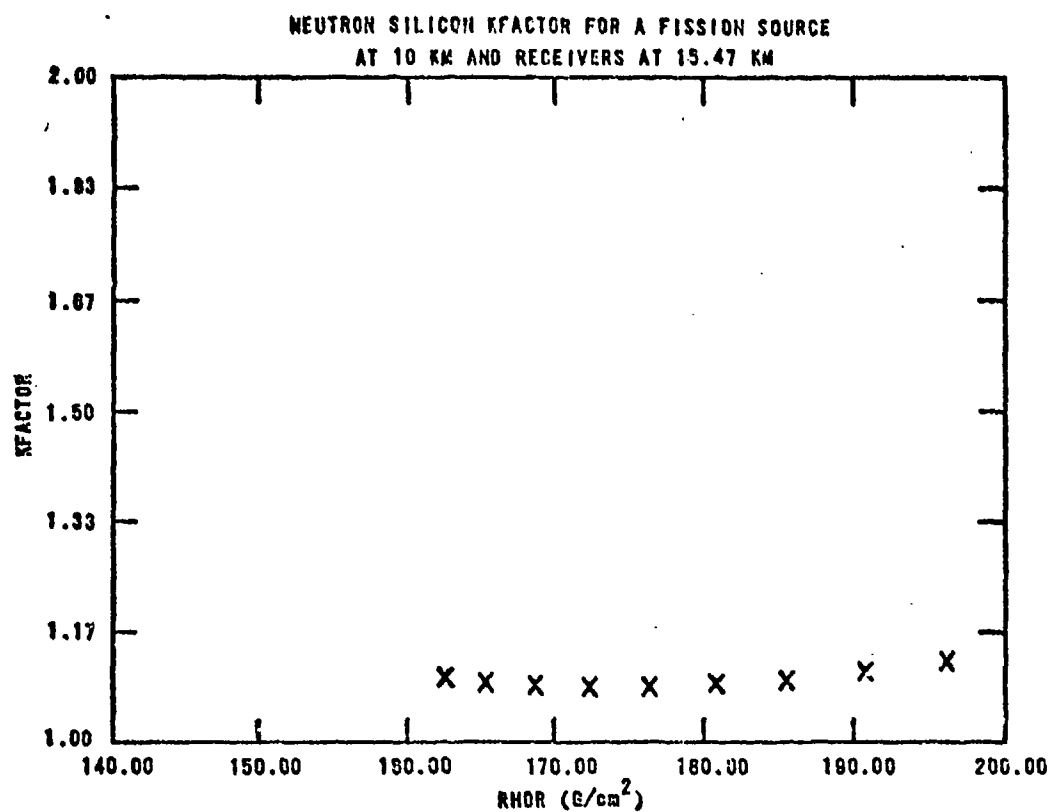


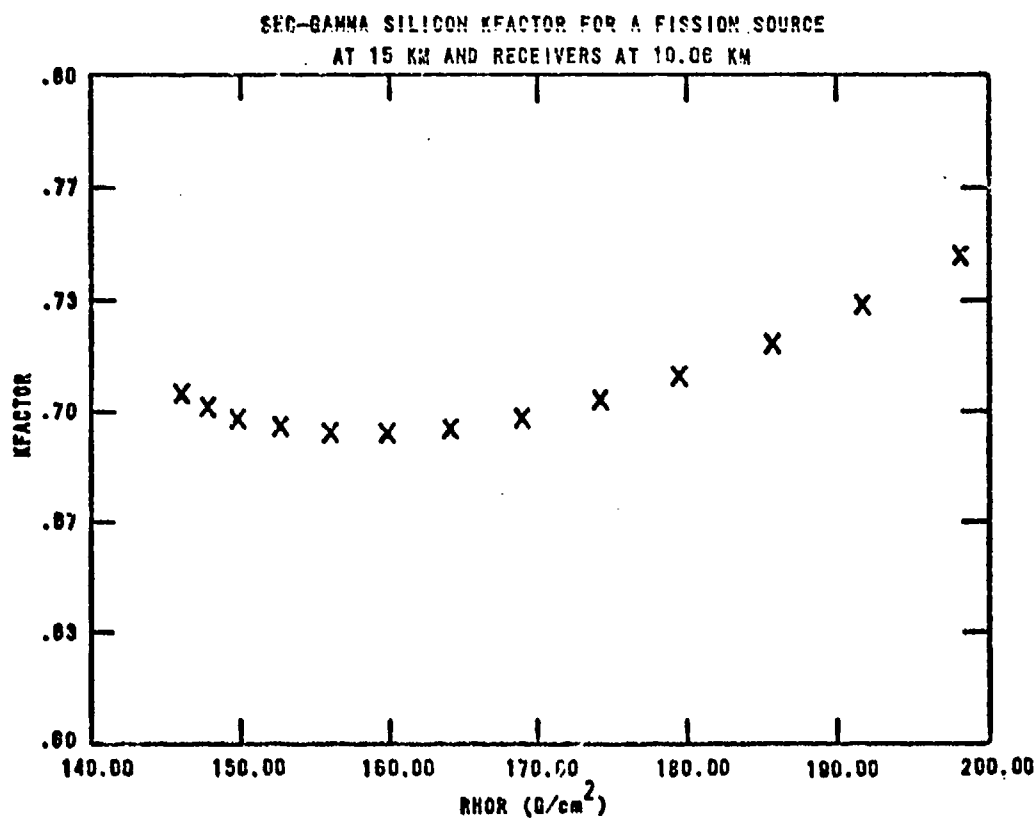
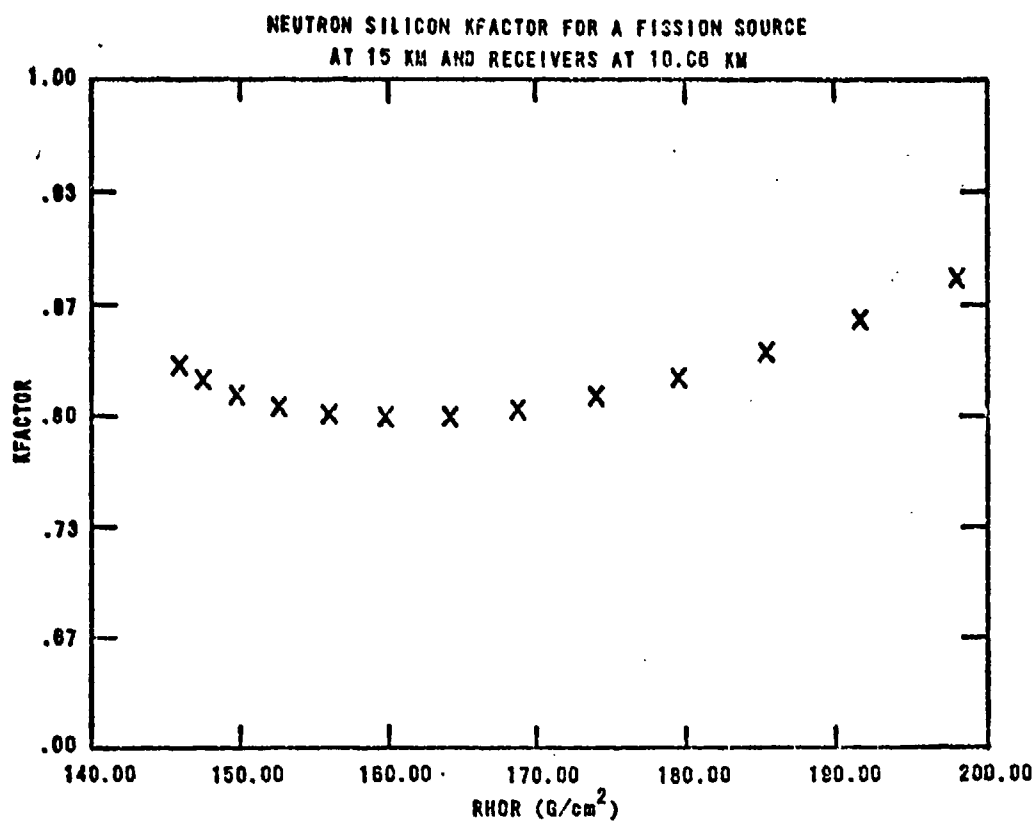
NEUTRON SILICON KFACTOR FOR A FISSION SOURCE
AT 10 KM AND RECEIVERS AT 13.37 KM



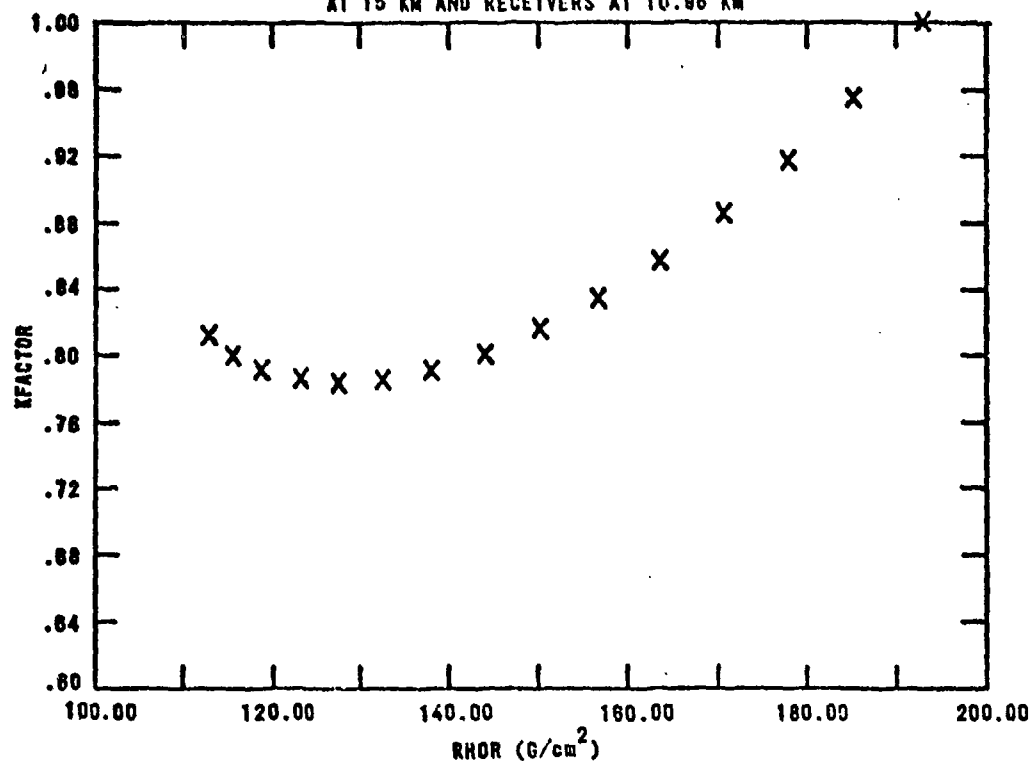
SEC-GAMMA SILICON KFACTOR FOR A FISSION SOURCE
AT 10 KM AND RECEIVERS AT 13.37 KM



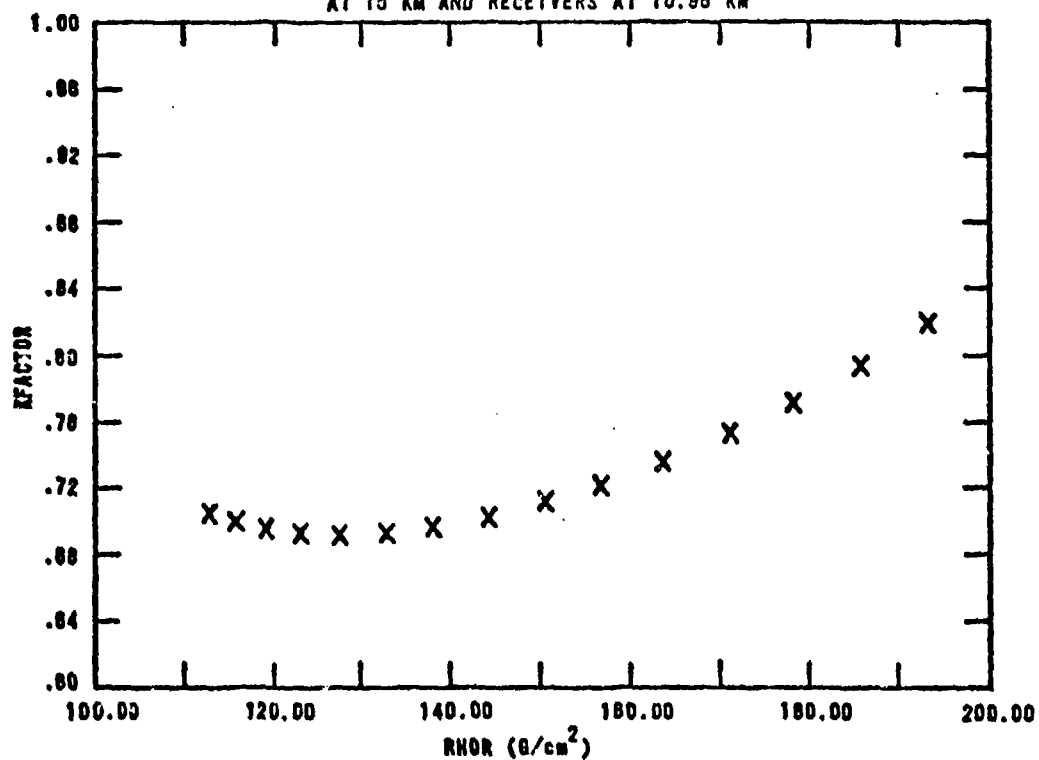




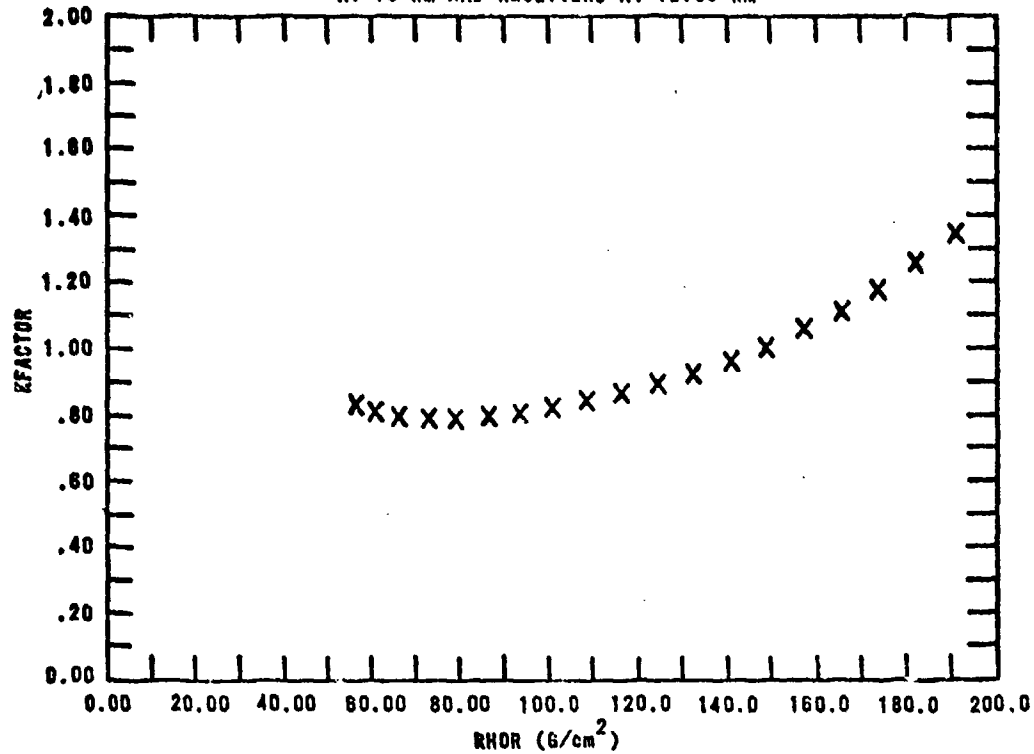
NEUTRON SILICON KFACTOR FOR A FISSION SOURCE
AT 15 KM AND RECEIVERS AT 10.98 KM



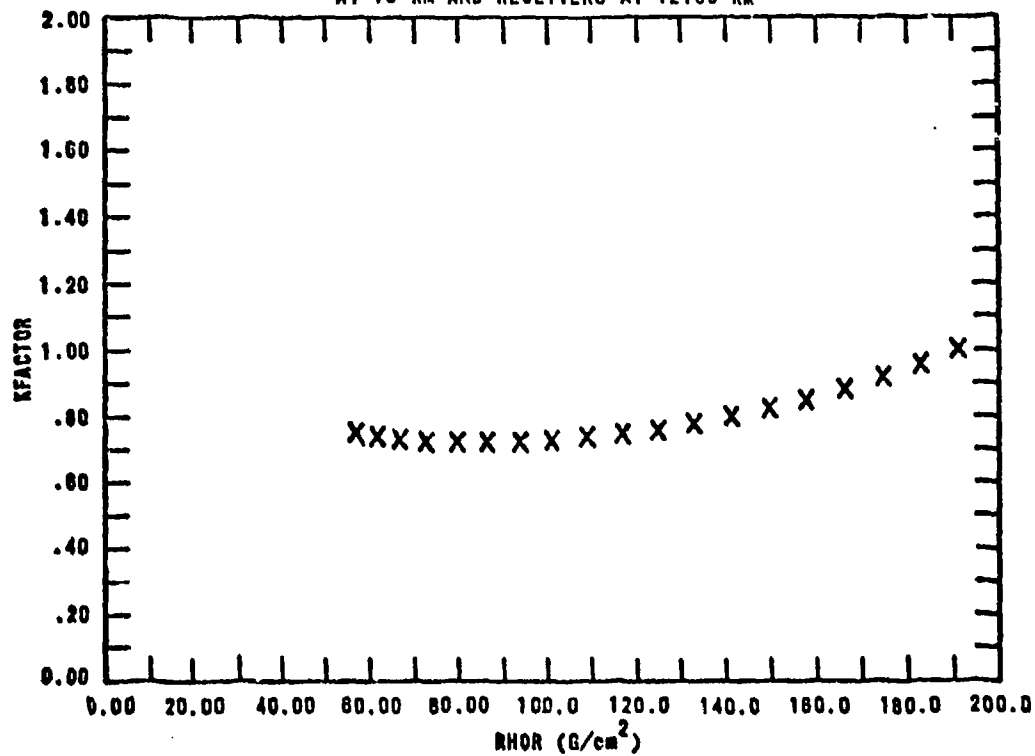
SEC-GAMMA SILICON KFACTOR FOR A FISSION SOURCE
AT 15 KM AND RECEIVERS AT 10.98 KM



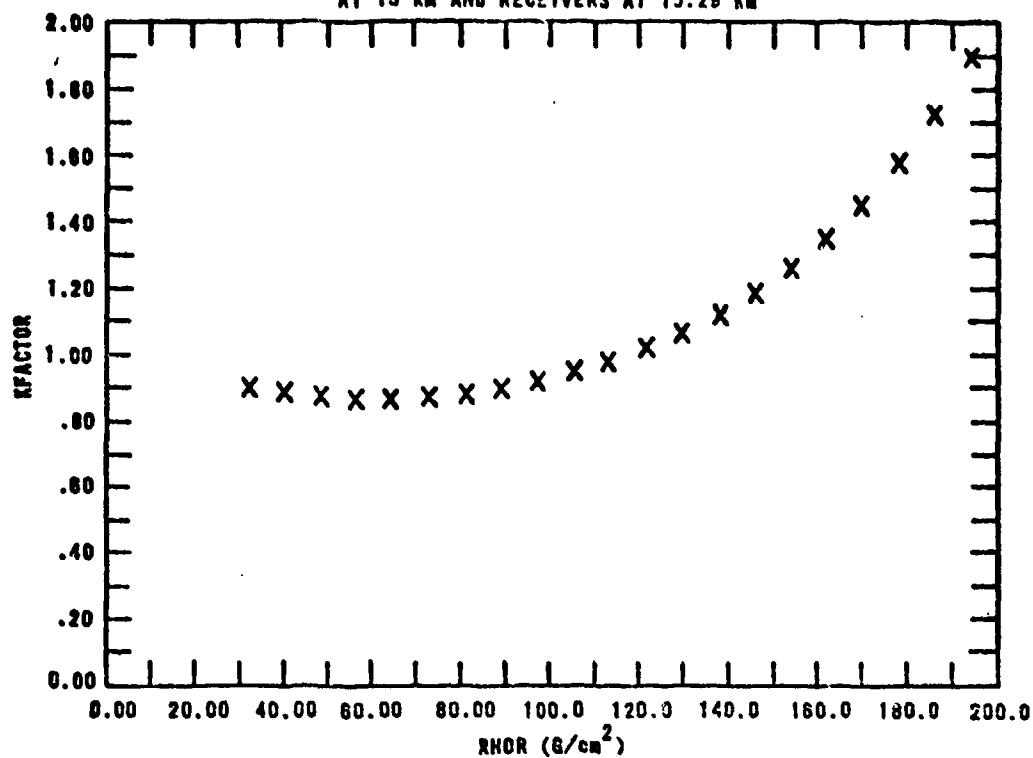
NEUTRON SILICON KFACTOR FOR A FISSION SOURCE
AT 15 KM AND RECEIVERS AT 12.80 KM



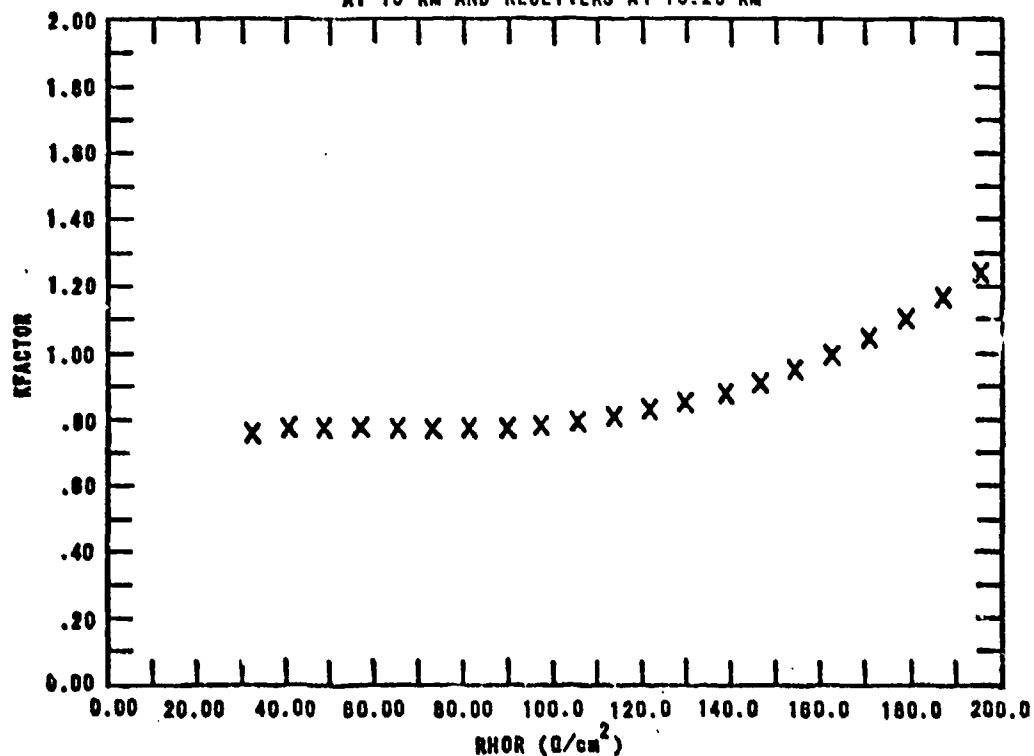
SEC-GAMMA SILICON KFACTOR FOR A FISSION SOURCE
AT 15 KM AND RECEIVERS AT 12.80 KM



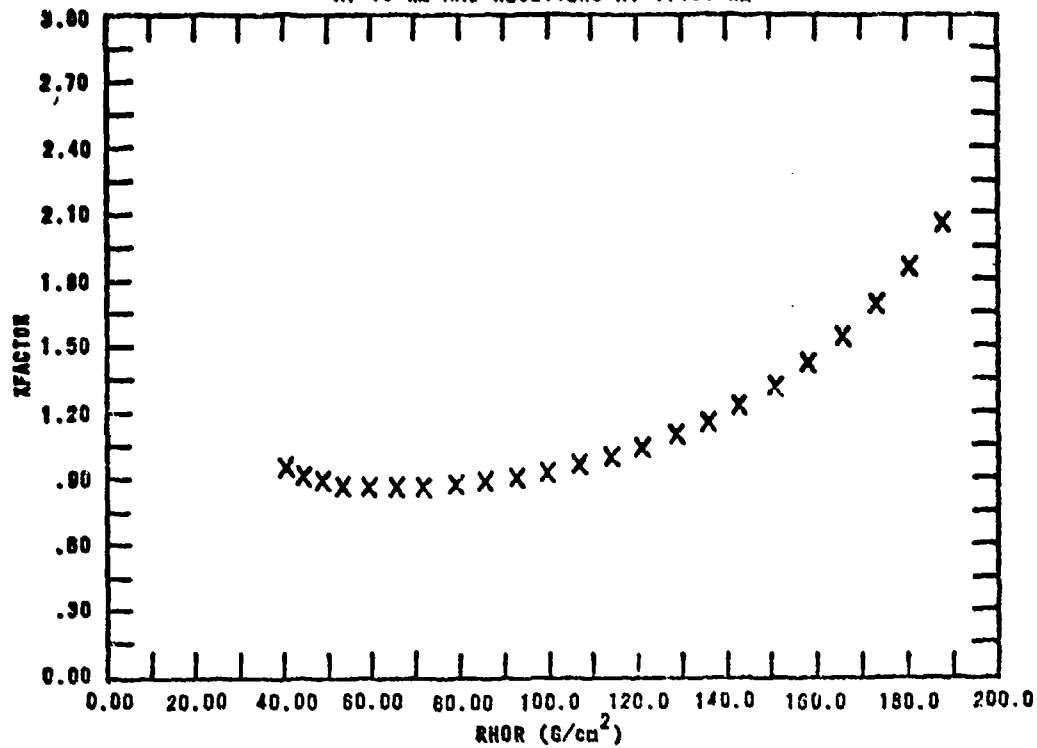
NEUTRON SILICON KFACTOR FOR A FISSION SOURCE
AT 15 KM AND RECEIVERS AT 15.29 KM



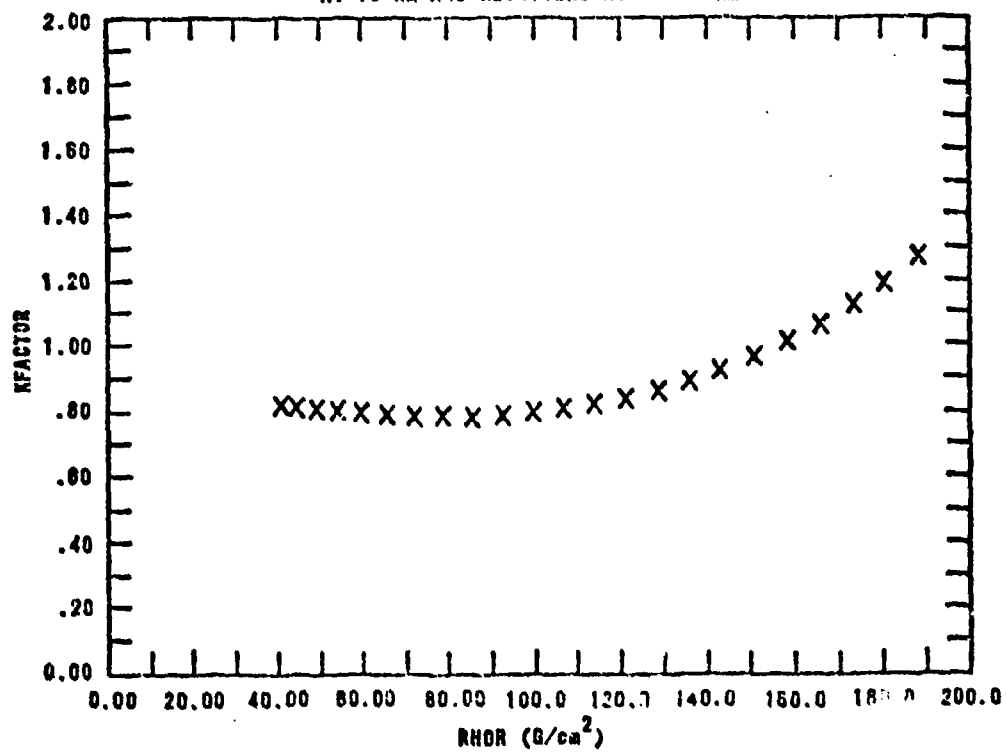
SEC-GAMMA SILICON KFACTOR FOR A FISSION SOURCE
AT 15 KM AND RECEIVERS AT 15.29 KM



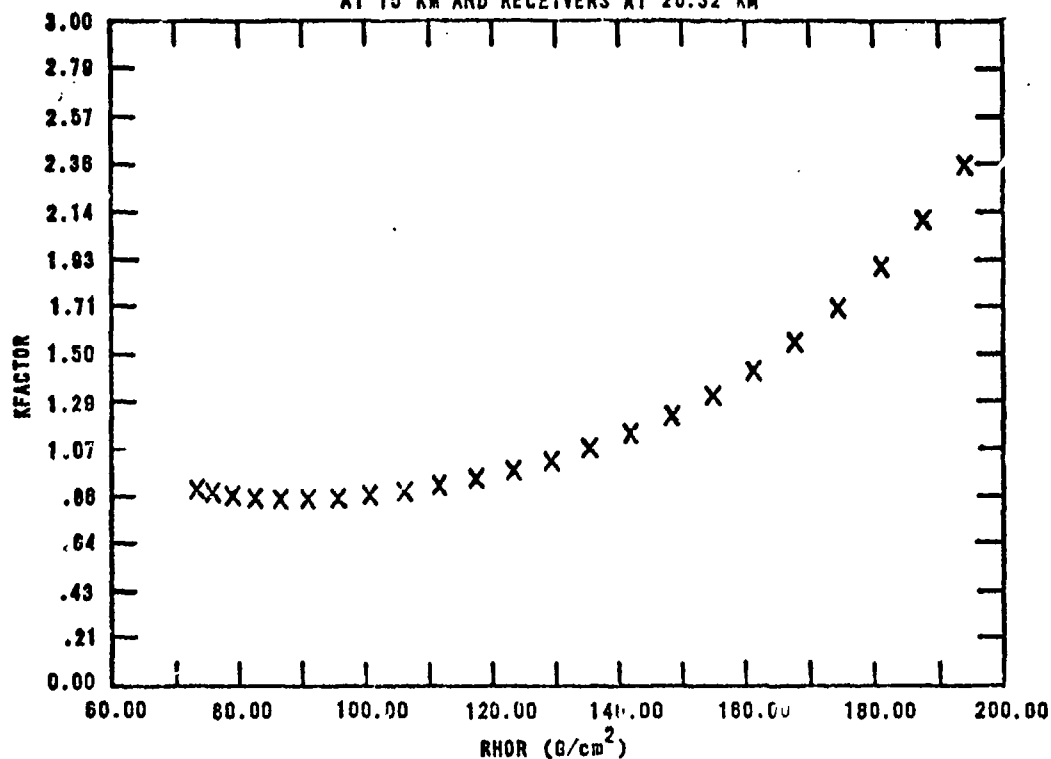
NEUTRON SILICON KFACTOR FOR A FISSION SOURCE
AT 15 KM AND RECEIVERS AT 17.36 KM



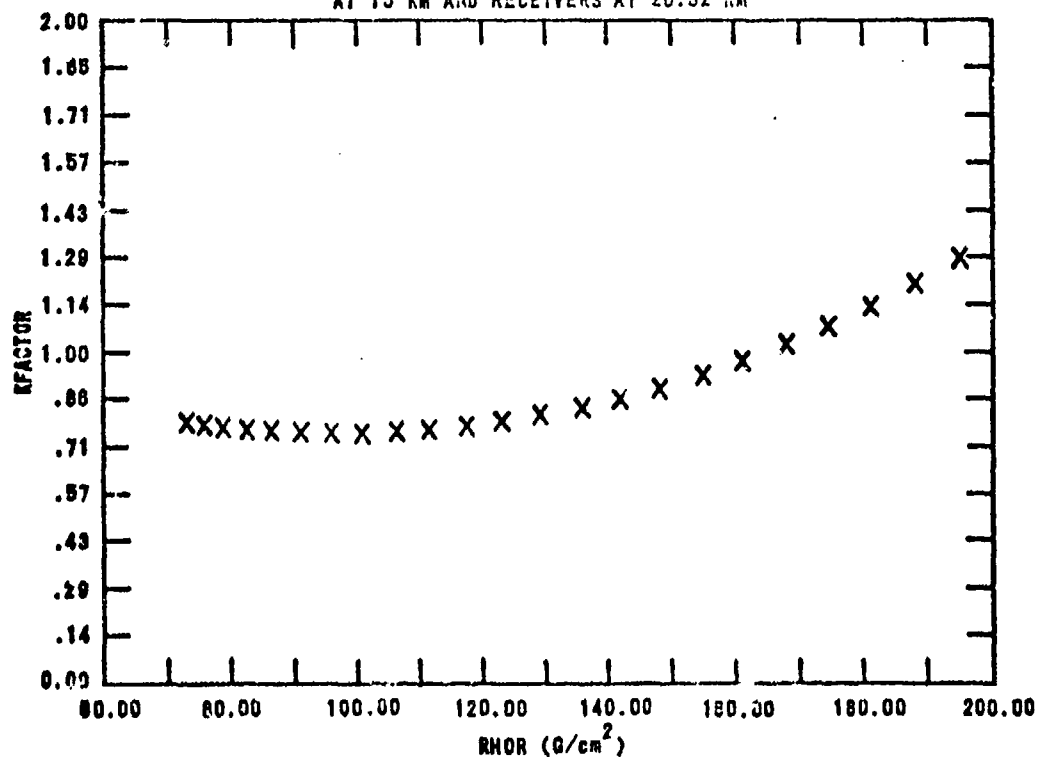
SEC-GAMMA SILICON KFACTOR FOR A FISSION SOURCE
AT 15 KM AND RECEIVERS AT 17.36 KM

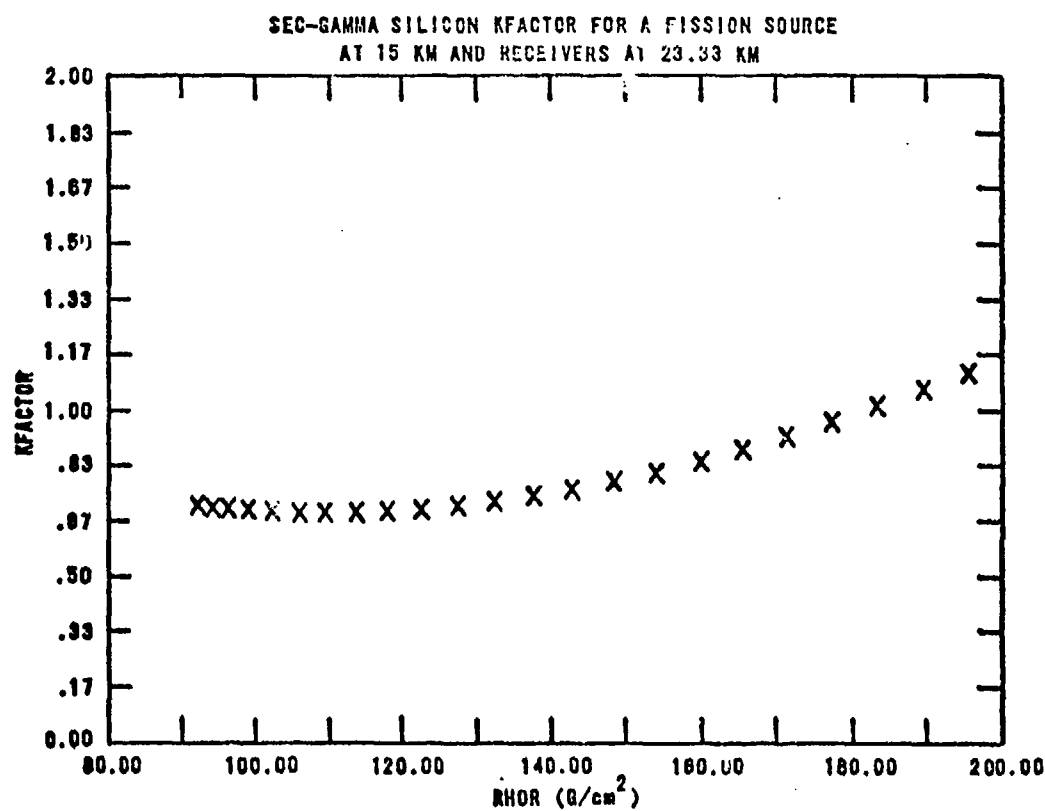
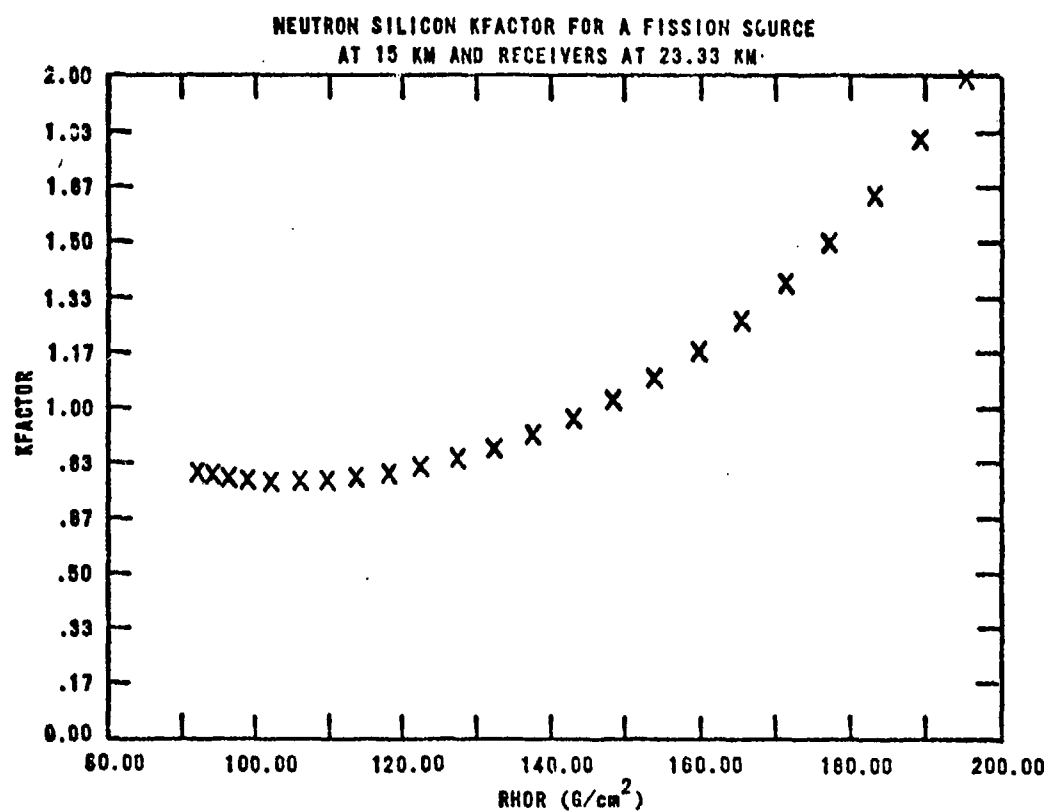


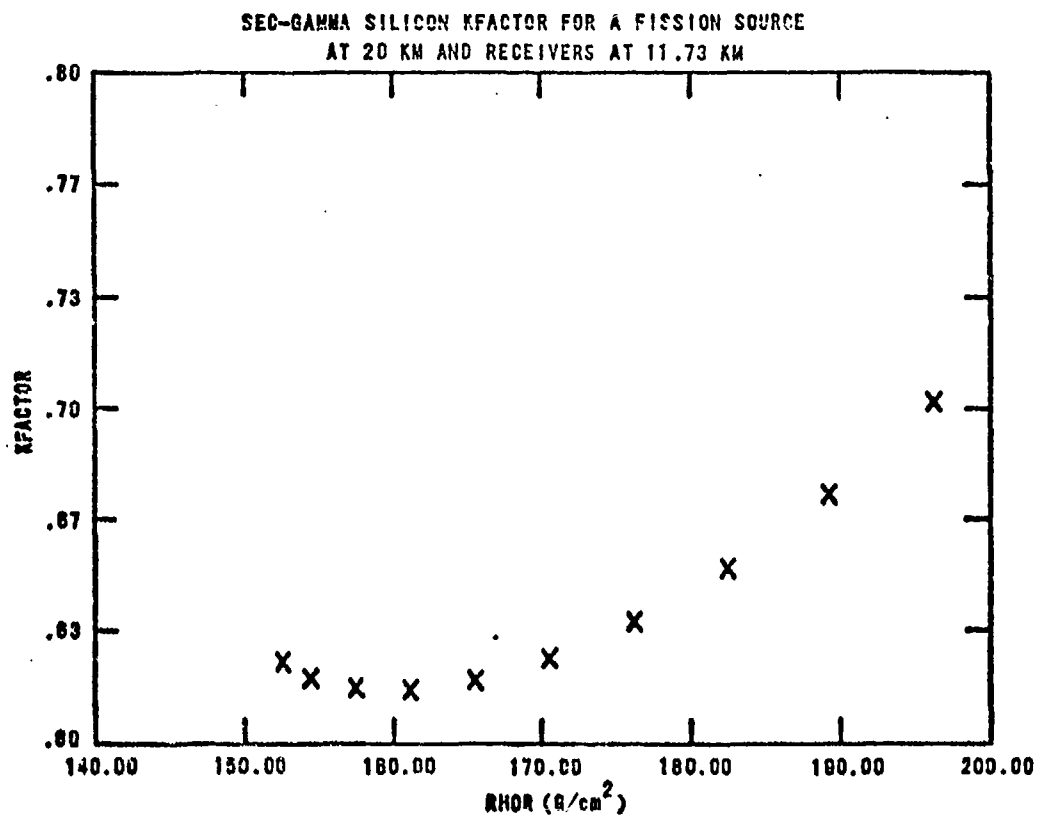
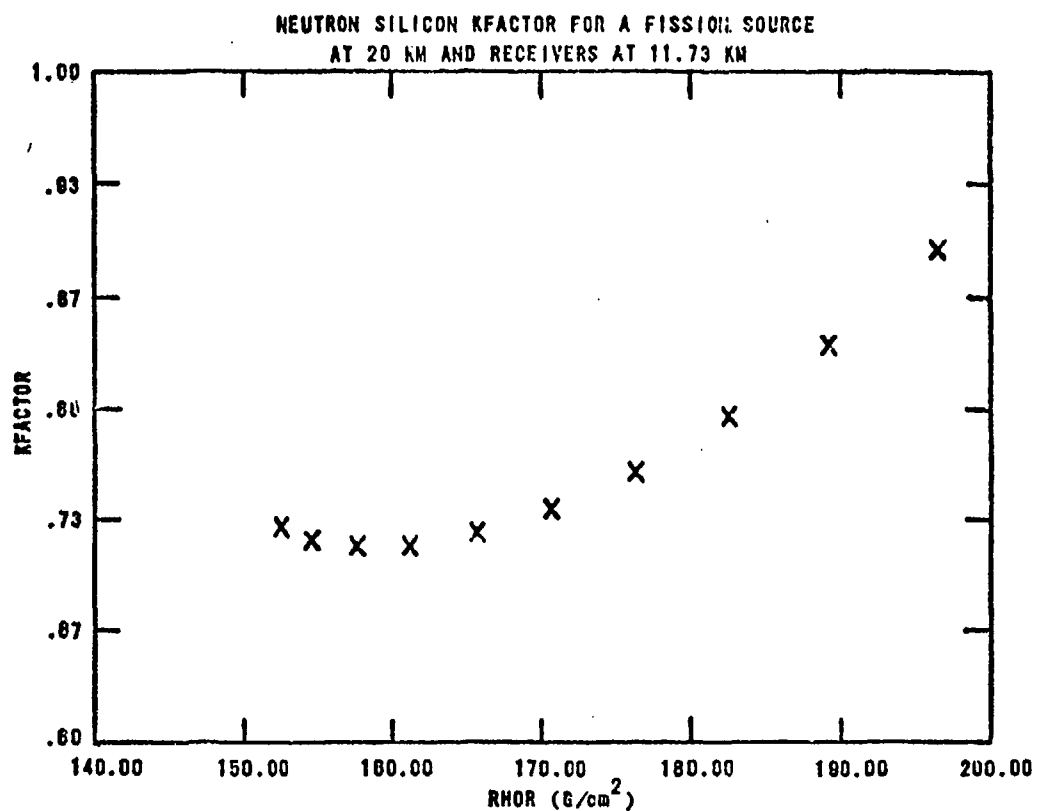
NEUTRON SILICON KFACTOR FOR A FISSION SOURCE
AT 15 KM AND RECEIVERS AT 20.32 KM



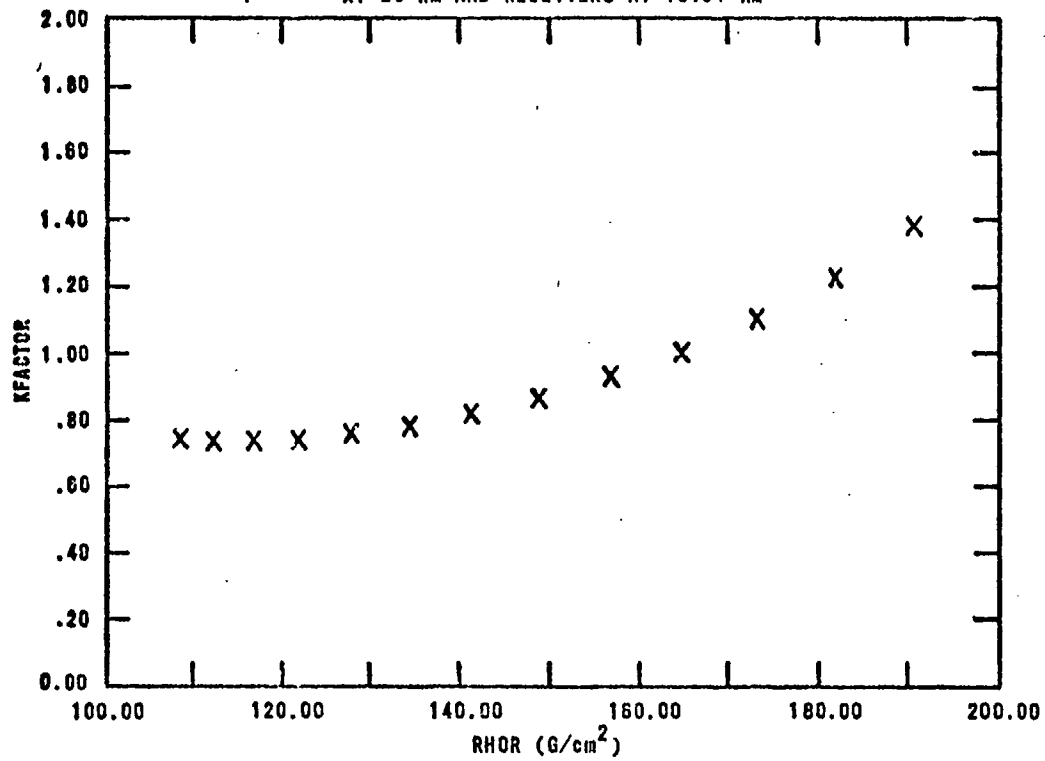
SEC-GAMMA SILICON KFACTOR FOR A FISSION SOURCE
AT 15 KM AND RECEIVERS AT 20.32 KM



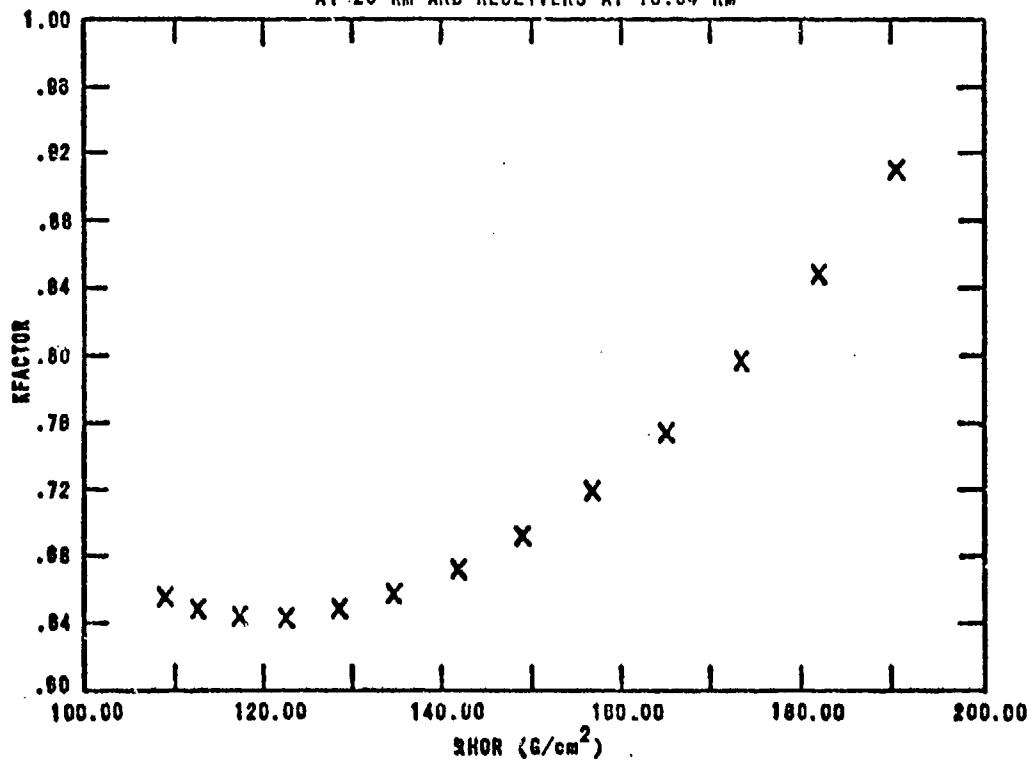




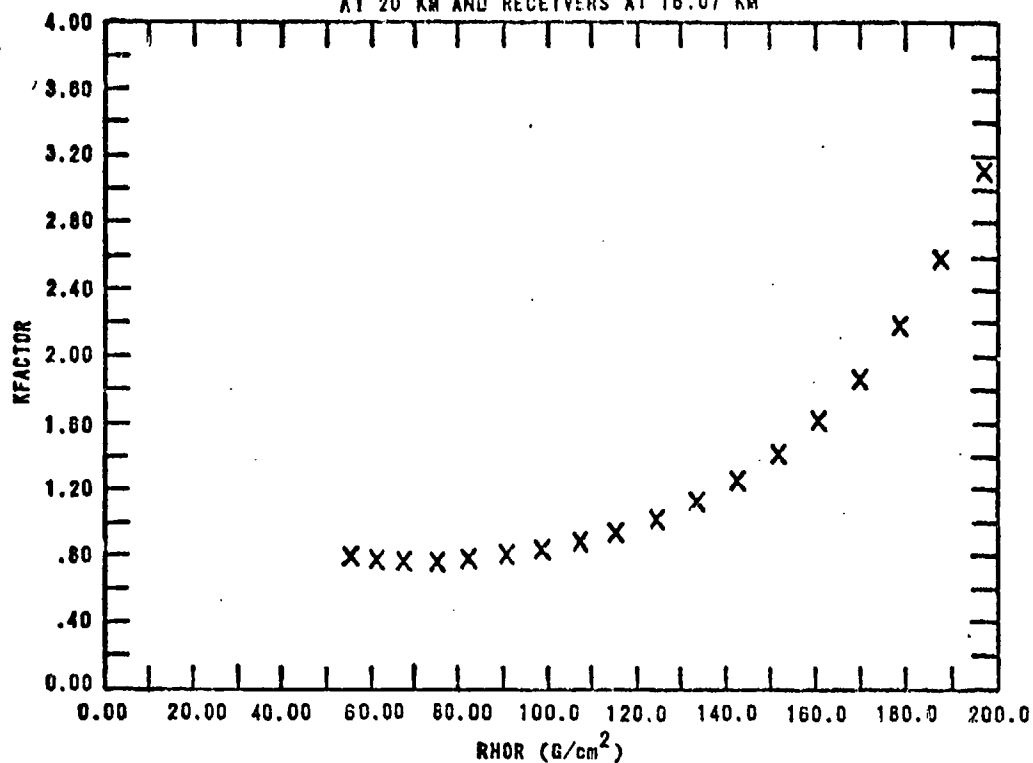
NEUTRON SILICON KFACTOR FOR A FISSION SOURCE
AT 20 KM AND RECEIVERS AT 13.34 KM



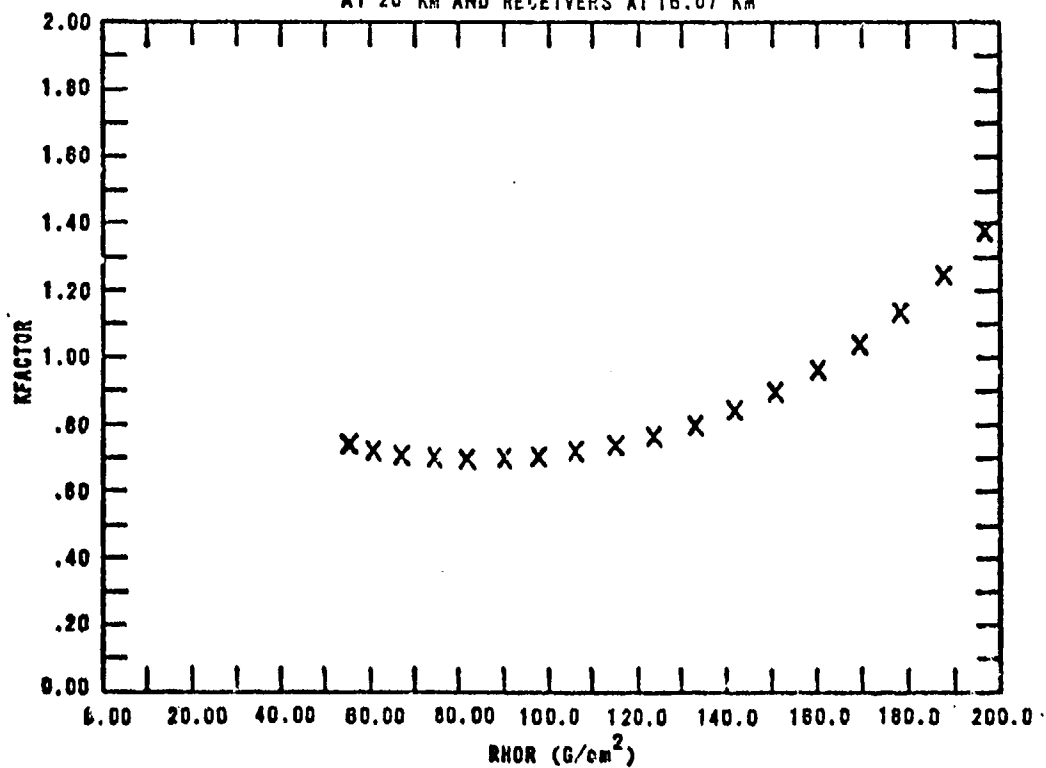
SEC-CAMMA SILICON KFACTOR FOR A FISSION SOURCE
AT 20 KM AND RECEIVERS AT 13.34 KM



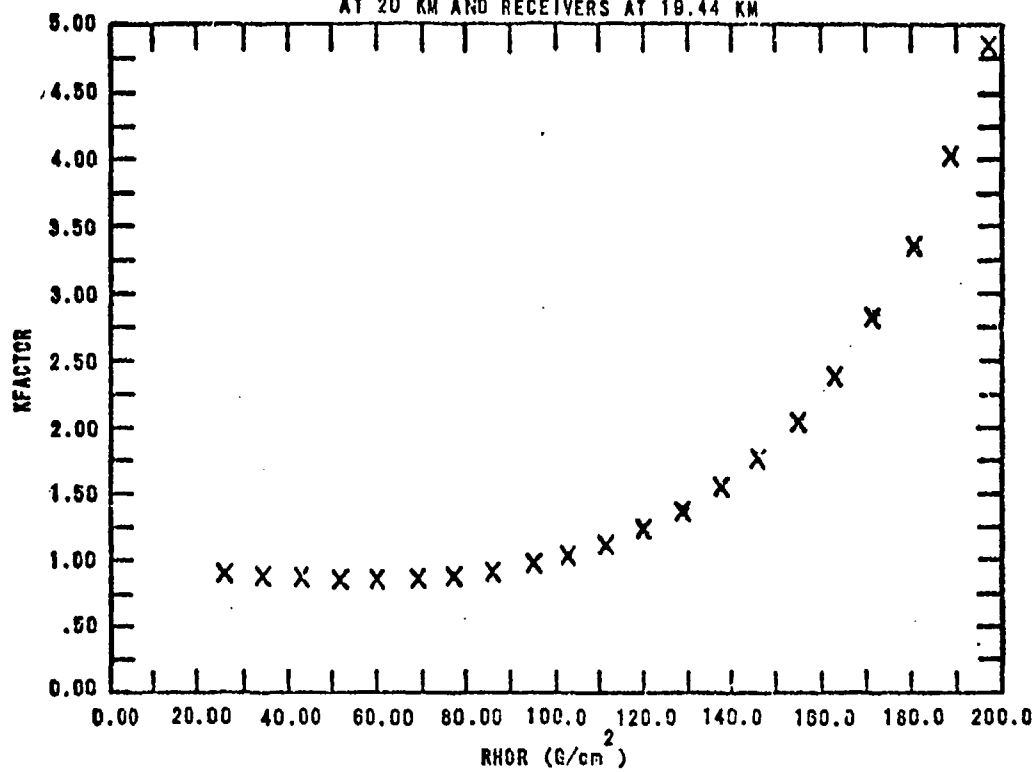
NEUTRON SILICON KFACTOR A FOR A FISSION SOURCE
AT 20 KM AND RECEIVERS AT 16.07 KM



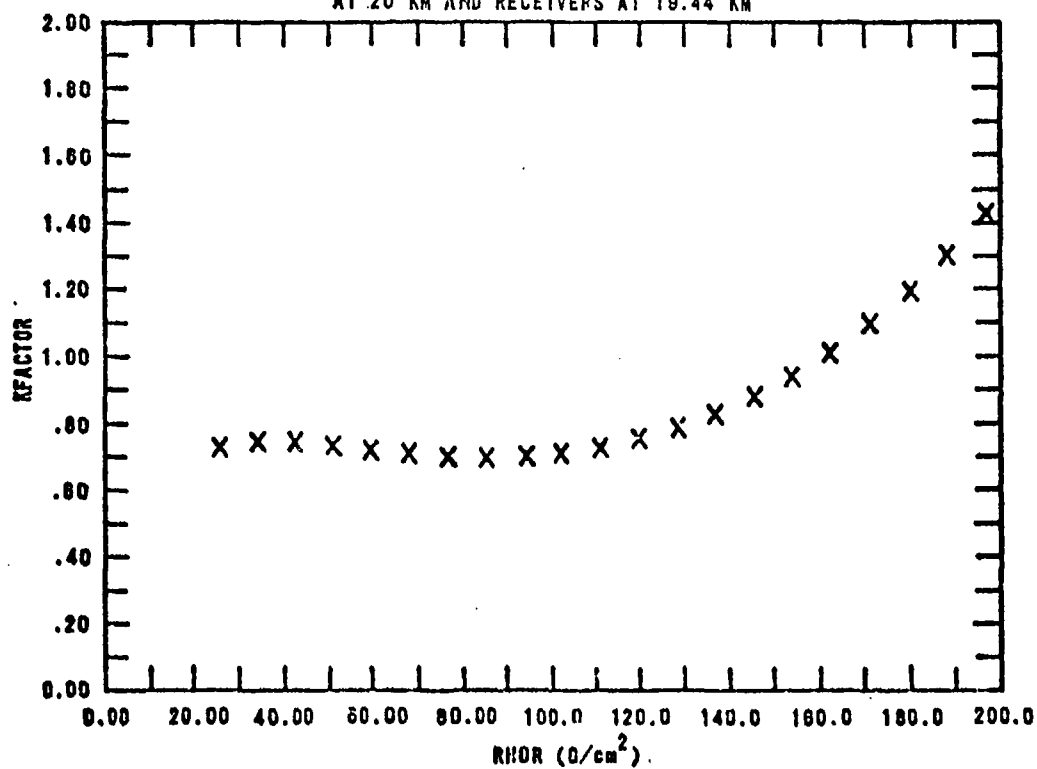
SEC-BAMMA SILICON KFACTOR FOR A FISSION SOURCE
AT 20 KM AND RECEIVERS AT 16.07 KM



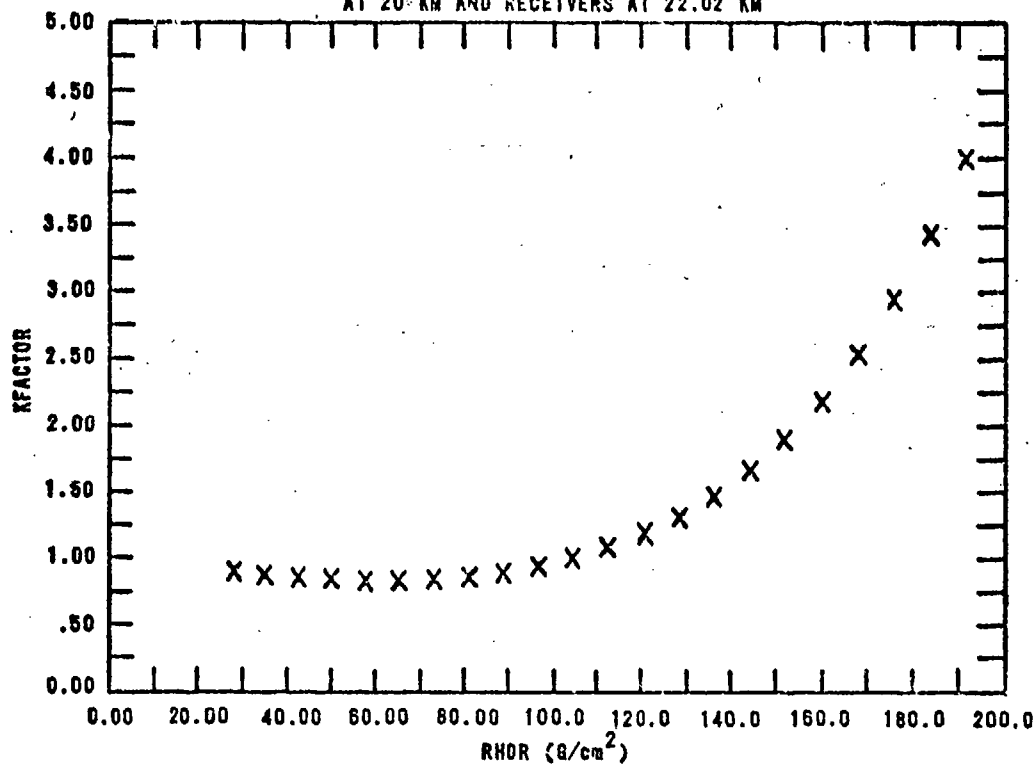
NEUTRON SILICON KFACTOR FOR A FISSION SOURCE
AT 20 KM AND RECEIVERS AT 19.44 KM



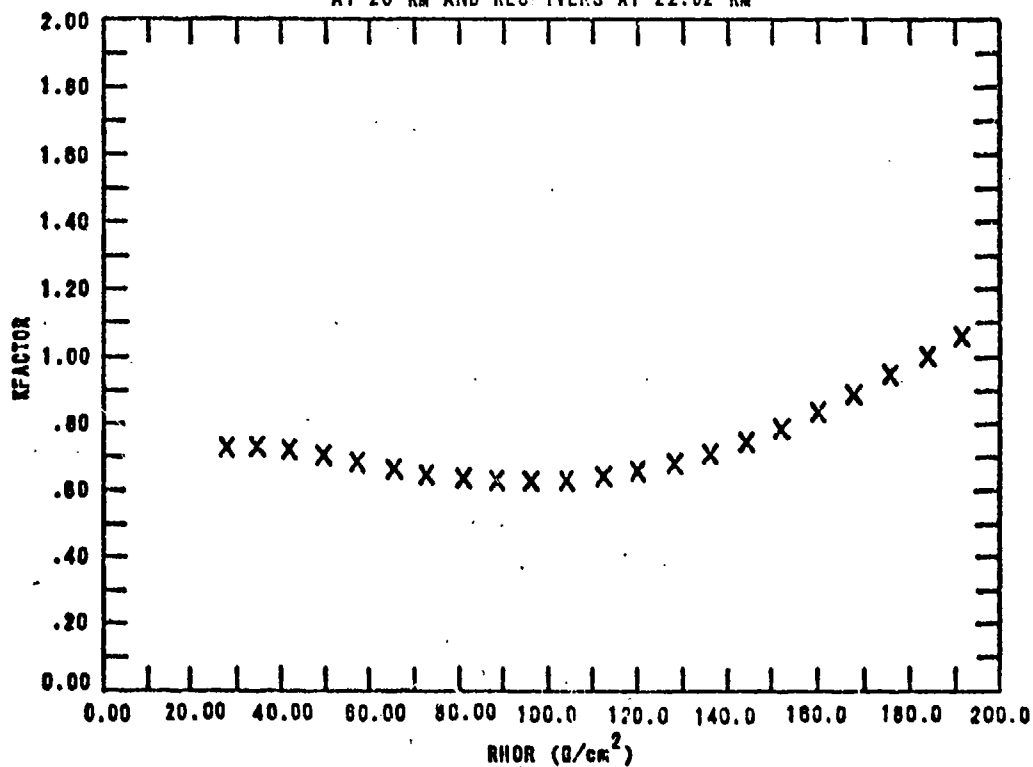
SEC-GAMMA SILICON KFACTOR FOR A FISSION SOURCE
AT 20 KM AND RECEIVERS AT 19.44 KM



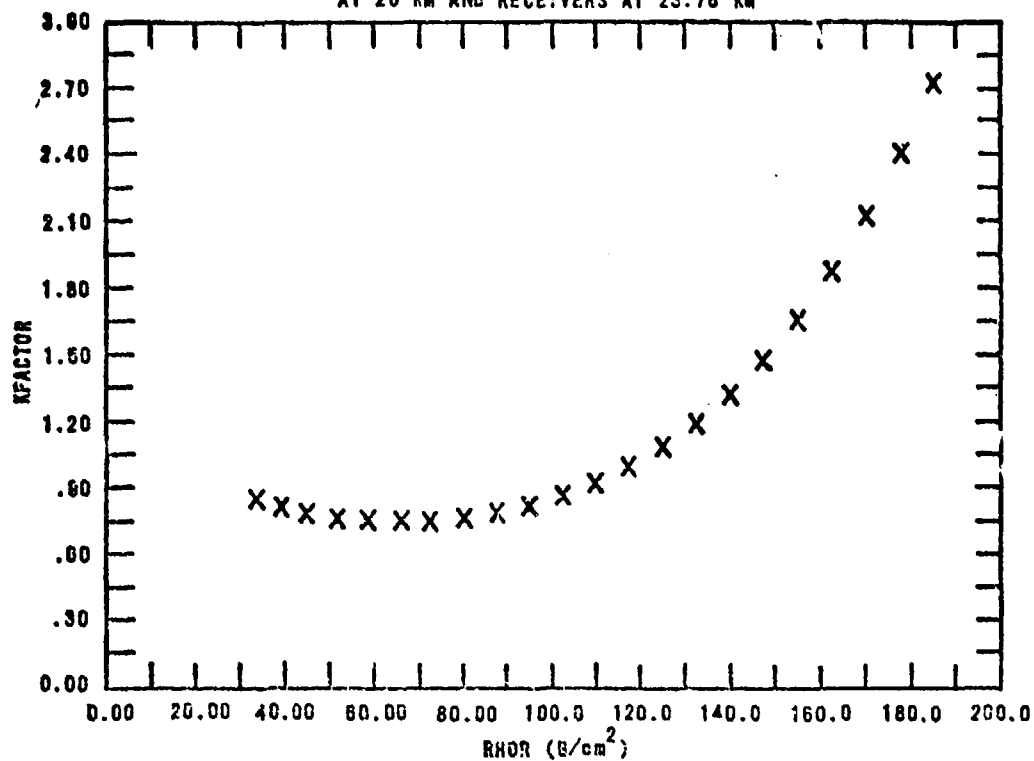
NEUTRON SILICON KFACTOR FOR A FISSION SOURCE
AT 20 KM AND RECEIVERS AT 22.02 KM



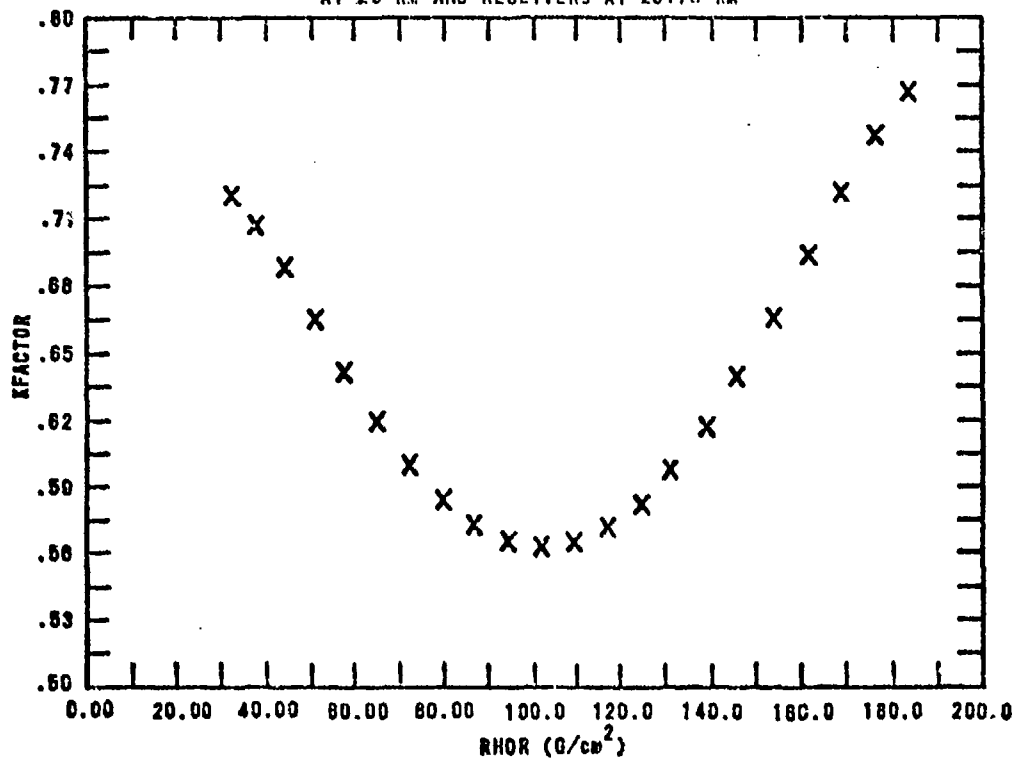
SEC-GAMMA SILICON KFACTOR FOR A FISSION SOURCE
AT 20 KM AND RECEIVERS AT 22.02 KM



NEUTRON SILICON KFACTOR FOR A FISSION SOURCE
AT 20 KM AND RECEIVERS AT 23.78 KM



SEC-GAMMA SILICON KFACTOR FOR A FISSION SOURCE
AT 20 KM AND RECEIVERS AT 23.78 KM



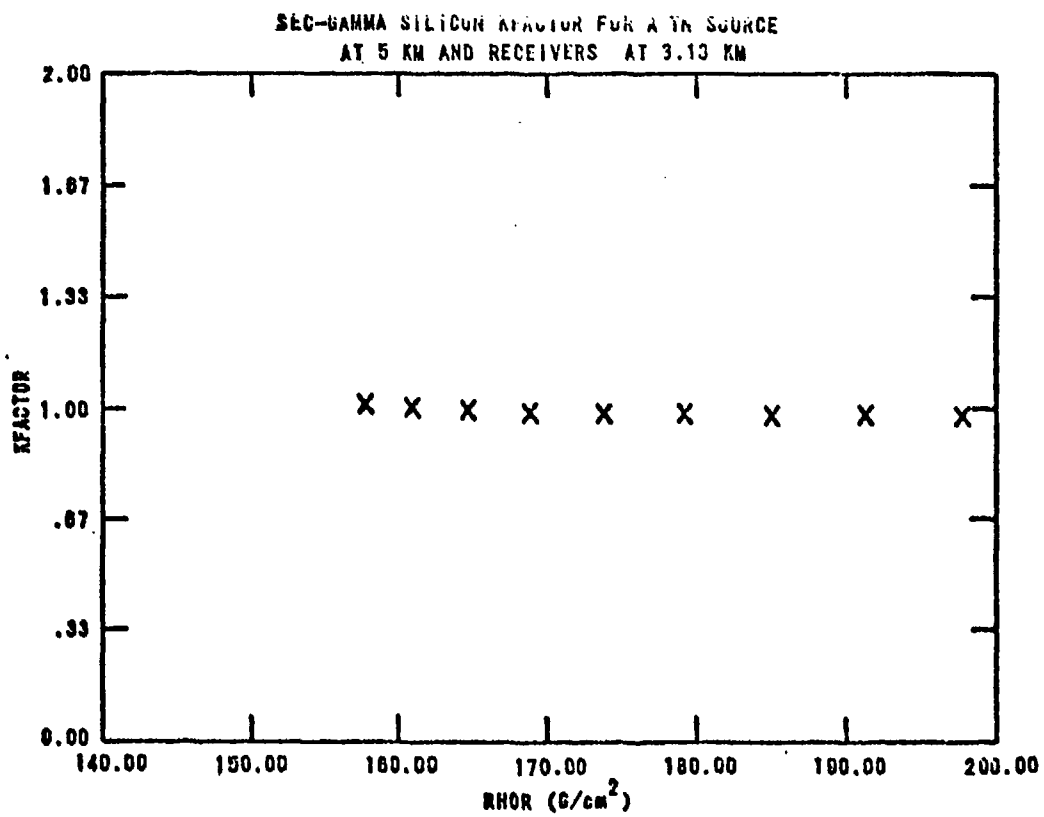
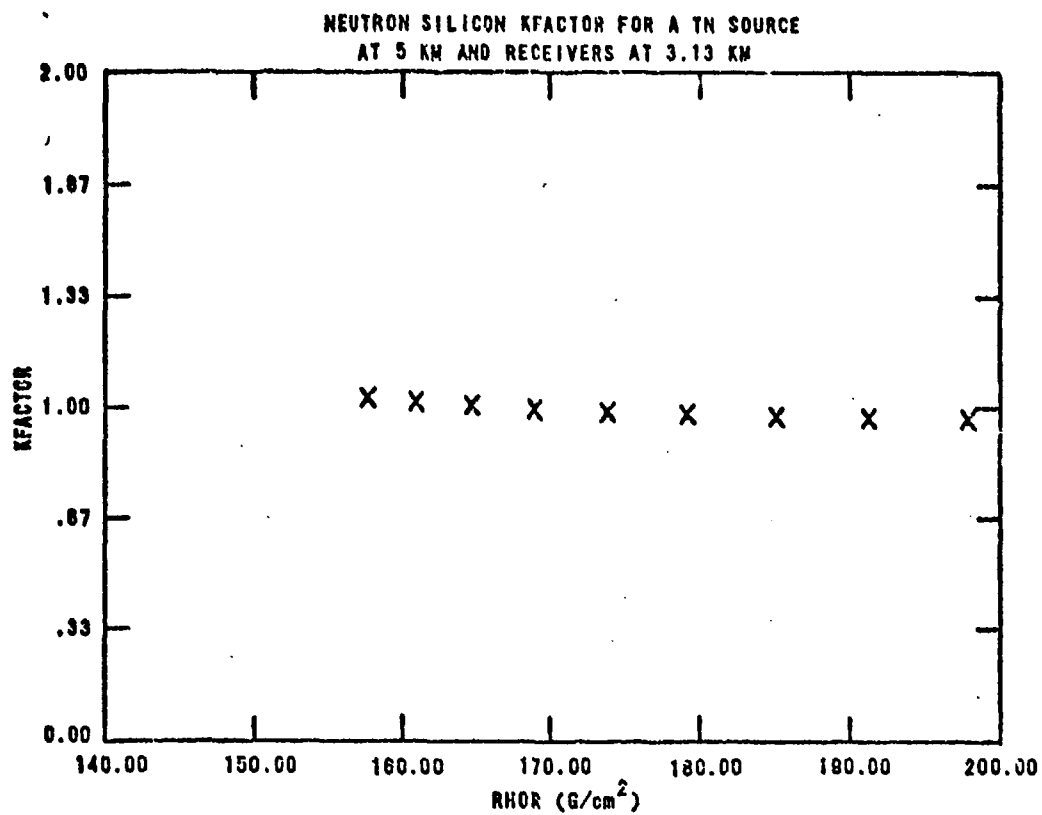
Appendix F

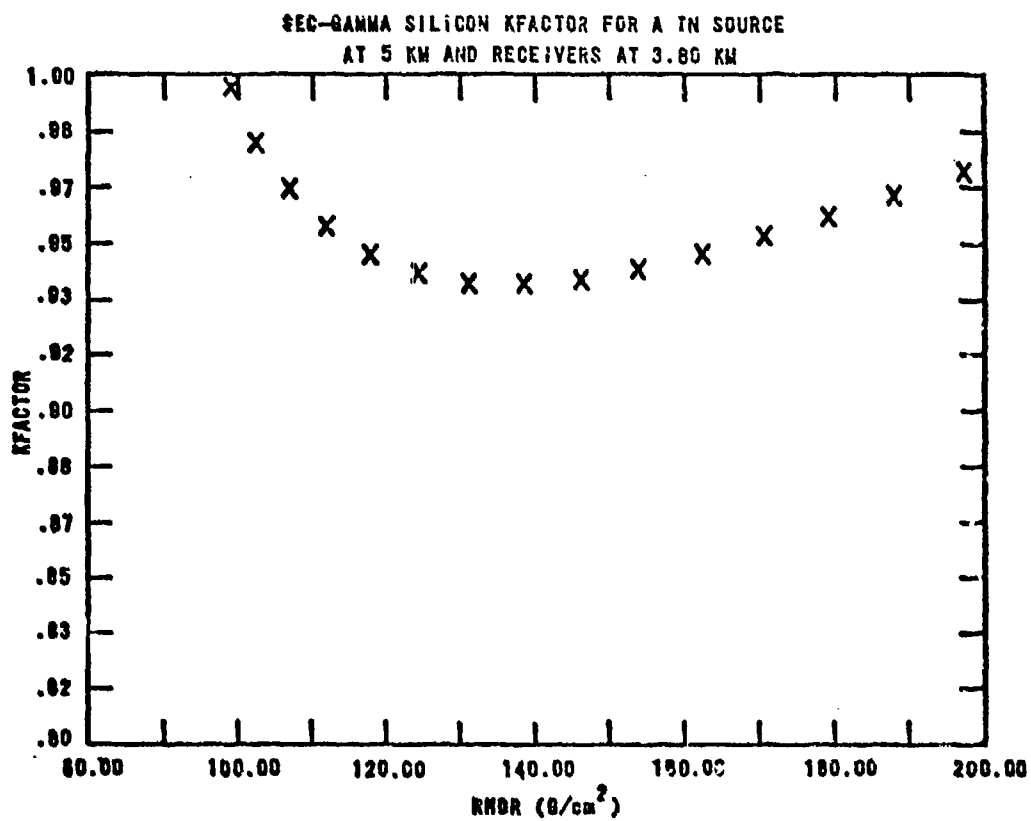
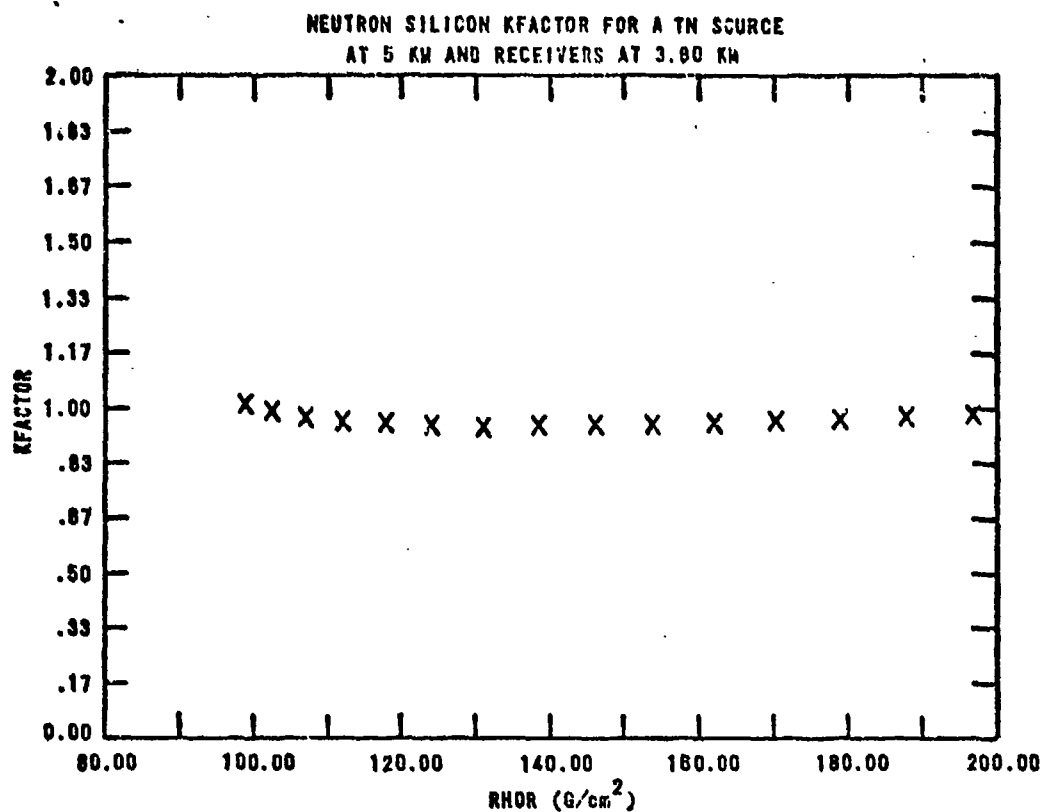
K Factor versus Mass Range Plots for a Thermonuclear Source

This appendix presents a series of K factor versus mass range* plots for the thermonuclear source in Table V. The K factors are based on the silicon dose response functions shown in Tables III and IV. Plots are included for neutrons and secondary gammas, at source altitudes of 5, 10, 15, and 20 km, and at seven receiver altitudes for each source altitude.

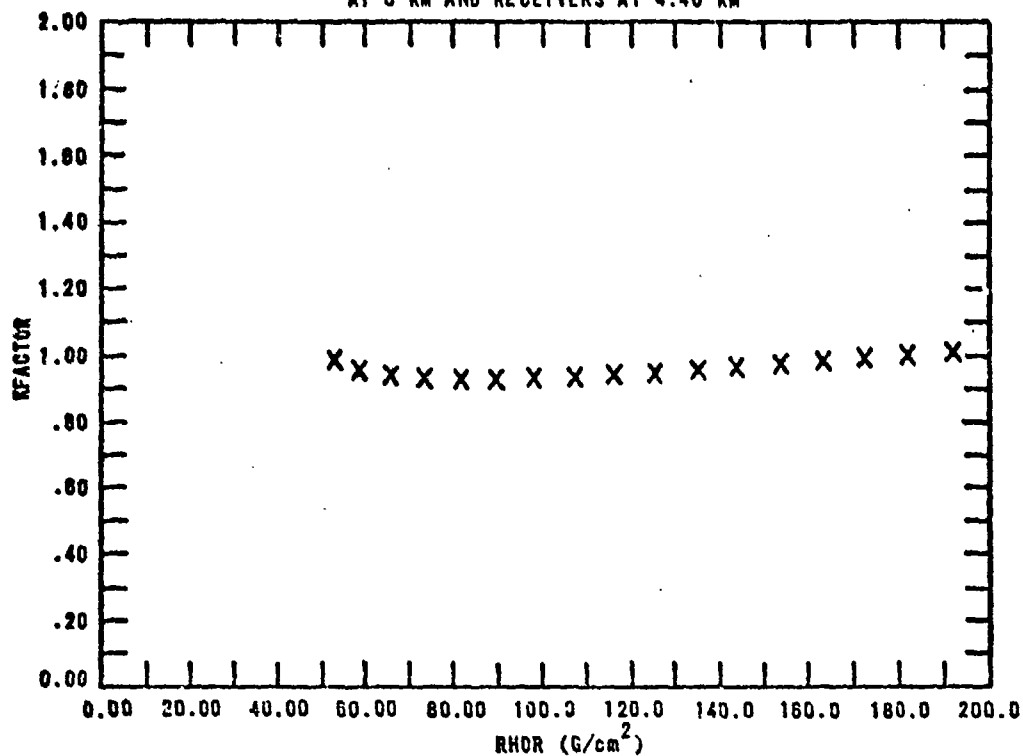
<u>Run No.</u>	<u>Index</u>	<u>Page</u>
	<u>Source Altitude (km)</u>	
1	5	155
2	10	162
3	15	169
4	20	176

*Mass range, $\langle \rho R \rangle$, is defined by equation (2.3) in Section II. In this appendix, the symbol "RHOR" is used for $\langle \rho R \rangle$.

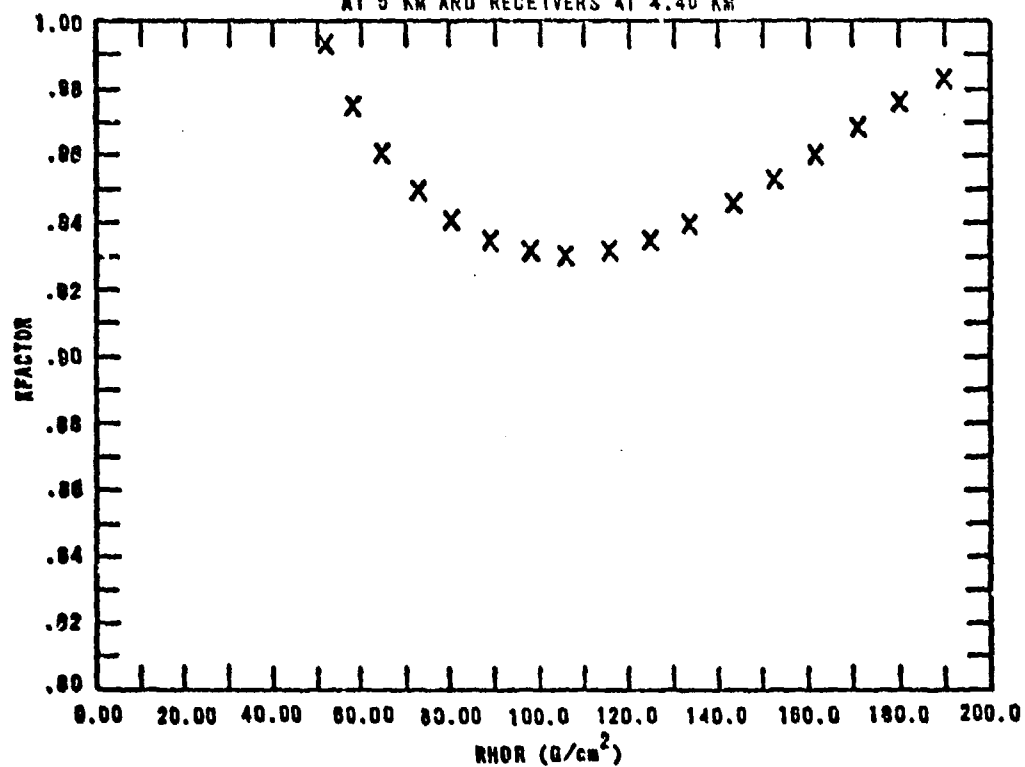




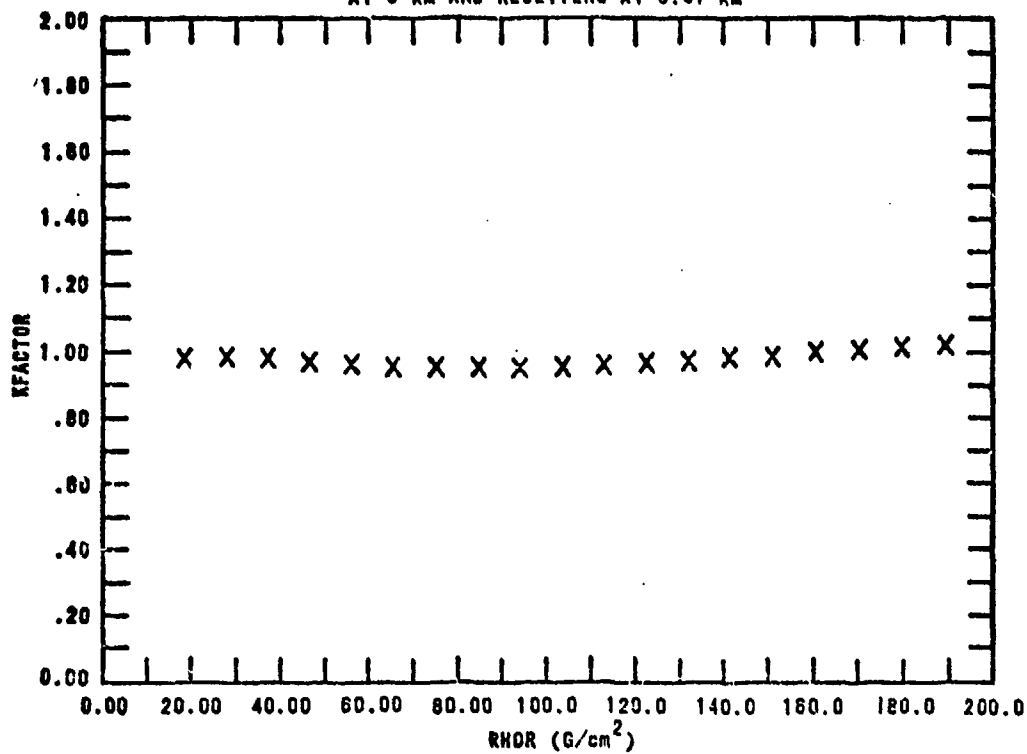
NEUTRON SILICON KFACTOR FOR A TN SOURCE
AT 5 KM AND RECEIVERS AT 4.40 KM



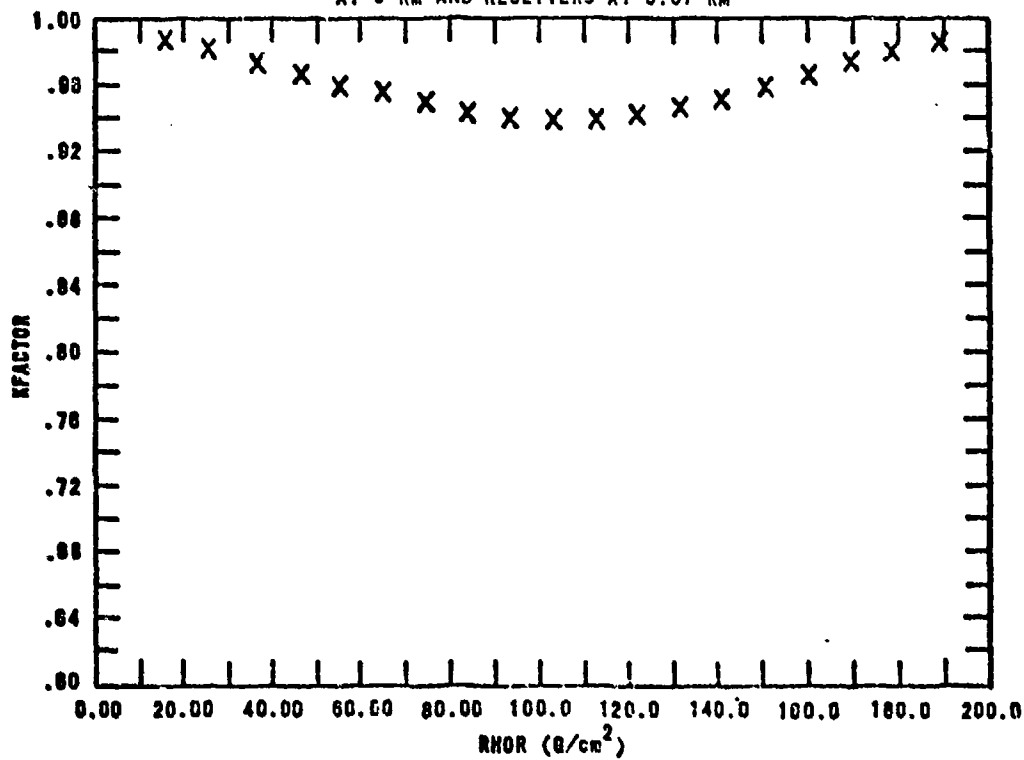
SEC-GAMMA SILICON KFACTOR FOR A TN SOURCE
AT 5 KM AND RECEIVERS AT 4.40 KM



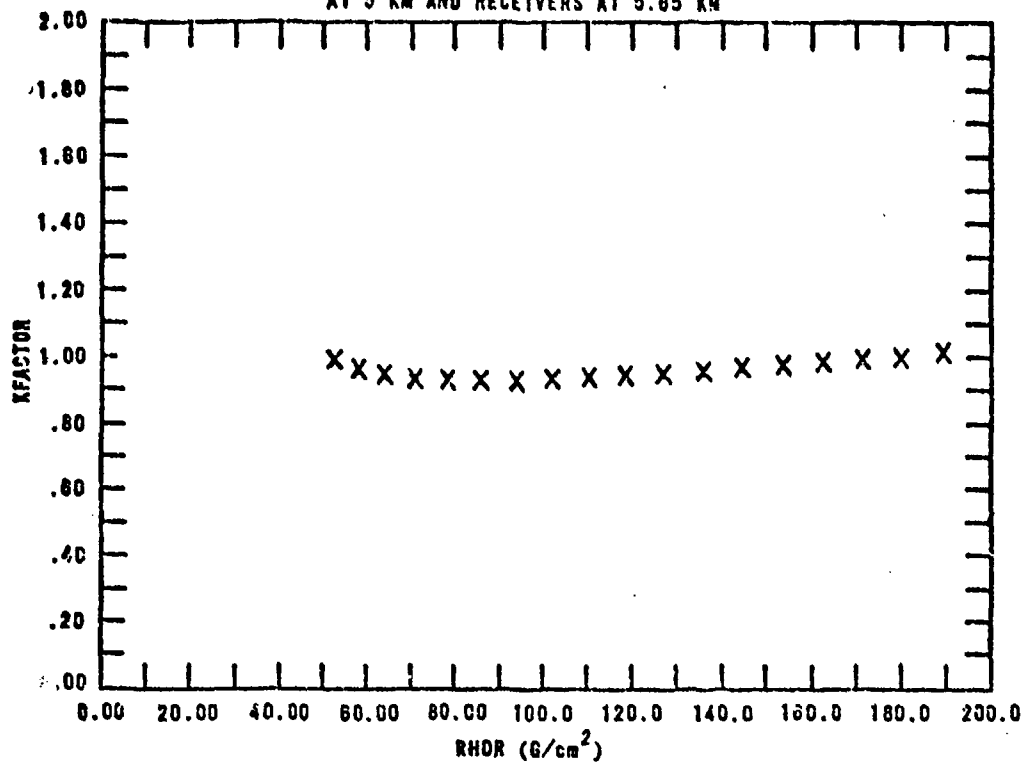
NEUTRON SILICON KFACTOR FOR A TN SOURCE
AT 5 KM AND RECEIVERS AT 5.07 KM



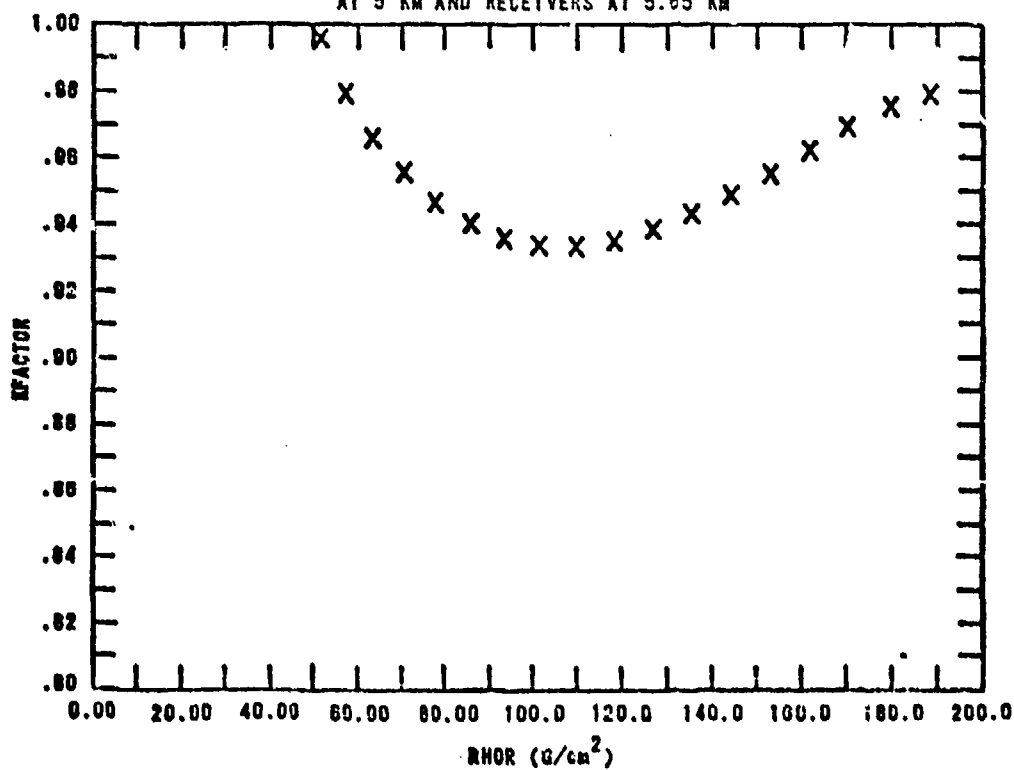
SEC-GAMMA SILICON KFACTOR FOR A TN SOURCE
AT 5 KM AND RECEIVERS AT 5.07 KM

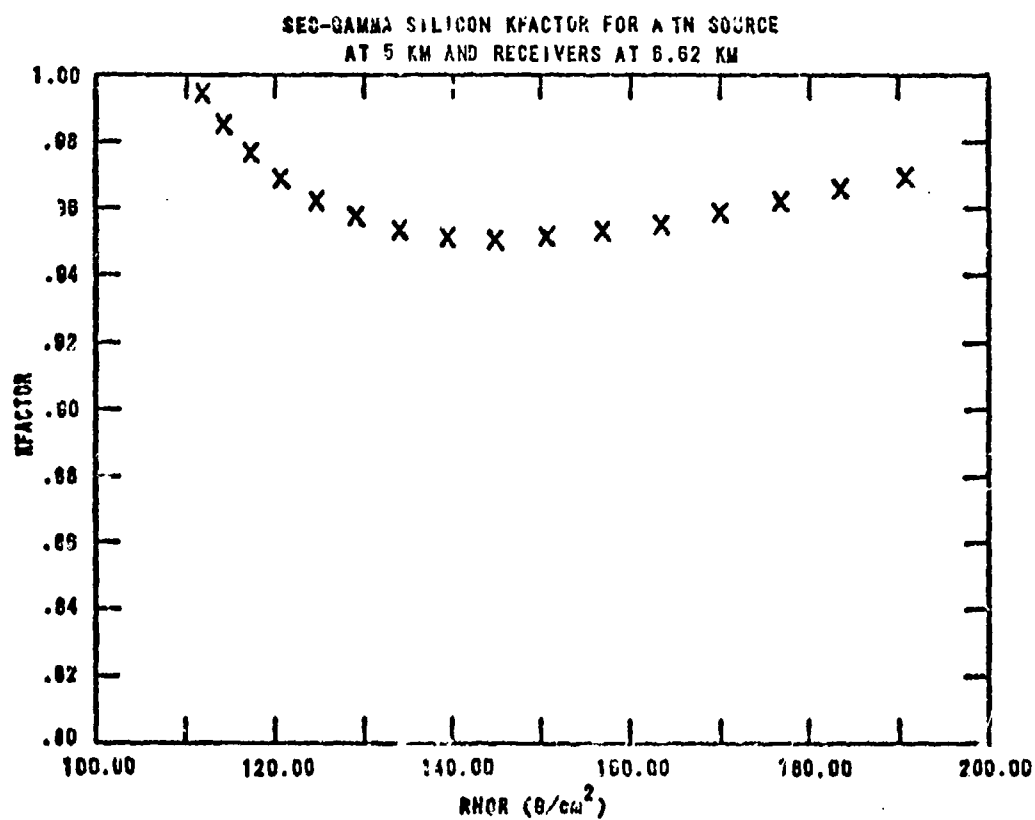
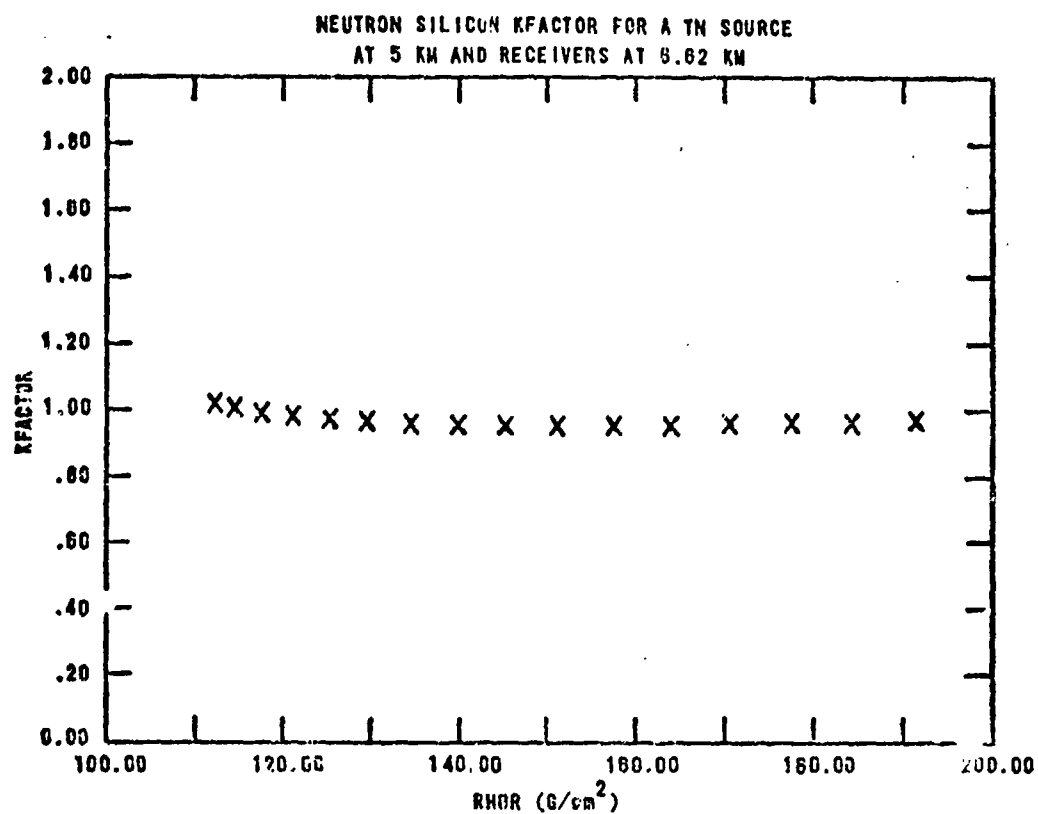


NEUTRON SILICON KFACTOR FOR A TN SOURCE
AT 5 KM AND RECEIVERS AT 5.65 KM

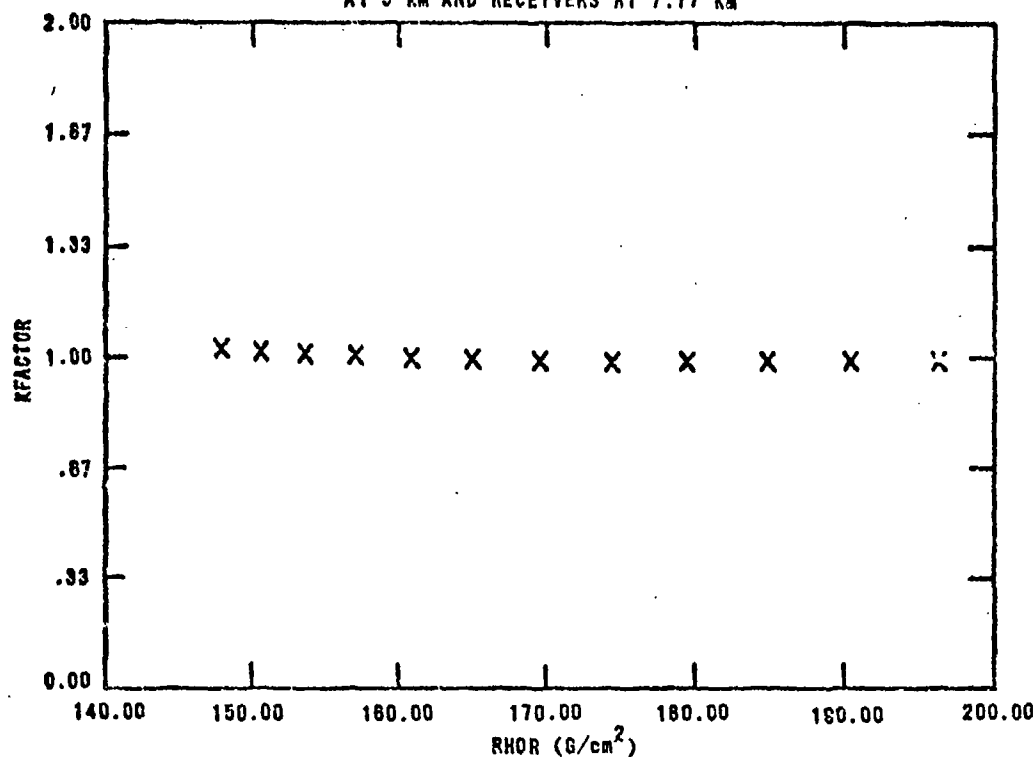


SEC-GAMMA SILICON KFACTOR FOR A TN SOURCE
AT 5 KM AND RECEIVERS AT 5.65 KM

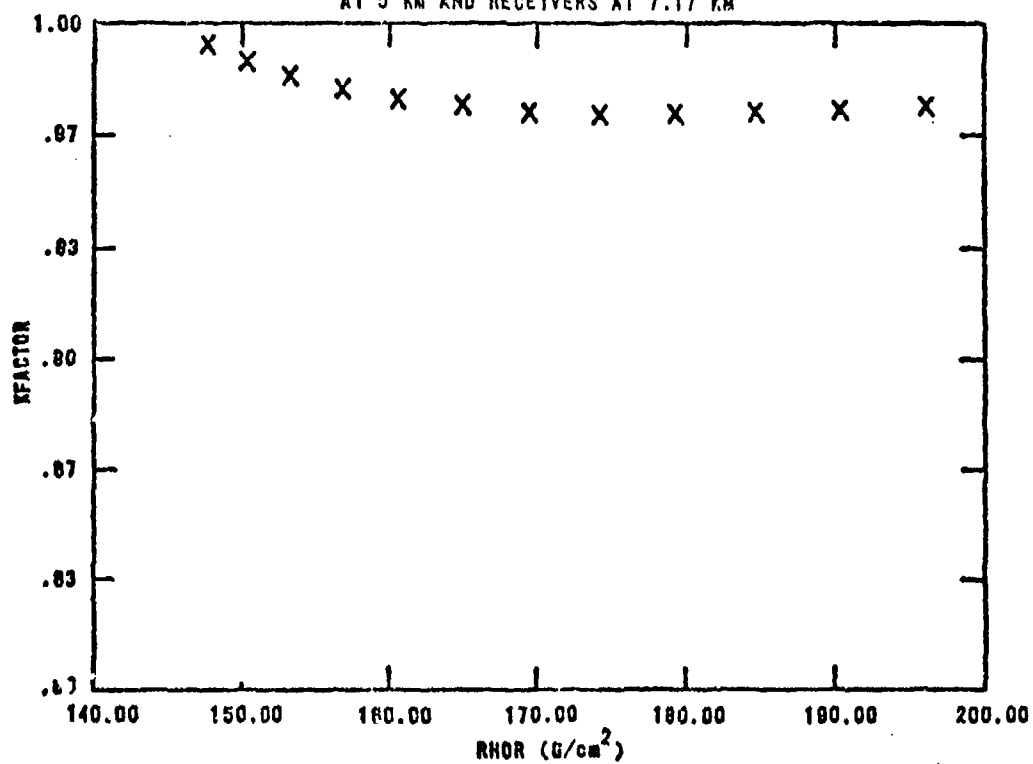


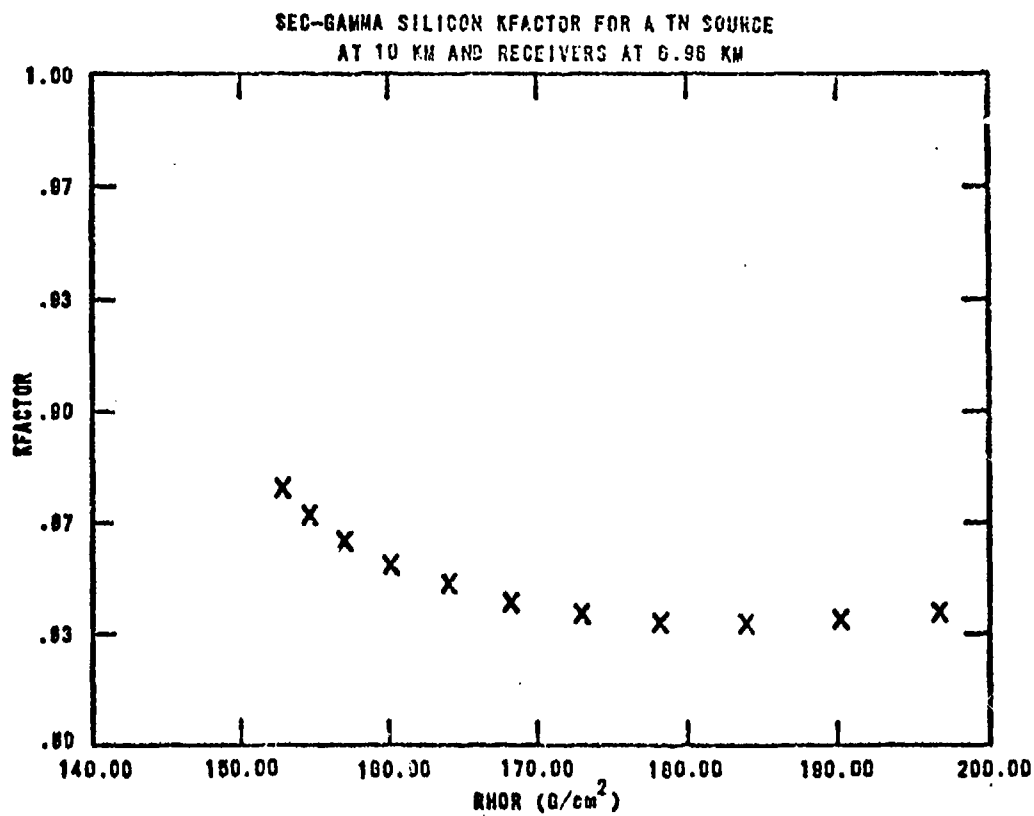
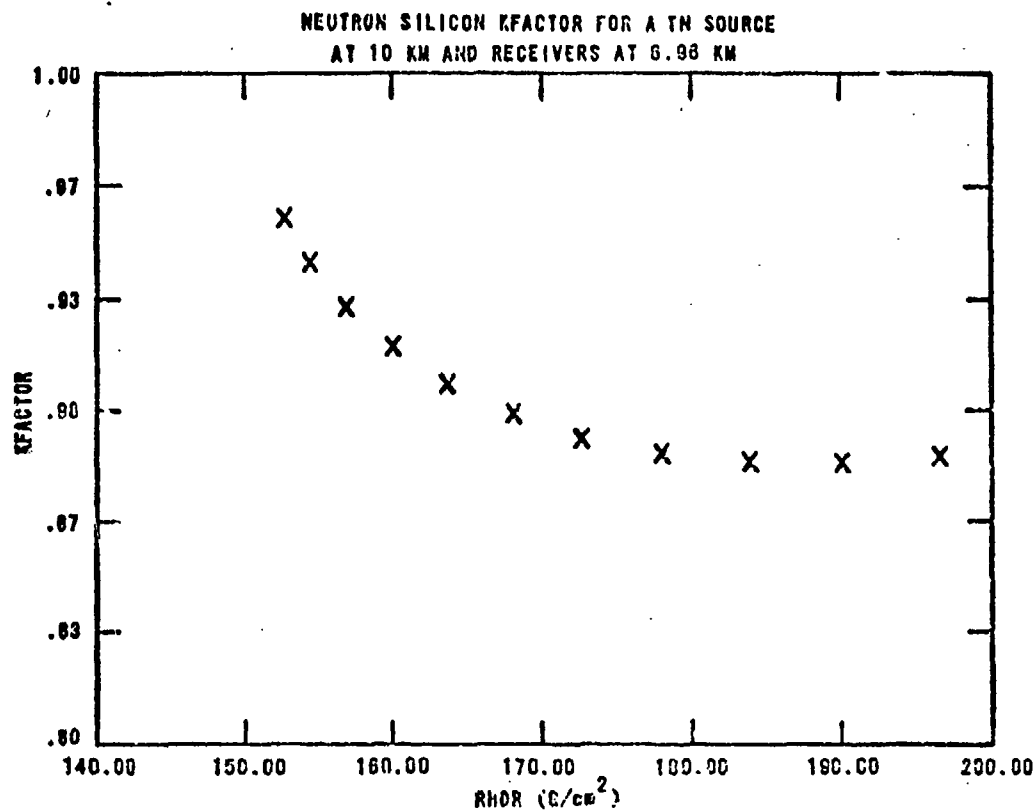


NEUTRON SILICON KFACTOR FOR A TN SOURCE
AT 5 KM AND RECEIVERS AT 7.17 KM

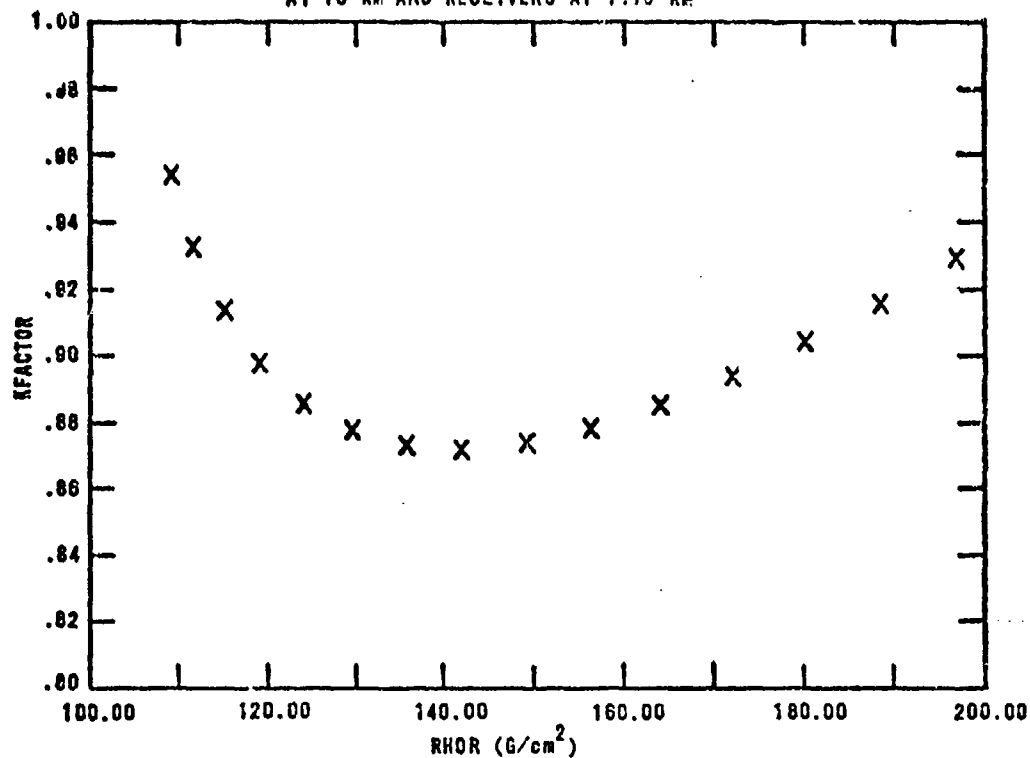


SEC-GAMMA SILICON KFACTOR FOR A TN SOURCE
AT 5 KM AND RECEIVERS AT 7.17 KM

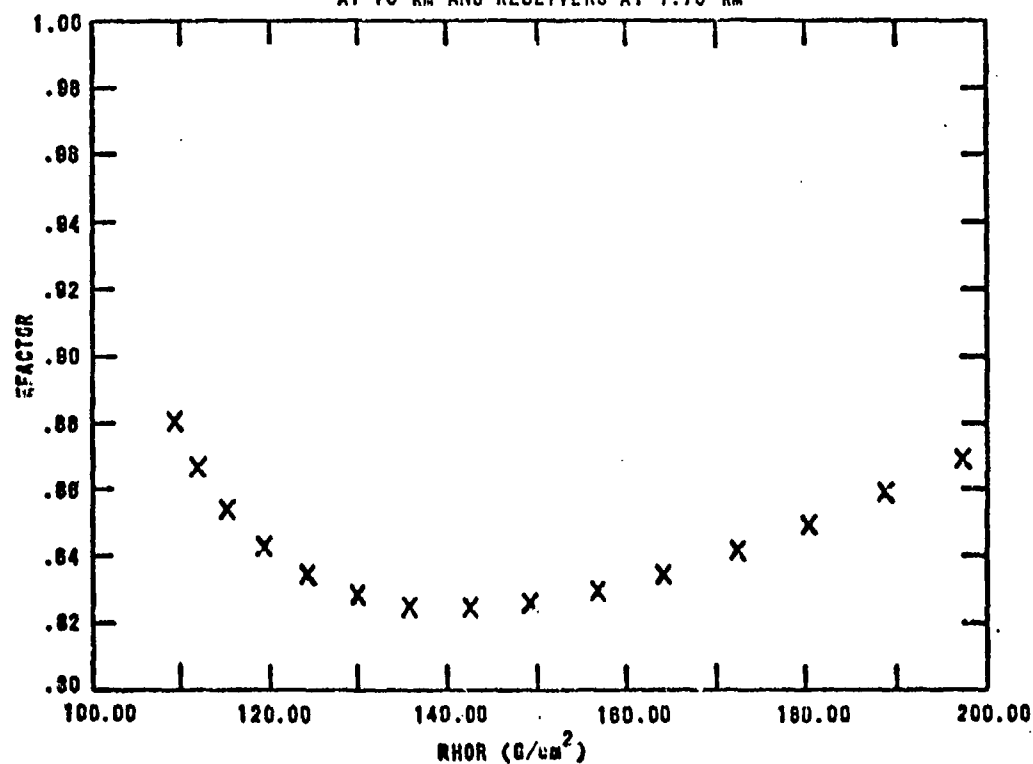




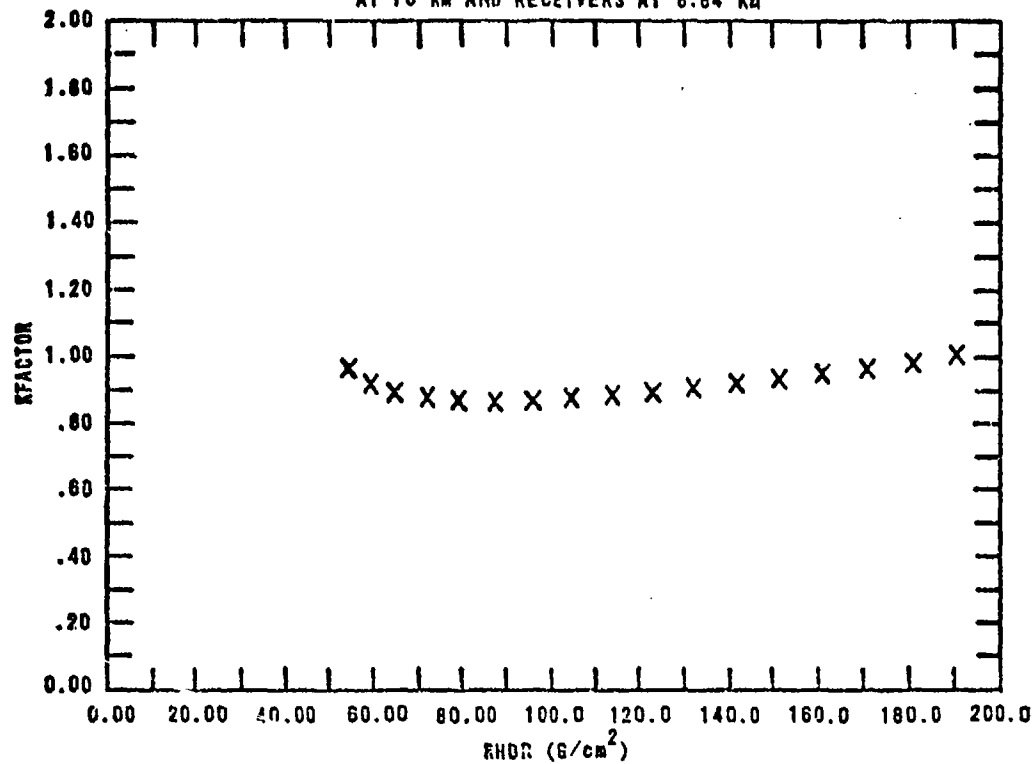
NEUTRON SILICON KFACTOR FOR A TN SOURCE
AT 10 KM AND RECEIVERS AT 7.73 KM



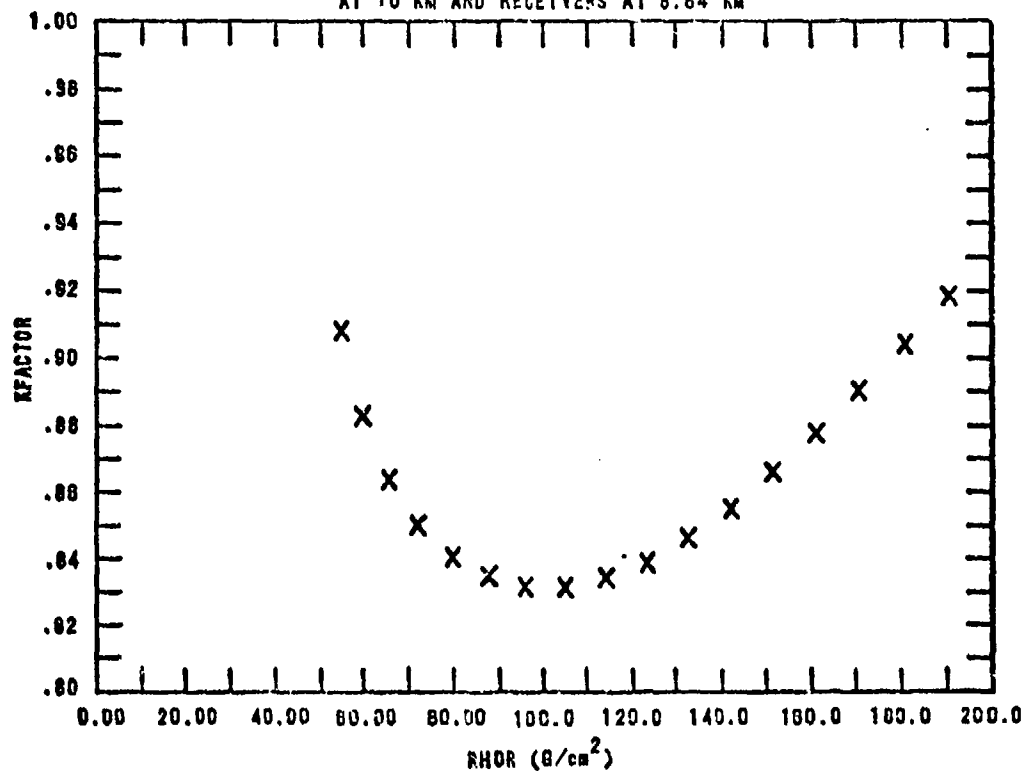
SEC-GAMMA SILICON KFACTOR FOR A TN SOURCE
AT 10 KM AND RECEIVERS AT 7.73 KM



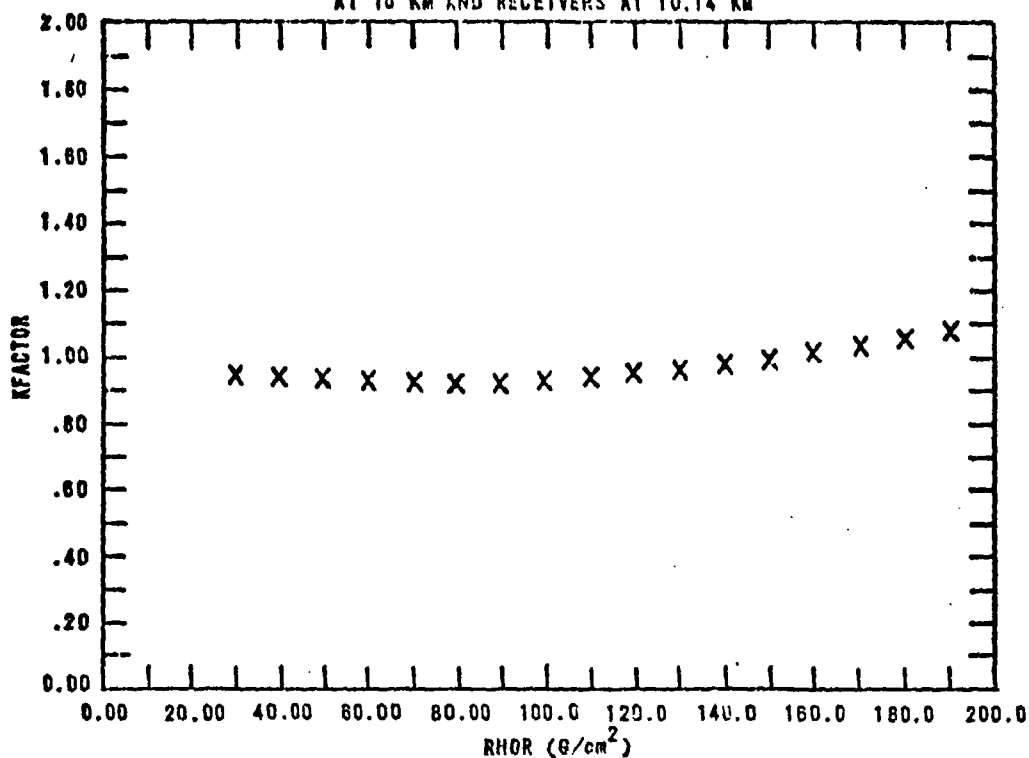
NEUTRON SILICON KFACTOR FOR A 1N SOURCE
AT 10 KM AND RECEIVERS AT 8.64 KM



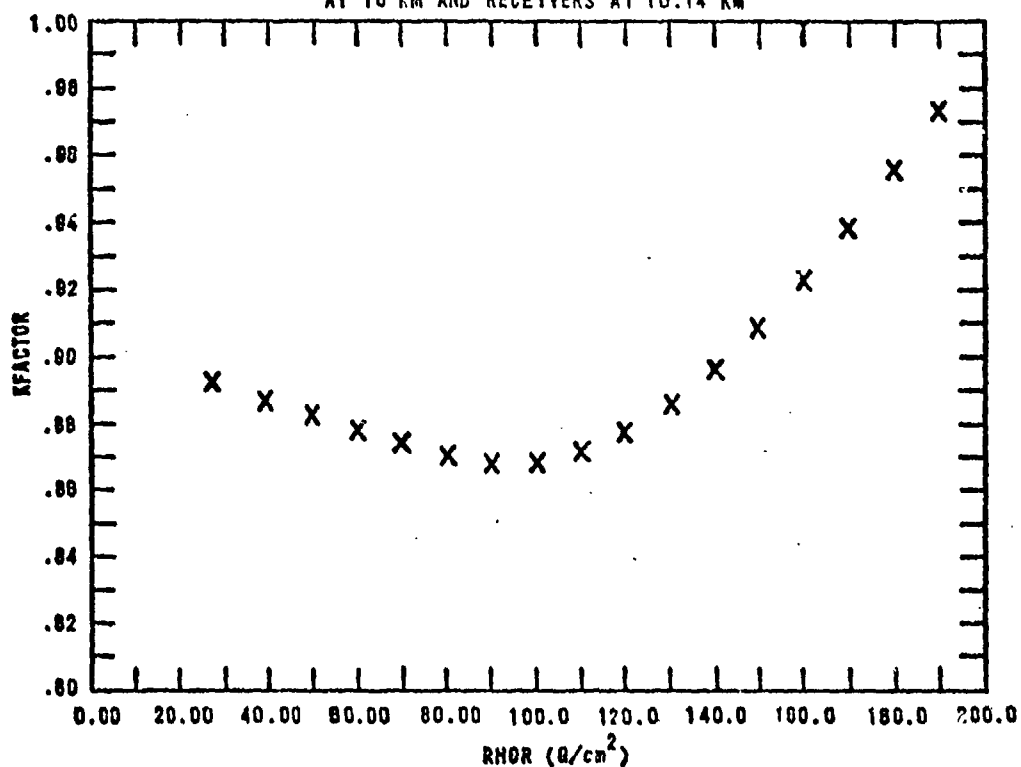
SEC-GAMMA SILICON KFACTOR FOR A 1N SOURCE
AT 10 KM AND RECEIVERS AT 8.64 KM



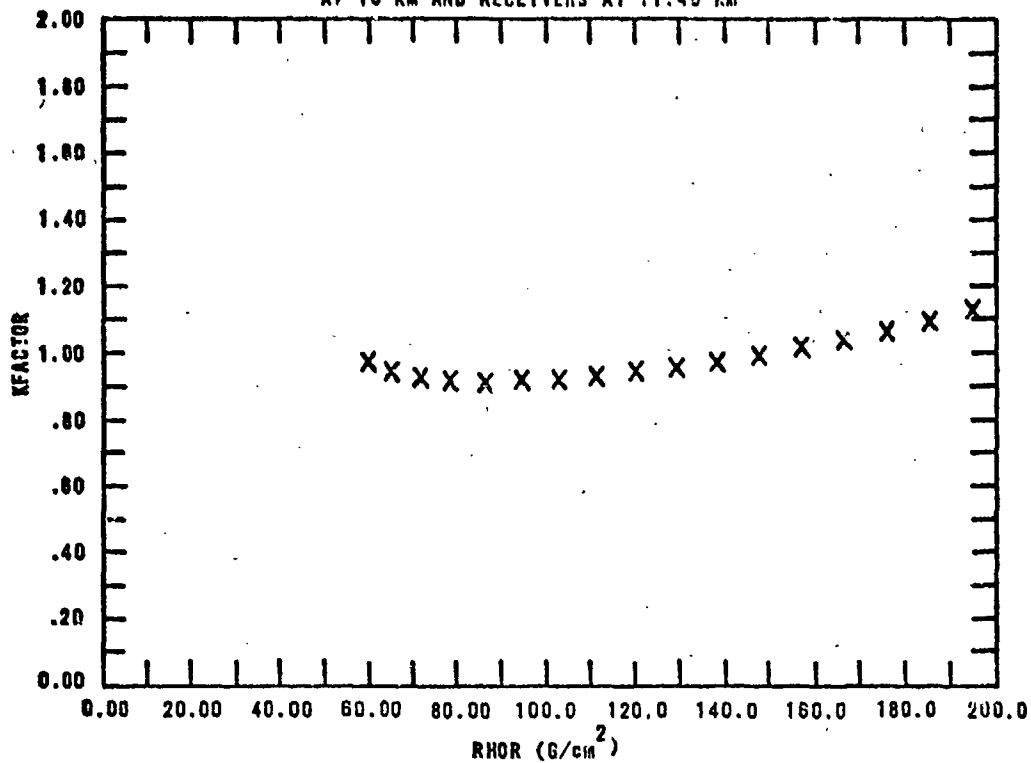
NEUTRON SILICON KFACTOR FOR A TN SOURCE
AT 10 KM AND RECEIVERS AT 10.14 KM



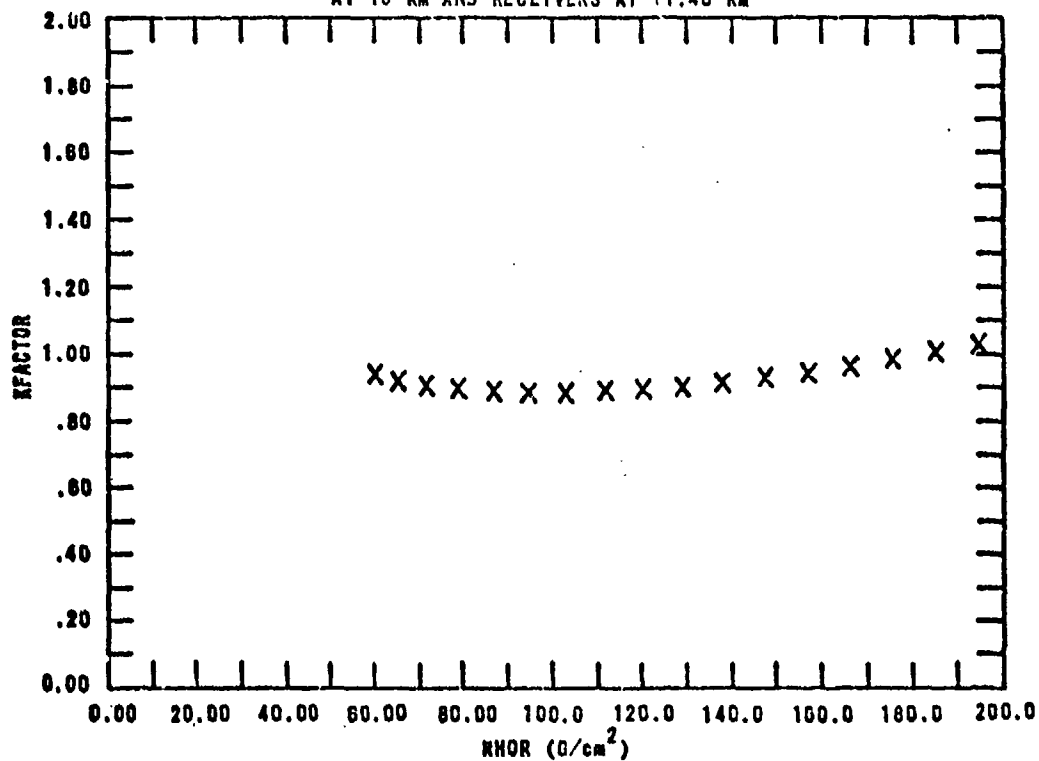
SEC-GAMMA SILICON KFACTOR FOR A TN SOURCE
AT 10 KM AND RECEIVERS AT 10.14 KM

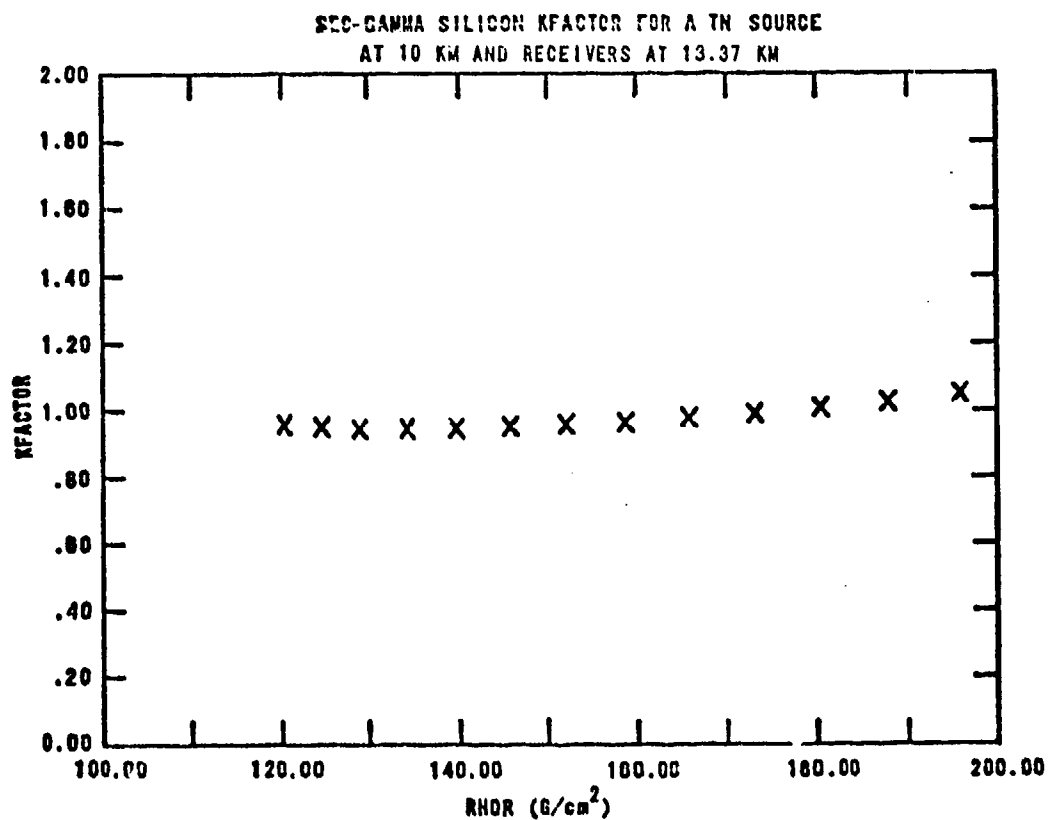
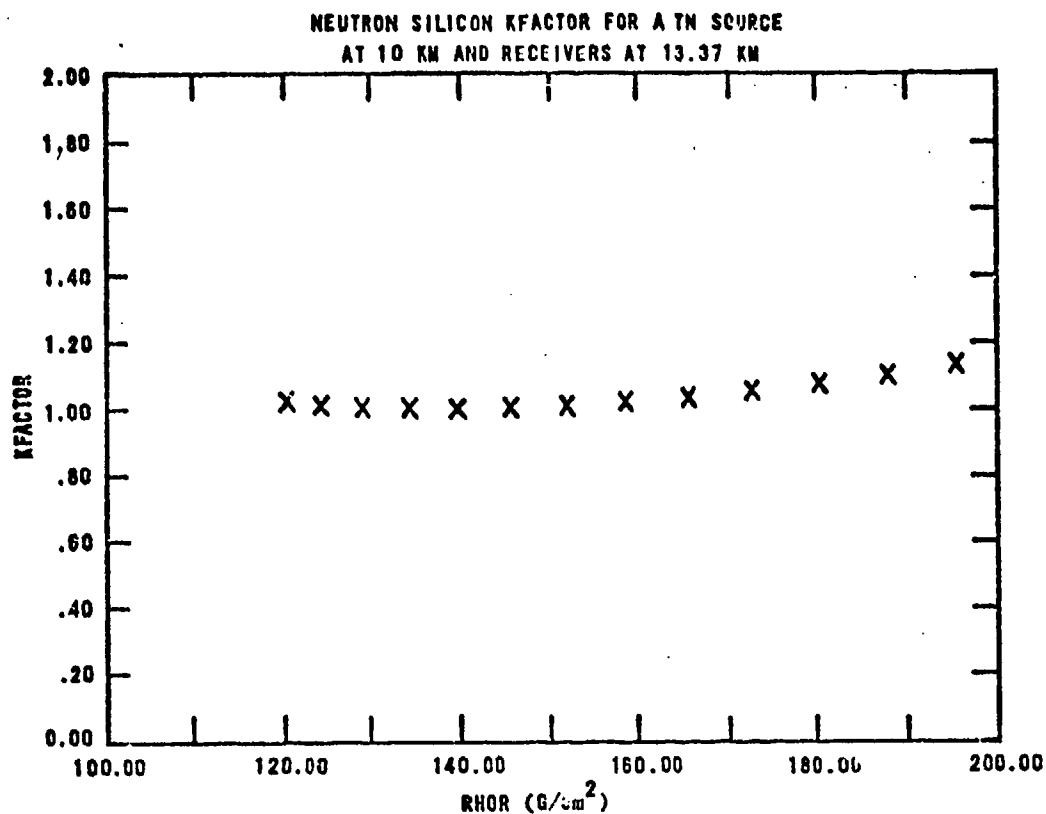


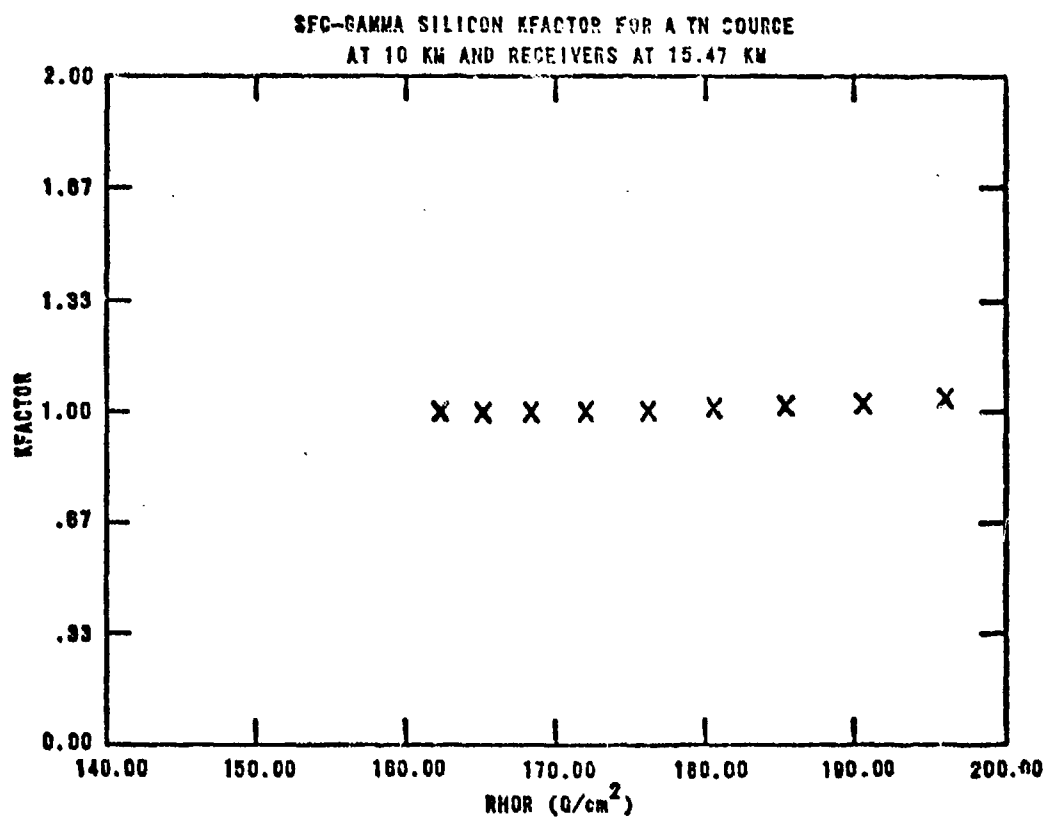
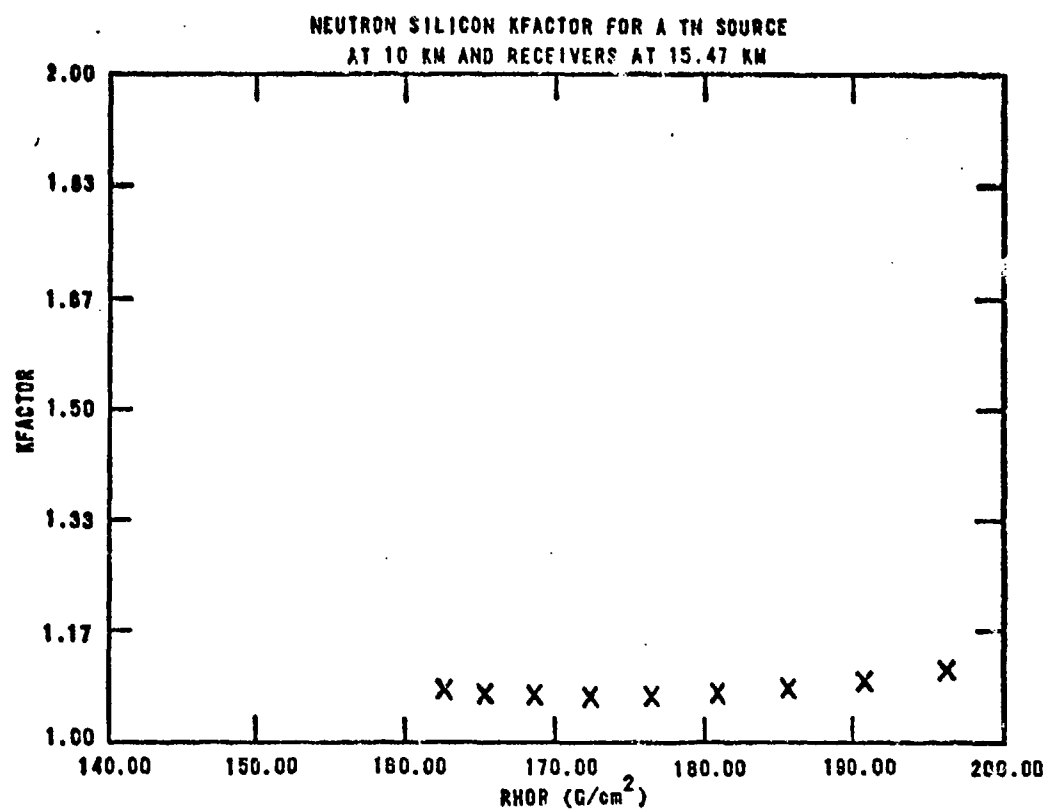
NEUTRON SILICON KFACTOR FOR A TM SOURCE
AT 10 KM AND RECEIVERS AT 11.40 KM

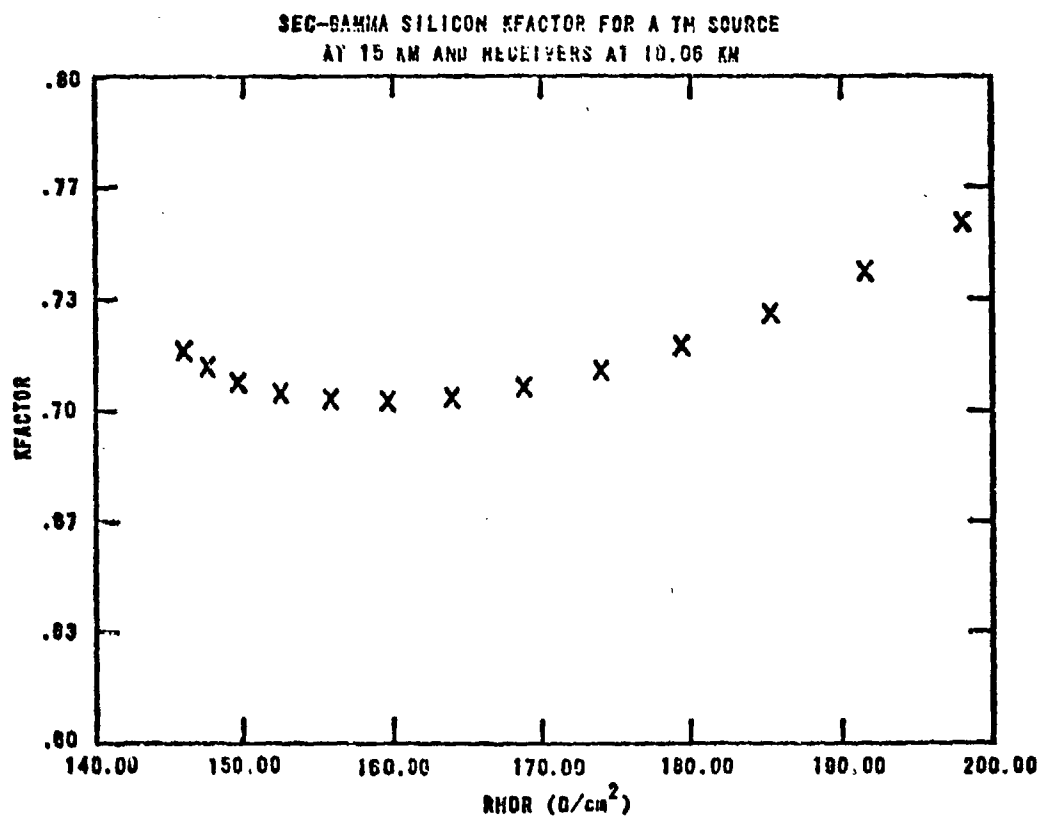
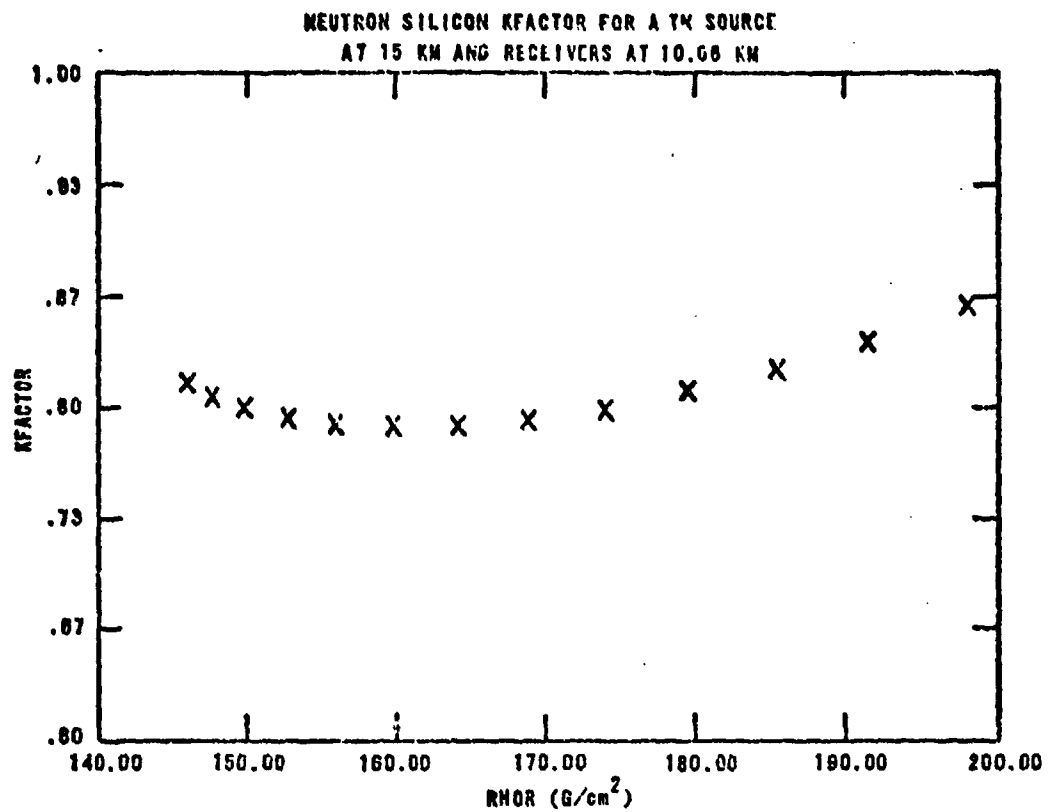


SEC-GAMMA SILICON KFACTOR FOR A TM SOURCE
AT 10 KM AND RECEIVERS AT 11.40 KM

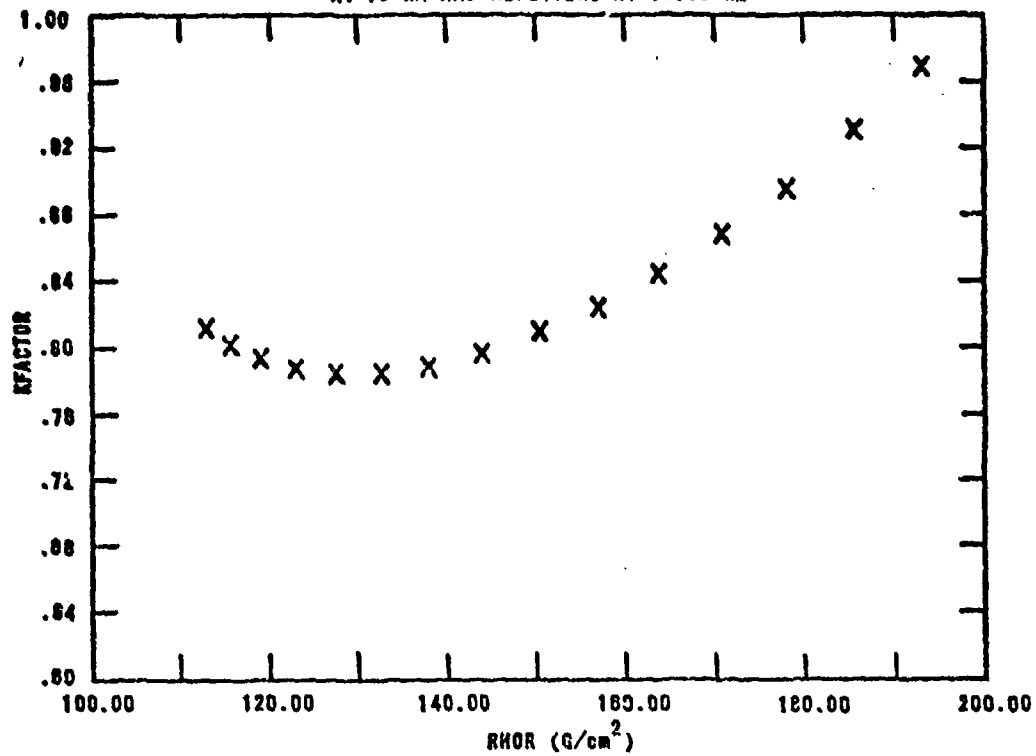




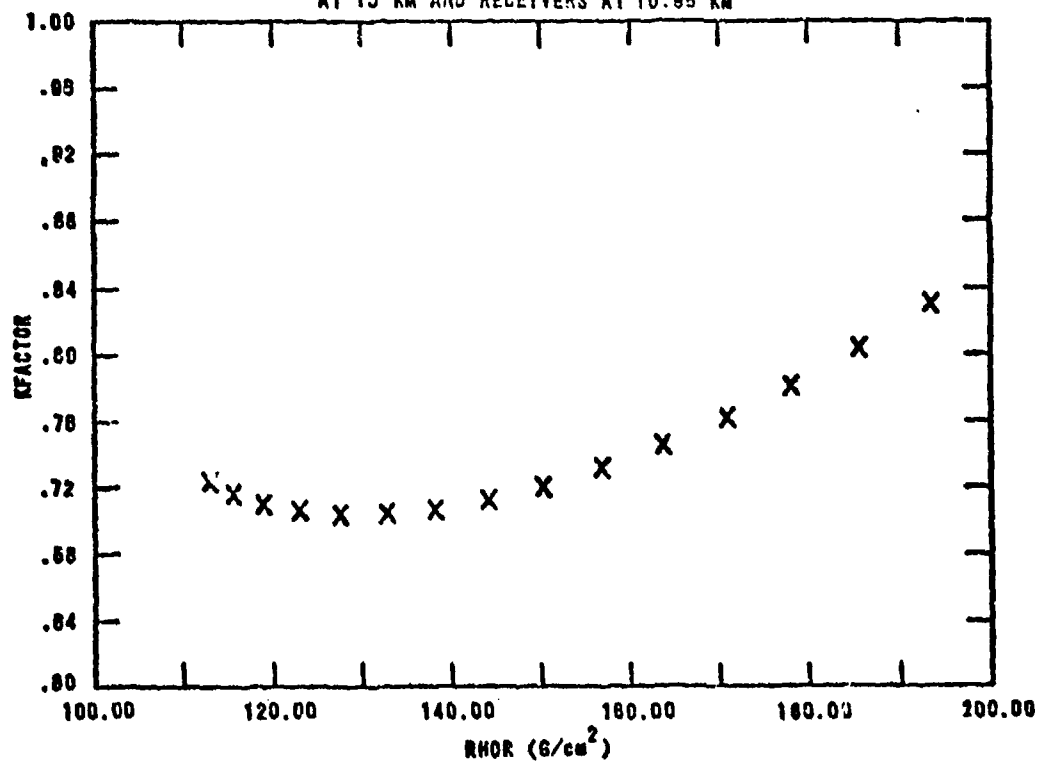




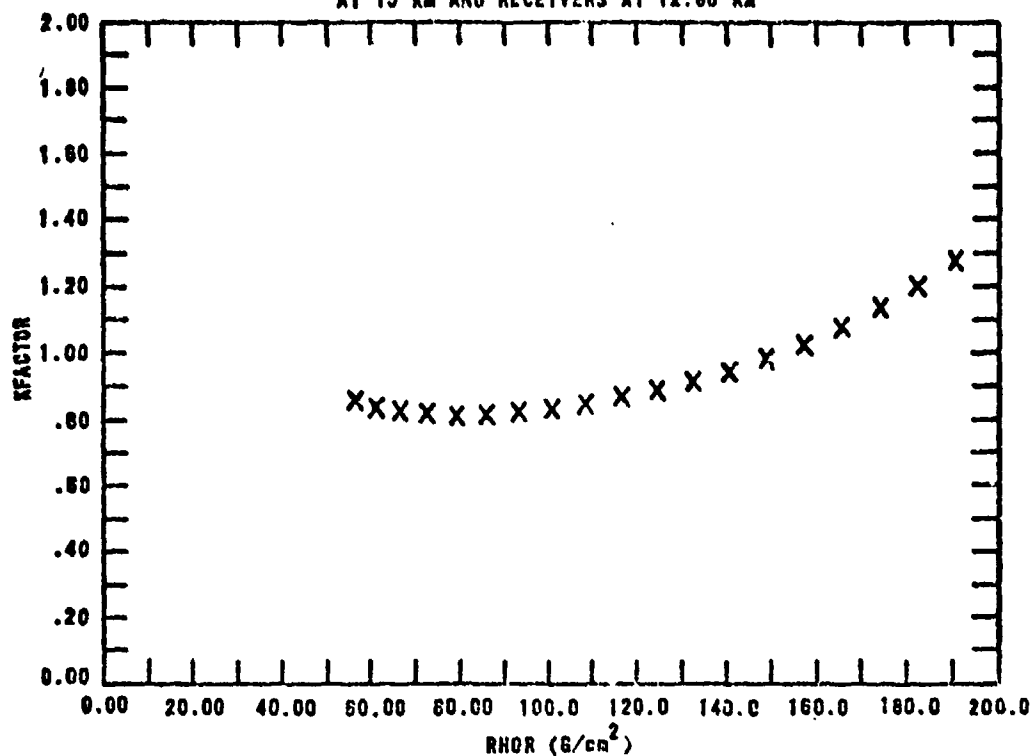
NEUTRON SILICON KFACTOR FOR A TN SOURCE
AT 15 KM AND RECEIVERS AT 10.96 KM



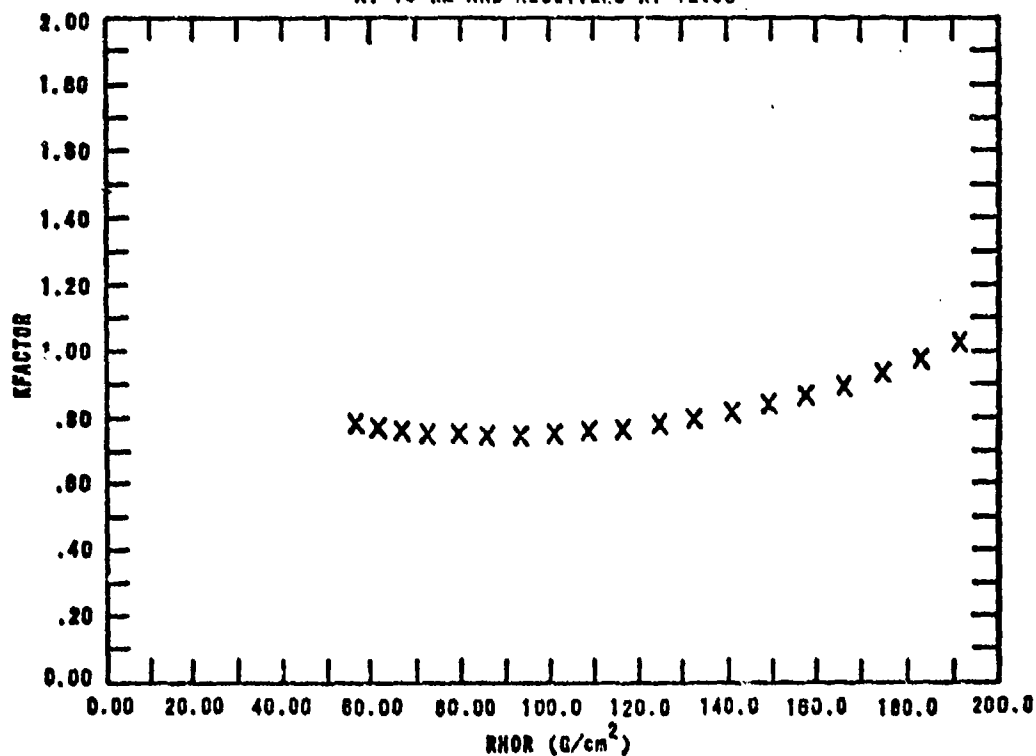
SEC-GAMMA SILICON KFACTOR FOR A TN SOURCE
AT 15 KM AND RECEIVERS AT 10.96 KM



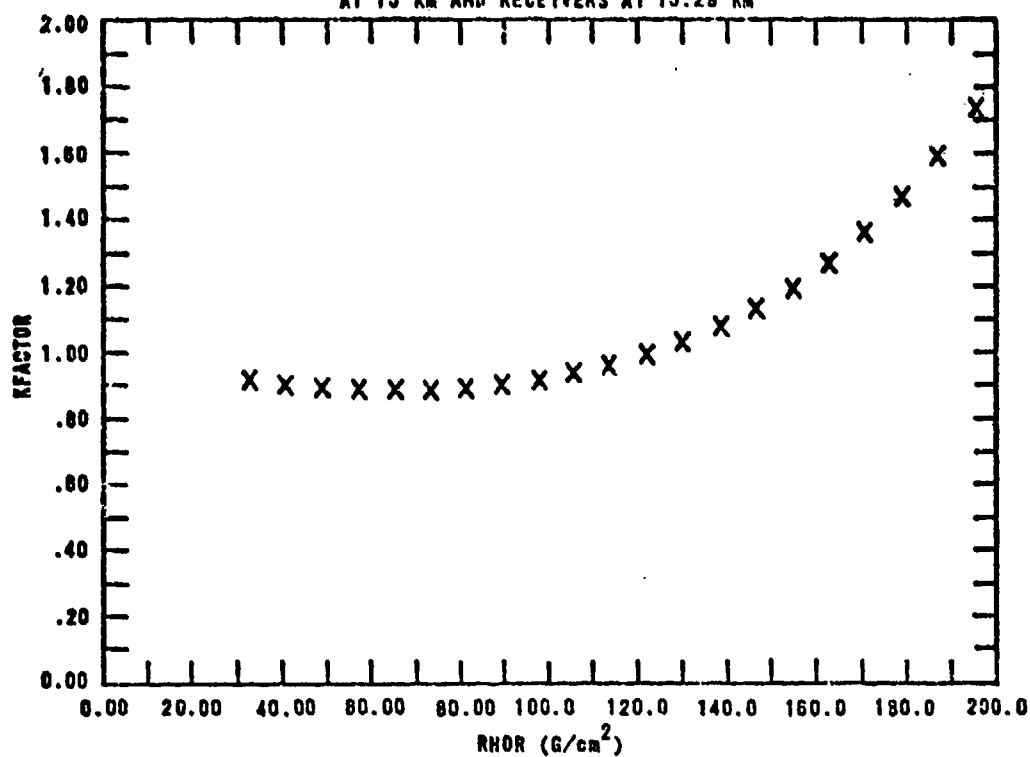
NEUTRON SILICON KFACTOR FOR A TN SOURCE
AT 15 KM AND RECEIVERS AT 12.80 KM



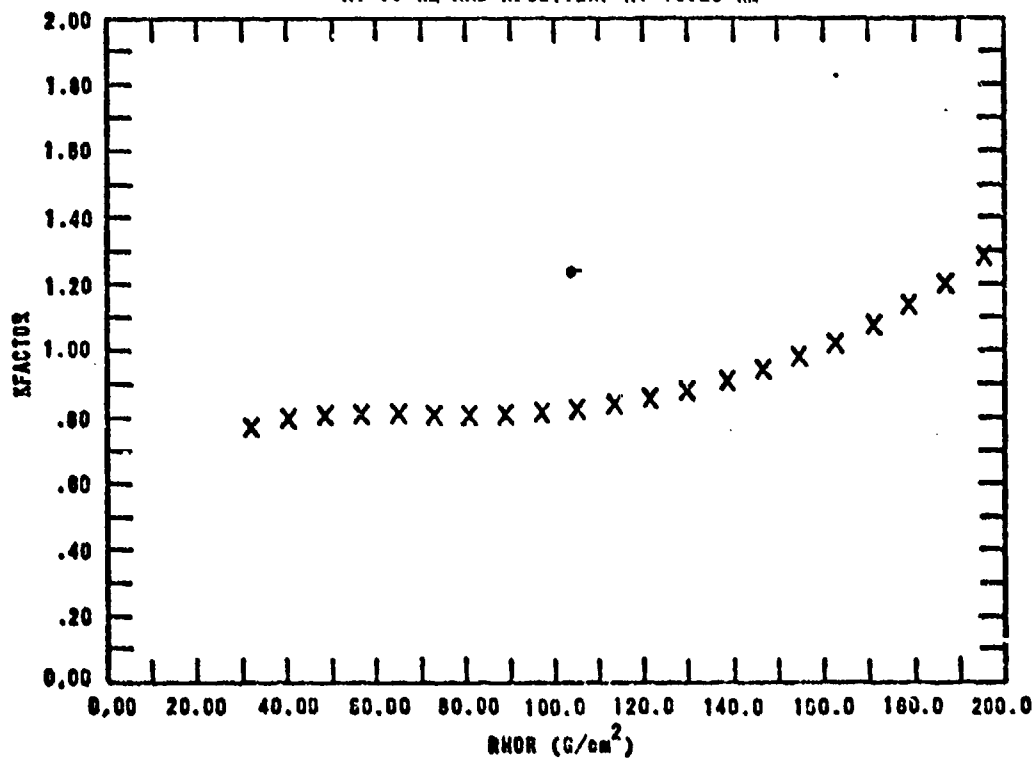
SEC-GAMMA SILICON KFACTOR FOR A TN SOURCE
AT 15 KM AND RECEIVERS AT 12.80

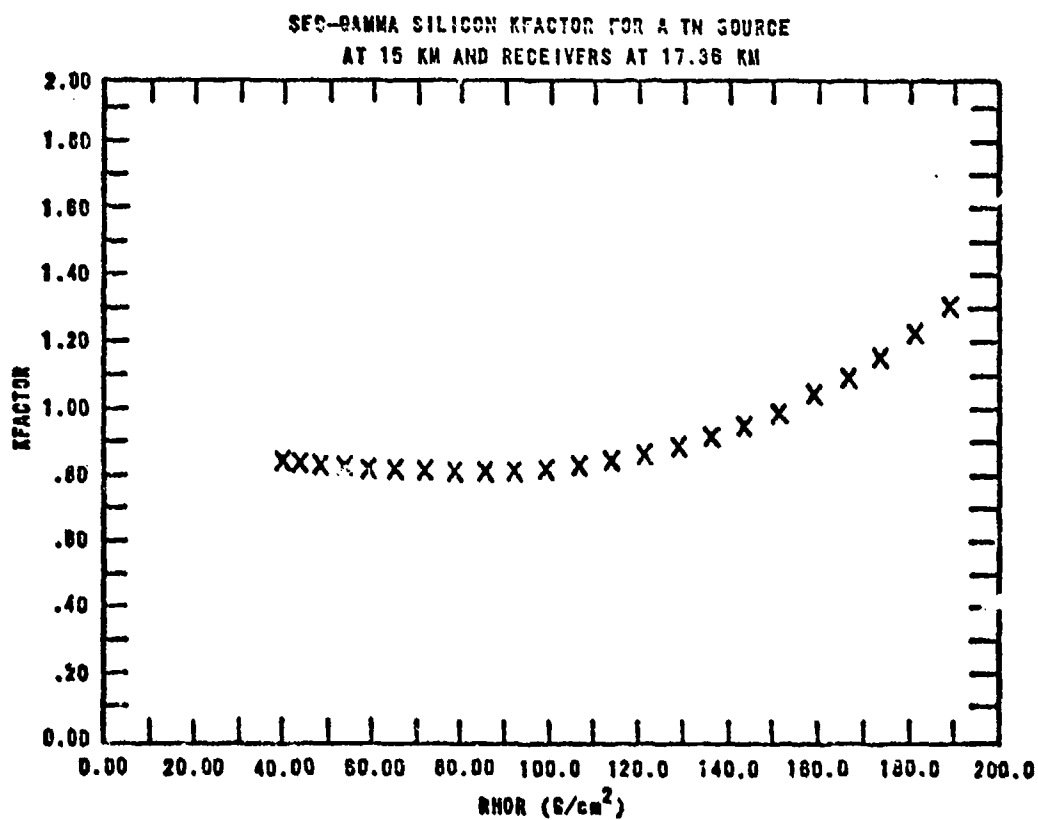
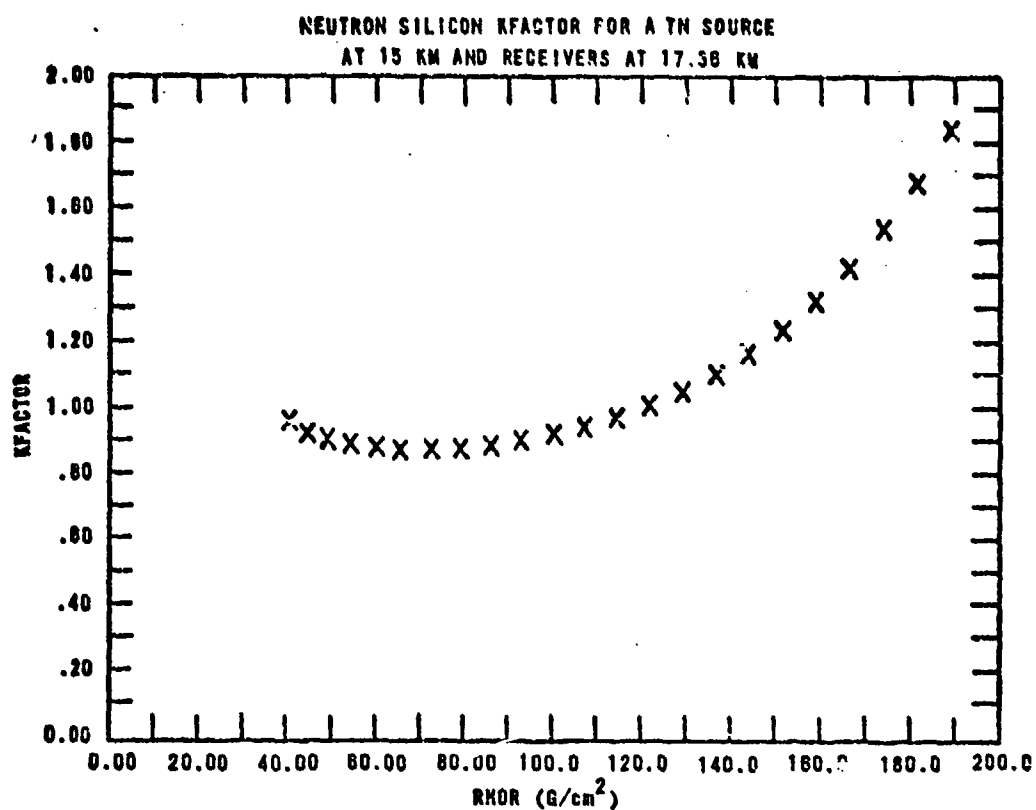


NEUTRON SILICON KFACTOR FOR A TN SOURCE
AT 15 KM AND RECEIVERS AT 15.29 KM

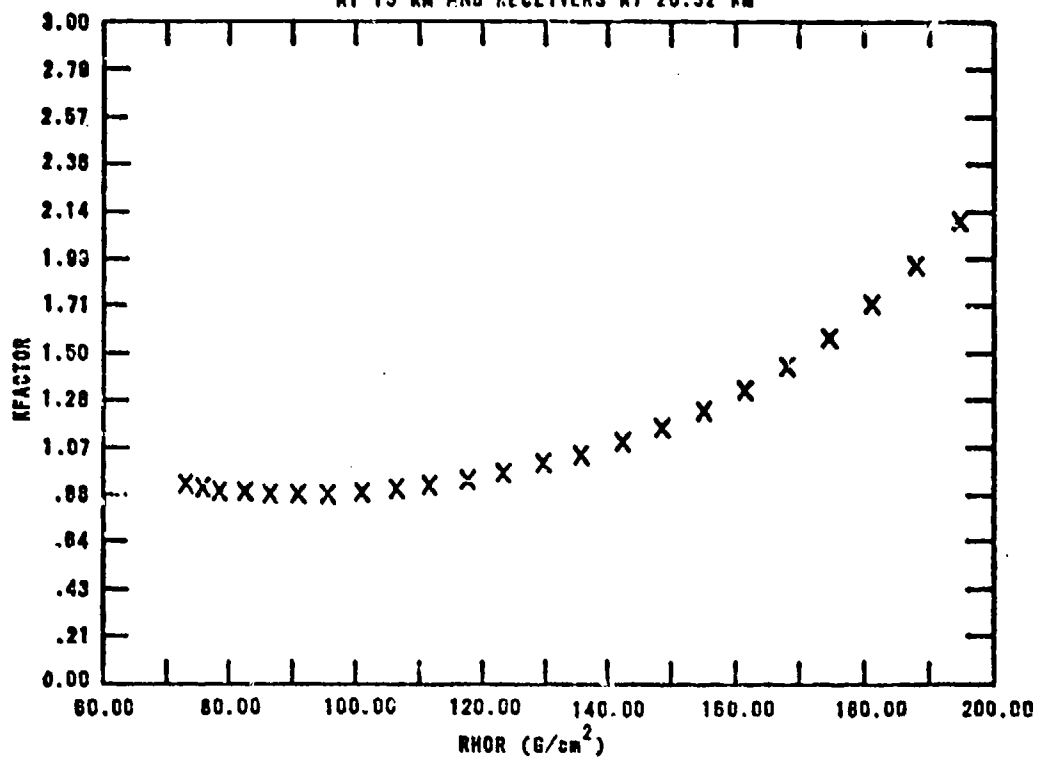


S2C-GAMMA SILICON KFACTOR FOR A TN SOURCE
AT 15 KM AND RECEIVERS AT 15.29 KM

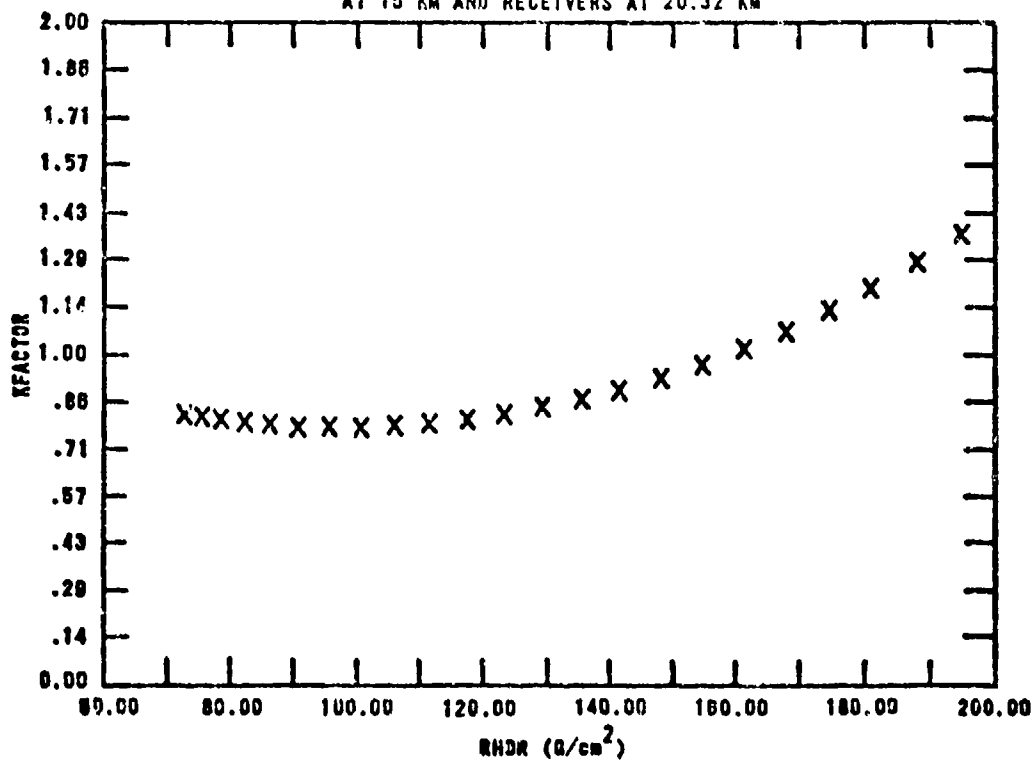


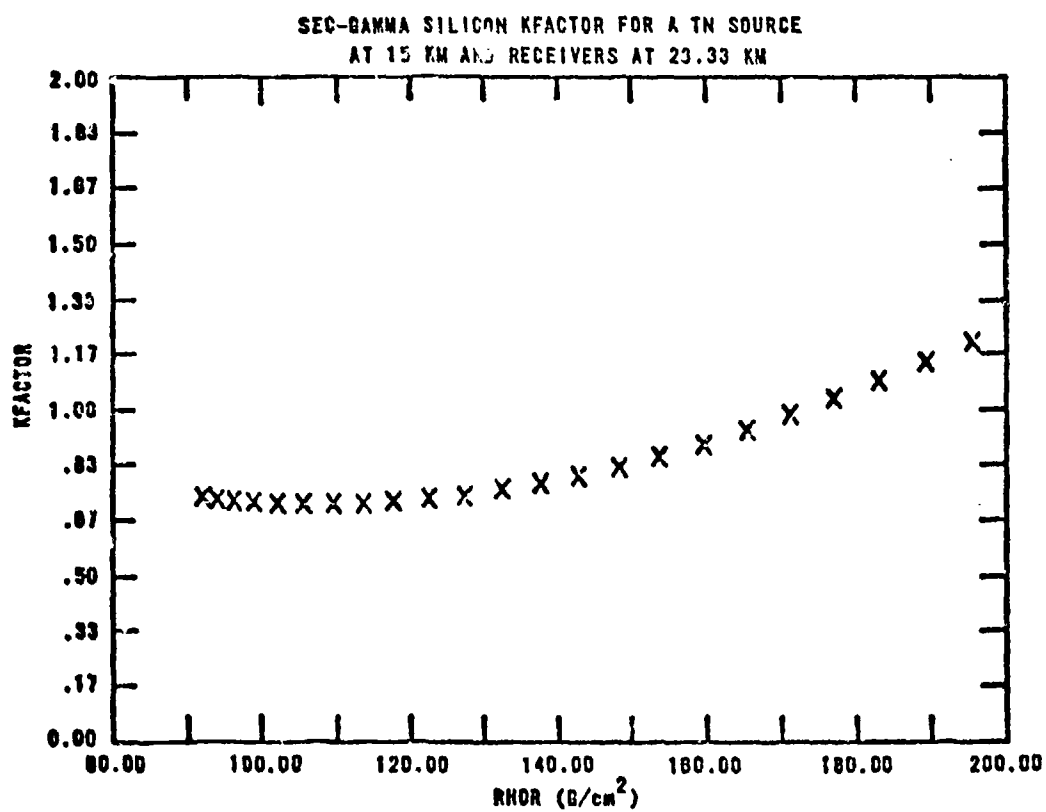
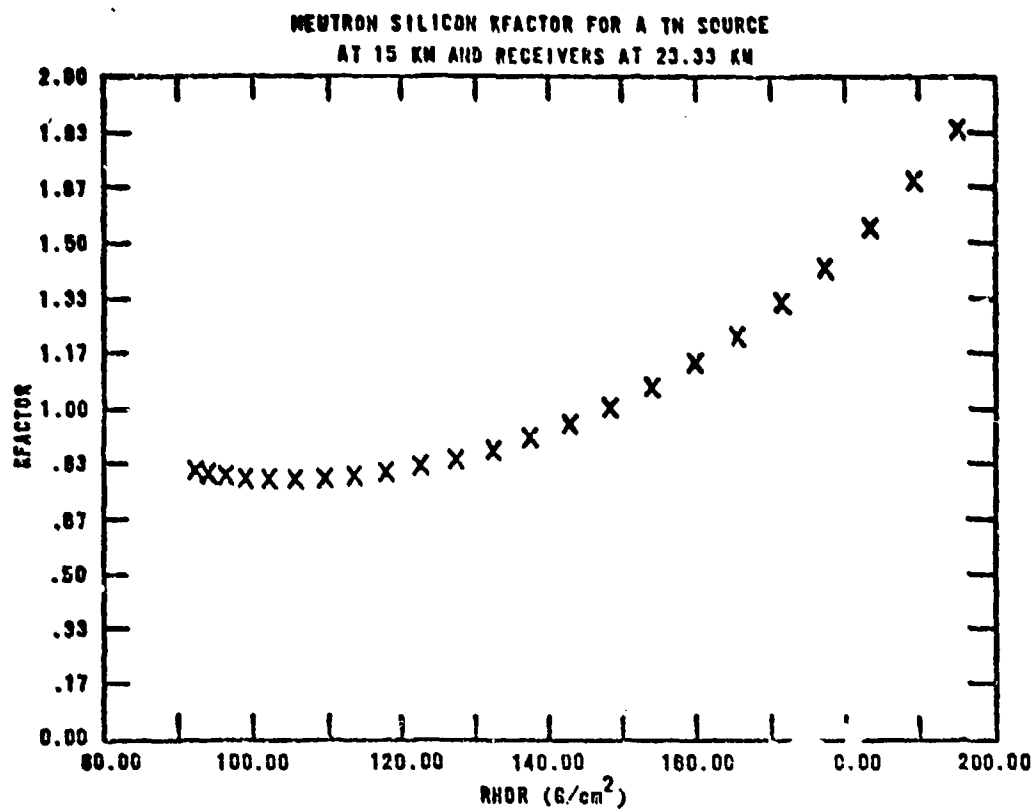


NEUTRON SILICON KFACTOR FOR A TN SOURCE
AT 15 KM AND RECEIVERS AT 20.32 KM

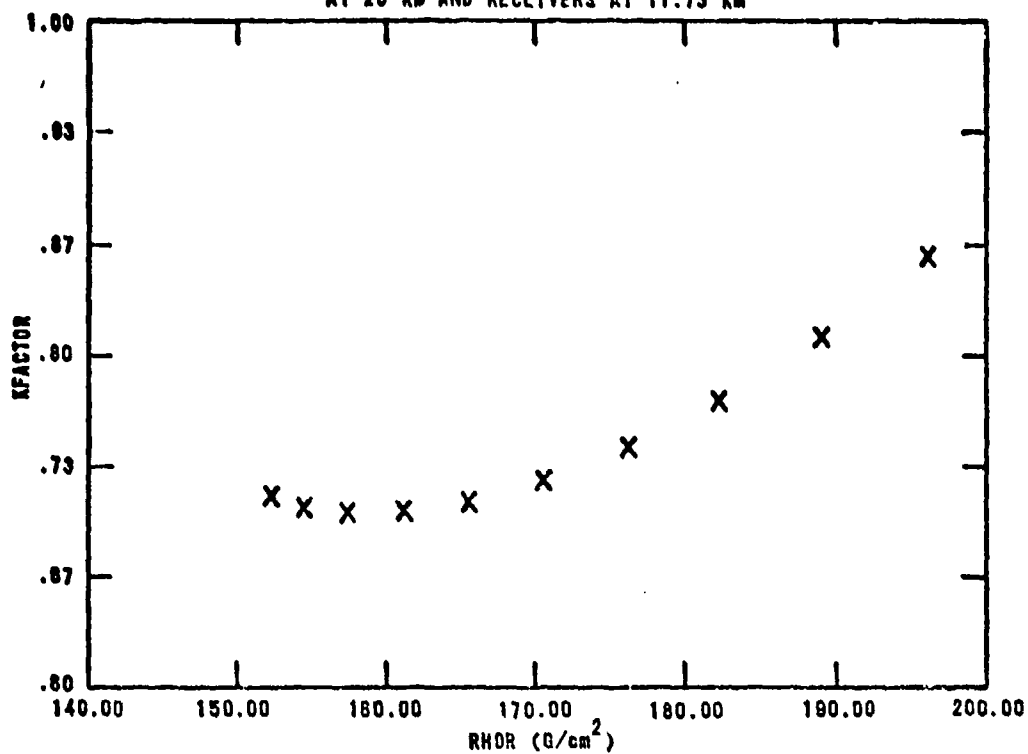


SEC GAMMA SILICON KFACTOR FOR A TN SOURCE
AT 15 KM AND RECEIVERS AT 20.32 KM

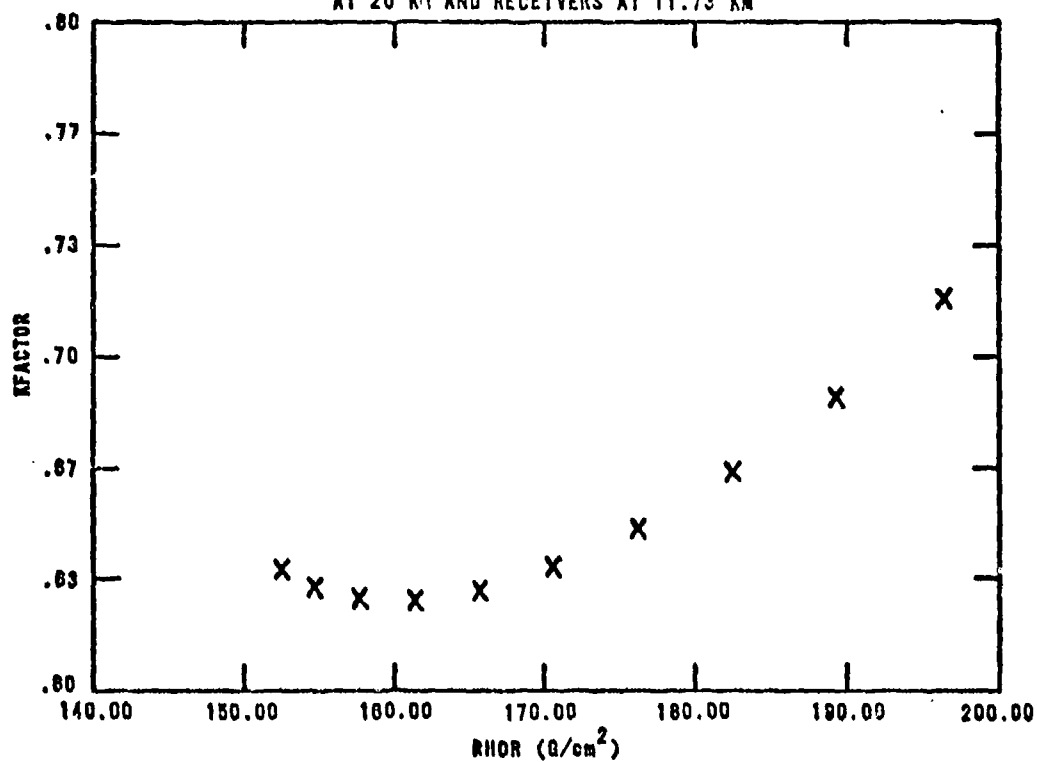




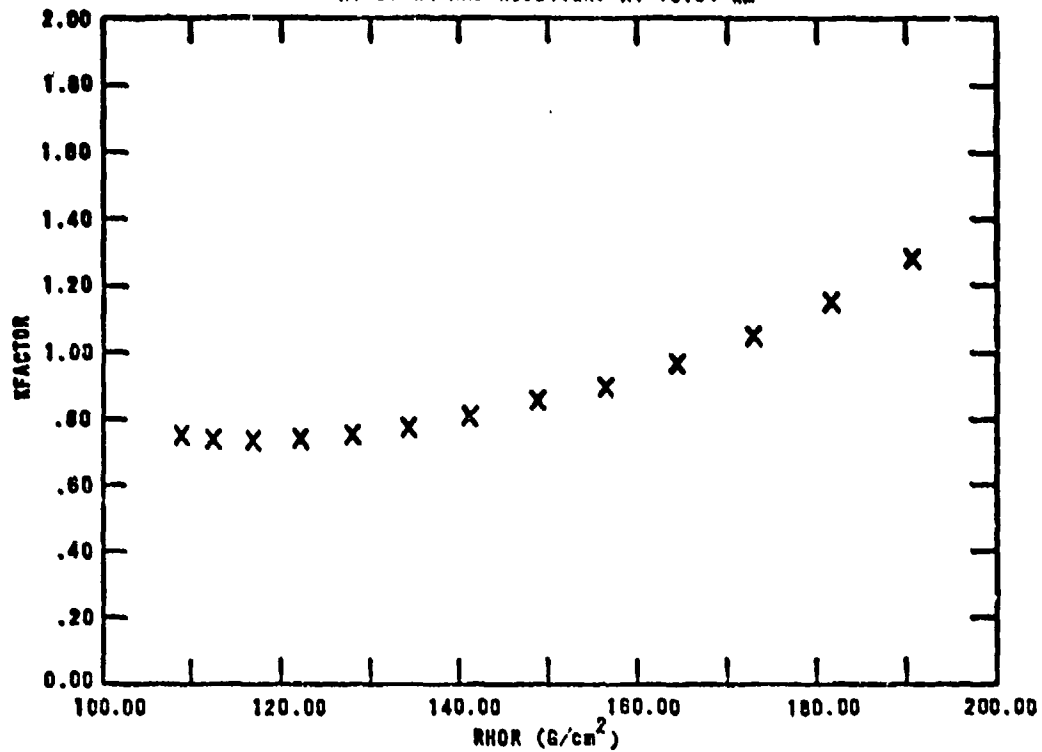
NEUTRON SILICON KFACTOR FOR A TN SOURCE
AT 20 KM AND RECEIVERS AT 11.73 KM



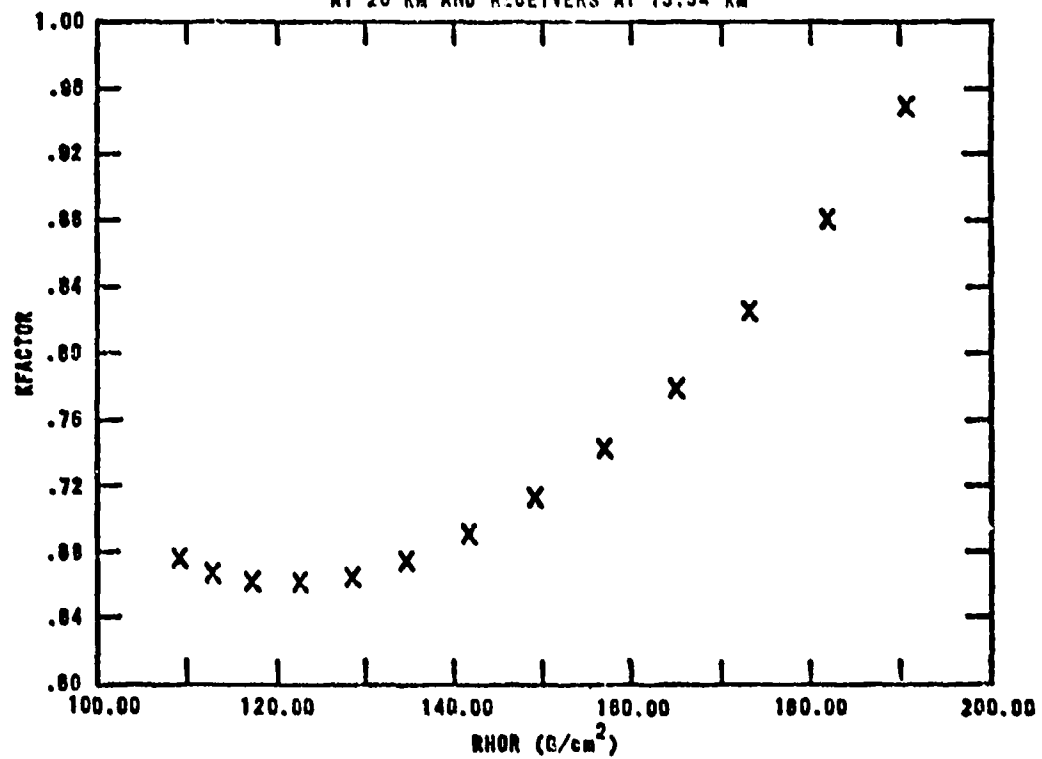
SEU-GAMMA SILICON KFACTOR FOR A TN SOURCE
AT 20 KM AND RECEIVERS AT 11.73 KM



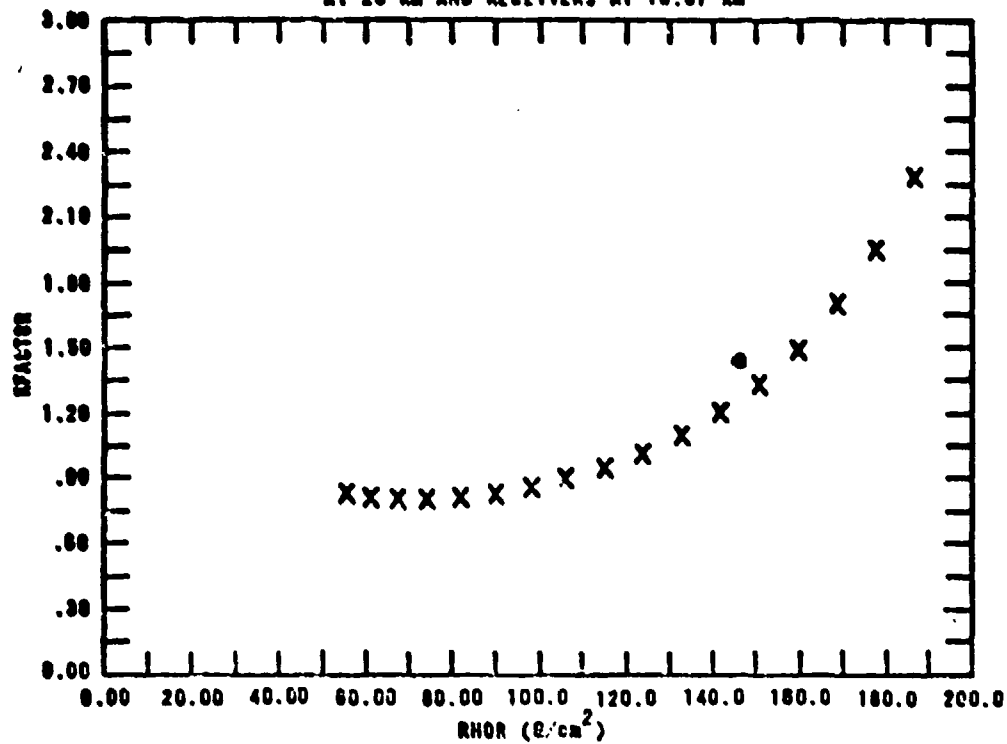
NEUTRON SILICON KFACTOR FOR A TM SOURCE
AT 20 KM AND RECEIVERS AT 13.34 KM



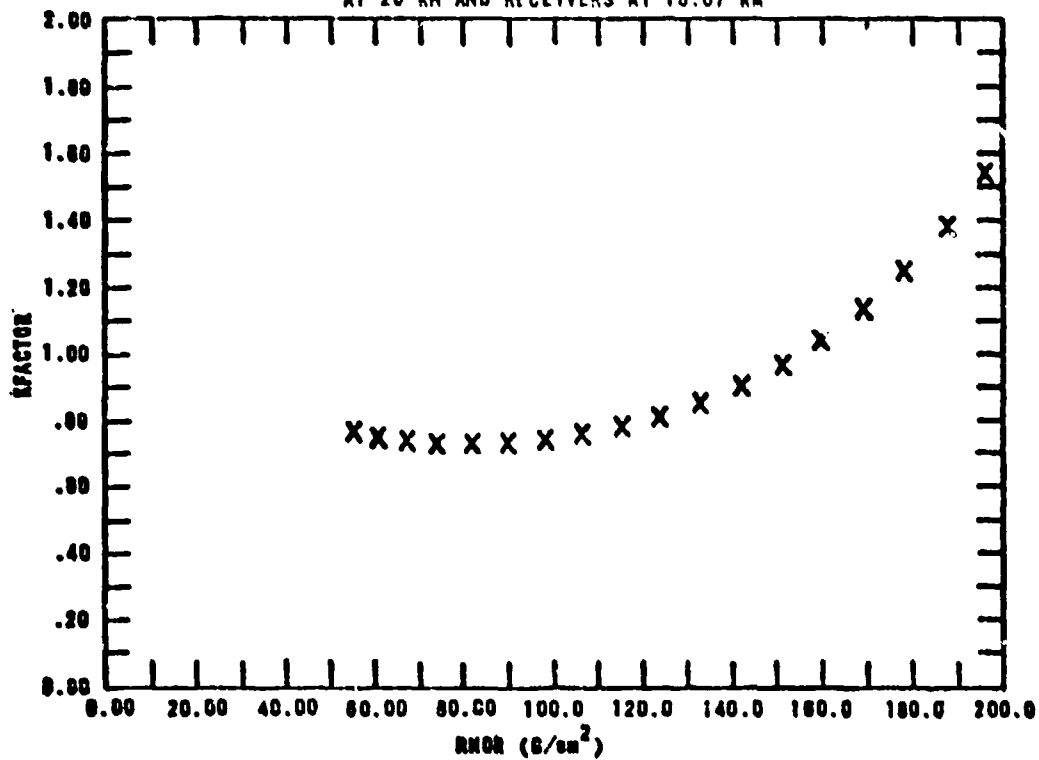
SEC-GAMMA SILICON KFACTOR FOR A TM SOURCE
AT 20 KM AND RECEIVERS AT 13.34 KM



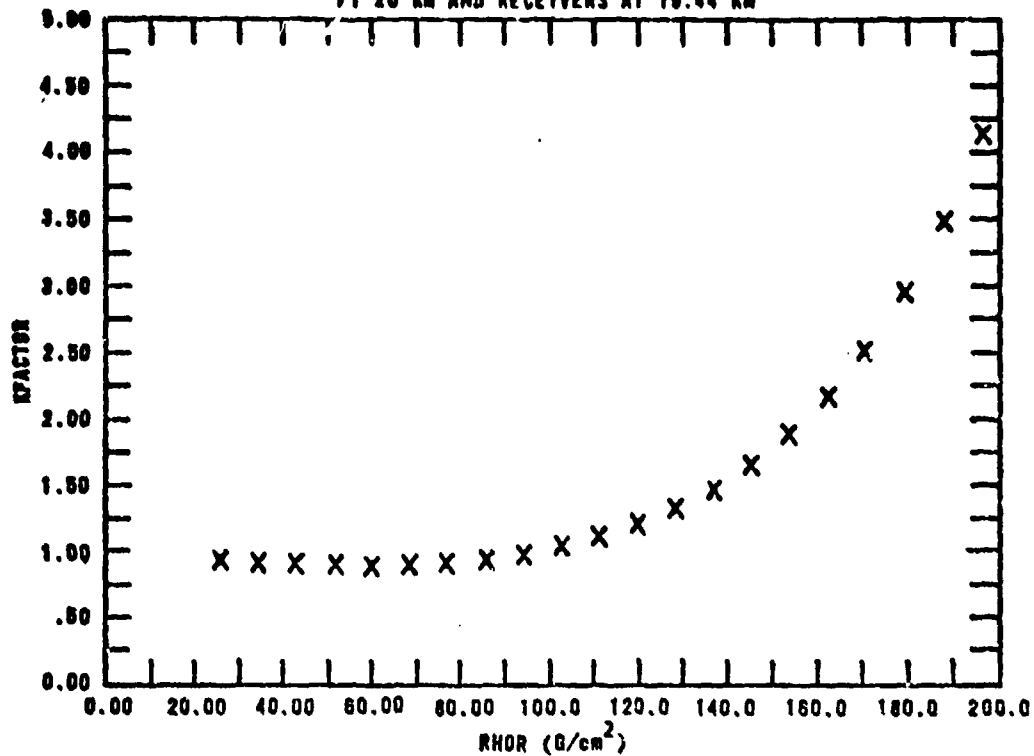
NEUTRON SILICON REACTOR FOR A 1M SOURCE
AT 20 KM AND RECEIVERS AT 16.07 KM



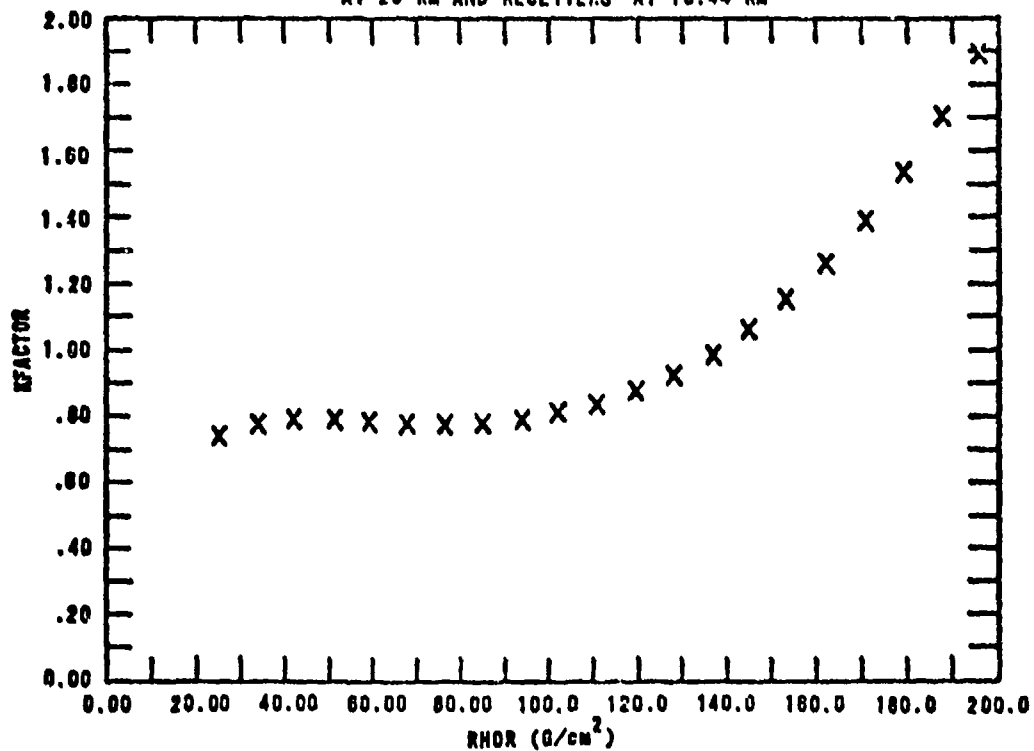
SEC-SAMMA SILICON REACTOR FOR A 1M SOURCE
AT 20 KM AND RECEIVERS AT 16.07 KM



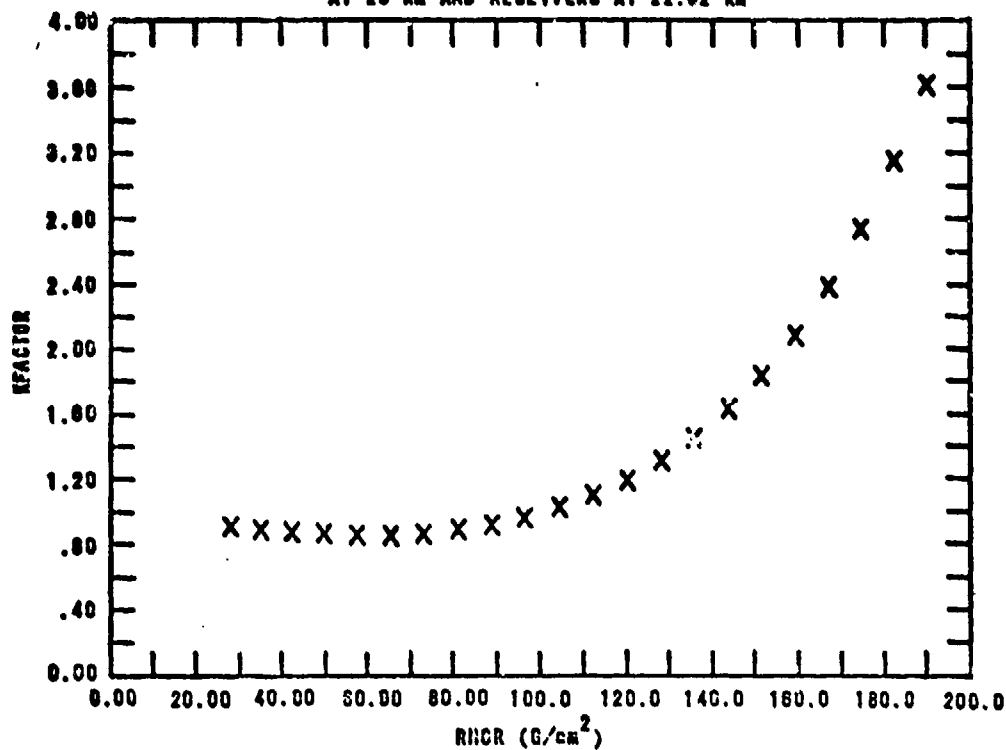
NEUTRON SILICON KFACTOR FOR A TN SOURCE
AT 20 KM AND RECEIVERS AT 19.44 KM



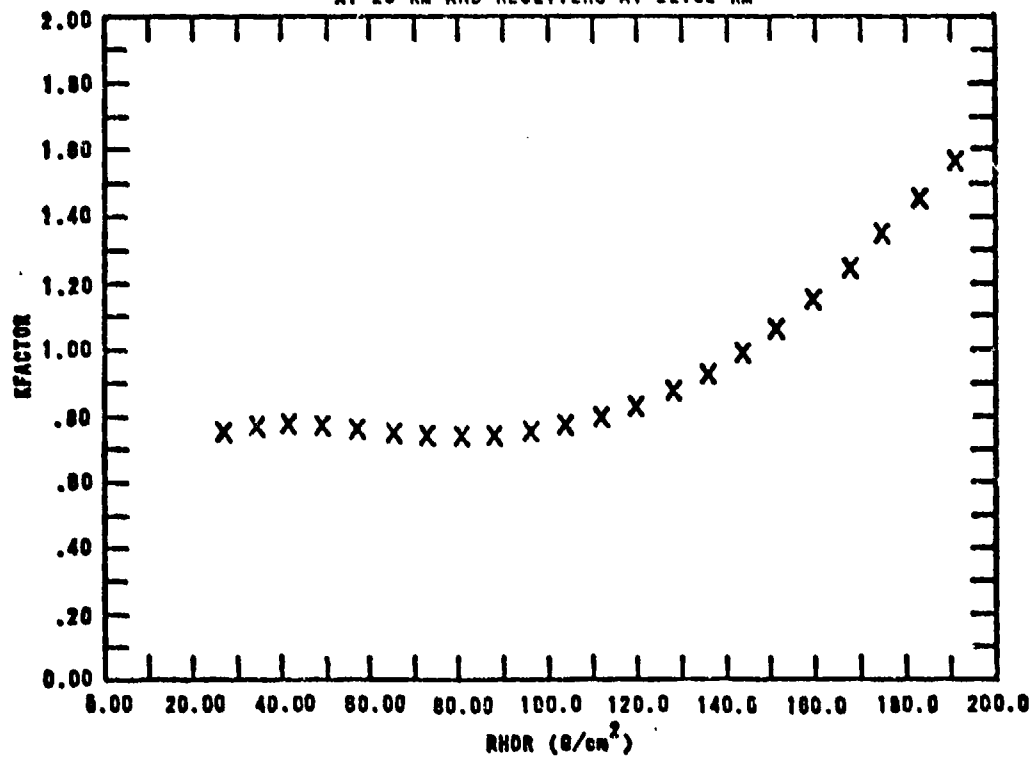
SEC-GAMMA SILICON KFACTOR FOR A TN SOURCE
AT 20 KM AND RECEIVERS AT 19.44 KM



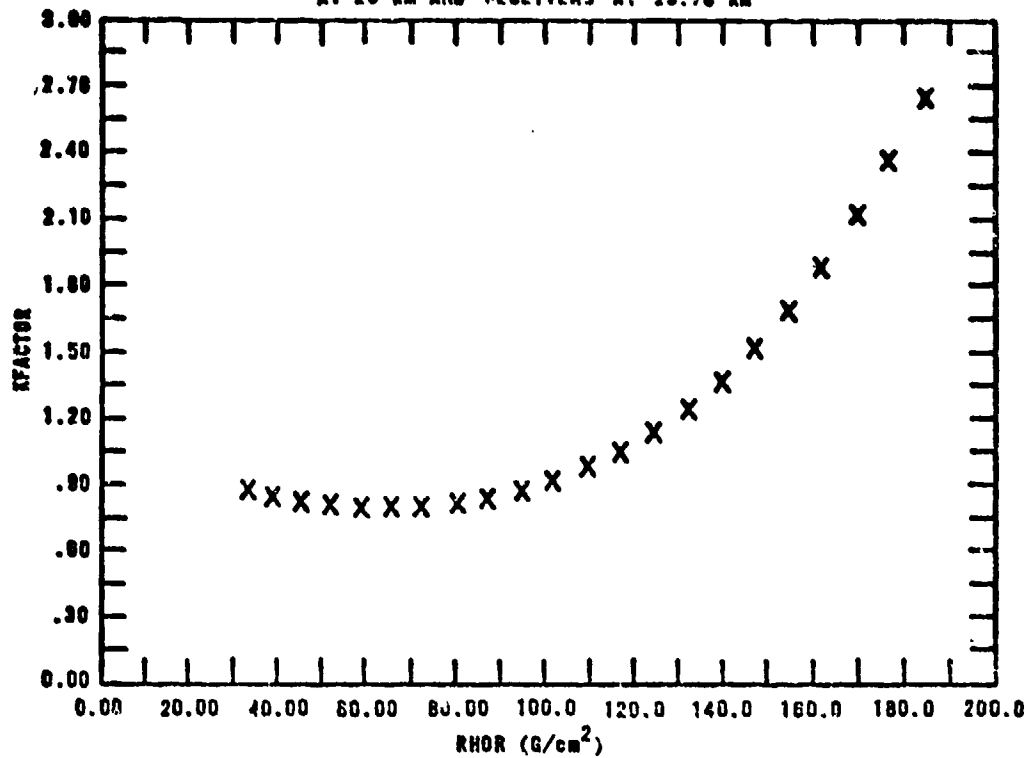
NEUTRON SILICON KFACTOR FOR A TN SOURCE
AT 20 KM AND RECEIVERS AT 22.02 KM



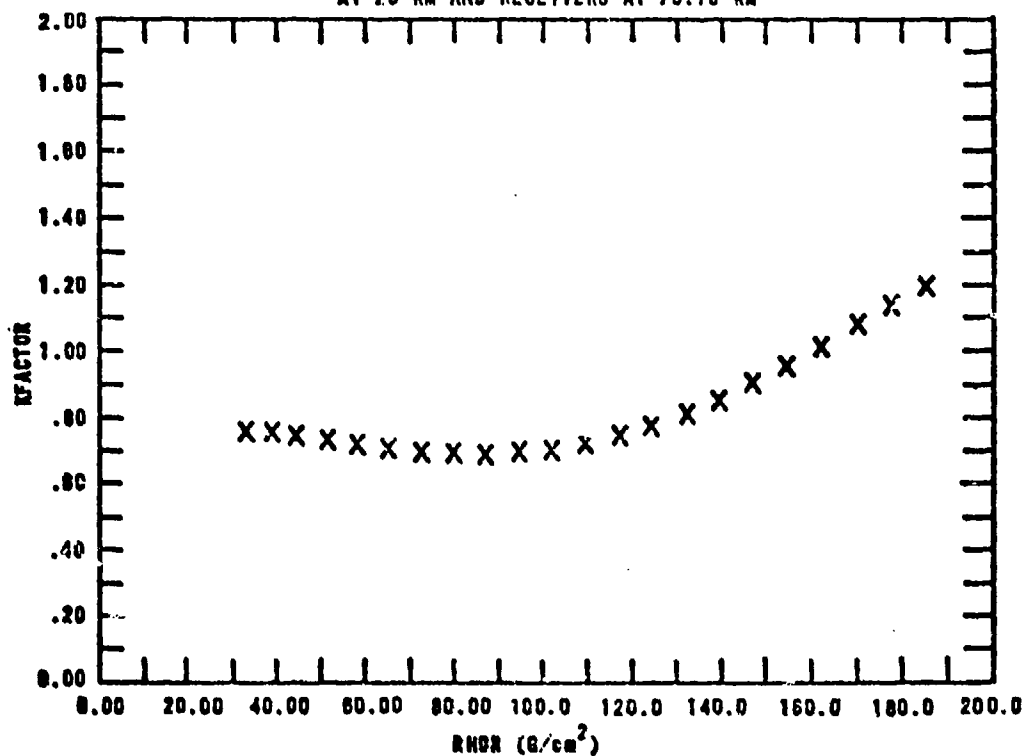
SEC-GAMMA SILICON KFACTOR FOR A TN SOURCE
AT 20 KM AND RECEIVERS AT 22.02 KM



NEUTRON SILICON KFACTOR FOR A TN SOURCE
AT 20 KM AND RECEIVERS AT 23.76 KM



SEC-GAMMA SILICON KFACTOR FOR A TN SOURCE
AT 20 KM AND RECEIVERS AT 23.76 KM



Vita

Raymond Alfred Shulstad, the son of Alfred K. and Gwendolyn G. Shulstad, was born 24 April 1944 in Salina, Kansas. He graduated from Catholic High School in Montgomery, Alabama, in 1962 and entered the University of Alabama. He was awarded a Bachelor of Science Degree in chemistry from that university in January of 1966 and was commissioned through the ROTC program as a Second Lieutenant in the United States Air Force. He entered active duty in June of 1966. His first assignment was as a full-time graduate student at the Air Force Institute of Technology (AFIT), Wright-Patterson AFB, Ohio. Upon graduation from this institution with a Master of Science Degree in Nuclear Engineering in June of 1968, he was transferred to the 1155th Technical Operations Squadron, McClellan AFB, California, where he served as a radiochemist until June of 1972. At that time, he returned to AFIT and began working toward a Doctor of Philosophy Degree in Aerospace Engineering. He majored in Nuclear Weapon Effects and completed the required course work and comprehensive examinations in April of 1974. He was then transferred to the Air Force Weapons Laboratory (AFWL), Kirtland AFB, New Mexico, and began working on his doctoral dissertation. He is currently assigned to the AFWL as a staff scientist in the Battle Environments Branch, Analysis Division.

Permanent address: 1033 Quintilia Avenue
Orlando, Florida 32809

This dissertation was typed by Mrs. Bette Shannon.